Spring 2019

The effects of low aspect ratio and heat exchanging internals on the bubble properties and flow regime in a pilot-plant bubble/ slurry bubble column for Fischer-Tropsch synthesis

Hayder Al-Naseri

Department: Chemical and Biochemical Engineering

THE EFFECTS OF LOW ASPECT RATIO AND HEAT EXCHANGING INTERNALS ON THE BUBBLE PROPERTIES AND FLOW REGIME IN A PILOT-PLANT BUBBLE/SLURRY BUBBLE COLUMN FOR FISCHER-TROPSCH SYNTHESIS

by

HAYDER AL-NASERI

A DISSERTATION

Presented to the Faculty of the Graduate School of the

MISSOURI UNIVERSITY OF SCIENCE AND TECHNOLOGY

In Partial Fulfillment of the Requirements for the Degree

DOCTOR OF PHILOSOPHY

in

CHEMICAL ENGINEERING

2019

Approved by

Dr. Muthanna Al-Dahhan, Advisor
Dr. Joshua P. Schlegel, Co-advisor
Dr. Parthasakha Neogi
Dr. Joseph Smith
Dr. Dipak Barua

PUBLICATION DISSERTATION OPTION

This dissertation consists of the following three articles, formatted in the style used by the Missouri University of Science and Technology:

Paper I pages 27-80 have been submitted to Experimental Thermal and Fluid Science Journal.

Paper II pages 81-129 ready to submit.

Paper III pages 130-169 have been submitted to Chemical Engineering Science Journal.

Paper IV pages 170-204 have been submitted to Chemical Engineering Journal.

Paper V pages 205-269 have been submitted to Chemical Engineering Science Journal.

ABSTRACT

Fischer-Tropsch synthesis (F-T) is a process utilized to convert the syngas mixture of CO and H_2 to synthetic fuel and chemicals that executed commercially by using the bubble/slurry bubble column reactor. The experimental results reveal that the investigated parameters, in terms the presence of internals, and reducing the aspect ratio and the solids loading, increase the local gas holdup, interfacial area, bubble passage frequency, and decrease the bubble rise velocity, bubble chord length. Meanwhile, the aspect ratio *H/D* = 4, and 5 provide enough height to established the fully developed flow regime. As a result of the variation in the bubble properties that in turn reflected on the flow regime transition, therefore, the presence of internals and decreasing the aspect ratio delay the transition from the transition flow regime to churn turbulent flow regime. The validated CFD codes, using Eulerian-Eulerian approach incorporated with the population balance model PBM, exhibit the capability to simulate the bubble column in bubbly and turbulent flow regimes. However, results revealed that the presence of internals enhanced the gas holdup significantly in the wall region of the column. The gas holdup radial profiles in the presence of internals in different configurations provide a uniform gas holdup profile. While the results of the effect of internals diameter exhibit that the gas holdup was increased remarkably in the center and the wall regions of the bubble column equipped by internals of 1-inch diameter more than in using internals of 0.5-inch. However, the effect of internals configurations reported that the internals with hexagonal arrangement increases the gas holdup in the center region more than the circular arrangement, and less in the wall region comparing with the circular arrangement.

ACKNOWLEDGMENTS

First and foremost, thanks and praises to ALLAH for his kindness and blessing. Thanks for giving me faith to believe in myself and guidance to overcome my weakness. Thanks for granting me patience through the hard times and thankfulness through the good times. I also wish to thank the Iraqi government that represented by the Higher Committee for Education Development in Iraq (**HCED**) for the financial support to earn the Ph.D. degree in the Chemical Engineering. I wish to express my sincere gratitude and thanks to my advisor, Dr. Muthanna H. Al-Dahhan, and my co-advisor, Dr. Joshua P. Schlegel. Dr. Muthanna H. Al-Dahhan introduced me to Missouri University of Science and Technology and encouraged me to pursue my Ph.D. under his guidance with his research team at this great university. Also, I would like to thank Dr. Joshua P. Schlegel for his support and affording me in the early stages of the research until I gained the required skills to understand and complete the work independently. To the Chemical Engineering staff, thank you for answering my questions and clearing my doubts.

In addition, I would like to thank all my colleagues for their support, help; and I want to say that I will never forget the hard and fun times we have faced together during these years of friendship, study, and work. I am very lucky to be a member of such a team and hope to keep our friendship forever. Warm and special thanks are due to my family: Mom and my brother Muhammad Al-Naseri. Finally, and forever, I don't find words to thank my lovely wife, Dhabya. Thanks for believing in me and for supporting our dream which today comes true as a result of her sacrifices. As I head towards other places to meet other peoples, I hope I left a good memory as I gathered many.

TABLE OF CONTENTS

Page

LIST OF ILLUSTRATIONS

SECTION Page

PAPER I

PAPER II

PAPER III

PAPER IV

PAPER V

LIST OF TABLES

1. INTRODUCTION

The growing in the economics of developing countries, and the rising in the world population, and the remarkable development in the technologies led to increase in the energy demand globally (i.e., increase the consumption of energy). Furthermore, new technologies for recovering crude oil, changes in the yields of existing crude oil fields, and a global increase in exploration have expanded the number and variety of crude oil types. The increase in the energy demand is one of prime reasons for increases the CO_2 emission and the global warming leading to climate change, however, according to International Energy Outlook-2018 [1], the estimated fraction of global fuel consumption increases by 60% from 2012 to 2040 accounting for 82% of the total increase in world liquid fuel consumption as shown in Figure 1.1. Therefore, the seeking clean alternative energy sources is critical in order to reduce the growing environmental concerns and the risk of the global warming, thereby, global production of natural gas, coal, biomass and biofuel is growing rapidly.

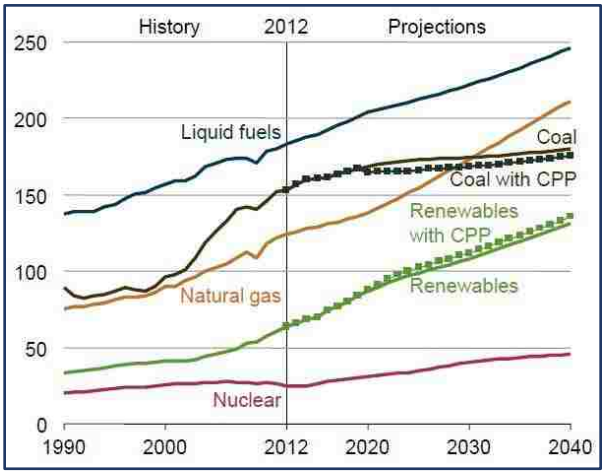

Figure 1.1. Total world energy consumption by energy source, 1990–2040 (quadrillion Btu) [1]

Among the alternative energy sources is the synthesis gas (syngas) (a mixture of CO and H2) produced via gasification of coal, natural gas and biomass are increasingly becoming reliable sources of energy and chemicals due to its product is free from the inorganic compounds (sulfur, nitrogen, oxygen) that makes it friendly to the environment [2]. Fischer-Tropsch (F-T) synthesis process is one of the robust technology that used for this purpose, which is a set of catalytic processes that can be used to produce the clean synthetic liquid fuel and chemicals from synthesis gas (CO_2 and H_2) that derived from several different carbon-containing feedstocks such as natural gas, coal, or biomass to converted to liquid fuel that typically the process termed gas to liquid (GTL), coal to liquid (CTL), and biomass to liquid (BTL), respectively[3,4].

Fischer-Tropsch (F-T) reaction was discovered in 1923 by Franz Fischer, Hans Tropsch, and Helmut Pichler, at Kaiser Wilhelm Institute when they reacted synthesis gas over cobalt catalyst, resulting in the production of gasoline, diesel, middle and heavy distillate oils [5]. First industrial FT reactor was the Ruhrchemie atmospheric fixed bed reactor established in 1935 with a gross annual capacity of 100,000-120,000 metric tons. All plants used Cocatalyst (100Co, 5ThO2, 8MgO, 200kieselguhr), operated at medium pressure in the range of 5-15 atm and 180-200 °C, and used syngas produced by reacting coke with steam utilizing water gas shift reaction. Recently, three types of the reactor that used in the process are multiphase reactor such as multi-tubular fixed bed, slurry bubble column, fixed fluidized bed, and circulating fluidized bed as shown in Figure 1.2, while, the operating conditions with the features of some initially developed Fischer-Tropsch (F-T) reactors are listed in Table 1.1. Currently, there are two operating modes for the FT reactors-high temperature mode (300–350 °C) and low-temperature mode (200–240 °C).

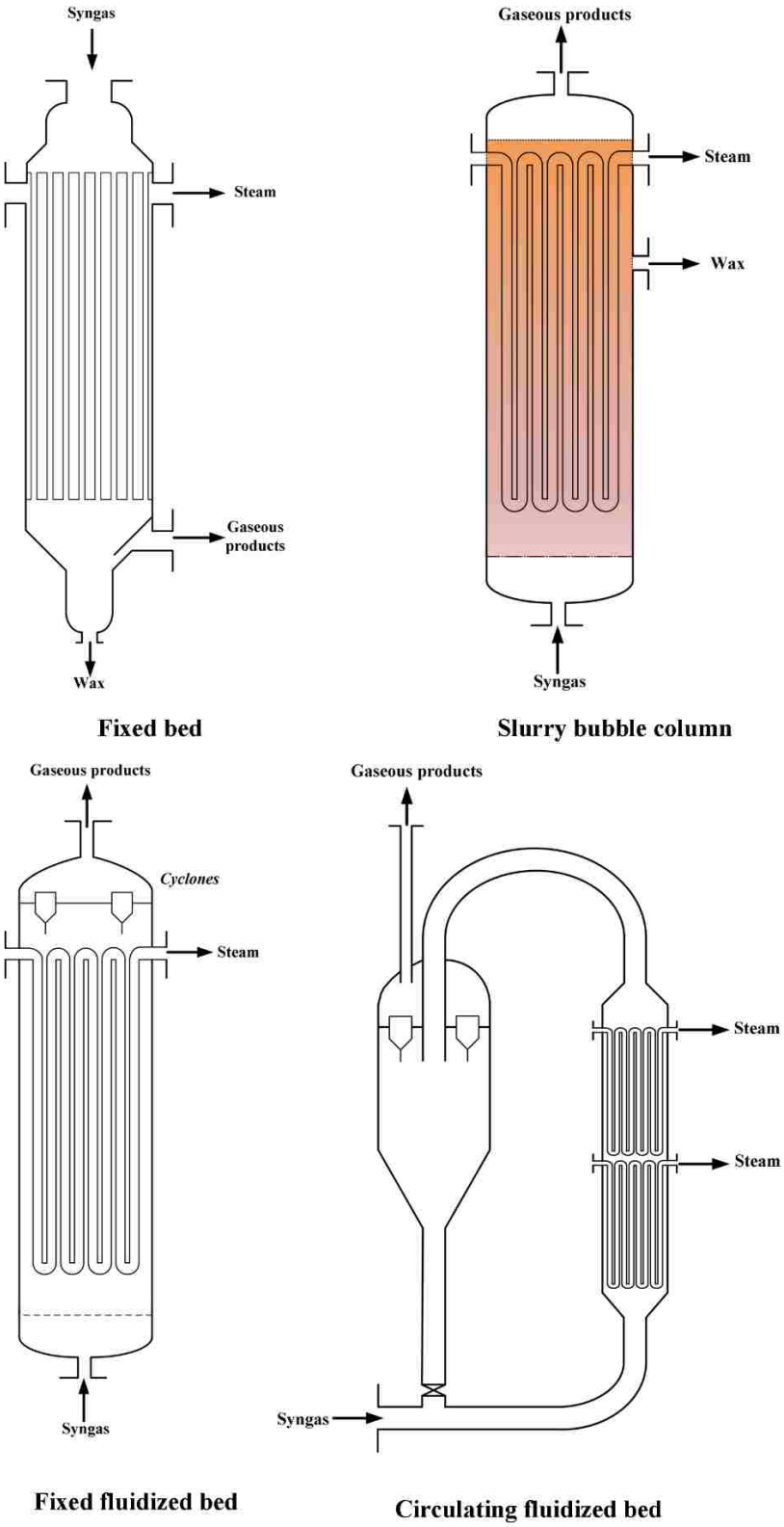

Figure 1.2. Commercial F-T reactors [6]

Nevertheless, slurry bubble column reactors have been selected for low-temperature (200-250 C^{o}) FT synthesis in recent years because they offer many advantages during operation and maintenance processes, particularly trickle bed reactors that have been also utilized for Fischer-Tropsch (F-T) synthesis in the form of shell and tubes configuration where the heat is removed by water passing through the shell [7,8].

Table 1.1. The structural features and operating temperature

Type of reactors	**Structural features**	**Operating temp (^{o}C)**
Old fixed bed (German)	Shell & double tube (concentric)	200-260
Improved fixed bed	Shell & tube	220-260
Multi-bed	Shell & tube and tray	220-260
Tubular-cum tray	Shell & tube and tray	200-260
Hot gas recycles	Single catalyst bed (cylindrical shell)	300-350
Oil recirculation	Single catalyst bed (cylindrical shell)	220-270
Fixed fluidized bed	Cylindrical shell Heat transfer through tube bundle in bed	300-330
Slurry bubble column	Cylindrical shell Heat transfer through tube bundle in bed	200-320

Bubble/Slurry bubble columns reactors as shown in Figure 1.3, in their simplest form, are cylindrical vessels in which gas is injected as bubbles from the bottom of column through a distributor (sparger), into a liquid (a two-phase column) or into a suspension of fine solids in a liquid (a three-phase column). The concentration of the solid phase in the slurry bubble column reactor, which represents the particles of the catalyst of particle diameter (5-150 μm), are varied 25-40% vol.[9]. The flow in a three-phase column is

sometimes approached as a pseudo two-phase flow: the fine solids follow the liquid phase, so a pseudo-homogeneous assumption can be made for the slurry (liquid-solid) phase [10]. In a continuous flow system, the gas may either flow with or counter to the liquid flow direction. In a semi-batch system, gas is sparged into a static liquid (slurry) medium. In either case, a high interfacial contacting area is provided between the liquid (or slurry) and gas phases.

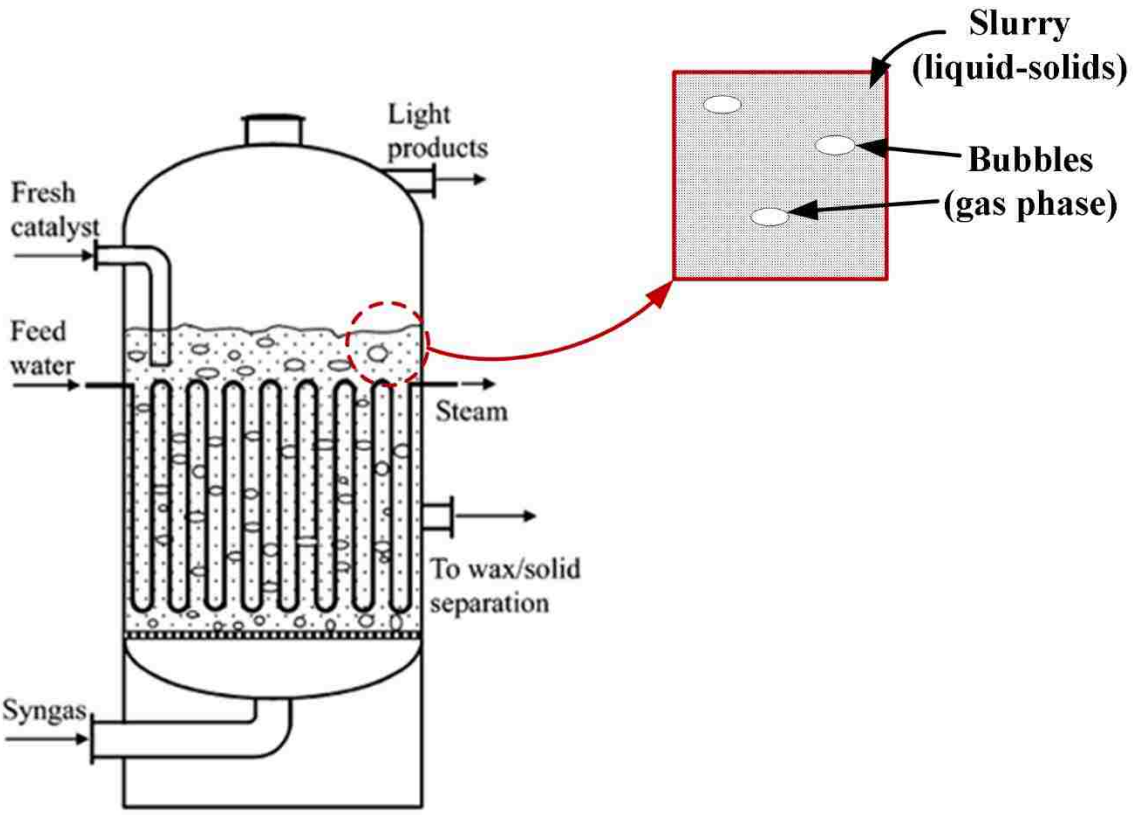

Figure 1.3. Slurry bubble column reactor with vertical heat exchanging internals

Bubble/Slurry bubble columns as multiphase reactors (or contactors) are favored for a wide range of applications in the chemical, biochemical, petrochemical, and metallurgical industries [11]. Chlorination, oxychlorination, carbonylation, and alkylation

are examples of two-phase bubble column applications. On the other hand, three-phase slurry bubble columns are used for hydrogenation, polymerization, coal liquefaction, and Fischer-Tropsch (F-T) synthesis among many other uses. Bubble/Slurry bubble columns reactors are preferred to different types of multiphase reactors in these applications for some reasons [12,13];

- Uniform reactor temperature and providing a high rate of heat transfer and mass transfer characteristics due to phase interaction and strong mixing.
- Excellent in temperature control (i.e., the operating under the designed temperature of reactions) and sufficient heat recovery due to equipping these reactors with a bundle of cooling tubes, therefore, there is no local overheating of the catalyst particle.
- The capability for online catalyst addition and withdrawal, therefore, handling of high catalyst loading is easy and catalyst regeneration is accomplished under favorable conditions.
- Simple to construct structures which do not involve mechanically moving parts, hence competitive investment, operating and maintenance costs.
- The capability to absorption and handling the troubles of operating.
- There are no catalyst attrition and erosion problems, and the reactor provides a high single pass conversion, a high yield, and high selectivity of product.

Accordingly, these features of the bubble/slurry bubble column reactors led to utilize these reactors in widespread applications comparing with the other multiphase reactors. However, most of the applications of these bubble/slurry bubble column reactors involve exothermic reactions such as Fischer-Tropsch synthesis and many others as

displayed in Table 1.2, therefore, removing the heat of reactions is a critical aspect in the design of the bubble/slurry bubble column reactors in order to ensure safe process operation and to maintain the operating of the reactor under the design temperature.

Table 1.2. Industrial two- and three-phase reactions carried out in bubble/slurry column reactors [14]

Product	**Heat of reaction (kJ/mol)**	**Pressure (bar)**	**Temperature (ºC)**
Fischer-Tropsch Synthesis	-210	30-40	250-290
Acetaldehyde	-243	3	120-130
Acetone	-255	10-14	110-120
Ethyl Benzene	-113	2-4	125-140
Benzoic Acid	-628	2-3	110-120
Cyclohexane	-214	50	200-225
Acetic Acid	-294	8-15	125-165
Vinyl Acetate	-176	30-40	110-130
Methanol synthesis	-91	50-100	220-270

Basically, there are five different methods have been used to maintain the operating of the reactor under the design temperature that so-called indirect methods: (a) external heat exchanger, (b) jacket heat exchanger, (c) coil, (d) heat exchanger horizontal internals tube, and (e) heat exchanger vertical internals tube as illustrated in Figure 1.4 (a, b, c, d, and e), respectively. Indirect heat transfer is very important for industrial practice since it can be applied in most cases [14]. The heat exchanger vertical internals tube preferred to utilized among these five types of heat exchangers, due to its capability to transfer high heat capacity which in turn generating the high-pressure steam (H.P steam), and

significantly control the liquid flow pattern (i.e., global liquid circulation, bubble dynamics, and back mixing) [15–17]. It is well known that the process of scale-up and design of these reactors in the absence of heat-exchanging tubes are still challenging engineering tasks due to the absence of phenomenological models which can describe the hydrodynamics of these reactors accurately.

Even though these features that render the bubble/slurry bubble columns as an attractive reactor choice, the disadvantages of these reactors lie in the difficulty in the scale-up and the design, the liquid circulation, and back-mixing due to the complexity in the interaction among the phases (gas-liquid-solid). Furthermore, numerous design and operating variables, physicochemical and thermodynamic properties of the fluids together affect the various hydrodynamic and transport parameters such as of heat and mass.

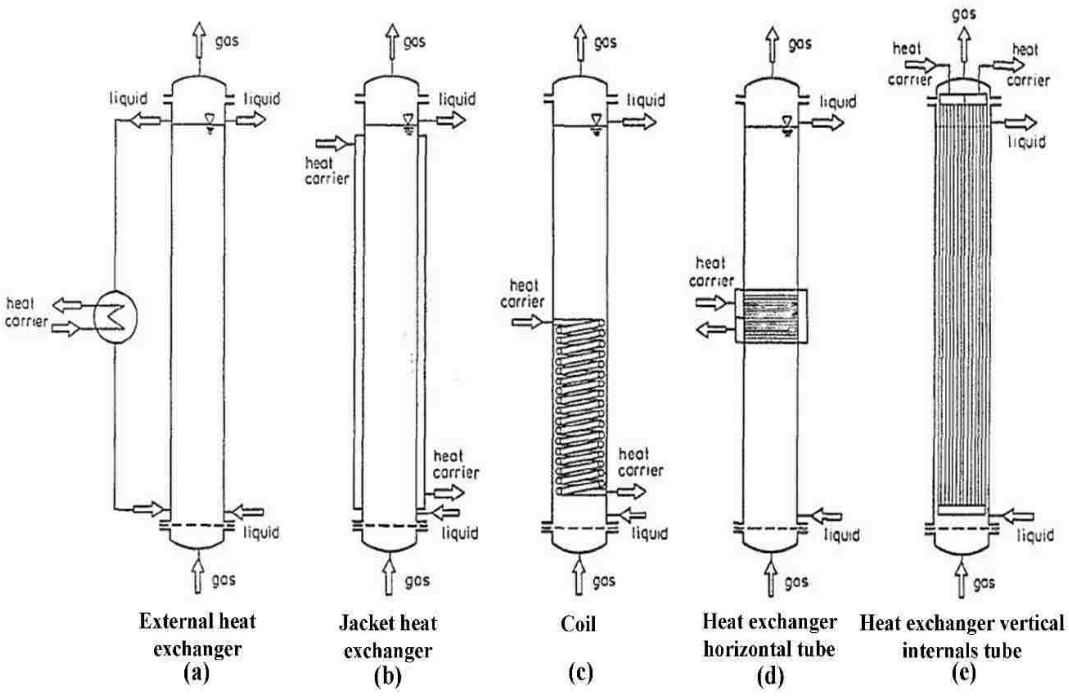

Figure 1.4. Types of the indirect heat exchanger in bubble/slurry column reactors [14]

1.1. RESEARCH MOTIVATION

In order to accomplish high-efficiency reaction systems that offer lower capital and operational costs for syngas conversion into high-value fuels and chemicals via Fischer-Tropsch processes, further investigations of the fluid dynamics and transport properties are needed. Furthermore, bubble dynamics, which including the local gas holdup, bubble rise velocity, bubble pass frequency, interfacial bubble area, and bubble chord length, administrate the hydrodynamics and the flow regime in the bubble/slurry bubble column reactors [18]. Hence, numerous studies have been conducted to investigate the effect of different design parameters on the hydrodynamics and the flow regime of the bubble/slurry bubble column reactor performance such as the physical properties of the fluid, the operating condition (pressure and temperature), the bubble column dimension (height H_s and diameter D_c), and the effect of the presence of internals. These studies have led to reduce the gap between the design and experimental results, enhance mass and heat transfer, and improve the scale-up tools.

Xue [19] executed the first comprehensive study in terms the effects of pressure, superficial gas velocity, and sparger design on the bubble properties, including the local gas hold-up, bubble frequency, bubble velocity, bubble chord length (which is characteristic of bubble sizes), and the specific interfacial area in bubble columns. The experiments were conducted by using 0.162 m diameter bubble column. While, the operating pressures is varied up to 1.0 MPa, and superficial gas velocity, up to 0.6 m/s. It was established that the radial profiles of the local gas holdup, specific interfacial area, mean bubble velocity, and bubble frequency profiles exhibit the same trends. The radial profiles evolve from flat at the low superficial gas velocity to highly parabolic at high

superficial gas velocity. Xue et al. [20], and Xue [19] showed that the effect of sparger diminishes at higher gas velocities in the fully developed flow region. Moreover, Xue [19] demonstrated that higher pressure tends to the evolution of smaller bubbles with low bubble velocity and enhanced frequency, hence higher residence time, consequently increasing both the overall and local gas holdup. Within the fully developed flow region at axial position $z/D \geq 2.0$, above the gas distributor, the bubble properties did not exhibit any significant change.

Wu et al. [21] studied the effect of the solids loading on the bubble dynamics, including the local gas holdup, bubble chord length, bubble velocity, bubble frequency, and specific interfacial area, using for the first time the four-point optical probe technique. The experiments were conducted using a Plexiglas column of 0.1 m inner diameter and 1.05 m high. F-T catalyst carrier with an average diameter of 75 μm was used as the solid phase, and the solids loadings in the experiments were used are 0.0, 9.1, and 25vol %. Results exhibit that with an increase in solids loading, the local gas holdup, specific interfacial area, and bubble frequency decreased, while the bubble velocity changed slightly. Bubble chord length increased noticeably, and the bubble chord length distribution spread more widely at high solids loading.

Youssef and Al-Dahhan [10,22,23] conducted the first systematic and comprehensive study of bubble properties in bubble columns equipped with mimicked dense heat-exchanging internals. The studies were conducted in two bubble columns of diameter 0.19 m and 0.44 m with superficial gas velocity varied between 0.03-0.45 m/s. The internals used were of different configurations with a cross-sectional area covering 5-25 % of the total CSA of the bubble columns. The details of internals bundle and

configurations used in the 0.44 m bubble column are shown in Figure 1.5. Their data obtained report that the overall gas holdup enhanced progressively with increased percentage coverage of column cross-sectional area by internals. Furthermore, the presence of dense internals that obstructed high fraction of the column promotes the local gas holdup radial profiles. Meanwhile, the presence of internals also led to increasing the bubble break-up rate-giving rise to smaller bubble chord lengths. Thus, increased specific interfacial area between the gas and liquid phases was higher for systems equipped with internals. No significant differences were noted on the bubble velocity probability distributions at the column's center between the case of no internals and that of 25 % CSA internals, particularly at high superficial gas velocity. However, at the 0.44 m diameter column's wall region, a higher probability of bubbles moving downward was obtained with nearly no bubbles moving upwards at the wall region.

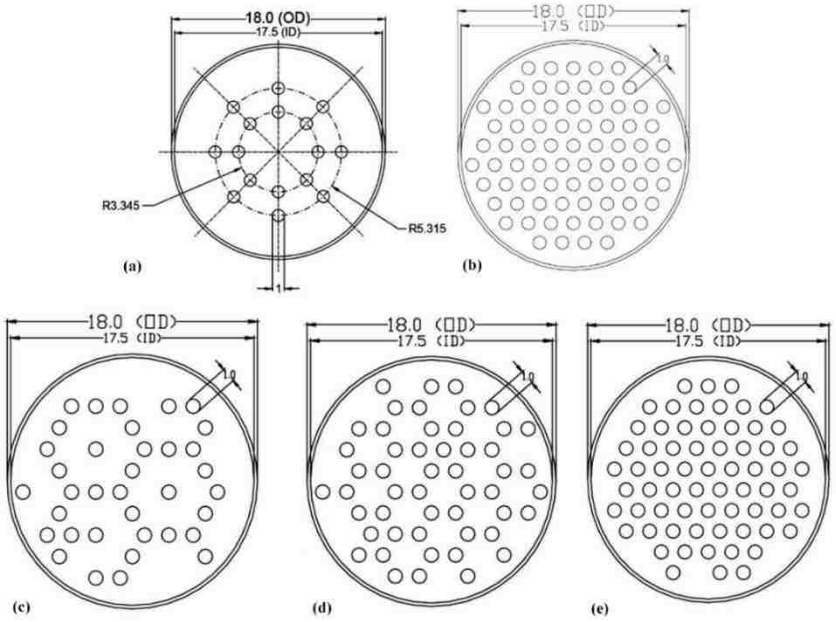

Figure 1.5. Different configurations of internals tubes covering (a) 5%, (b) 25%, (c) 10%, (d) 15%, (e) 20% of the total cross-section area of the bubble column

Moreover, Kagumba and Al-Dahhan [24] investigated the impacts of the presence of dense internals that encountered in Fischer-Tropsch (F-T) synthesis process on the bubble properties. An advanced four-point optical probe has been utilized to measure the bubble properties in a bubble column of 0.14 m diameter and 1.83 m height. The studied internals, as shown in Figure 1.6, with two configurations the hexagonal arrangement of 0.5-inch diameter tube and the circular arrangement of 1-inch diameter tube cover 25% of the CSA of the bubble column. Whereas, the superficial gas velocities applied based on both total cross-sectional area and free cross-sectional area available for the flow were in the range 0.03−0.45 m/s covering the bubbly flow regime through the churn turbulent flow regime. Their data revealed that the presence of internals exhibits insignificant effect at high gas velocity on both overall and local gas holdups, an enhancement of bubble passage frequency, increased interfacial area, and a decrease in bubble velocity and bubble chord length which was smaller with internals as result of enhancement in bubble breakup rate. Results of the effect of internals tube diameter show that the internals of 0.5-inch gave consistently overall and local gas holdup, specific interfacial area, and bubble passage frequency higher than the 1-inch.

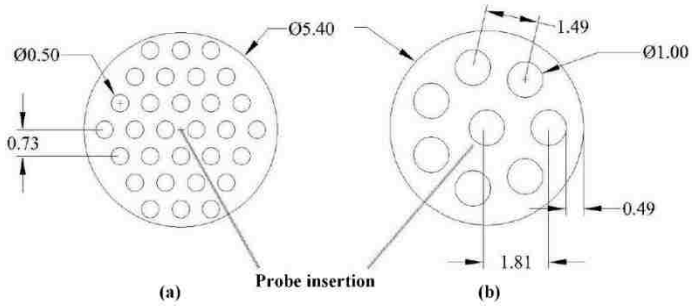

Figure 1.6. Internals configurations covering 25% CSA: (a) 0.5 in. diameter; (b) 1 in. diameter [24].

Shaikh and Al-Dahhan [25] studied the effect of the pressure on the local gas holdup and the flow regime transitions in a bubble column of 0.162 m diameter by using the Computed Tomography (CT) technique. Results reported that the increase in the pressure would increase the local gas holdup and delay the transition in the flow regime. However, although the bubble properties have not been examined, Shaikh and Al-Dahhan [25] attributed that to a decrease in the mean bubble chord length, which in turn, increases the interfacial area and decreases the bubble rise velocity. Meanwhile, the geometry of bubble columns, including diameter (D_C), height (static liquid level) (H_S), and sparger design has also been investigated by several researchers [18,26–32]. Their data obtained indicate that the effect of sparger design on the gas holdup and its profile is limited only to the region that is close to the sparger and to the bubbly (homogeneous) flow regime. Thus, the impact of the diameter (D_C) and the static liquid level (H_S) on the global gas holdup is ignored when scaling up from experiments to industrial systems, although a gas holdup tends to decrease with an increase in the reactor's diameter [30]. Meanwhile, Thorat and Joshi [33], and Besagni et al. [34] investigated the impact of the sparger design of different open area used coarse and fine hole diameter of the sparger. Their results exhibited that the increasing in the open area of the sparger would inhibit the gas holdup, and hence, the coarse sparger would produce a ''pseudo-homogeneous" flow regime, while, the fine sparger produces the mono-dispersed homogeneous flow regime, thus stabilizing the homogeneous flow regime

The impact of liquid viscosity on the gas holdup distribution using water and Drakeoil has been conducted by Chen et al. [35]. Their results revealed that the gas holdup was increased significantly with increase the superficial gas velocity, while a slight

increase was observed for the profile of gas holdup with increase the axial distance above the sparger, moreover increasing the viscosity of the liquid phase would inhibit the gas holdup, which was attributed to the formation of larger bubbles in viscous liquids.

Furthermore, Besagni et al. [36] investigated the dual effects of viscosity on the gas holdup, the flow regime transition, and the bubble distribution in a large-scale bubble column of inner diameter = 0.29 m and 5.2 m a height using water-monoethylene as a liquid phase with different concentrations. Their results reported that a larger number of small bubbles, which stabilizes the homogeneous flow regime, thus increasing the gas holdup, characterizes the low viscosity liquid phase. In contrast, moderate/high viscosity is characterized by larger bubbles, which destabilize the homogeneous flow regime and, thus, decrease the gas holdup.

The flow regime in the bubble/slurry bubble column reactor is related to the superficial gas velocity; therefore, As the superficial gas velocity increases, the transition flow regime is encountered where the flow pattern transits gradually from bubbly to the churn regime. Hence, the flow pattern was investigated extensively by utilizing different techniques such as gamma-ray computed tomography (CT)[25,37], pressure transducer [38–44], four-point optical probe [45], conductivity probe [46,47], and liquid extension (overall gas holdup) [45,48–51]. Their experiments result illustrated that the flow regime is sensitive toward the bubble column dimension, the gas-liquid properties, and the solid loading and particle size, that in turn reflects on the hydrodynamic properties of bubble column will change as well.

The impact of operating pressure on the flow regime transition has been studied by Shaikh and Al-Dahhan [25] using the radial profile of gas holdup, which was measured by

gamma-ray computed tomography (CT) technique. The results reported that the increase in pressure leads to a delay in the transition velocity. Furthermore, the transition in flow regime was demarcated clearly under ambient pressure, in contrast to high pressure where the transition occurs gradually. Nedeltchev et al. [52] identified the flow regime transition by utilizing the pressure transducer technique and used two types of organic liquids, 1-Butanol and gasoline, at different pressures. The study revealed that the pressure influence on flow regime transition varied according to the liquid properties. Moreover, the second and fourth transition velocities under ambient pressure occur earlier in 1-butanol than in gasoline.

Zhang et al. [46] studied and demarcated the flow regime in a bubble column using a local measurement technique. Zhang et al. [46] used the bubble properties as a criterion to identify the flow regime transition and developed an empirical correlation to predict the flow regime boundaries. The bubble properties were measured using a two-element conductivity probe that placed at the center of a bubble column at the height of $H/D = 7.87$ above the distributor. The regimes have been identified locally by bubble properties since each regime has an individual dynamic. According to the data obtained, reported the capability of the bubble properties to demarcate the flow regime transition, whereas, the experimental results exhibit alignment with the prediction results.

Chen et al. [53] using gamma-ray computed tomography (CT) and computer automated radioactive particle tracking (CARPT) techniques, investigated the effect of the internals on gas holdup, liquid velocity, turbulent stresses, and eddy diffusivities both radial and axial in a 0.44 m diameter column. The column was equipped with internals similar to those used in industrial scale units covering 5 % of the total CSA of the bubble column to

mimic liquid phase methanol (LPMeOH) synthesis using both air-water and air-drakeoil 10 and superficial gas velocities from 0.02-0.1 m/s. The configuration of the studied internals is illustrated in Figure 1.7. They reported that internals covering 5 % of the total CSA have insignificant effect on liquid recirculation velocity, while gas holdup increases slightly. The turbulent stresses and eddy diffusivities were lower in the presence of internals. In this work, the range of superficial gas velocity covered was low. Thus, it is not possible to evaluate with confidence the effect of internals at a high superficial gas velocity that would guarantee high volumetric productivity as desired especially in the Fischer-Tropsch (F-T) synthesis process.

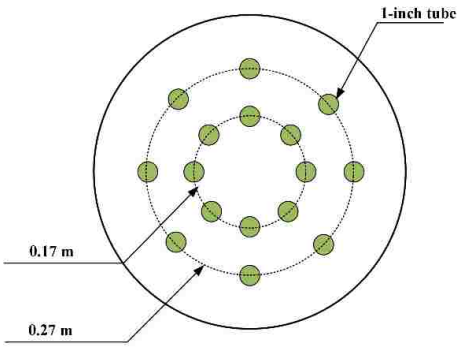

Figure 1.7. The configuration of internals covering 5% of the column's cross-section area [35]

Al Mesfer et al. [16] investigated the effect of heat exchanging internals, which is similar to those used in Fischer–Tropsch (F-T) synthesis process, time-averaged gas holdup distributions in a bubble column using gamma-ray Computed Tomography (CT) in a 0.14 m inner diameter Plexiglas bubble column operated at atmospheric condition with air-water system. Thirty vertical Plexiglas rods of 0.5-inch outer diameter were used which covered

~25% of the total CSA and were arranged in a triangular pitch of 2.14 cm as illustrated in Figure 1.8. The superficial gas velocities that calculated based on both total CSA and free CSA for the flow column, varied from 0.05 to 0.45 m/s to cover the bubbly and churn-turbulent flow regimes. They reported that in churn turbulent flow regime, the overall gas holdup and the profiles of gas holdup obtained in bubble columns without internals can be extrapolated to those with internals in the central region of the column if the superficial gas velocity is based on the CSA available for the flow of the phases provide that symmetric time-averaged cross-sectional gas holdup distributions are achieved. Further, the presence of internals significantly increases the overall and the local gas holdup when the velocity calculated based on the total CSA of the column as shown in Figure 1.9. At a high superficial gas velocity that is based on free CSA for the flow, the influence of dense internal becomes insignificant at the central region of the column. However, the profiles of the gas holdup in the column with internals become less steeper compared to those that are like parabolic shape at high gas velocity in the column without internals due to higher gas holdup was obtained in the region near the wall with internals.

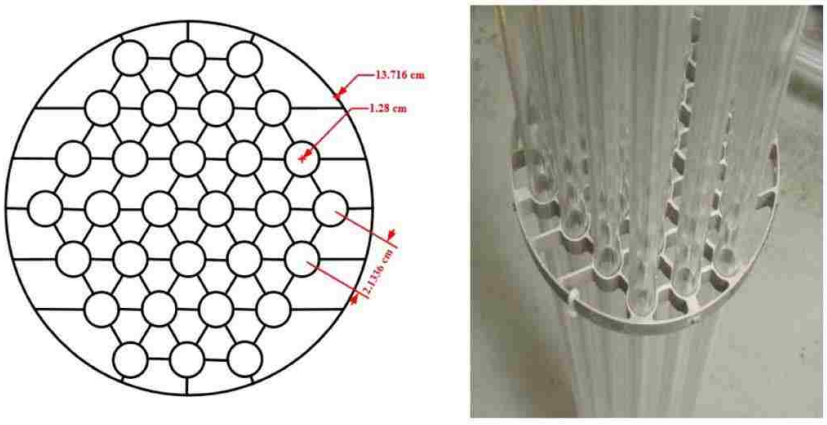

Figure 1.8. Schematic diagram and photo of Honeycomb with 0.5-in. internals [16].

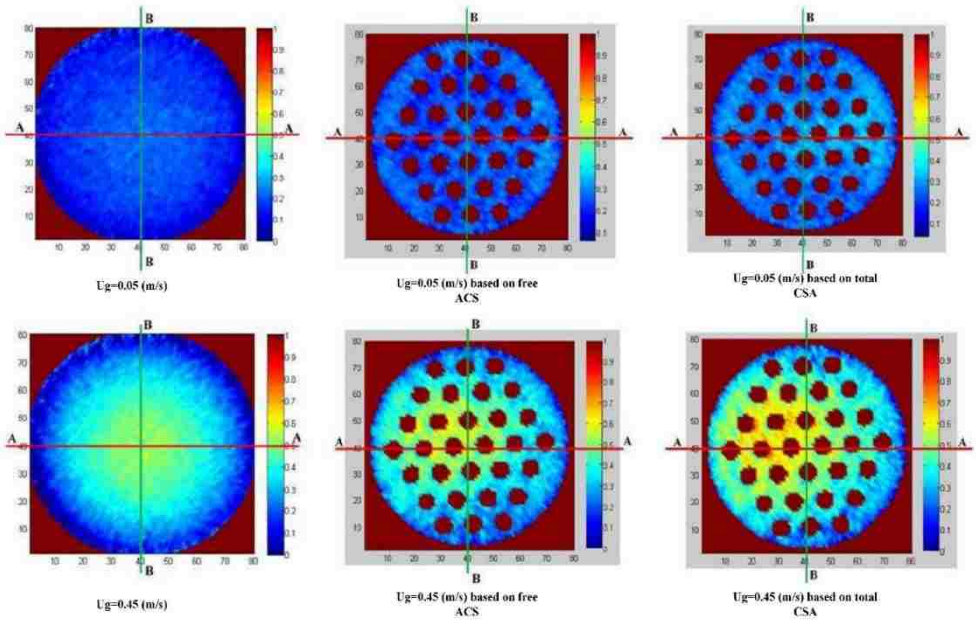

Figure 1.9. The effect of internals on the time-averaged cross-sectional gas holdup distributions at various superficial gas velocities based on total and free CSA [16].

Later, Al Mesfer et al. [15] studied the effects of the presence of internals on the liquid velocity field and turbulence parameters, including Reynolds stresses, turbulent kinetic energy, and turbulent eddy diffusivities, using an advanced radioactive particle tracking (RPT) technique in the same setup that used in Al Mesfer et al. [16]. The superficial gas velocities based on both total cross-sectional area and free cross-sectional area available for the flow were utilized (0.08, 0.2, and 0.45 m/s), which covered the transition and churn-turbulent flow regime to meet the industrial applications of Fischer-Tropsch (F-T) synthesis process. Data obtained show that the presence of the internals at a given superficial gas velocity causes an increase in the axial centerline liquid velocity, as shown in Figure 1.10, and a sharp decrease in turbulence parameters while the increase in superficial gas velocity in the presence of internals causes an increase in axial centerline liquid velocity and turbulent parameters.

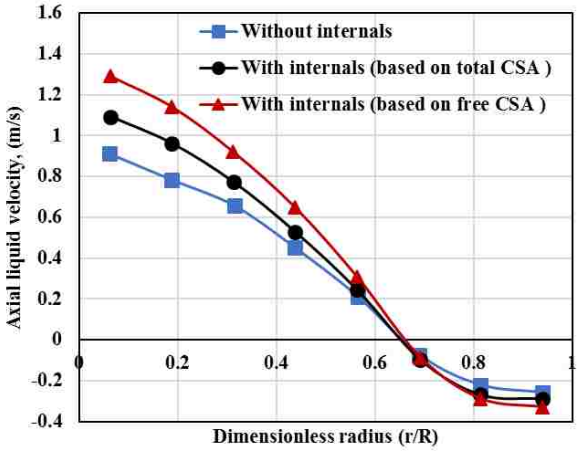

Figure 1.10. The effect of the presence of internals on the liquid axial velocity at superficial gas velocities based on the total and free CSA in the gas-liquid system [15].

Sultan et al. [17,54,55] introduced comprehensive investigations in terms of the effects of the presence of internals, the configuration of internals (hexagonal, circular, and circular with central tube), the diameter of internals tubes (0.5-inch and 1-inch), and the diameter of the bubble column (0.15m and 0.4 m) on the time-averaged cross-sectional gas holdup using an advanced gamma-ray computed tomography (CT) technique and all the used internals cover 25% of the CSA of bubble column. Data obtained revealed, that all the studied superficial gas velocities resulted in symmetrical gas holdup distributions over the CSA of the bubble columns without vertical internals; however, the columns equipped densely with vertical internals did not have symmetrical gas holdup distributions as shown in Figure 1.11. The presence of an extra central tube in the circular configuration played a key role in the gas-liquid distribution over the CSA of the bubble column. The hexagonal configuration (in both bubble columns 0.14 m and 0.4 m) had the advantage of providing the best spread of the gas phase over the entire CSA of the column. Furthermore, as shown

in Figure 1.12 the bubble column equipped with 1-inch vertical internals exhibited more uniform gas holdup distribution than the column with 0.5-in. Internals. Also, the visualization of the gas-liquid distributions for bubble columns with and without internals reveal that the well-known phenomenon of the core-annular liquid circulation pattern that observed in the bubble column without internals still exists in bubble column packed densely with vertical internals.

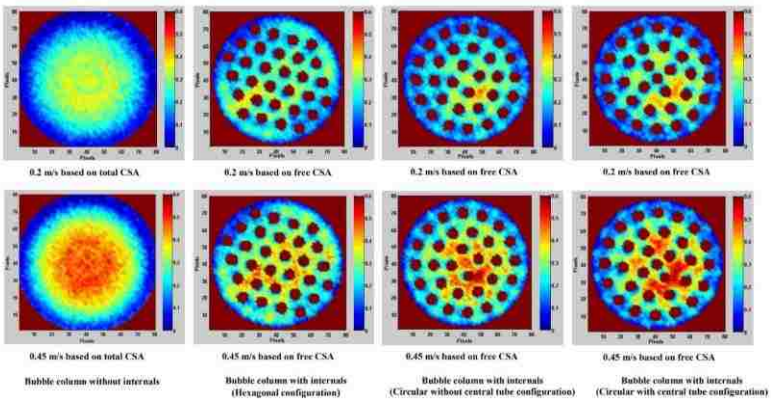

Figure 1.11. The effect of the vertical internal tubes configuration and superficial gas velocity on the time-averaged cross-sectional gas holdup distributions [54].

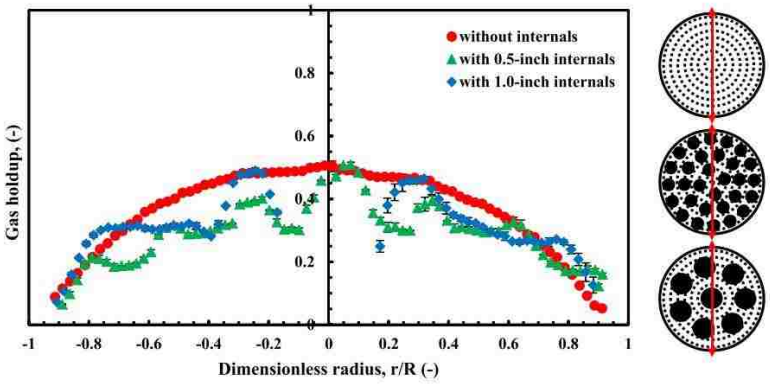

Figure 1.12. The effect of the presence of internals and internals tube diameters on the azimuthally averaged gas holdup profiles, U_g= 0.45 m/s based on the free CSA [55].

The recent development in the numerical solution approaches that followed by huge increases in the capability of the computer let to providing the opportunity to simulate the flow dynamics in the bubble column and addressing the influences of the studied-parameters such as, superficial gas velocity, sparger design, and the presence of internals. Nowadays computational fluid dynamics (CFD) provides the state-of-the-art capabilities of simulating the hydrodynamics in bubble column reactors.

Larachi et al. [56] investigated, for the first time, the effect of internals and their configuration on the hydrodynamics of the bubble column using computational fluid dynamics (CFD). They used vertical heat-exchange tubes with occluded cross-sectional area ranging between 2 to 16.2 %, and tubes of 1-inch diameter arranged in a triangular pitch configuration as shown in Figure 1.13. Transient 3-D computational fluid dynamic simulations were carried out for five bubble column internals geometries. The simulation results revealed that the liquid circulation and the mixing patterns in bubble columns with internals were significantly affected by the inserted tubes, as illustrated in Figure 1.14. They concluded that in the presence of internals, the large-scale and coherent meandering gas winding around, as observed in hollow bubble columns, could not be sustained and were replaced by smaller pockets whose size was dictated by the inter-tube gaps. They also reported that the gap scale was important in the longitudinal funneling of liquid flow. A sharp decrease of the liquid kinetic turbulent energy upon insertion of the heat-exchange tubes in the bubble column was also observed. They assumed a constant bubble size (neglecting coalescence/dispersion effects) and a steady drag force as the sole interfacial force (neglecting all other forces such as lift, wall, and turbulent diffusion). Whereas the occluded column cross-sectional area was reasonably high, these CFD results were not

evaluated and validated against any benchmark experimental data due to the lack of such data. Further work which utilizes solids is still required.

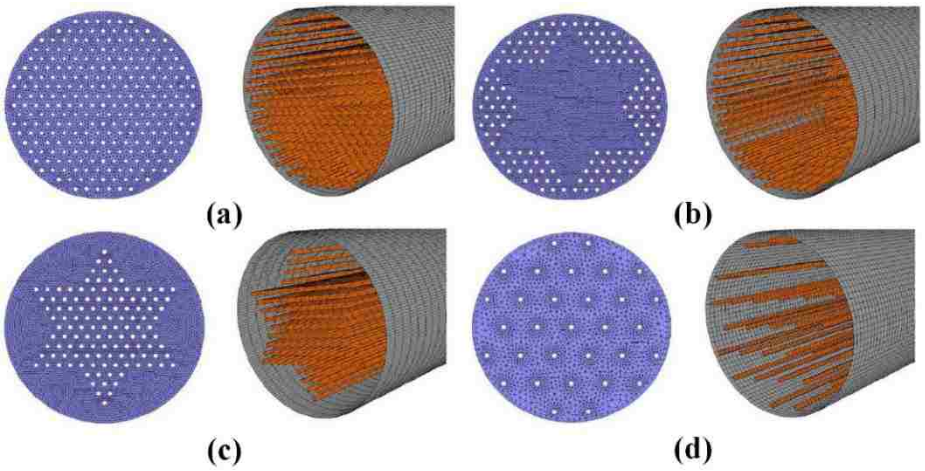

Figure 1.13. Numerical mesh used: (a) dense arrangement of internals, (b) star arrangement: core clearance: (c) star arrangement: wall clearance: (d) sparse arrangement of internals.

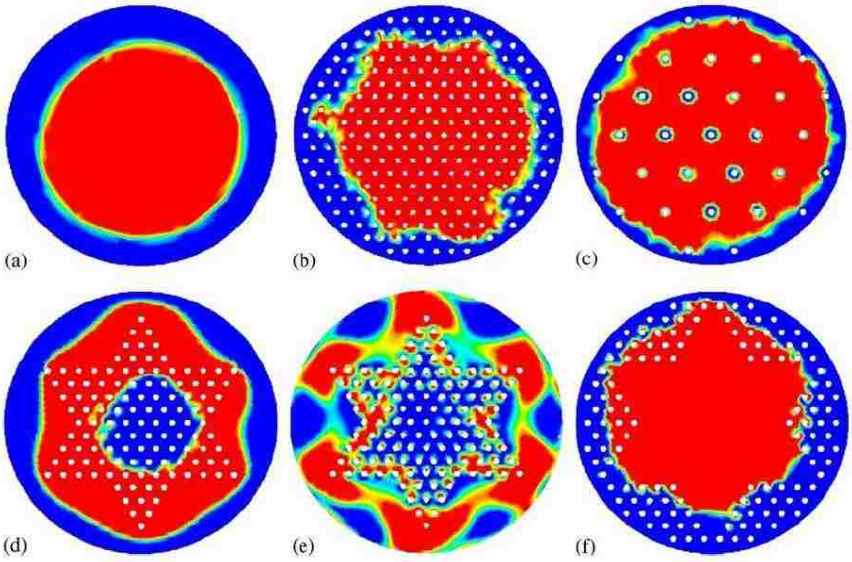

Figure 1.14. The effect of the presence of internals on the time-averaged axial liquid velocity at *Z/D*= 5. Color scale was voluntarily exaggerated to distinguish up-flowing (red) and down-flowing (blue) regions

Guang et al. [57] simulated the effect of the configuration of gas distributors on hydrodynamic behavior, gas hold-up and mixing characteristics in the bubble column reactor utilizing the CFD. Numerical simulations of gas-liquid flow were conducted in a cylindrical bubble column of 0.4 m in diameter at the superficial gas velocity Ug = 0.1 m/s using eight different gas distributors were adopted in the simulation as illustrated Figure 1.15. The simulation results show that the configuration of the gas distributor has an important impact on liquid velocity and local gas hold-up in the vicinity of the gas distributor. Further, the CFD modeling results reveal that an increase in the number of gas sparging pipes used in gas distributors is beneficial in improving the gas hold-up, illustrated in Figure 1.16, but is disadvantageous in reducing bubble size due to a decrease in turbulent kinetic dissipation. It has been demonstrated from the simulations that the appearance of asymmetrical flow patterns in the bubble column and the adoption of smaller gas sparging pipes for gas distributors are effective in improving the mixing characteristics.

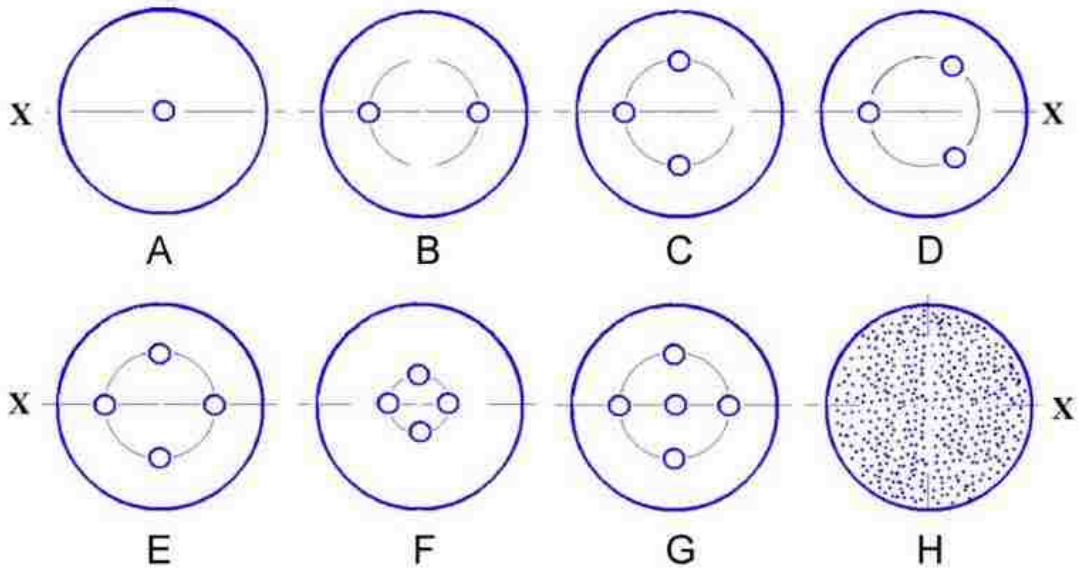

Figure 1.15. Configurations of gas distributors used in the bubble column [57].

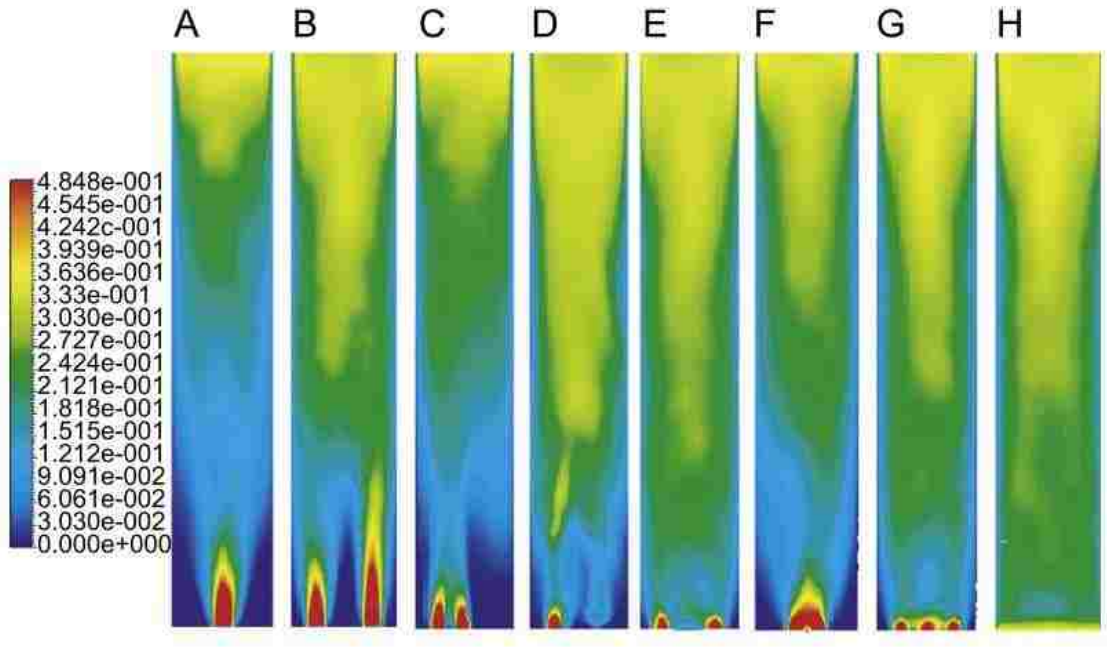

Figure 1.16. Predicted contours of time-averaged gas hold-up inside the bubble column for different configurations of gas distributors [57].

Guo and Chen [58] used Eulerian two-fluid model coupled with a population balance method (TFM-PBM) to simulate the effects of vertical internals on hydrodynamic of bubble columns. The interfacial drag force, the shear-induced lift force, and the radial wall lubrication force exerted on bubbles were included in the model. The numerical results showed the radial wall lubrication force greatly influences the radial distribution of time-averaged gas holdup. When the internals was present, the turbulent dissipation rates increased significantly in the gaps between the internal walls, and more bubbles with smaller bubble size were predicted in the bubble column. Meanwhile, the gas holdup increased with dense internals insertion, especially in r/R equal to 0.6–0.9 region. The internals and the configurations influence the overall liquid circulation. When 31 thin internals is inserted in the column at a low superficial gas velocity, large-scale liquid

circulations are replaced by small local vortex. However, the variations of liquid circulations are different at a high superficial gas velocity, when the large-scale liquid circulations are always present in the column regardless of inserting 31 thin internals or 8 thick internals.

The lack of open literature on the design aspects of large-scale reactors burdens researchers of bubble/slurry column scale-up and renders the process even harder to achieve. One of the most reason that can explain this issue is that the most studies were conducted in a bubble column of lab-scale and the operating dynamic liquid level is greater than nine, although, the used size in the practical field is H/D = 3-5. Therefore, none the aforementioned studies has accounted for the effect of the presence of internals and the solids loading on the bubble properties and the flow regime transition in low aspect ratio (i.e., low dynamic liquid level $H/D \leq 3$, 4, and 5) that used in Fischer-Tropsch (F-T) synthesis process.

1.2. RESEARCH OBJECTIVES

Accordingly, the purposes of this study experimentally are to improve and advance the fundamental understanding and knowledge of the effects of heat exchanging internal, the variation in the aspect ratio (H/D = 3, 4, and 5), and the solids loading on the bubble properties and the flow regime transition in bubble/slurry bubble column. While the CFD simulation for the bubble column has been addressed to validate the interfacial forces azimuthally and demarcate the capability of validated CFD codes to simulate the flow dynamics in a bubble column with different designed internals. To accomplish these goals, the bubble properties and the flow regime will be examined in industrial size pilot-plant

scale bubble/slurry bubble column occupied by heat exchanging internals covers 24% of the CSA of the column using an advanced four-point optical probe and pressure transducer. Therefore, the following objectives are set for this study:

1. Investigate the effect of the presence of heat exchanging internals and low aspect ratios on the bubble properties and the fully developed flow region.
2. Investigate the effect of solids loading and low aspect ratios on the bubble properties and fully developed flow region in the bubble column with internals.
3. Demarcate the effect of the variation in the low aspect ratio on the flow regime transition and exam the bubble properties.
4. Demarcate the effect of the presence of heat exchanging internals and the variation in the low aspect ratio on the flow regime transition and exam the bubble properties.
5. Validate the interfacial forces azimuthally with the experimental results and investigate the effect of the presence of internals, internals configuration, and internals tube diameters on the time-averaged gas holdup distributions.

PAPER

I. THE EFFECTS OF INTERNALS AND LOW ASPECT RATIO ON THE FULLY DEVELOPED FLOW REGION AND BUBBLE PROPERTIES IN A PILOT-PLANT BUBBLE COLUMN

ABSTRACT

This work investigates, for the first time, the effects of the presence of internals and low dynamic liquid levels on the bubble dynamics in industrial-size pilot plant bubble columns. Experimental work that conducted in a bubble column of 0.6 m inner diameter and 3.9 m height with an air-water system was utilizing our advanced four-point fiber optical probe technique to measure the radial profiles of the bubble properties. The superficial gas velocity varied from 0.2-0.45 m/s to cover the churn turbulent flow regime. PVC pipe of 0.06 m diameter used to represent the heat exchanging internals, occupying 24% of the column cross-section area, and three different aspect ratios (H/D = 3, 4, and 5) were used. Data obtained show that the presence of internals slightly increases the overall gas holdup and significantly affects the radial profiles and distribution of the bubble properties, particularly in the fully developed flow region. However, the presence of internals increases the local gas holdup, the bubble pass frequency, and the interfacial bubble area, especially in the wall region, while decreases the bubble chord length and the bubble rise velocity. The variation in the aspect ratio (H/D) and the presence of internals exhibited a slight impact on the bubble dynamics in the sparger region, whereas the effect of internal on the local gas holdup was concentrated in the wall region. Meanwhile, the axial location (Z), where the fully developed flow region occurs, appears a high sensitivity

toward the internals existence and the variations in the aspect ratio and the superficial gas velocity. However, the presence of internals and the increase in aspect ratio both show that the fully developed flow region begins at lower axial locations, while an increase of the superficial gas velocity delays the transition to fully developed flow to a higher axial location.

1. INTRODUCTION

Bubble/slurry bubble column multiphase reactors are widely used in various fields of chemical and biochemical, petrochemical, and wastewater treatment processes [1–3]. Bubble/slurry bubble column reactors are characterized by high heat and mass transfer coefficients, excellent thermal control, few movable parts that contribute to a low cost, and high selectivity and conversion [4–8]. The disadvantages are the global liquid circulation and back mixing, which increase the prevalence of undesirable products and difficulty in the design due to the interaction among the phases [9]. Such reactors are used for processes such as Fischer-Tropsch synthesis (F-T), hydrogenation, oxidation, fermentation, coal liquefaction, liquid phase methanol synthesis, and many others. The bubble/slurry bubble column carries out exothermal reactions, and hence, using the heat exchanging internals is critical to maintain the reactions at desired temperature. Therefore, internals have been utilized with different coverage area of the cross-section area CSA of the bubble column. The exothermic process requires the removal of heat from the reactor; therefore heat exchanging tubes, which occupy about 5−25% of the column's cross-sectional area CSA depending on the type of process that used [5], [10]–[13], are an essential part of the reactor

design. However, in this study heat exchanging internals, which covers 24% of CSA of column, has been used, the same that used in the Fischer-Tropsch synthesis (F-T).

Significant effort has gone into addressing the shortcomings in understanding the interaction between the gas and liquid phases that complicate bubble/slurry bubble column reactors' design. This is because the bubble/slurry bubble columns are characterized with multi-scale phenomena that make the interaction among the phase complex. Therefore, multi-scale approach is needed in understanding such multi-scale phenomena, which is the case for all multiphase flows. The mixing intensity and gas-liquid interfacial area, which affect the transport coefficients embedded in gas-liquid mass transfer models, are affected by the hydrodynamics of the reactor. This, in turn, affects the conversion and selectivity of the reactors [5]. Because of these complex interactions, the flow field in a bubble column is very complex. Bubble properties, which are characterized by the local gas holdup, bubble rise velocity, bubble frequency, interfacial area, and bubble diameter, are necessary to understand the hydrodynamics and interphase transfer in a bubble/slurry bubble column [14]. Therefore, numerous researchers have investigated bubble dynamics to optimize the performance of bubble column reactors. These have led to reduce the gap between the design and experimental results, enhance mass and heat transfer, and improve the assessment of the scale-up methods [15], [16]. The effect of pressure has been studied by numerous researchers [10–15]. Shaikh and Al-Dahhan [20] studied the effect of the pressure on the local gas holdup and the flow regime transitions in a bubble column of 0.162 m diameter by using the Computed Tomography (CT) technique. Results reported that the increase in the pressure would increase the local gas holdup and delay the transition in the flow regime. Although the bubble properties have not been examined, they attribute

that to a decrease in the mean bubble chord length, which in turn, increases the interfacial area and decreases the bubble rise velocity. The geometry of bubble columns, including diameter (D_C), height of static liquid level (H_S), and sparger design has also been investigated by several researchers [4], [10], [16–22]. The Data obtained indicate that the effect of sparger design on the gas holdup and its profile is significant, particularly, in the region that is close to the sparger and in the bubbly (homogeneous) flow regime. Whereas, Besagni et al. [28] reported that the effect of the column dimensions and sparger design on the gas holdup is insignificant as long as three criteria are satisfied: the diameter of the bubble column is larger than 0.15 m, hole dimeter of sparger is larger than 1–2 mm and the aspect ratio is larger than 5. The effect of the height of static liquid level (H_S)on the gas holdup has been investigated extensively by S. Sasaki et al. [25], [29], and G. Besagni et al. [22]. Accourding to S. Sasaki et al. [25],[29] revealed that the efect of initial liquid level H_S, and the column diameter D_C on the overall gas holdup are insignificant when the scaling up from small to large bubble columns, while, for $H_S \leq 2.2\ m$ and $D_C \leq 0.2\ m$, the overall gas holdup decreases with increasing initial liquid level. Furthermore, Haque et al. [26] confirmed during investigating the effect of nine different spargers on the time mixing and the gas holdup that when the aspect ratio is relatively low (less than 2-5 depending upon the column diameter, sparger design and the physical properties) the liquid phase flow pattern is not completely devloped. The bubble behaviour and the flow pattern strongly depend on the sparger design. Thus, the impact of D_C and H_S on the global gas holdup is ignored when scaling up from experiments to industrial systems, although a gas holdup tends to decrease with an increase in the reactor's diameter [25]. The impact of liquid viscosity on the gas holdup distribution using water and Drakeoil has been conducted by

Chen et al. [30]. Their results revealed that the gas holdup was increased significantly with increase the superficial gas velocity, while a slight increase was observed for the profile of gas holdup with increase the axial distance above the sparger, moreover increasing the viscosity of the liquid phase would inhibit the gas holdup, which was attributed to the formation of larger bubbles in viscous liquids. Furthermore, Besagni et al. [31] investigated the dual effects of viscosity on the gas holdup, the flow regime transition, and the bubble distribution in a large-scale bubble column of inner diameter = 0.29 m and 5.2 m a height using water-monoethylene as liquid phase with different concentrations. Their results reported that a larger number of small bubbles, which stabilizes the homogeneous flow regime, thus increasing the gas holdup, characterizes the low viscosity liquid phase. In contrast, moderate/high viscosity is characterized by larger bubbles, which destabilize the homogeneous flow regime and, thus, decrease the gas holdup. Meanwhile, Thorat and Joshi [32], and Besagni et al. [33] studied the effect of the sparger design in terms the open area using coarse and fine hole diameter of the sparger. Their results indicate that the gas holdup was increased with a decrease in the open area of the sparger, and hence, the coarse sparger would produce a ‘‘pseudo-homogeneous” flow regime, while, the fine sparger produces the mono-dispersed homogeneous flow regime, thus stabilizing the homogeneous flow regime

In addition to using the internal heat exchanger to maintained the reaction at desired temperature, it provides better control to the back mixing and flow pattern as well. Therefore, having heat-exchanging tubes inside the bubble/slurry bubble columns add challenges related to the lack of understanding of these effects on the multi-scale phenomena and interactions among phases encountered in these reactions. Furthermore,

the presence of internals complicates the experimental investigations and the implementation of the techniques whether they are invasive techniques such as optical fiber probes, heat transfer probes or non-invasive techniques as it complicates as well the data processing such as gamma ray computed tomography, electrical tomography etc., and prevent the use of light-based techniques. According to Chen [10], Youssef and Al-Dahhan [14], Forret et al. [34], Jhawar and Prakash [35], and Al Mesfer [7], the internals impacts the hydrodynamics of the bubble column; nevertheless, this impact has not been fully quantified very well. Table lists experimental studies on the effects of vertical internal tubes and the column dimensions on the hydrodynamics of the bubble column. Chen et al. [10] carried out experiments using air-water and air-Drakeoil 10 and utilizing Gamma-ray Computed Tomography (CT) technique and Radioactive Particle Tracking (RPT) technique to measure the gas holdup, the time-averaged axial liquid velocity, and the turbulence parameters (included normal stress, shear stress, and eddy diffusivity). This study reported that the internals, which is covering about 5% of the total cross-section of the bubble column, slightly increase the gas holdup and have some effect on the flow pattern and turbulence parameters in the column. Larachi et al. [36] presented a computational study for the influence of internals in five different configurations on the hydrodynamics in a pilot-scale bubble column by using transient 3D computational fluid dynamic simulation. This work revealed that liquid structure, which consists of circulation and mixing patterns, is impacted by the presence of internals. Moreover, this study remarked that internals significantly decreases the liquid kinetic energy and break down the large-scale and coherent meandering gas twirls to small pockets whose size depends on the inter-tube gap, with the turbulent eddies behaving similarly. Subsequently, Youssef and

Al-Dahhan [6] investigated the impact of vertical internals which covering 5% and 22% of the total cross-section of the bubble column. This mimics those typical for liquid-phase methanol synthesis and the Fischer-Tropsch process. The results of this work indicated that the impact of the vertical internals depends significantly on the coverage area (i.e., the tube pitch). With 22% coverage by internals, the overall gas holdup, local gas holdup, and interfacial area increased, while the bubble chord length and bubble rise velocity decreased. Little change was measured in the case of internals covering 5% of the cross-section area. Investigation of the bubbles' downward velocity has indicated that less small-scale recirculation exists with densely packed internals as compared to an empty column. Recently, Kagumba and Al-Dahhan [5] investigated the influence of different sizes and configurations of the dense internals on the bubble dynamics. Data obtained indicate that internals with tubes of 0.5-inch diameter increases the overall and local gas holdup, bubble frequency, and interfacial area, in particular in the center region, more than other cases (such as a bubble column without internals and a bubble column with internals with tubes of 1-inch diameter). A lower bubble rise velocity, and a smaller chord length have also been measured with the internals of 0.5 in diameter. Guo and Chen [37] simulated the effect of vertical internals with a circular configuration on the hydrodynamic properties of a bubble column using a Eulerian two-fluid model with a population balance model (TFM-PBM) and interfacial forces, including the drag force, lift force, and wall lubrication force. Simulations were performed under two superficial gas velocities to cover the pseudo-homogeneous flow regime [38] and heterogeneous flow regime [39]. Guan and Yang [40] studied the influence of internals, which covers 5% of the cross-section area of the bubble column with hexagonal configuration on the hydrodynamics of pilot-scale bubble columns.

The CFD results revealed the insignificant effect for the internals on the gas holdup and the presence of internals gives rise to an enhancement of large-scale liquid circulation due to the remarkable decrease of turbulent viscosity. The presence of internals increased the turbulent dissipation rates significantly in the gaps between the internal walls while decreasing the mean bubble chord length in the bubble column. Thereby, the gas holdup increased with the dense internal structures. Internals and their configurations influence the overall liquid circulation at a low superficial gas velocity, where the liquid circulation by small, local vortices was eliminated. At a high superficial gas velocity, the impact of turbulence induced by the bubble coalescence and the bubble breakup overwhelms the effect of internals. Unfortunately, most of these investigations have been conducted in lab-scale facilities of bubble column with a diameter ($D < 0.44$ m) were operated either without the presence of internals [25], [31-32] or at a high dynamic liquid level with aspect ratio $H/D \geq 9$ [22], [30], [41].

Based on the studies mentioned, the internals has a significant impact on the hydrodynamic and transport properties in bubble column reactors. Typical applications for bubble/slurry bubble column reactors have a low dynamic liquid level with aspect ratio $H/D \leq 5$ for cost and thermohydraulic reasons [41]. The relative shortage in the data regarding the effect of internals and scale-up at low dynamic liquid levels interferes with the design and scale-up of bubble/slurry bubble column reactors. Therefore, this study aims to investigate the effect of industrial heat exchanger internals structure on the bubble dynamics at three different low aspect ratios (H/D = 3, 4, and 5) using an industrial-size pilot plant bubble column of D = 0.6 m, equipped with a heat exchanger of internals structure of hexagonal configuration and consisting of 12 dual pipes of 0.06 m diameter,

covering 24% of CSA of the bubble column. The most of the previous studies were conducted using water and air as liquid phase and gas phase, respectively, at ambient temperature and pressure. therefore, this work has been accomplished in the same conditions to have a good base for comparison between the data obtained in this work and the results of these previous studies. The Data obtained will be useful to assess the numerical simulations in terms of using the population balance model (PBM), particularly the simulation at high superficial gas velocity by utilizing the bubble chord length distribution, and validate the simulation result with the experiment results.

2. EXPERIMENTAL SETUP

The experiments were carried out using a cylindrical bubble column with an inner diameter of 24 inches (~0.6 m) and a height of 152.5 inches (3.9 m) as shown in its schematic diagram in Figure 1 and 2. Deionized water in a batch mode was used as a liquid phase, while oil-free and dry compressed air was used as a gas phase. In industrial practices, some processes, the liquid phase is flowing either co-current or counter-current with a flow rate much smaller than the flow rate of the gas phase. Accordingly, the flow rate and the mode of operation whether batch, co-current, and counter-current would not affect the hydrodynamics of the bubble column. The compressed air was fed into the bubble column from the bottom through a gas distributor (sparger). The gas distributor, which was designed in our laboratory based on previous work using perforated plate with open area 1.09% [14], has 600 holes of 3 mm diameter that are arranged in a triangular pattern with 20 mm pitch as shown in Figure 2(c).

Table 1. Summarize of the effect of dense vertical internals tubes and bubble column dimension on the bubble dynamics and liquid structure previous work.

Authors	Technique of measurement	Setup dimension	Internals arrangement and structure	Operation conditions	Findings
Sultan et al. [42]	Gamma-ray Computed Tomography (CT)	D = 0.14, 0.46 m H = 1.8, 3.66 m	Hexagonal and circularly arranged in a triangular pitch = 2.1, 4.5 and 5 cm Covers ~25% of CSA of the column	Ug = 0.05, 0.3 and 0.45 m/s T and P = ambient *H/D* = 11.3 and 6 Two-phase system	• The arrangement of internals impacts the radial profile of gas holdup significantly • The hexagonal arrangement significantly increases the gas holdup values
S. Sasaki et al. [25]	Image processing method, high-speed video camera (IDT, Motion Pro X-3)	$0.16 \leq D \geq 2$ m $0.4 \leq H_0 \geq 4$ m	Bubble column without internals	Ug = 0.025 to 0.35 m/s T and P = ambient Two-phase system (batch condition)	• The ratio of H_0 to D is useless to evaluate the critical height • The overall gas holdup decreased with increasing the D and decreasing the H_0 • Insignificant effect for the D and H_0 on the overall gas holdup as long the bubble column scaled up
G. Besagni et al. [28]	Expansion bed technique	D = 0.24 m H = 5.3 m	Bubble column without internals	Ug = 0.004 to 0.23 m/s T and P = ambient *H/D* = 5 to 10 Two-phase system (batch condition and counter-current)	• In batch bubble column model, the changing in the aspect ratio has turned out to decrease the gas holdup and destabilize the homogeneous flow regime. While, in the counter-current bubble column model, has turned out to increase the gas holdup and destabilize the homogeneous flow regime • Three flow regimes are available in the bubble column (batch model) • The critical value of the aspect ratio *H/D* ranged between 5 and 10, based on the bubble column operating model (batch or counter-current)
S. Sasaki et al. [29]	Image processing method, high-speed video camera (IDT, Motion Pro X-3)	cylindrical: D = 0.2 m rectangular: W = 0.2 m D_r = 0.2 m	Bubble column without internals	Ug = 0.025 to 0.4 m/s T and P = ambient *H/D* = 1.5 to 5 Two-phase system (batch condition)	• The flow pattern depends on Ug, whereas no significant effect for the height on the flow regime • The capability of overall gas holdup to demarcate the flow regime transition
Besagni and Inzoli [43]	Double-fiber optical probe, and expansion bed techniques	D = 0.24 m H = 5.3 m	Annular gap configuration: Two-tube (Ø = 0.06, 0.075 m)	Ug = 0.0037 to 0.23 m/s U_L = 0.0 to 0.11 m/s T and P = ambient Two-phase system (batch condition and counter-current)	• Insignificant effect for the internals on the local gas holdup • The presence of internals has a limited effect on the global hydrodynamic. • The presence of internals stabilizes the homogeneous regime in terms of transition gas velocity and holdup.

Table 1. Summarize of the effect of dense vertical internals tubes and bubble column dimension on the bubble dynamics and liquid structure previous work (cont.).

Thorat and Joshi [32]	Expansion bed technique	D = 0.385 m H = 3.2 m	Bubble column without internals	Ug = 0.0 to 0.3 m/s T and P = ambient *H/D* = 1 to 8 Two-phase system (batch condition)	• Increasing the gas holdup with a decrease the open area of sparger and the hole diameter • Increasing the gas holdup with an increase the aspect ratio *H/D* • Reducing the coalescing nature in turn delay the transition in the flow regime
Forret et al. [34]	Pitot tube Tracer conductivity method	D = 1 m H = 3.7 m	Arranged in a square pitch of 108 mm. of 56 tubes, each 63 mm in diameter	Ug = 0.15 m/s T and P = ambient *H/D* was not defined Two-phase system	The presence of internals enhances both the large liquid recirculation scale and local dispersion and decreases the velocity fluctuation.
Al Mesfer et al. [44]	Radioactive Particle Tracking (RPT)	D = 0.14 m H = 1.8 m	Hexagonal arranged in a triangular pitch = 2.1cm Covers ~25% of CSA of the column	Ug=0.08, 0.2 and 0.45 m/s T and P = ambient *H/D* = 11.3 Two-phase system	Internals increase the axial centerline liquid velocity and decreases the turbulent parameters (Reynold normal stress, Reynold shear stress, and the turbulent kinetic energy) significantly.
George et al. [45]	Fast response heat-transfer probe Liquid tracer	D = 0.15 m H = 2.5 m	Concentric tube bundle + baffle Coverage area was not defined	Ug = 0.03-0.3 m/s T and P = ambient *H/D* = 6 Two-phase system	The liquid back-mixing is affected in the internals presence, while this impact could be reduced by placing the baffle in the sparger region.
Al Mesfer [7]	gamma ray Computed Tomography (CT)	D = 0.14 m H = 1.8 m	Hexagonal arranged in a triangular pitch = 2.1 Covers ~25% of CSA of the column	Ug=0.08, 0.2 and 0.45 m/s T and P = ambient *H/D* = 11.3 Two-phase system	Internals presence increases the overall gas holdup and the local gas holdup when the Ug is calculated based on the total CSA.
Abdulmohsin and Al-Dahhan [46]	Fast response heat-transfer probe	D = 0.19 m H = 2 m	Hexagonal and circular Covers 5%, and 22% of the total CSA, respectively	Ug=0.03-0.2 m/s T and P = ambient *H/D* = 8.5 Two-phase system	Internals presence increases the heat transfer coefficient significantly.
Youssef et al. [47]	Four-point fiber optical probe	D = 0.45 m H = 3.75 m	Hexagonal and circular Coverage (5 and 25%) of total CSA	Ug = 0.05-0.45 m/s T and P = ambient *H/D* = 7.1 Two-phase system	• The dense internals of 25% coverage area increases the overall and radial profile of gas holdup significantly and the wall region, in particular • The presence of internals decreases the mean bubble chord length and bubble velocity.
Jhawar and Prakash [35]	Fast response heat-transfer probe	D = 0.15 m H = 2.5 m	Concentric tube bundle + baffle Coverage area was not defined	Ug=0.03-35 m/s T and P = ambient *H/D* = 11.3 Two-phase system	The internals and their position significantly affect the heat transfer and the hydrodynamics of the bubble column.
Youssef and Al-Dahhan [6]	Four-point fiber optical probe	D = 0.19 m H = 2 m	Hexagonal and circular Coverage (5 and 22%) of total CSA	Ug=0.03-0.3 m/s T and P = ambient *H/D* = 8.5 Two-phase system	• The local gas holdup and interfacial bubble area increased by increasing the coverage area of the internals • The presence on internals reduces the liquid recirculation scale • The presence of internals increases the bubble breakup rate.

A screen made from stainless steel of mesh size 400 has covered the distributor. Two parallel rotameters were connected to measure and control the superficial gas velocity U_g, which calculated based on the free CSA of flow in the bubble column and varied from 0.2 to 0.45 m/s. The calculation of the superficial gas velocity has been calibrated with an equation that provided by the manufacturing company for the rotameters (Omega). However, this equation calibrates the pressure, temperature, and the molecular weight of the gas. Therefore, the difference in the density of air has been considered in this work. An internal heat exchanger structure, as shown in Figure 3 that covers 24% of the CSA of the bubble column and consists of 12 dual pipes of 0.06 m diameter has been utilized in this research. Two sections of vertical tubes with a length of 1.55 m were used. This mimics the heat exchangers used in the Fischer-Tropsch process. Sultan [42] visualized and quantified the impact of internals configuration and bubble column size on the loacl gas holdup profiles using gamma-ray computed tomography CT technique. Their results exhibit that an enhancement in the cross-sectional gas holdup distribution was obtained when the internal (in both arrangements) were used. However, high cross-sectional gas holdup distribution was found in the internals of hexagonal configuration arrangement, therefore, the hexagonal arrangement has been utilized in this work. Experiments were carried out at three aspect ratios of dynamic height to the inner diameter of *H/D* = 3, 4, and 5. In this case, the initial bed height (liquid height) varied with the change in gas velocity to maintain the same studied bed dynamic heights with the change in gas velocity. It is worth to mention that we found in our previous work [12], [13] for high *H/D* bubble column with and without internals (*H/D* ~ 11.5), the variation in the initial bed height to maintain the same dynamic height with the change in gas velocity had no effect on the

hydrodynamics of the bubble column. However, for the low aspect ratio bubble column, the effect in the change in the initial bed height or when the bed height was kept constant, can be related directly to the effect of the dynamic aspect ratio (*H/D*) on the bubble dynamics and on the hydrodynamics of the bubble column with and without internals found in this study. The bubble properties have been measured radially at five dimensionless radial positions (r/R=0.0, 0.23, 0.46, 0.69, and 0.92). According to Chen et al. [10], and Al Mesfer et al. [44] revealed that the reflected point for the axial liquid velocity is located at r/R=0.66-0.7, where after this point the liquid velocity is negative magnitude (i.e., the liquid moves from the top to the bottom of the bubble column). Thereby, in this work, the dimensionless r/R = 0.69, and 0.92 have been defined as wall region. Our four-point fiber optical probe was used as discussed in the following section to measure the local bubbly properties at various axial positions, starting from 0.3 m above the perforated plate moving upward with increments of 12 inch (~0.3 m). At each axial position, five radial locations were measured as shown in Figure 2(a-b). The optical probe has been inserted vertically from the top of the bubble column to have flexibility in positioning the probe and to reduce the effect of the probe on the hydrodynamic properties. In addition, due to the space limitation in the experiment setup, the four-point fiber optical probe was oriented into the downward direction, and hence, the bubbles that are moving in a downward direction were not measured either in center or wall region, and hence, all bubble properties have been measured based on the bubbles that move in the upward direction.

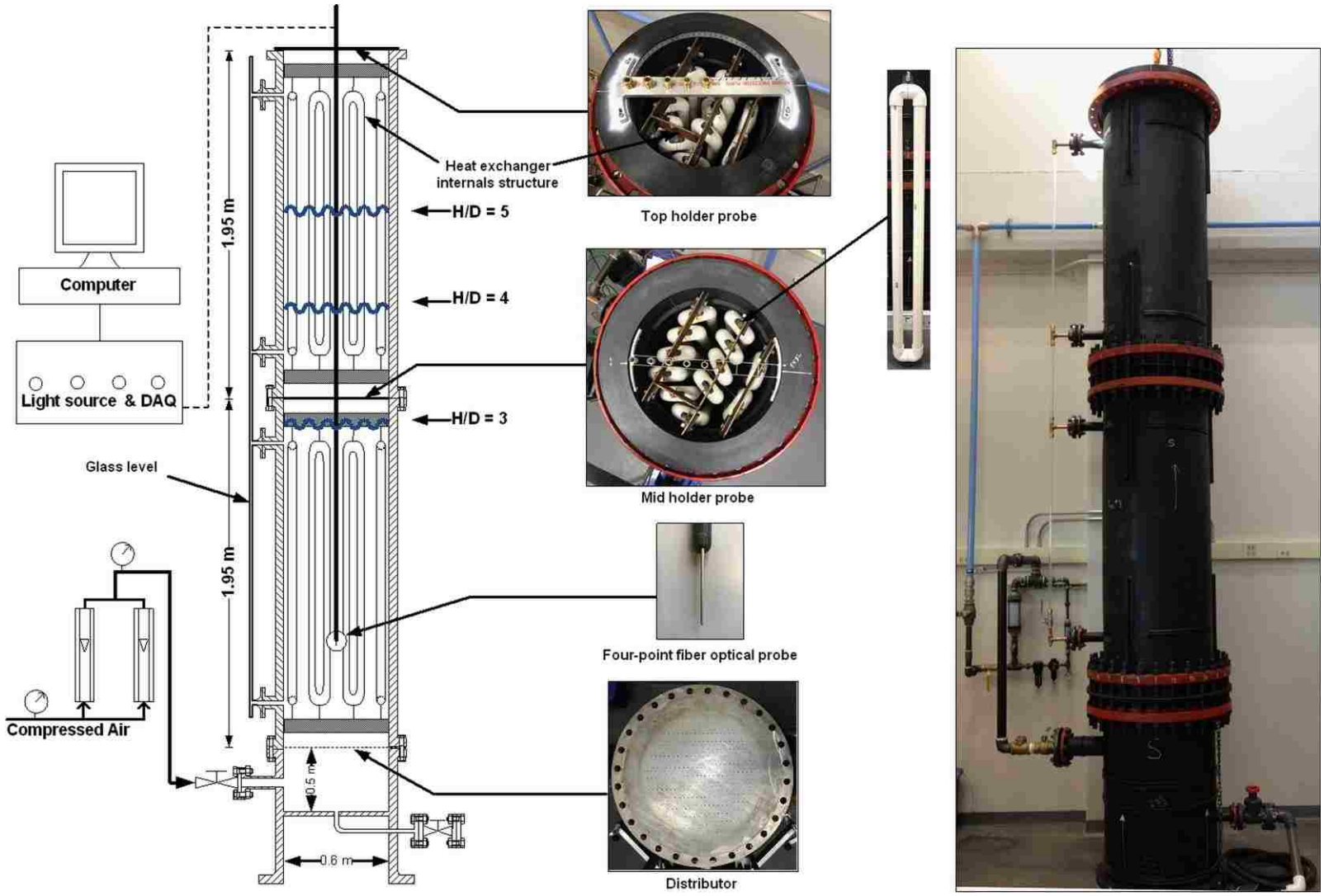

Figure 1. Schematic diagram of the industrial-size pilot plant bubble column reactor with its internals

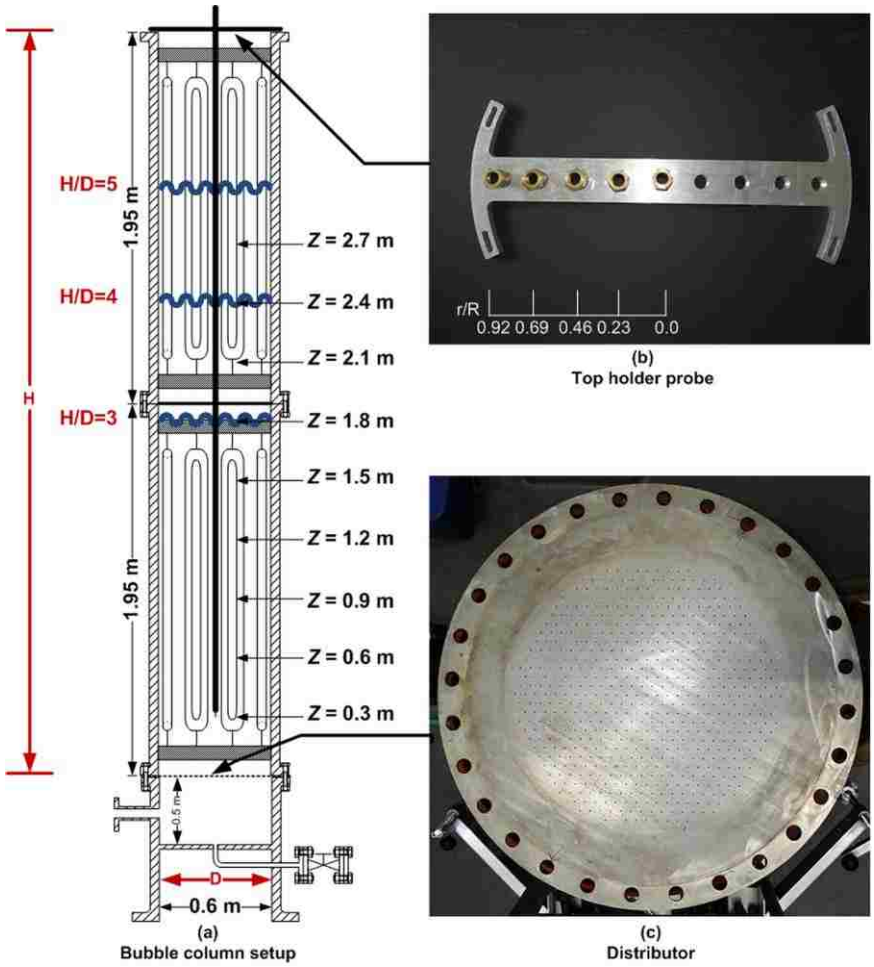

Figure 2. Schematic of the axial and radial movement locations for the four-point fiber optical probe

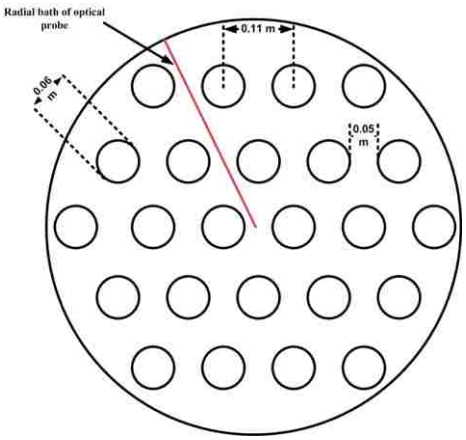

Figure 3. Internals of hexagonal configuration covering 24% of the (CSA) of bubble column

3. MEASURMENT TECHNIQUE

3.1. FOUR-POINT OPTICAL PROBE

Our four-point fiber optical probes have been utilized in these experiments to measure the bubble properties as illustrated in Figure 4. The four-point fiber optical probe was developed by Frijlink [48] at Delft University, and then Xue et al. [49] developed a data processing algorithm in the Chemical Reaction Engineering Laboratory (CREL) at Washington University. Further, Xue et al. [50] quantified the uncertainty in the measurement of the four-point optical probe for the bubble properties against high speed and high resolution camera in a separate effect experiment of 2D bubble column. Their findings confirm the reliability of using this technique and the data processing algorithm that developed. In this study, our advanced version was employed to measure bubble properties (chord length, local gas holdup, interfacial area, bubble rise velocity, and bubble frequency). The structure of the four-point optical probe technique primarily consists of four quartz glass tips. The diameter of each tip is 200μm, clad by silicon with 380 μm diameter and a protective layer of Teflon with an overall diameter of 600 μm. Three tips are arranged in an equilateral triangle. The fourth tip, which is about 2 mm longer than the other tips, is located in the center of the equilateral triangle. The probe was manufactured in the mFReal (Multiphase Flow and Multiphase Reactors Engineering Laboratory) in the Chemical and Biochemical Engineering Department at Missouri University of Science and Technology. The principal work of the fiber optical probe depends on a laser beam, which is generated by Light Emitting Diode (LED). The laser is sent into each optical tip, and

then the reflected light is converted from light photons into a voltage signal collected in the data acquisition board (Power DAQ PD2-MFS-8-1M/12) with a sample rate of 40 kHz.

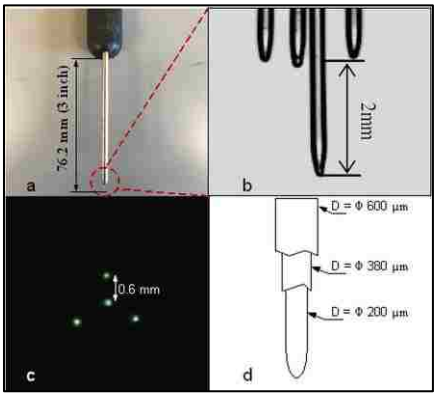

Figure 4. Configurations of four-point fiber optical probe. (a) Optical probe. (b) Side view of four optical tips. (c) Top view of four-point fiber optical probe tips. (d) TEM image of fiber tip

Due to the difference in refractive index in between the gas phase and liquid phase, the intensity of reflected light changes depending on the phase present at the optical probe tips as shown in Figure 4 e.

4. METHODS AND DATA PROCESSING

4.1. GLOBAL GAS HOLDUP

The expansion bed technique was used to obtain the overall gas holdup during the bubble column operation as shown in Equation (1):

$$\varepsilon_G = \frac{H_D - H_S}{H_D} \tag{1}$$

where H_S and H_D are the heights of the static and dynamic liquid level, respectively. The static liquid level, which monitored by using a glass level, was changed to maintain the dynamic liquid level at a desired height to make *H/D* = 3, 4, and 5.

4.2. ANALYSIS OF VARIANCE BY ANOVA METHOD

An ANOVA test, a two-way means model, is a statistical method that has been utilized to identify the axial location of the fully developed flow region if it occurs. The principle of this method is evaluating the variance of the mean variables, which are the local gas holdup, and the variation in the axial location, in this case. Furthermore, the criterion that used to identify the transition between different regions in different conditions (U_g= 0.2-0.45 m/s, *H/D* = 3-5, and with and without internals bubble column) is the radial profile of the local gas holdup because it is a fundamental parameter among other bubble properties in design and scale-up [5]. In this method, the variation in the radial profile of local gas holdup at a specific axial location would be compared with a radial profile of next axial position to calculate the variances of the local gas holdup if it is significant or insignificant. Therefore, when the variance of the local gas holdup with the axial positions is insignificant, that indicates the presence of the fully developed flow at this position [51].

4.3. BUBBLE DYNAMIC PROPERTIES

The data processing algorithm developed by Xue et al. [49] assumes an ellipsoidal bubble shape and considers surface curvature. Figure 5 (a) shows the bubble when it hits the probe with a deviation angle equal to β, which is the angle between Tip 0 and the normal vector *n*, and *n* is the perpendicular vector on the bubble's symmetry plane. Equations (2-

4) calculate the bubble's velocity by using the bubble's time traveling from Tip 0 to another Tip *i*, i=1, 2, 3.

$$\Delta t_1 - \frac{T_1 - T_0}{2} = \frac{Z_1'/\cos\emptyset}{V} = \frac{X_1.\sin\beta\cos\gamma + Y_1.\sin\beta\sin\gamma + Z_1.\cos\beta}{V.\cos\emptyset} \quad (2)$$

$$\Delta t_2 - \frac{T_2 - T_0}{2} = \frac{Z_2'/\cos\emptyset}{V} = \frac{X_2.\sin\beta\cos\gamma + Y_2.\sin\beta\sin\gamma + Z_2.\cos\beta}{V.\cos\emptyset} \quad (3)$$

$$\Delta t_3 - \frac{T_3 - T_0}{2} = \frac{Z_3'/\cos\emptyset}{V} = \frac{X_3.\sin\beta\cos\gamma + Y_3.\sin\beta\sin\gamma + Z_3.\cos\beta}{V.\cos\emptyset} \quad (4)$$

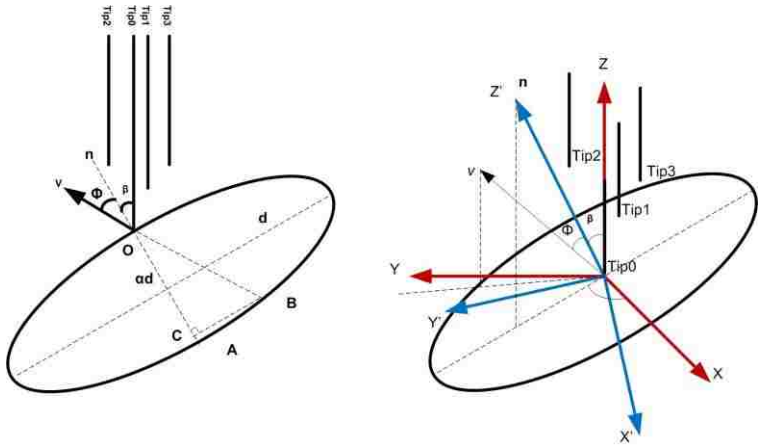

Figure 5 (a) Schematic of bubble hitting the Probe Tips (b) Bubble Velocity Vector with Coordinate Transformation

where *V* is the bubble velocity vector magnitude, X_i, Y_i, Z_i for *i*=1, 2, 3 are the cartesian coordinate for Tips 1, 2, and 3 (measured photographically), $\emptyset$ is the angle between the bubble's velocity vector and the normal vector of the symmetry plane of the bubble, and γ is the angle between the x-axis and the projection of the normal vector on the XY plane as shown in Figure 5 (b). After the bubble's velocity was calculated, the bubble's chord length, which can be expressed by $dl_i = v.T_i.\cos\emptyset$, can be found. The chord length will represent the distance AC in Figure 5. However, if the bubble hits the tips with deviation

$\emptyset$ as in Figure 5 (b), $v.T_i.\cos\emptyset$ is actually represents the length AD. Thus, the chord length and bubble velocity values have some errors. Kataoka et al. [52] found the value of $\emptyset$ is 10^o to 22^o in an air-water system for different operating conditions. Xue et al. [49] assume that in most cases, $\emptyset$ less than 30^o, hence the chord length and velocity are that measured with errors less than 13.4%, which was considered acceptable.

Kataoka et al. [52] found equation (5) to calculate the interfacial area by using $v.\cos\emptyset$. This equation can measure the interfacial area for all bubbles that hit all the tips or hit the center tip and miss the others. Therefore, the ship bubble effect in this equation is ignored:

$$a = \frac{1}{\Delta T}\cdot\sum_{N}\frac{1}{V.cos\,\emptyset} \cong \frac{1}{\Delta T}\cdot\frac{N}{N_{measured}}\sum_{N_{measured}}\frac{1}{V.cos\,\emptyset} \tag{5}$$

$$N = N_{measured} + N_{missed} \tag{6}$$

Finally, from the center tip's response, the local gas holdup can be measured by using equation (7), where *N* is the total number of sample points in the probe's central tip:

$$\varepsilon_g = \frac{Time\ spent\ in\ bubbles\ by\ probe's\ central\ tip}{Total\ sample\ time} = \frac{\sum T_0}{\Delta T} \tag{7}$$

After the bubble velocity is calculated by solving equations (2-4), the bubble chord length can be calculated by solving the following equations:

$$\left(\frac{L_0}{2}\right)^2 + \alpha^2[(X_0' - O_{X'})^2 + (Y_0' - O_{Y'})^2] = \alpha^2 d^2 \tag{8}$$

$$\left(\frac{L_1}{2}\right)^2 + \alpha^2[(X_1' - O_{X'})^2 + (Y_1' - O_{Y'})^2] = \alpha^2 d^2 \tag{9}$$

$$\left(\frac{L_2}{2}\right)^2 + \alpha^2[(X_2' - O_{X'})^2 + (Y_2' - O_{Y'})^2] = \alpha^2 d^2 \tag{10}$$

$$\left(\frac{L_3}{2}\right)^2 + \alpha^2[(X_3' - O_{X'})^2 + (Y_3' - O_{Y'})^2] = \alpha^2 d^2 \quad (11)$$

where L_i is the chord length pierced by Tip i, α is equal the aspect ratio of an ellipsoidal bubble, d is the length of the major axis of the bubble, and $O_{Y'}$ and $O_{X'}$ are the X' and Y' coordinates of the center of bubble in the X'Y'Z' coordinate system shown in Figure 5 (b).

5. RESULTS

5.1. THE FULLY DEVELOPED FLOW REGION

A bubble column reactor consists of three regions: sparger, fully developed flow, and disengagement [17], [53]. Meanwhile, bubble properties are constantly changing due to the coalescence and breakup rates in each region [17], [54]. Most of the bubble properties in previous work have been examined in the fully developed flow region where a high ratio of *H/D* has been used (*H/D* $\geq$ 9) because the coalescences and breakup rates are in an equilibrium state [5]. Thereby, the radial profile of the dynamic properties is nearly invariant with the axial position, which is the fully developed flow region [25], [55]. Identifying the fully developed region and the sparger region (if it occurs) is crucial for this work due to the low aspect ratios, *H/D*, and aim to investigate the effect of internals and dynamic liquid level on the bubble dynamics in the fully developed flow region and the sparger region. Figure 6 (a) and (b) depict the radial profiles of local gas holdup in different axial positions for the bubble column with and without internals, operated at the dynamic liquid level *H/D* = 5 and the superficial gas velocity U_g= 0.45 m/s, which is calculated based on the free CSA of the bubble column. By utilizing the ANOVA method, the radial

profiles of the local gas holdup have an insignificant variance at Z = 1.2 m, and Z = 1.5 m above the distributor for the bubble column with, and without internals, respectively. The impact of superficial gas velocity, the presence of internals, and aspect ratios on the fully developed flow region has been listed in Table 2. All parameters exhibit a significant effect on the fully developed flow region. A decrease in superficial gas velocity and the existence of internals enhance the fully developed flow region to appear early at lower axial postion. The increasing in the superficial gas velocity and the absence of internals increase the chaotic behavior of the bubble columns by increasing the turbulent kinetic energy (TKE) and the eddy diffusivity [10], [44].

The pronounced impact of increasing the superficial gas velocity on the fully developed flow region was indicated in a decrease in the aspect ratios. At H/D = 3, the height of the dynamic liquid level was not enough to yield a fully developed flow region and neither without the presence of internals, through all the velocities except at U_g = 0.2 m/s. Hence, in Table 2, N/A (not applicable) has been indicated for the conditions in which the fully developed region has not appeared. Except at low-velocity, U_g= 0.2 m/s, in the bubble column with the internal case, the fully developed flow region has been indicated in Z = 0.9 m. At the aspect ratios of H/D = 4 and 5, no effect has been observed on the the fully developed flow region by the presence of internals. In contrast, increasing the aspect ratio in the absence of internals delays the transition to the developed flow region, and hence, the transion occurs at higher axial position. In general, the data listed in Table 2 show for the design of the distributer used that internals and superficial gas velocity have a significant effect on the existence of the fully developed flow region, whereas, the variation in the aspect ratio has slightly effect and limited in the bubble column without

internals. Therefore, the data reflect a similar perspective toward the effect on the bubble dynamic. Based on data obtained, the impact of internals and low aspect ratio on the bubble properties would be studied in the fully developed flow region, and the sparger region, which were demarcated in the axial level at Z = 1.5 m, and Z = 0.6 m, respectively, including the bubble column with and without internals for all operation aspect ratios, although the bubble column, that is operated with the aspect ratio of H/D = 3 does not show the fully developed region. In addition, the radial profile at the aeration liquid level has been excluded to prevent the disengagement region effect on the local gas holdup measurements

Table 2 Aspect ratio, *H/D*, for fully developed flow region under different operating conditions

Superficial gas velocity U_g (m/s)	Axial location of the fully developed flow in bubble column with internals, Z (m)			Axial location of the fully developed flow in bubble column without internals, Z (m)		
	H/D = 3	H/D = 4	H/D = 5	H/D = 3	H/D = 4	H/D = 5
0.2	0.9 m	0.9 m	0.9 m	N/A	1.2 m	1.2 m
0.3	N/A	1.2 m	1.2 m	N/A	1.2 m	1.5 m
0.45	N/A	1.2 m	1.2 m	N/A	N/A	1.5 m

5.2. OVERALL GAS HOLDUP

The overall gas holdup is a volume fraction of a gas phase in the dispersion of the gas-liquid system [56] during the gas phase sparged through the bubble column [5]. Figure 7 illustrates, with error bars, the impact of internals on the overall gas holdup in the bubble column running under different aspect ratios. An increase in the aspect ratio increases the overall gas holdup, and this effect was significant in the absence of internals. This is attributed to the fluctuations in the dynamic liquid level during no-internals cases. The

presence of internals increases the overall gas holdup by ~ 15, 12, and 6 % for the aspect ratios *H/D* = 3, 4, and 5, respectively, at a superficial gas velocity based on free CSA for the flow of U_g = 0.2 m/s.

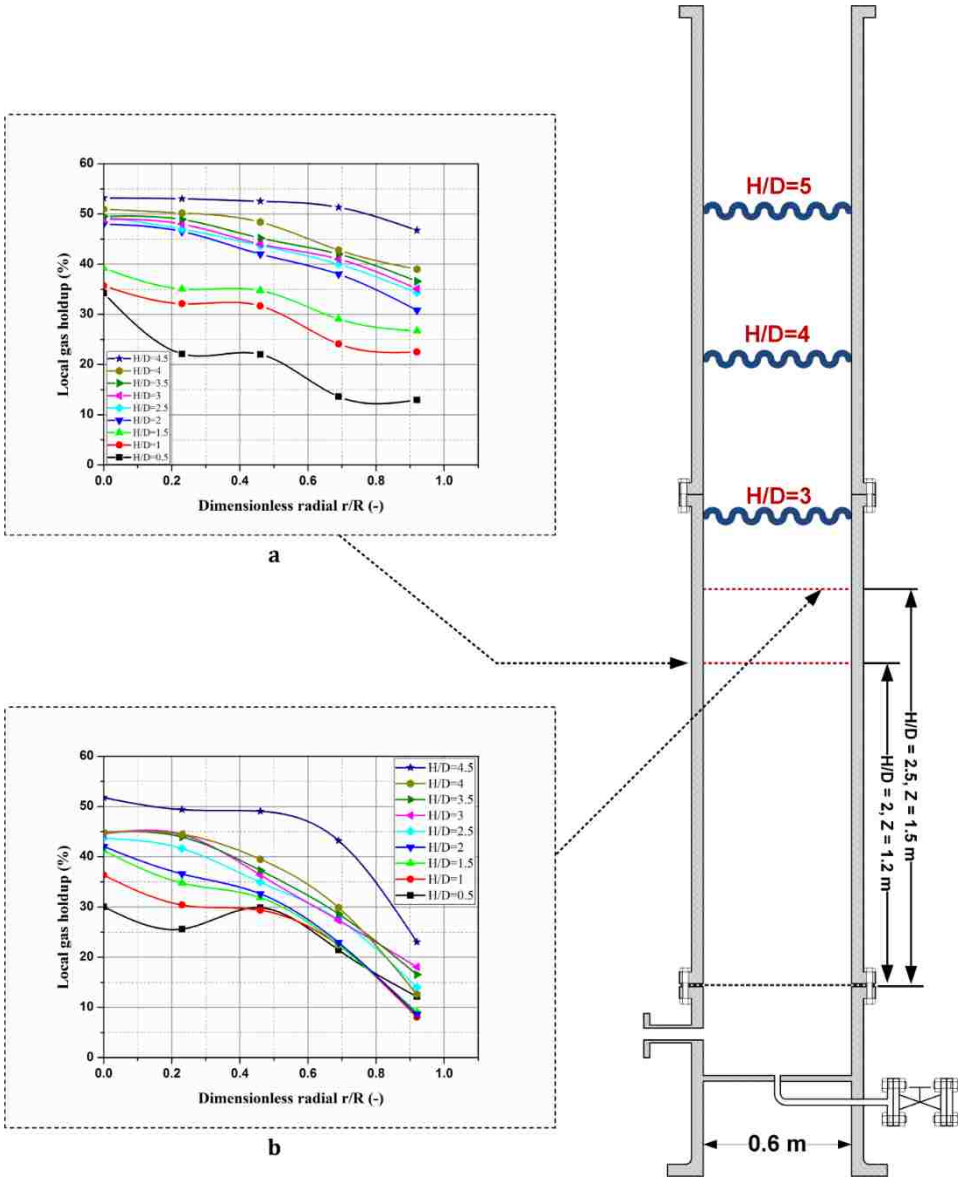

Figure 6. (a); Fully developed flow region in bubble column with internals, *H/D*=5, and Ug=0.45 m/s (b); Fully developed flow region in bubble column without internals, *H/D*=5, and Ug=0.45 m/s

This enhancement increased by increasing the superficial gas velocity to reach ~ 25, 17, and 9 % for aspect ratio *H/D* = 3, 4, and 5, respectively, at U_g= 0.45 m/s. Consequently, the influence of the presence of internals is greater than the variation in the aspect ratio, which indicates a similar effect toward the bubble dynamics. Although the gas velocity was calculated based on the free CSA of the column, the data obtained of the overall gas holdup show alignment with the results of Youssef et al. [47] for the internals that cover 25% CSA area of the column.

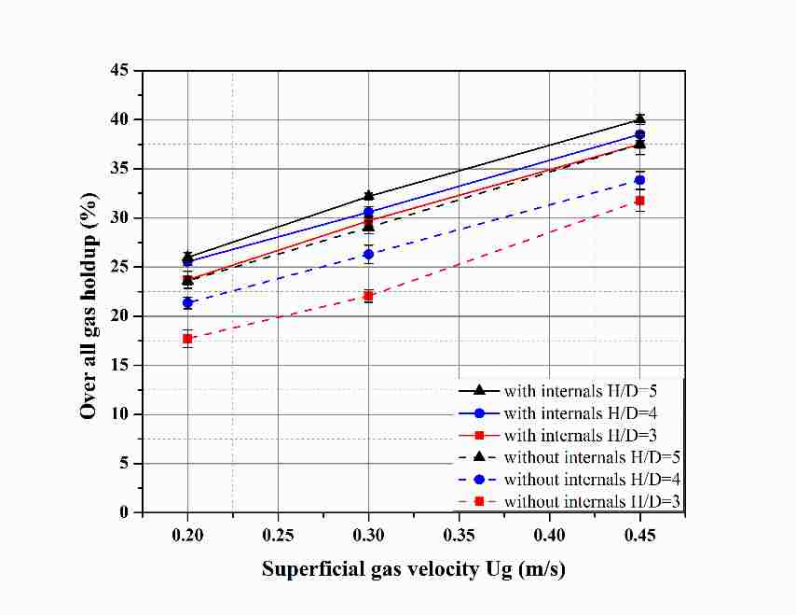

Figure 7. Internals effect on the overall gas holdup at different dynamic liquid level operations

5.3. LOCAL GAS HOLDUP

The local gas holdup is defined as a local volume fraction for the gas phase. It represents the brief of the physical phenomena for other bubble properties, such as the interfacial bubble area, bubble chord length, bubble pass frequency, and bubble rise

velocity [5]. Therefore, through the local gas profiles, the liquid back-mixing and the efficiency of the heat and mass coefficient are determined [10], [30], [35]. The effect of the internals and the variation in aspect ratio on the local gas holdup in the fully developed flow region, and the sparger region has been illustrated in Figure 8, and Figure 9, respectively. However, as mentioned previously, the fully developed flow region and the sparger region are demarcated in an axial position located in Z = 1.5 m, and Z = 0.6 m, respectively, for all used superficial gas velocities (U_g= 0.2, 0.3, and 0.45 m/s). In the case of the absence of internals, the local gas holdup of the fully developed flow region exhibits steeper radial profiles than the profiles in the sparger region. Further, as the aspect ratio increases, the radial local gas holdup profile decreases. In contrast in the sparger region, the variation in the aspect ratio does not have a clear effect on the local gas holdup, which is aligning with the results of Parasu and Joshi [57]. This phenomenon could be attributed to the hole's diameter d_0 < 3 mm of the distributor and it's configuration and design, and hence, the primary bubble diameter is smaller than the bubble size in the fully developed flow region. Therefore, the highest aspect ratio *H/D* provides enough distance for the bubbles to reach the equilibrium bubble size by increasing the coalescence rate where being in an equilibrium state with the breakup rate. Consequently, it can attribute the disappearing of the fully developed flow region in aspect ratio *H/D* =3.

Meanwhile, as can be seen in Figure 8, the presence of internals shows a significant increase in the fully developed flow region on the local gas holdup by about ~5%, 6%, and 8% for *H/D* = 3, 4, and 5, respectively, in the center region and by about ~26%, 22%, and 19 % for *H/D* = 3, 4, and 5, respectively, in the wall region. This effect is consistent with the results of Youssef and Al-Dahhan [6], Youssef et al. [47], and Al Mesfer et al. [7].

They reported that this enhancement for the internals to the local gas holdup is a result of increasing the bubble breakup rate, which in turn, decreases the bubble size and thus decreases the bubble rise velocity, which in turn increases the residence time for the bubble in the bubble column and afterward increases the local gas holdup.

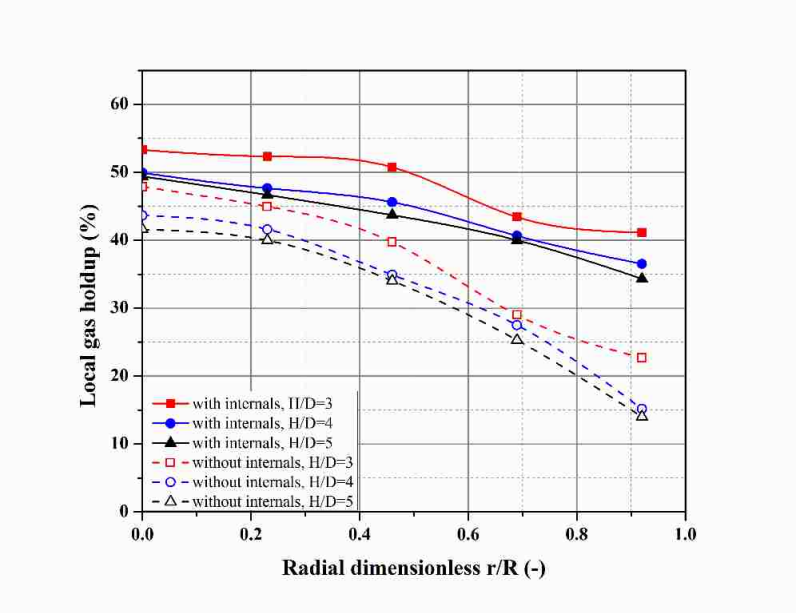

Figure 8. The effect of internals and the aspect ratio on the radial profiles of the local gas holdup for the fully developed flow region at Ug=0.45m/s

While, as can be seen in Figure 9, the sparger region appears to be an insignificant impact for the internals on the local gas holdup in the central region of the bubble column, except for the wall region where the local gas holdup has been increased about ~17%. It is worth mentioning, the internals enhances the local gas holdup in the wall region more than in the central region. This implies that the presence of internals reduces the difference in the local gas holdup between the center and the wall region by administrating the bubble

size distribution along the radial profile, which will be discussed in more detail in section 5.4 of the bubble chord length distribution.

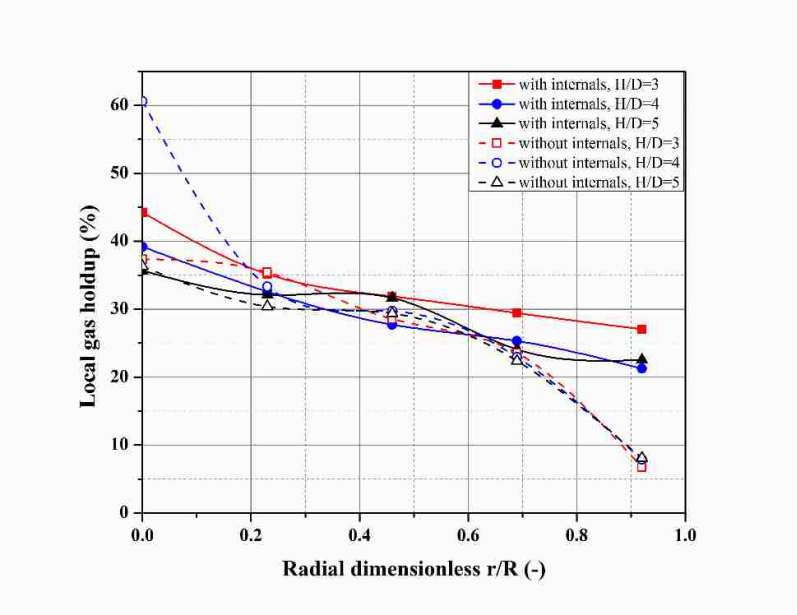

Figure 9. The effect of internals and the aspect ratio on the radial profiles of the local gas holdup for the sparger region at Ug=0.45m/s

The difference in the local gas holdup between the center region and the wall region is the main reason to enhance the global liquid recirculation, where the liquid moves upward in the center of the bubble column, while moves downward close to the wall region of the bubble column. Figure 10 illustrates the effect of superficial gas velocity U_g, presence of internals, and aspect ratios (*H/D* = 3, 4, and 5) on the difference of the local gas holdup between the central region, and the wall region. As shown in Figure 10, during the with internals case the difference in the local gas holdup at U_g= 0.2 m/s is ~ 3%, 5%, and 7% for *H/D* = 3, 4, and 5, respectively, and as increasing the superficial gas velocity to U_g= 0.45 m/s, the difference increases to ~12%, 13%, and 15% for *H/D* = 3, 4, and 5,

respectively. In contrast, in the absence of internals, the difference in the local gas holdup at U_g= 0.2 m/s is ~14%, 15%, and 17% for *H/D* = 3, 4, and 5, respectively, and as the U_g increases to U_g= 0.45, the difference in the local gas holdup increased to ~25%, 28%, and 30% for *H/D* = 3, 4, and 5, respectively. Based on the data obtained in Figure 10, the increasing in the superficial gas velocity U_g enhances the different in the local gas holdup, which in turn, promptes the global liquid circulation, and this agrees with most previously conducted work [44]. While, the presence of internals inhibits the effect of the superficial gas velocity U_g to increase the liquid circulation by reducing the gaps in the local gas holdup between the center region and the wall region. This attribution has been concluded since the global liquid circulation is due to the difference in the local gas holdup between the wall and the center regions [35]. Comparing with the results of Chen et al. [10], and Al Mesfer et al. [7], [44], they observed that the increase in the liquid circulation was related with an increase the difference in the local gas holdup between the center region and the wall region. Accordingly, current work shows different effect for the presence of internals towards inhibiting the liquid circulation, and this difference could be attributed to using low aspect ratio of the dynamic liquid level *H/D* and the presence of internals with big gap between the tubes of internals, which in turn, keeps the bubble size small and thus allows the bubble to pass without resistance through the internals and then increases the local gas holdup in the wall region as well. Hence, the effects of the distance between the tubes of internals, the internals configuration, and the size of tubes on the bubble properties and the liquid velocity are essential to consider in further investigations.

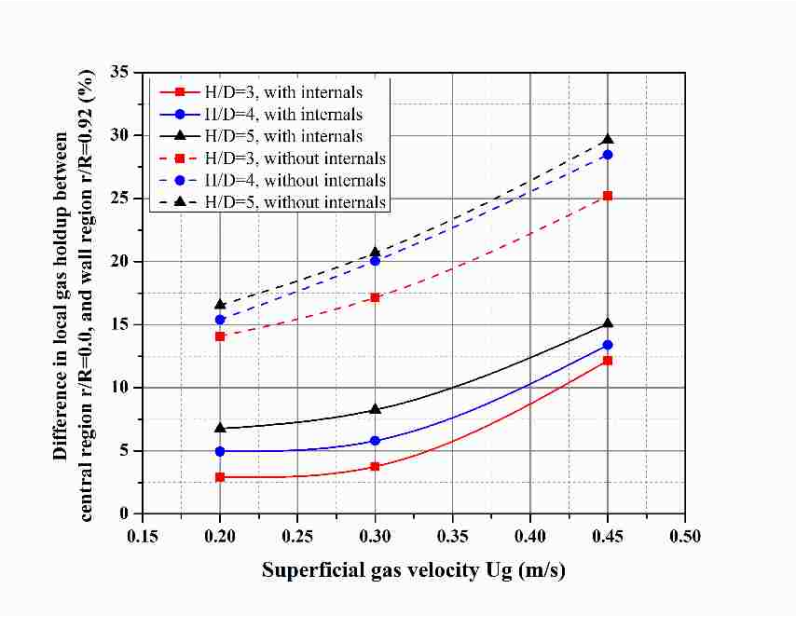

Figure 10. The difference in the local gas holdup between the center and the wall regions in the fully developed region at different aspect ratios in a bubble column with and without internals

5.4. BUBBLE CHORD LENGTH DISTRIBUTION

The bubble chord length directly administrates bubble properties such as the interfacial bubble area, bubble velocity, and local gas holdup. Therefore, a better understanding of the influence of different parameters, such as the presence of internals and the superficial gas velocity on the bubble size, would provide by inference a physical attribution about how these parameters impact the entire bubble properties at the same conditions.

Unfortunately, bubbles exist in a wide range of size distribution, and hence, the mean value is not adequate to represent the bubble size properly. Based on that, the probability density function has been associated with statistical parameters of the mean and variance. Hence, the findings for low aspect ratios (up to $H/D = 5$) of this study, are critical

for the assessment of the scale-up methods reported in the literature which have been assessed for the bubble column of high aspect ratios (up to *H/D* ≅ 9and more). These methods need further considerations to include the effect of low aspect ratios and the presence of internals with their configurations. As the superficial gas velocity changed, the bubble dynamics alter based on this changing. Consequently, the flow regime of the bubble column transits from a regime to another depending on the superficial gas velocity. Figure 11(a-c) and Figure 12(a-c) illustrate the effect of gas velocity on the bubble chord length distribution in a bubble column with, and without internals, respectively, and the statistical parameters have been summarized in Table 3. However, the results show a slight effect for the superficial gas velocity on the bubble chord lengths along the fully developed flow region and the sparger region for all the aspect ratios (*H/D* = 3, 4, and 5). The increase in gas velocity slightly decreases the bubble chord length in the fully developed flow region and the sparger regions. This could be attributed to the fact that the experiments were conducted in a range of velocities are located in one region, the churn turbulent flow regime [58]. Where in this region, the turbulent eddies were promoted significantly, which in turn, increases the bubble breakup rate that reduces the bubble size [59].

Further, although the gas velocity U_g impacts slightly on the chord length, that does not explain the reason behind the increase in the local gas holdup with an increase in the superficial gas velocity unless there is a massive increase in the bubble number. It is worth mentioning that Table 3 displays that the mean value of the bubble chord lengths at the sparger region appears smaller than in the fully developed flow region which indicates that the bubble size increased during axial rising. Similar results have been revealed by Esmarili et al. [17], where they measure the gas hold up in the middle and the top zone of the bubble

column, and they report that the gas holdup in the middle zone is lower than in the top zone, especially at high gas velocity U_g. As well as, the most height of the aspect ratio exhibits a slight increase, which aligns with the results of Parasu and Joshi [57].

The effect of the internals on the chord lengths has been illustrated in Figure 13 (a-b), and the statistical parameters of the mean and variance for the chord length distribution are summarized in Table 4. These results are aligned with the results reported in the literature [5], [6], [48–51]. Table 4 shows that the existence of internals decreases the bubble chord length, which attributes the increase in the local gas holdup with internals. Although the chord length distribution with internals exhibits a slight increase in the mean value of 0.63 cm, compared to 0.67 cm for the bubble column without internals, the variance was lower for the existence of internals than for the bubble column without internals, revealing that a narrower range of bubble chord lengths exists with the internals. While at the wall region different phenomena appear, where the mean bubble chord length in the absence of internals case is smaller than these in the presence of internals case. Data obtained from the bubble column with internals, suggest that the mean bubble chord lengths in the center and the wall regions are close to each other, indicating that the presence of internals is significantly administrating the radial profile of the bubble size distribution. The observed fact that relates to the effect of internal on the hydrodynamic properties were supported by the results reported previously [5], [6], revealing that smaller bubbles are generated in the internals system due to enhancing the bubble breakup rate.

5.5. BUBBLE FREQUENCY

Number of bubbles that hit the central tip of the probe divided by the sampling time is defined as bubble pass frequency (1/sec), according to Wu et al. [64]. The bubble chord length does not adequately attribute the effect of internals and different aspect ratios on the bubble dynamics. As well, based on the renewal layer theory of Schluter et al. [65], the bubble pass frequency is a critical parameter for the heat and mass transfer in a bubble column since it determines the contact times between the eddies and the surface or the interface of the multiphase fluid [66]. Therefore, it has been essential in this work to investigate the impact of internals and aspect ratio on the bubble frequency. The effect of internals and superficial gas velocity on the bubble pass frequency in the fully developed flow region and the sparger region has been illustrated in Figure 14 (a-c) and Figure 15 (a-c), respectively.

Table 3. Summary of the statistical parameters for the bubble chord length distribution in bubble columns with and without internals at different dynamic liquid levels

H/D=3								
Ug m/s	With internals				Without internals			
	Fully developed		Sparger		Fully developed		Sparger	
	Mean	Var	Mean	Var	Mean	Var	Mean	Var
0.2	0.61	0.8582	0.51	0.3564	0.76	0.8327	0.67	0.8922
0.3	0.69	1.0653	0.50	0.4602	0.69	0.6443	0.65	0.5925
0.45	0.53	0.7504	0.50	0.4265	0.62	0.5843	0.52	0.4705
H/D=4								
Ug m/s	With internals				Without internals			
	Fully developed		Sparger		Fully developed		Sparger	
	Mean	Var	Mean	Var	Mean	Var	Mean	Var
0.2	0.74	0.6552	0.72	0.2419	0.78	0.8433	0.76	0.9046
0.3	0.67	1.0375	0.50	0.8065	0.69	0.6415	0.65	0.5013
0.45	0.60	0.6194	0.46	0.4602	0.63	0.5806	0.61	0.4091
H/D=5								
Ug m/s	With internals				Without internals			
	Fully developed		Sparger		Fully developed		Sparger	
	Mean	Var	Mean	Var	Mean	Var	Mean	Var
0.2	0.75	0.8177	0.66	0.3791	0.79	0.8142	0.77	0.9527
0.3	0.70	0.9470	0.52	0.7307	0.70	0.6591	0.67	0.5320
0.45	0.63	0.4692	0.51	0.6063	0.67	0.5346	0.61	0.4796

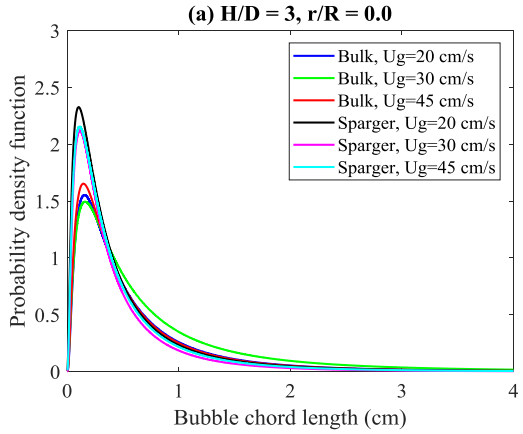

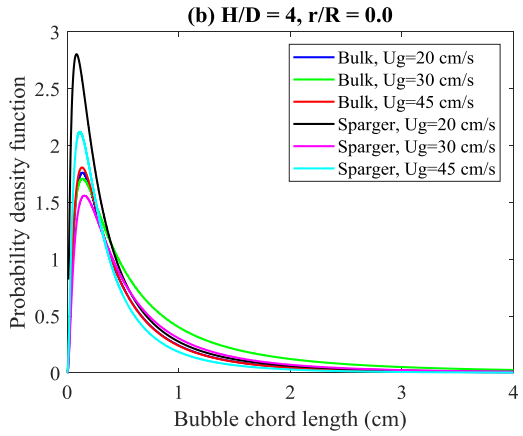

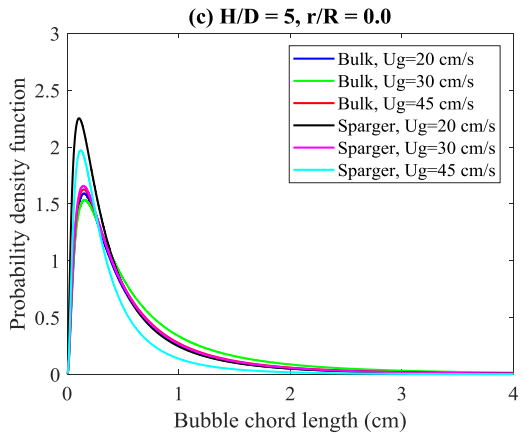

Figure 11. The effect of superficial gas velocity on the bubble chord length distribution in the bubble column with internals r/R = 0.0 (a) *H/D* = 3 (b) *H/D* = 4, and (c) *H/D* =5

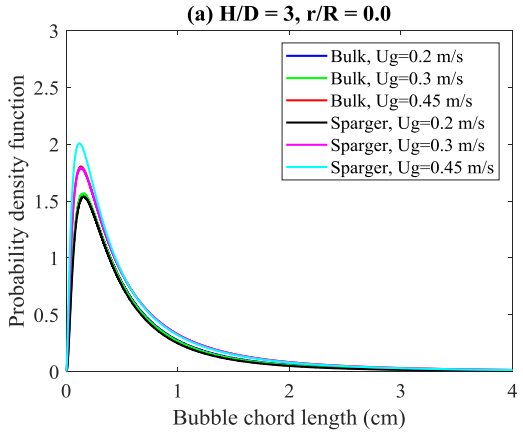

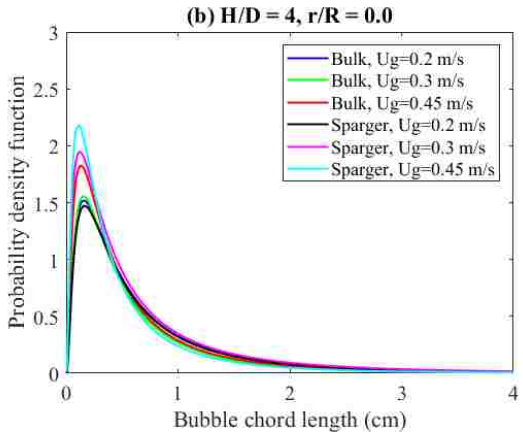

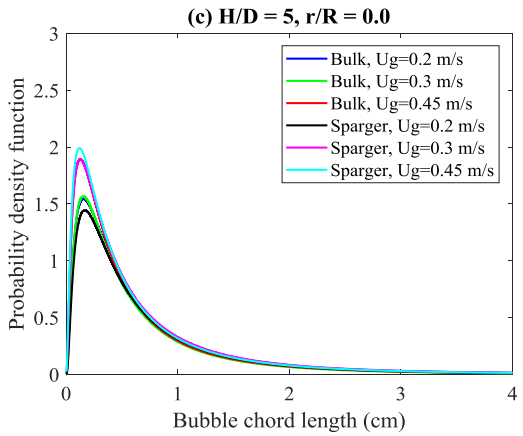

Figure 12. The effect of superficial gas velocity on the bubble chord length distribution in the bubble column without internals r/R = 0.0 (a) *H/D* = 3 (b) *H/D* = 4, and (c) *H/D* =5

Table 4. Summary of the statistical measures for the bubble chord length distribution in a bubble column with and without internals at *H/D* = 5 and Ug=0.45 m/s

measurements	Fully developed region				Sparger region			
	With internals		Without internals		With internals		Without internals	
	Center	Wall	Center	Wall	Center	Wall	Center	Wall
Mean (cm)	0.63	0.59	0.67	0.50	0.51	0.50	0.61	0.52
Varince (cm^2)	0.4692	0.7032	0.5346	0.6770	0.6063	0.3633	0.4796	0.3830

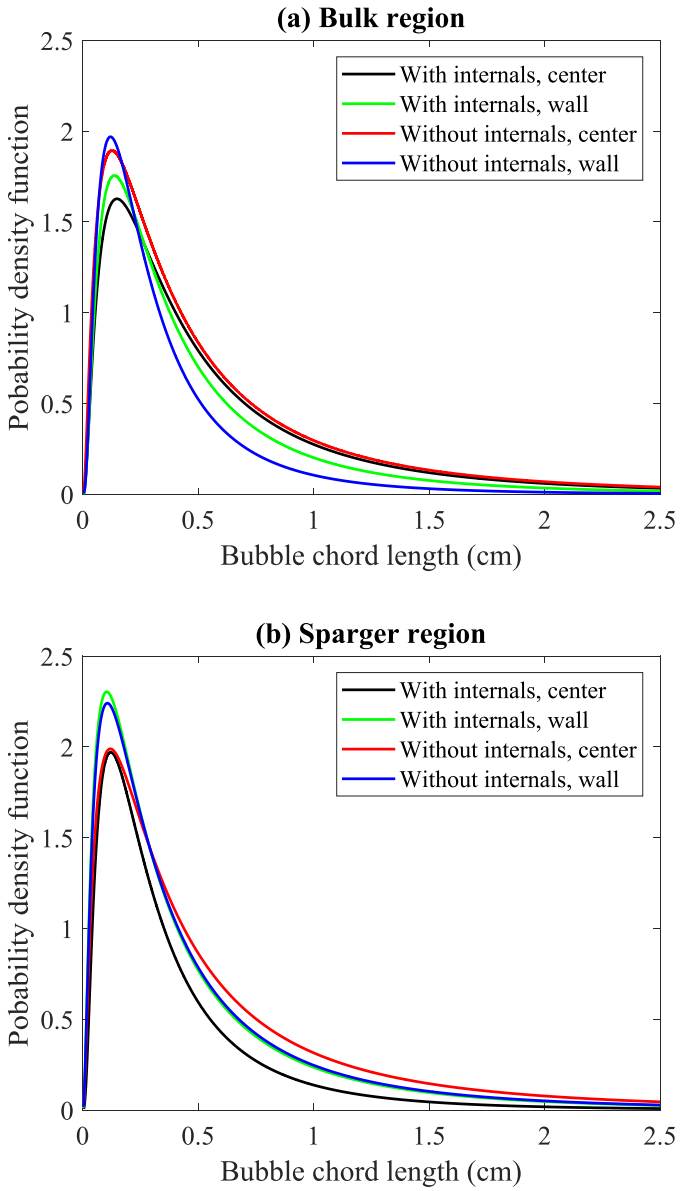

Figure 13. The effect of internals on the bubble chord lengths in the center and wall region of the bubble column at Ug=0.45 m/s (a) The fully developed flow region and (b) The sparger region.

Results show a remarkable increase in the bubble pass frequency accompanying with increasing the superficial gas velocity, and the presence of internals. The same phenomena have been found by Manjrekar and Dudukovic [52] and Wu et al. [55] regarding the superficial gas velocity effect and Kagumba and Al-Dahhan [5] regarding the internals effect. The increase in the bubble pass frequency is the result of the increase in the rate of breakup, which is enhanced significantly by the presence of internals and an increase in the superficial gas velocity, while, slightly increased with a decrease the aspect ratio. However, bubble passage frequency in sparger region is less than that in the fully developed flow region which indicates an increase in the rate of breakup with the coalescence rate along axial rising.

Combining the results of the bubble pass frequency and the bubble chord length distribution, help to enhance the understanding of the variations in local gas holdups at different dynamic liquid levels and internals existence with the increase in the superficial gas velocity. In the case of a bubble column without internals, an increase in the superficial gas velocity increases the breakup rate. The large bubbles, by nature, move in the center of bubble column as a result of the effect of wall shear stress and the difference in buoyancy force, including the newly created large bubbles in the center of the column. Therefore, bubbles move at a high frequency, which means more bubbles appear in the center region and cause the increase in the gas holdup. Meanwhile, most small bubbles are concentrating in the wall region due to encountering a low drag force and move with low frequency. Thus, the local gas holdup in the center of the bubble column becomes larger than that in the wall region, and with a further increase in gas velocity, the difference becomes much more apparent.

In the presence of internals increase the breakup rate, and that would reduce the bubble chord length, as mentioned earlier. Therefore, the population of small bubble size will be increased, especially in the wall region, in turn, increases the local gas holdup in this region.

5.6. BUBBLE RISE VELOCITY

As mentioned before, all the bubble properties were measured depending on that bubbles which moving in the upward direction. Therefore, the bubble rise velocity as a concept has been used to explain the bubble velocity. Further, as a result to the effect of global liquid circulation, most of the bubbles that are close to the wall of the bubble column are moving in a downward direction [47], and hence, the bubble rise velocity in the wall region has not been considered in this work. Although the bubble rise velocity represents the residence time of the gas phase in the reactor, which is the reactant material, it also provides insightful information that is related to the liquid structure. Moreover, the bubble rise velocity confirms the integrity of the attribution for the impact of parameters on the bubble properties. As much as the bubble size increases the bubble rise velocity is being increased. Figure 16 and Figure 17 illustrate the impact of the aspect ratio variation on the bubble rise velocity distribution in histogram form with normal distribution the fully developed flow region, and sparger region, respectively. However, increasing the aspect ratio exhibits no significant effect on the bubble rise velocity in case of the bubble column with and without internals both in the fully developed flow region and the sparger region, in a similar trend of the impact on the bubble chord length. While the existence of internals and the increasing in the superficial gas velocity significantly would promot the bubble rise

velocity in the fully developed flow region and the sparger region as illustrated in Figure 18 and Figure 19, respectively. Meanwhile, the effect of the superficial gas velocity is higher compared to the presence of internals. However, the change in the bubble rise velocity is attributed to the increase in the bubble breakup rate, which in turn reduces the bubble size. Therefore, the presence of internals and the superficial gas velocity appear to have the most impact compared to the aspect ratio. Similar results have been reported by Youssef et al. [47], and Kagumba and Al-Dahhan [5], where the presence of internals and the superficial gas velocity effects have been investigated in a bubble column with a covering cross area of 25%. According to Youssef et al. [47], and Kagumba and Al-Dahhan [5], the existence of internals and an increase in the superficial gas velocity significantly enhance the decrease of the bubble rise velocity, and this is attributed to the enhancement in the bubble breakup rate.

5.7. BUBBLE SPECIFIC INTERFACIAL AREA

Specific interfacial area is defined as the interface area per unit volume of the liquid phase. It is directly related to enhancing the mass transfer rate, and hence, it is a key indicator to increase the rate of reaction. Based on that, the interfacial bubble area is increasing as long the volume of the bubble is reduced, and in the meantime there is an increase in the bubble pass frequency, or in other words, an increase in the bubble break-up rate. In addition, the bubbles with spherical shape give a lower interfacial area due to the low surface area and the large volume that occupied. While bubbles with the same surface area but with an irregular shape give a high interfacial area.

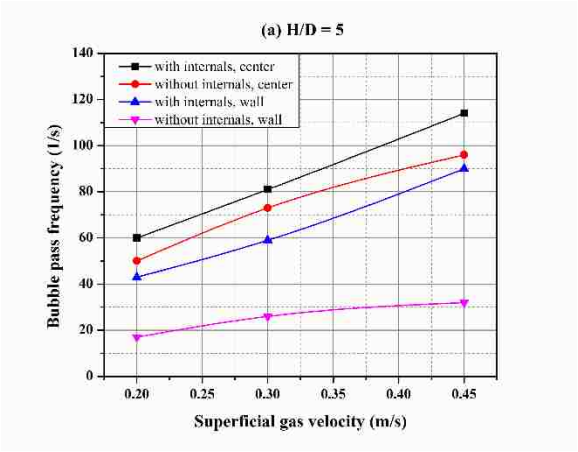

Figure 14. The effect of the internals and superficial gas velocity on the bubble pass frequency in the fully developed region

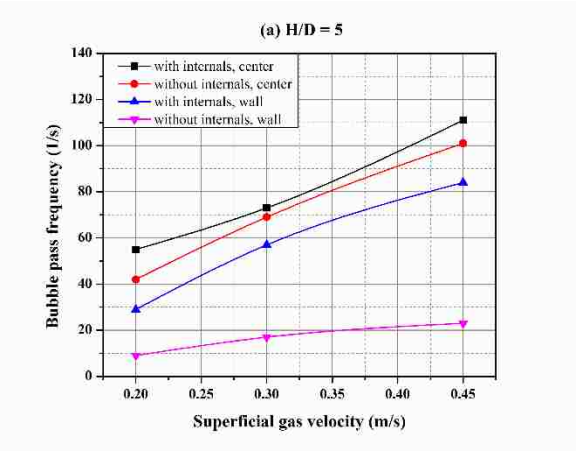

Figure 15. The effect of the internals and superficial gas velocity on the bubble pass frequency in the sparger region

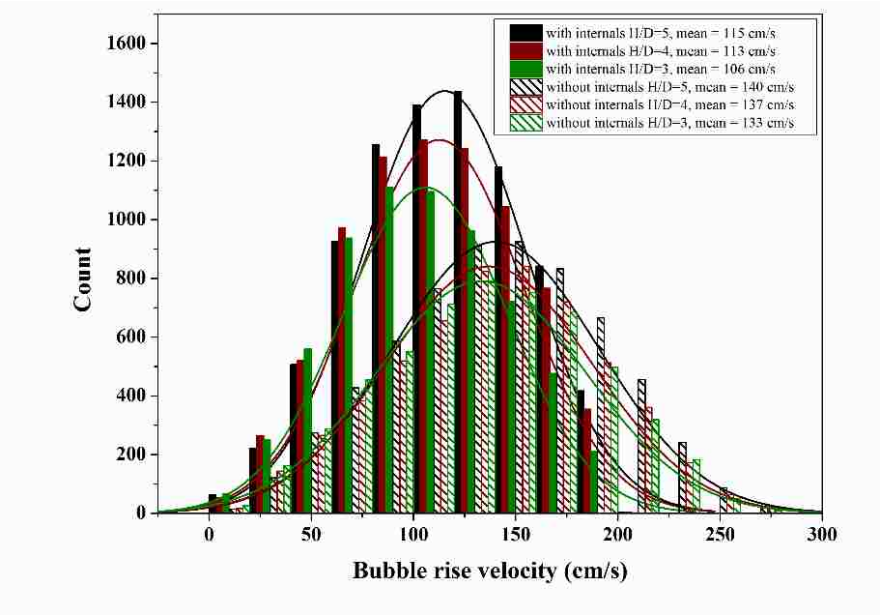

Figure 16. Aspect ratio effect on the bubble rise velocity in the fully developed flow region of a bubble column with and without internals, Ug=0.45 m/s

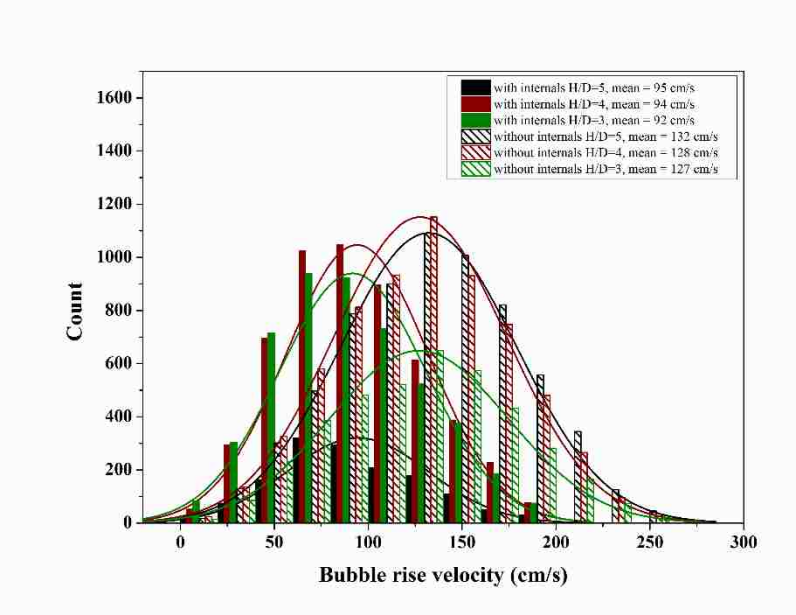

Figure 17. Aspect ratio effect on the bubble rise velocity in the sparger region of a bubble column with and without internals, Ug=0.45 m/s

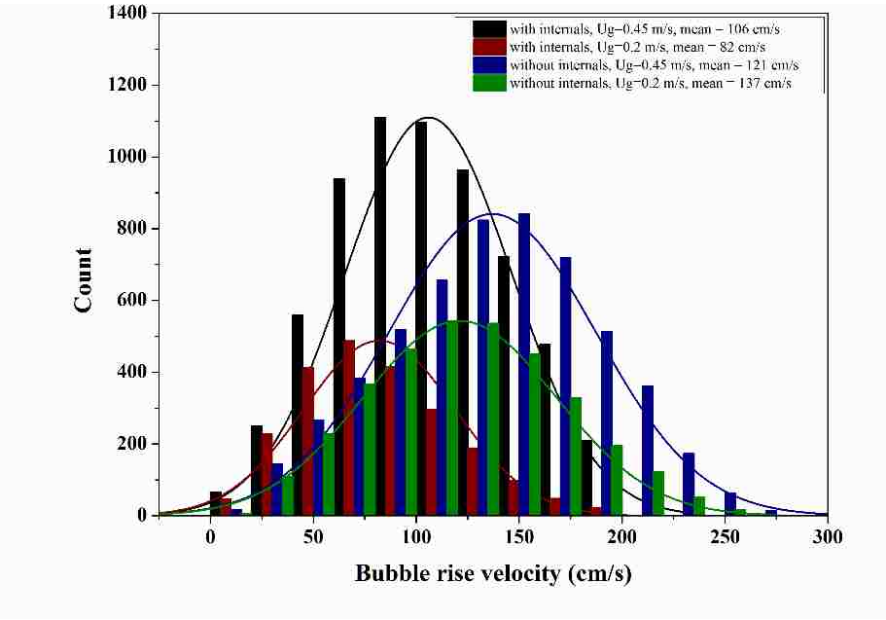

Figure 18. Internals effect on the bubble rise velocity in the fully developed flow region, *H/D* = 5 and r/R = 0.0

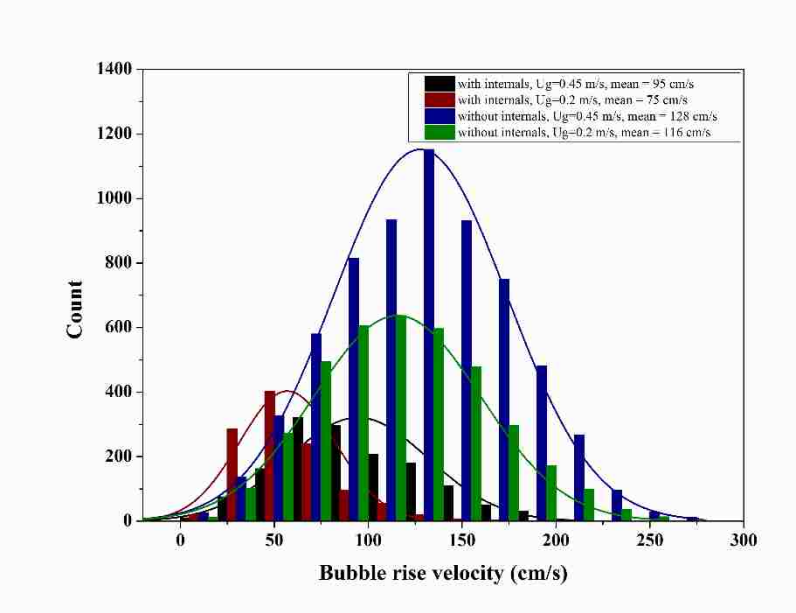

Figure 19. Internals effect on the bubble rise velocity in the sparger region, *H/D* = 5 and r/R = 0.0

Therefore, the matter attribution of the effect of internals and gas velocity on the interfacial bubble area is related to the shape of the bubbles as well. The impact of internals and superficial gas velocity U_g that calculated based on the free CSA of bubble column in the fully developed flow region and the sparger region are illustrated in Figure 20. The trend of the specific interfacial area is similar to that of the radial profiles of local gas holdup and the bubble frequency in the center and wall region of the bubble column. A remarkable increase in the interfacial bubble area is exhibited with the presence of internals and an increase in the gas velocity U_g. Although the bubbles' shape deformed as the superficial gas velocity increases, gas velocity appears to have a lower effect than the effect of internals. This could be that attributed to the fact that all the gas velocities are in the range of the churn turbulence region, and hence, most bubbles are deformed and have an irregular shape. Therefore, an increase in the bubble break-up rate is the key upfront attribution to explain the internals effect, which in turn increases the bubble pass frequency and reduces the bubble chord length distribution. Consequently, in the presence of internals, increasing the superficial gas velocity exhibits a significant effect on the interfacial area in both the fully developed flow region and the sparger region. In contrast, in the absence of internals, the superficial gas velocity effect was limited in the fully developed flow region.

Figure 21 shows the impact of the aspect ratio variation on the interfacial bubble area in the fully developed flow region and the sparger region. The variation in the aspect ratio shows a slight effect in a bubble column with internals. While this variation appears to have more influence in the absence of internals, typically in the radial profile range r/R = 0 to 0.69 (i.e., until the inversion point) where the axial liquid velocity moves in the

negative direction. Therefore, most of the bubbles in this region will be in the same direction due to the setup limitation (the four-point fiber optical probe was inserted in a downward orientation, which in turn measures bubble direction upward). In general, the existence of internals administrates the enhancement in the bubble interfacial area as a reasonable cause to increase the bubble break-up rate, and hence, increases the bubble numbers, and decreases the bubble chord length distribution. Meanwhile, as shown in Figures 20 and 21, the wall region exhibits an enhancement in the specific interfacial area by the presence of internals more than the central region. That could be attributed to the configuration of the internals and the distance between the tubes that have the capability to distribute the bubbles radially based on the size and in turn uniformly increase the number of bubbles along with the wall region.

6. CONCLUSIONS

In this work, the effects of the heat exchanger internals and the low aspect ratios of dynamic liquid level on the bubble properties have been investigated using a pilot-plant bubble column reactor. Radial profiles of the local gas holdup in the fully developed flow region and the sparger region were examined, and the fully developed flow region was demarcated. In addition, the radial profile distributions of the bubble chord lengths, rise velocity, bubble frequency, and interfacial area were studied. All bubble properties have been measured based on the bubbles that move in the upward direction. The results show that the presence of internals slightly increases the overall gas holdup, whereas,

significantly increases the local gas holdup, particularly at the wall region of the bubble column.

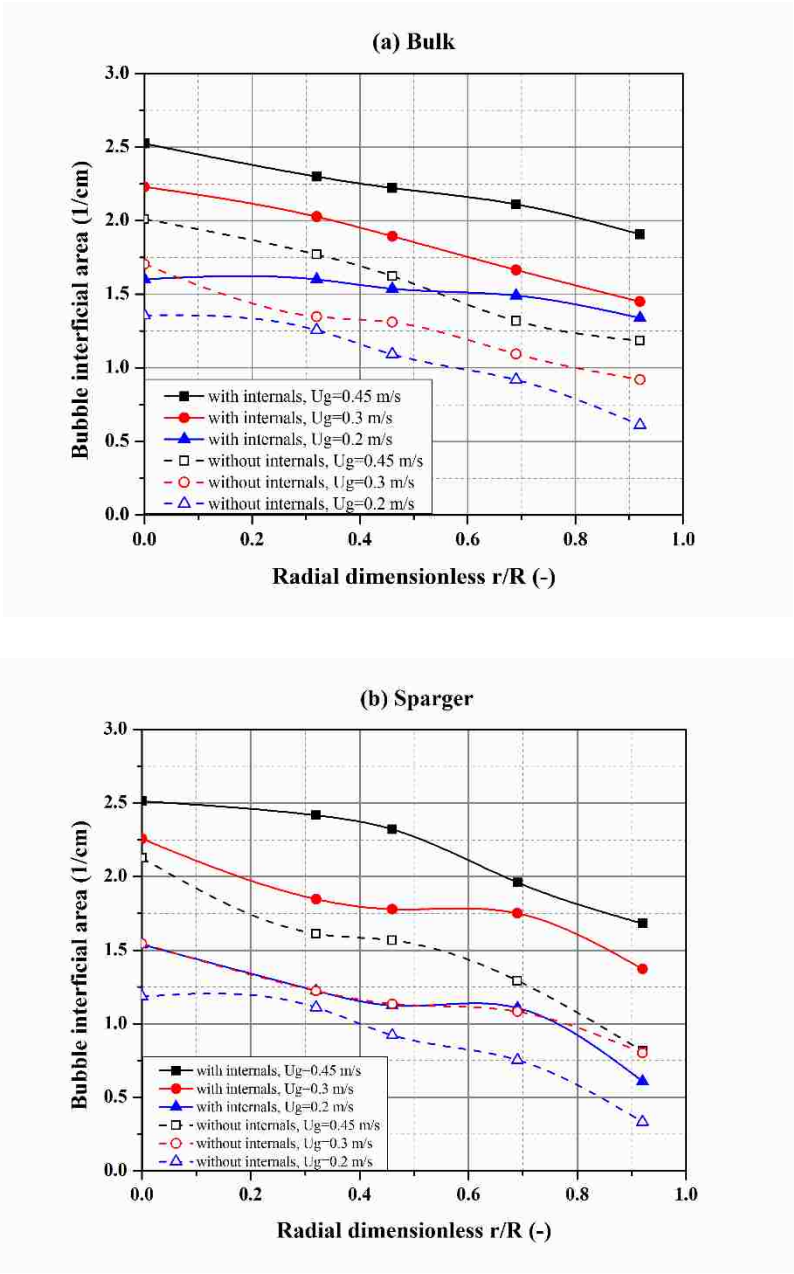

Figure 20. Internal and superficial gas velocity Ug effects on the interfacial area at *H/D*=5 in (a) Fully developed flow region, and (b) Sparger region

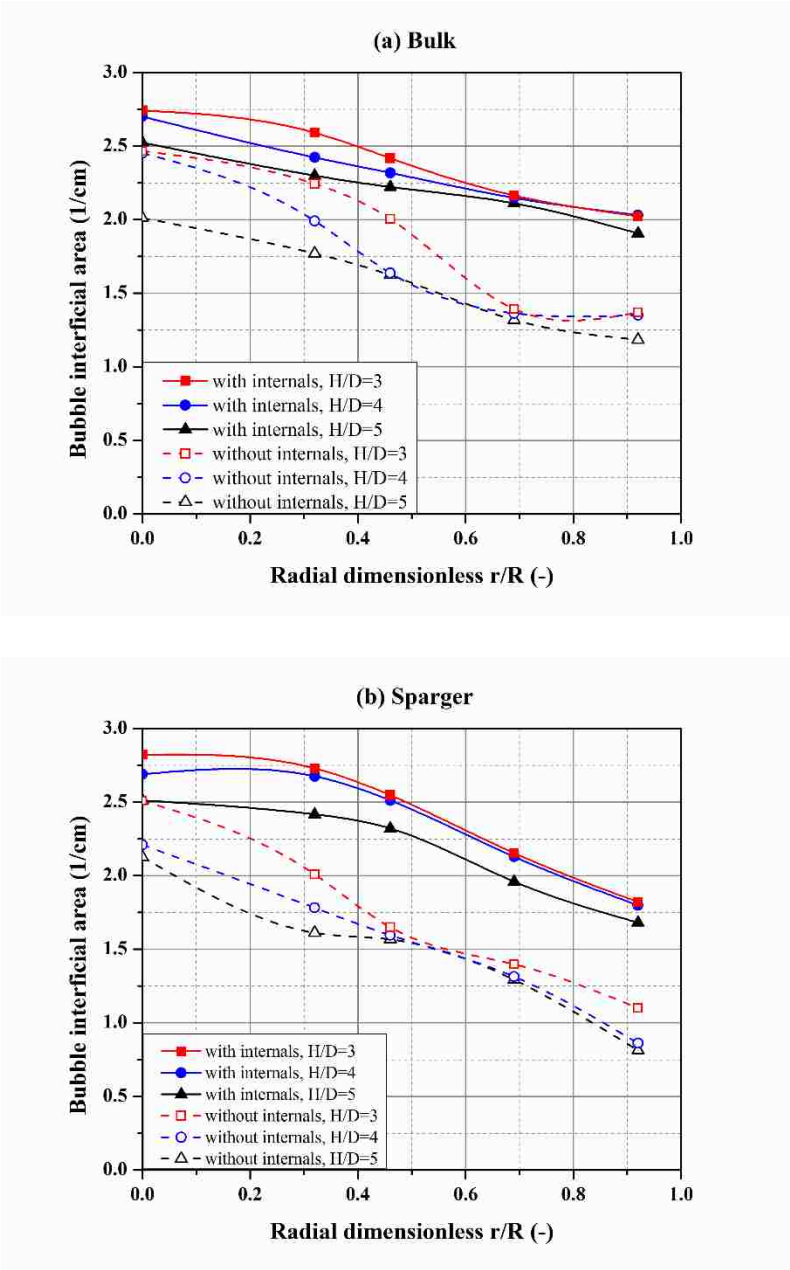

Figure 21. Aspect ratio effect on the radial profile of the bubble interfacial area in (a) Fully developed flow region, and (b) Sparger region

Meanwhile, an increasing the superficial gas velocity U_g promotes the overall gas holdup and the local gas holdup, and this impact increases with the presence of the internals, particularly in the wall region of the bubble column. Thus, the presence of

internals would decrease the difference in the local gas holdup between the center and wall region of the bubble column, and hence, it is expected that inhibits the liquid recirculation.

The presence of internals and decreasing the superficial gas velocity, in turn, inhibit the bubble chord length. This phenomenon could be attributed to the increasing the bubble breakup rate due to the turbulent eddies effects, which results in the reduction the bubble rise velocity and increasing the local gas holdup, interfacial area, and bubble frequency. in bubble column with internals, the radial profile of the local gas holdup exhibits a nearly flat profile due to reducing the difference in the local gas holdup between the wall and the center regions. Therefore, the radial profiles of the bubble properties are significantly affected by the structure of the internals. Hence, the effects of the distances between the tubes, the internals configuration, and the size of the tubes on the bubble properties and the liquid velocity are worth to being conducted experimentally and considered properly in the modeling and the CFD simulations.

The effects of the internals and the superficial gas velocity have exhibited significant effects on the fully developed flow region. While, the aspect ratio of the dynamic liquid level has a slight effect on the fully developed flow regime, particularly, in the case of bubble column with internals. The flow develops rapidly during the existence of internals and the operating in low superficial gas velocity U_g. An increase in the dynamic liquid level also tends to delays the appearance of the fully developed region, and this effect is limited in the absence of internals.

Finally, a high aspect ratio provides the bubbles enough residence time to reach the stable bubble size, where the bubble coalescence and breakup rates reach the equilibrium state. Therefore, as the aspect ratio increases, the local gas holdup decreases. In addition,

the variation of the aspect ratio and the presence of internals exhibit a slight influence on the sparger region. This shows alignment with the previous studies, which report that the sparger region is sensitive to the distributor design.

NOMENCLATURE

a = bubble interfacial area (cm^2)

H = height of bubble column reactor (m)

H_0 = initial liquid level (m)

H_S = static liquid level (m)

D, D_C = bubble column diameter (m)

D_r = depth of rectangular bubble column (m)

H/D = aspect ratio, ratio of height of dynamic liquid level to bubble column diameter (-)

CFM = cube foot per minute

d_0 = diameter of hole distribution (mm)

N = total number of bubbles

$N_{measured}$ = accept bubble

L_i = bubble chord length (cm)

TFM-PBM = two fluid model-population bubble model

TKE = turbulent kinetic energy

T = operating temperature (K)

P = operating presser (psi)

T_i = time of bubble hits the tip (i)

U_g = superficial gas velocity (m/s)

U_L = liquid velocity (m/s)

V = velocity vector

X_i, Y_i, Z_i = Cartesian coordinates

$X^{'}$, $Y^{'}$, $Z^{'}$ = Spherical coordinates

Z = axial location (m)

Greek letters

ε_G = overall gas holdup (-)

ε_g = local gas holdup (-)

β, γ, ϕ = angles

α = aspect ratio of ellipsoidal bubble

Subscripts

g, G = gas phase

i = 1, 2, 3

REFERENCES

[1] F. M. Pereira *et al.*, "Evaluation of fatty acids production by Chlorella minutissima in batch bubble-column photobioreactor," *Fuel*, vol. 230, no. April, pp. 155–162, 2018.

[2] Joelianingsih, H. Nabetani, Y. Sagara, A. H. Tambunan, and K. Abdullah, "A continuous-flow bubble column reactor for biodiesel production by non-catalytic transesterification," *Fuel*, vol. 96, pp. 595–599, 2012.

[3] H. Ishibashi, M. Onozaki, M. Kobayashi, J. -i. Hayashi, H. Itoh, and T. Chiba, "Gas holdup in slurry bubble column reactors of a 150t/d coal liquefaction pilot plant process," *Fuel*, vol. 80, no. 5, pp. 655–664, 2001.

[4] P. Rollbusch *et al.*, "Experimental investigation of the influence of column scale, gas density and liquid properties on gas holdup in bubble columns," *Int. J. Multiph. Flow*, vol. 75, pp. 88–106, 2015.

[5] M. Kagumba and M. H. Al-Dahhan, "Impact of internals size and configuration on bubble dynamics in bubble columns for alternative clean fuels production," *Ind. Eng. Chem. Res.*, vol. 54, no. 4, pp. 1359–1372, 2015.

[6] A. A. Youssef and M. H. Al-Dahhan, "Impact of internals on the gas holdup and bubble properties of a bubble column," *Ind. Eng. Chem. Res.*, vol. 48, no. 17, pp. 8007–8013, 2009.

[7] M. K. Al Mesfer, A. J. Sultan, and M. H. Al-Dahhan, "Impacts of dense heat exchanging internals on gas holdup cross-sectional distributions and profiles of bubble column using gamma ray Computed Tomography (CT) for FT synthesis," *Chem. Eng. J.*, vol. 300, pp. 317–333, 2016.

[8] K. Zhang *et al.*, "Low-temperature methanol synthesis in a circulating slurry bubble reactor," *Fuel*, vol. 82, no. 2, pp. 233–239, 2003.

[9] W.-D. Deckwer and A. Schumpe, "Improved Tools For Bubble Column Reactor Design and scal-up," *Chem. Eng. Sci.*, vol. 48, no. 5, pp. 889–911, 1993.

[10] J. Chen *et al.*, "Fluid dynamic parameters in bubble columns with internals," *Chem. Eng. Sci.*, vol. 54, no. 13–14, pp. 2187–2197, 1999.

[11] M. Kagumba, H. Al-Naseri, and M. H. Al-Dahhan, "A new contact time model for the mechanistic assessment of local heat transfer coefficients in bubble column using both the four-optical fiber probe and the fast heat transfer probe-simultaneously," *Chem. Eng. J.*, vol. 361, no. December 2018, pp. 67–79, 2019.

[12] A. A. Jasim, A. J. Sultan, and M. H. Al-Dahhan, "Impact of heat exchanging internals configurations on the gas holdup and bubble properties in a bubble column," *Int. J. Multiph. flow*, vol. 112, pp. 63–82, 2019.

[13] A. A. Jasim, A. J. Sultan, and M. H. Al-Dahhan, "Influence of heat-exchanging tubes diameter on the gas holdup and bubble dynamics in a bubble column," *Fuel*, vol. 236, no. March 2018, pp. 1191–1203, 2019.

[14] B. C. Ong, P. Gupta, A. Youssef, M. Al-Dahhan, and M. P. Duduković, "Computed Tomographic Investigation of the Influence of Gas Sparger Design on Gas Holdup Distribution in a Bubble Column," *Ind. Eng. Chem. Res.*, vol. 48, no. 1, pp. 58–68, 2009.

[15] A. Shaikh and M. Al-Dahhan, “Scale-up of bubble column reactors: A review of current state-of-the-art,” *Ind. Eng. Chem. Res.*, vol. 52, no. 24, pp. 8091–8108, 2013.

[16] P. M. Wilkinson, A. P. Spek, and L. L. van Dierendonck, “Design parameters estimation for scale-up of high-pressure bubble columns,” *AIChE J.*, vol. 38, no. 4, pp. 544–554, 1992.

[17] A. Esmaeili, S. Farag, C. Guy, and J. Chaouki, “Effect of elevated pressure on the hydrodynamic aspects of a pilot-scale bubble column reactor operating with non-Newtonian liquids,” *Chem. Eng. J.*, vol. 288, pp. 377–389, 2016.

[18] S. Kumar and A. Khanna, “Experimental analysis and development of correlations for gas holdup in high pressure slurry co-current bubble columns,” *Korean J. Chem. Eng.*, vol. 31, no. 11, pp. 1964–1972, 2014.

[19] N. Rados, A. Shaikh, and M. H. Al-Dahhan, “Phase Distribution in a High Pressure Slurry Bubble Column via a Single Source Computed Tomography,” *Can. J. Chem. Eng.*, vol. 83, no. February, 2005.

[20] A. Shaikh and M. Al-Dahhan, “Characterization of the hydrodynamic flow regime in bubble columns via computed tomography,” *Flow Meas. Instrum.*, vol. 16, pp. 91–98, 2005.

[21] C. Wu, M. H. Al-Dahhan, and A. Prakash, “Heat transfer coefficients in a high pressure bubble column,” *Chem. Eng. Sci.*, vol. 62, no. 1–2, 2007.

[22] A. Forret, J. M. Schweitzer, T. Gauthier, R. Krishna, and D. Schweich, “Influence of scale on the hydrodynamics of bubble column reactors: An experimental study in columns of 0.1, 0.4 and 1 m diameters,” *Chem. Eng. Sci.*, vol. 58, no. 3–6, pp. 719–724, 2003.

[23] G. Hebrard, D. Bastoul, and M. Roustan, “Influence of the gas sparger on the hydrodynamic behavior of bubble columns,” *Chem. Eng. Res. Des.*, vol. 74, no. 3, pp. 406–414, 1996.

[24] S. B. Kumar, “Computed Tomographic Measurements of Void Fraction and Modeling of the Flow in Bubble Coulnms,” Washington Univeristy, St. Louis, MO, 1994.

[25] S. Sasaki, K. Uchida, K. Hayashi, and A. Tomiyama, “Effects of column diameter and liquid height on gas holdup in air-water bubble columns,” *Exp. Therm. Fluid Sci.*, vol. 72, pp. 67–74, 2017.

[26] M. W. Haque, K. D. P. Nigam, and J. B. Joshi, “Optimum gas sparger design for bubble columns with a low height-to-diameter ratio,” *Chem. Eng. J.*, vol. 33, no. 2, pp. 63–69, 1986.

[27] O. M. Basha and B. I. Morsi, “Effects of Sparger and Internals Designs on the Local Hydrodynamics in Slurry Bubble Column Reactors Operating under Typical Fischer-Tropsch Process Conditions - I,” *Int. J. Chem. React. Eng.*, vol. 0, no. 0, pp. 1–19, 2017.

[28] G. Besagni, A. Di Pasquali, L. Gallazzini, E. Gottardi, L. P. M. Colombo, and F. Inzoli, “The effect of aspect ratio in counter-current gas-liquid bubble columns: Experimental results and gas holdup correlations,” *Int. J. Multiph. Flow*, vol. 94, pp. 53–78, 2017.

[29] S. Sasaki, K. Hayashi, and A. Tomiyama, “Effects of liquid height on gas holdup in air–water bubble column,” *Exp. Therm. Fluid Sci.*, vol. 72, pp. 67–74, 2016.

[30] J. Chen, P. Gupta, S. Degaleesan, M. H. Al-Dahhan, M. P. Duduković, and B. A. Toseland, “Gas holdup distributions in large-diameter bubble columns measured by computed tomography,” *Flow Meas. Instrum.*, vol. 9, no. 2, pp. 91–101, 1998.

[31] G. Besagni, F. Inzoli, G. De Guido, and L. A. Pellegrini, “The dual effect of viscosity on bubble column hydrodynamics,” *Chem. Eng. Sci.*, vol. 158, no. June 2016, pp. 509–538, 2017.

[32] B. N. Thorat and J. B. Joshi, “Regime transition in bubble columns: Experimental and predictions,” *Exp. Therm. Fluid Sci.*, vol. 28, no. 5, pp. 423–430, 2004.

[33] G. Besagni, L. Gallazzini, and F. Inzoli, “Effect of gas sparger design on bubble column hydrodynamics using pure and binary liquid phases,” *Chem. Eng. Sci.*, vol. 176, pp. 116–126, 2018.

[34] A. Forret, J. M. Schweitzer, T. Gauthier, R. Krishna, and D. Schweich, “Liquid dispersion in large diameter bubble columns, with and without internals,” *Can. J. Chem. Eng.*, vol. 81, no. 3–4, pp. 360–366, 2003.

[35] A. K. Jhawar and A. Prakash, “Bubble column with internals: Effects on hydrodynamics and local heat transfer,” *Chem. Eng. Res. Des.*, vol. 92, no. 1, pp. 25–33, 2014.

[36] F. Larachi, D. Desvigne, L. Donnat, and D. Schweich, “Simulating the effects of liquid circulation in bubble columns with internals,” *Chem. Eng. Sci.*, vol. 61, no. 13, pp. 4195–4206, 2006.

[37] X. Guo and C. Chen, “Simulating the impacts of internals on gas–liquid hydrodynamics of bubble column,” *Chem. Eng. Sci.*, vol. 174, pp. 311–325, 2017.

[38] G. Besagni and F. Inzoli, “Comprehensive experimental investigation of counter-current bubble column hydrodynamics: Holdup, flow regime transition, bubble size distributions and local flow properties,” *Chem. Eng. Sci.*, vol. 146, pp. 259–290, 2016.

[39] S. Nedeltchev, S. Aradhya, F. Zaid, and M. Al-Dahhan, “Flow Regime Identification in Three Multiphase Reactors Based on Kolmogorov Entropies Devived from gauge Pressure Fluctuations,” *J. Chem. Eng. Japan*, vol. 45, no. 9, pp. 757–764, 2012.

[40] X. Guan and N. Yang, “CFD simulation of pilot-scale bubble columns with internals: Influence of interfacial forces,” *Chem. Eng. Res. Des.*, vol. 126, pp. 109–122, 2017.

[41] G. Bloch, “Axial and Radial Dispersion in a Large-Diameter Bubble Column Reactor at Low Height-to- Diameter Ratios,” *Chem. Ing. Tech.*, vol. 87, no. No. 6, pp. 756–761, 2015.

[42] A. J. Sultan, L. S. Sabri, and M. H. Al-Dahhan, “Investigating the influence of the configuration of the bundle of heat exchanging tubes and column size on the gas holdup distributions in bubble columns via gamma-ray computed tomography,” *Exp. Therm. Fluid Sci.*, vol. 98, no. February, pp. 68–85, 2018.

[43] G. Besagni and F. Inzoli, “Influence of internals on counter-current bubble column hydrodynamics: Holdup, flow regime transition and local flow properties,” *Chem. Eng. Sci.*, vol. 145, pp. 162–180, 2016.

[44] M. K. Al Mesfer, A. J. Sultan, and M. H. Al-Dahhan, “Study the Effect of Dense Internals on the Liquid Velocity Field and Turbulent Parameters in Bubble Column for Fischer–Tropsch (FT) Synthesis by Using Radioactive Particle Tracking (RPT) Technique,” *Chem. Eng. Sci.*, vol. 161, pp. 228–248, 2017.

[45] K. J. H. George, A. K. Jhawar, and A. Prakash, “Investigations of flow structure and liquid mixing in bubble column equipped with selected internals,” *Chem. Eng. Sci.*, vol. 170, pp. 297–305, 2017.

[46] R. S. Abdulmohsin and M. H. Al-Dahhan, “Impact of internals on the heat-transfer coefficient in a bubble column,” *Ind. Eng. Chem. Res.*, vol. 51, no. 7, pp. 2874–2881, 2012.

[47] A. A. Youssef, M. E. Hamed, J. T. Grimes, M. H. Al-Dahhan, and M. P. Duduković, “Hydrodynamics of pilot-scale bubble columns: Effect of internals,” *Ind. Eng. Chem. Res.*, vol. 52, no. 1, pp. 43–55, 2013.

[48] J. J. Frijlink, “Physical aspects of gassed suspension reactors,” Delft University of Technology, 1987.

[49] J. Xue, M. Al-dahhan, M. P. Dudukovic, and R. F. Mudde, “Bubble Dynamics Measurements Using Four-Point Optical Probe,” *Can. J. Chem. Eng.*, vol. 81, no. August, pp. 375–381, 2003.

[50] J. Xue, M. Al-Dahhan, M. P. Dudukovic, and R. F. Mudde, “Four-point optical probe for measurement of bubble dynamics: Validation of the technique,” *Flow Meas. Instrum.*, vol. 19, no. 5, pp. 293–300, 2008.

[51] G. E. P. Box, W. G. Hunter, and J. S. Hunter, *Statistics for Experimenters An Introduction to Design, Data Analysis, and Model Bulding*. Wiley, 1978.

[52] I. Kataoka, M. Ishii, and A. Serizawa, “Local Equationtion And Measurements Of Interfacial Area Concentration In Two-Phase Flow,” *Int. J. Multiph. Flow*, vol. 12, no. 4, pp. 505–529, 1986.

[53] A. B. Pandit and Y. K. Doshi, “Mixing time studies in bubble column reactor with and without internals,” *Int. J. Chem. React. Eng.*, vol. 3, pp. 1–23, 2005.

[54] D. Colella, D. Vinci, R. R. Bagatin, M. Masi, and E. A. Bakr, “A study on coalescence and breakage mechanisms in three different bubble columns,” *Chem. Eng. Sci.*, vol. 54, pp. 4767–4777, 1999.

[55] J. Xue, “Bubble Velocity, Size and Interfacial Area Measurements in Bubble columns,” Washington Univeristy, Saint Louis, 2004.

[56] D. B.Bukur and J. G.Daly, “Gas hold-up in bubble columns for Fischer-Tropsch synthesis,” *Chem. Eng. Sci.*, vol. 42, no. 12, pp. 2967–2969, 1987.

[57] U. Parasu Veera and J. B. Joshi, “Measurement of gas hold-up profiles by gamma ray tomography: Effect of spager design and height of dispersion in bubble columns,” *Chem. Eng. Res. Des.*, vol. 77, no. Part A, pp. 303–317, 1999.

[58] A. Shaikh and M. H. Al-Dahhan, “A Review on Flow Regime Transition in Bubble Columns,” *Int. J. Chem. React. Eng.*, vol. 5, 2007.

[59] A. Serizawa and I. Kataoka, “Turbulence suppression in bubbly two-phase flow,” *Nucl. Eng. Des.*, vol. 122, pp. 1–16, 1990.

[60] K. Akita and F. Yoshida, “Bubble Size, Interfacial Area, and Liquid-Phase Mass Transfer Coefficient in Bubble Columns,” *Ind. Eng. Chem. Process Des. Dev.*, vol. 13, no. 1, pp. 84–91, 1974.

[61] R. Pohorecki, W. Moniuk, A. Zdro, and P. Bielski, “Hydrodynamics of a pilot plant bubble column under elevated temperature and pressure,” vol. 56, pp. 1167–1174, 2001.

[62] W. Luewistutthichat, A. Tsutsumi, and K. Yoshida, “Bubble Characteristics in Multi-Phase flow system: Bubble Sizes and Size Distributions,” *J. Chem. Eng. Japan*, vol. 30, no. 3, pp. 461–466, 1986.

[63] A. Yasunishi, M. Fukuma, and K. Muroyama, “Measurement Of Behavior Of Gas Bubbles And Gas Holdup In A Slurry Bubble Column By A Dual Electroresistivity Probe Method,” *J. Chem. Eng. Japan*, vol. 19, no. 5, pp. 444–449, 1986.

[64] C. Wu, K. Suddard, and M. H. Al-Dahhan, “Bubble Dynamics Investigation in a Slurry Bubble Column,” *AIChE J.*, vol. 54, no. 5, pp. 1203–1212, Jan. 2008.

[65] S. Schlüter, A. Steiff, and P.-M. Weinspach, “Heat transfer in two- and three-phase bubble column reactors with internals,” *Chem. Eng. Process. Process Intensif.*, vol. 34, no. 3, pp. 157–172, Jun. 1995.

[66] M. Kagumba, “Heat transfer and bubble dynamics in bubble and slurry bubble columns with internals for Fischer-Tropsch synthesis of clean alternative fuels and chemicals,” Missouri University of Science and Technology, 2013.

[67] O. N. Manjrekar and M. P. Dudukovic, “Application of a 4-point optical probe to a Slurry Bubble Column Reactor,” *Chem. Eng. Sci.*, vol. 131, pp. 313–322, 2015.

II. THE IMPACTS OF SOLIDS LOADING AND LOW ASPECT RATIO ON THE BUBBLE PROPERTIES AND FULLY DEVELOPED REGION IN A PILOT-PLANT SCALE SLURRY BUBBLE COLUMN WITH INDUSTRIAL HEAT EXCHANGING INTERNALS FOR FISCHER-TROPSCH (F-T) SYNTHESIS

ABSTRACT

In this work, for the first time, the effects of the solids loading and the low aspect ratio on the bubble dynamics and the fully developed flow in an industrial-size pilot-plant bubble column with the presence of industrial heat exchanging internals, which covers 24% of the cross-section area of the column to simulate the Fischer-Tropsch (F-T) column, have been investigated using an advanced 4-point optical probe. The solids concentrations (glass beads of diameter 60-150 μm) and the superficial gas velocities (calculated based on the free cross-section for flow column) are varied from 0.0 to 25 vol% and 0.2 to 0.45 m/s, respectively, while, the studied aspect ratios are H/D = 3, 4, and 5. The results show that the presence of solids slightly increases the overall gas holdup and significantly affects the radial distributions of the bubble properties, including the local gas holdup, bubble chord length, bubble rise velocity, bubble passing frequency, and bubble interfacial area, in both the fully developed flow and the sparger regions. The increase in the solids loading decreases the local gas holdup, bubble frequency, and interfacial area, especially in the wall region, while, the presence of the solids increases the bubble chord length and bubble rise velocity. Further, the presence of internals decreases the solids loading influence on the bubble properties and exhibits a strong control for the distributions of bubble properties at all solids loading levels. The aspect ratio appears to have an insignificant effect on the

bubble properties in the presence of the solids. However, the fully developed flow region exhibits a high sensitivity toward the solids loading, aspect ratio, and changes in superficial gas velocity. Increase in aspect ratio and the solids loading show that the fully developed flow region begins at lower axial locations, while an increase the superficial gas velocity delays the transition to fully developed flow to a higher axial location.

1. INTRODUCTION

In the recent decade, the demand for energy has been increased due to an increase in the human population and technology development. This leads to increased oil consumption and the rated air pollution. An alternative, environmentally friendly fuel is a part of a possible solution to these problems. Fischer-Tropsch (F-T) synthesis is a well-established process to convert syngas (CO and H_2) obtained from coal, natural gas, biogas and biomass to liquid fuel (GTL), which has been used to produce alternative fuels of free sulfur and metals. Slurry bubble column reactor (SBCR) is a desirable reactor due to its high selectivity and conversion, excellent thermal control, low maintenance and high degree of mixing [1]–[3]. The SBCR is classified as a three-phase flow system including gas (syngas), liquid (fuel product), and fine solid (fine catalyst size). The reaction that takes place in the F-T process is highly exothermic, and hence, a heat exchanging internals are essential part of the reactor design and geometry to keep the reaction temperature under control at the desired level [4].

Numerous works have been conducted aim to improve the SBCR performance by investigating the impact of different parameters on the bubble dynamics and liquid

hydrodynamics. Among these parameters are gas and liquid phase properties, column dimension, sparger design, operating conditions (pressure, temperature), solids loading (concentration C_s) and particles size d_p. Chen et al. [5]. Schafer et al. [6], Besagni and Inzoli [7], Veera et al. [8], and Rollbusch et al. [9] studied the impact of fluid properties (liquid and gas) on the bubble dynamics in a bubble column reactor. Data obtained show a significant effect for the variation in the fluid properties on the bubble dynamics, where an increase in the viscosity of liquid phase led to increasing the bubble size and bubble rise velocity, which leads to reduce the gas holdup and interfacial area. Whereas increased density of gas phase drastically increases the gas holdup. The impact of operating conditions including pressure and temperature have been studied by Schafer et al. [6], Shin et al. [10], Esmaeili et al. [11], Rollbusch et al. [9], and Rados et al. [12]. They reported that high operating pressure and temperature significantly increase the gas holdup due to increased the gas density and reduced the surface tension.

The effects of the aspect ratio (*H/D*), static liquid level (H_S), bubble column diameter (D_C), and the sparger design on the bubble dynamics have been extensively investigated [2], [9], [13]–[17]. Their results revealed that the bubble dynamics are very sensitive towards the variation in the sparger design where the decreasing the hole diameter of the sparger in turn increases the local gas holdup, particularly in the region that is close to the gas distributor, and hence, the changing in the bubble dynamics were reflected on the liquid pattern and the flow regime. Besagni et al. [16] suggested that the bubble column dimensions and the sparger design have insignificant effect on the on gas holdup as long as three criteria are satisfied: the diameter of the bubble column is larger than 0.15 m, hole dimeter of sparger is larger than 1–2 mm and the aspect ratio is larger than 5. Meanwhile,

Al-Naseri et al. [2] studied the effect of the presence of internals and the low aspect ratios (*H/D* = 3, 4, and 5) on the bubble dynamics and the fully developed flow using four-point optical probe technique in a bubble column (using the same setup that used in current study). Al-Naseri et al. [2] revealed that the local gas holdup in the fully developed flow region was promoted significantly by the presence of internals and reducing the aspect ratio (*H/D*), whereas, in the sparger region the local gas holdup slightly increased. Furthermore, the present of internals inhibits the difference in the local gas holdup between the center and the wall regions on the bubble column and this effect extended to other bubble properties including the bubble passage frequency, bubble rise velocity, interfacial area, and the bubble chord length.

The influence of solids loading, particles size, sparger design, and bubble column diameter have been also investigated in previous works. A summary of the previous is listed in Table 1 using various measurement techniques. These studies found that the solids loading reduces the local gas holdup and the interfacial area which is a result of increase the bubble size and the bubble rise velocity, which attributed to an increase in the effective or apparent viscosity of the slurry (liquid and solid) since the catalyst is fine particles size (60-150 μm) and an increase in the effective surface tension. Decreasing the solids particle size enhances the solids loading effect on the bubble dynamics [18], [19]. Results obtained by Rados et al. [12] utilizing the gamma-ray Computed Tomography (CT) technique showed that an increase in the operating pressure enhances the bubble breakup rate and therefore, increases the gas holdup. The effect of solids loading on the solids and liquid velocity, and solids shear stress has been studied by Rados et al. [20] using the radioactive particle tracking technique. An increase in superficial gas velocity and operating pressure

increases the solid's axial velocity. Wu et al. [4] extended for the first time the four-point optical probe developed to a 0.1 inner diameter slurry bubble column to investigate the bubble properties (the local gas holdup, bubble chord length, bubble frequency, specific interfacial area, and bubble velocity). Results exhibited that with increase the superficial gas velocity, the local gas holdup, bubble chord length, bubble frequency, specific interfacial area, and bubble velocity were increased. While, with the presence of solids the local gas holdup, specific interfacial area, and bubble frequency decreases progressively with an increase the solids loading. Contrarily, an increase in the solids loading led to increase the bubble chord length and the bubble velocity slightly changed. Furthermore, the distribution of the bubble chord length in the center region exhibited a wide range of the bubble sizes with increasing solids loading. Bubble velocity distribution was analyzed in the center and wall regions of the column. The ratio of bubbles moving downward in the center and wall region increased with increasing superficial gas velocity, and the phenomenon was even apparent in the wall region at low solids loadings. However, Wu et al. [4] suggested their study was conducted in a lab-scale bubble column, in which the wall effect may be still important on the studied parameters, especially at high solids loading. Therefore, for a better understanding of the bubble dynamics in a commercial FT slurry bubble column, further experimentation in larger columns is recommended.

Regarding the impact of heat exchanging internals on the hydrodynamics, Al Mesfer et al. [21], [22], studied the effect of dense vertical internals in a bubble column on the gas holdup and liquid velocity by using gamma-ray CT and radioactive particle tracking techniques, respectively. The experiments were conducted under ambient conditions of pressure and temperature while, the superficial gas velocity, based on the total and free

CSA area for flow column, was varied from 0.05 to 0.45 m/s. They reported that the presence of internals increases the gas holdup slightly, while, at a given superficial gas velocity causes an increase in the axial centerline liquid velocity and a sharp decrease in turbulence parameters. Kagumba and Al-Dahhan [1], utilized the same setup that used by Mesfer et al. [21], [22] to measure the bubble properties using a four-point fiber optical probe in gas velocities ranged from 0.03 to 0.45 m/s that calculated based on free and total cross-section area CSA for flow column. Data obtained at velocity based on free cross-sectional area exhibited that the presence of internals increases insignificantly the local gas holdup, and hence, that it is possible to extrapolate the local gas holdup results obtained from empty bubble columns to those with dense internals, whereas, the bubble size and bubble rise velocity significantly decreased. Meanwhile, the experiments that conducted in gas velocity based on the total cross-section area CSA for flow column exhibited that the presence of internals increases significantly the local gas holdup. Sultan et al. [23]–[25] conducted comprehensive investigations in terms of the effects of the presence of internals, the configuration of internals (hexagonal, circular, and circular with central tube), and the diameter of internals tubes (0.5-inch and 1-inch) on the time-averaged cross-sectional gas holdup using an advanced gamma-ray computed tomography (CT) technique and all the used internals cover 25% of the cross-section area CSA for flow column. Data obtained revealed, that all the studied superficial gas velocities resulted in symmetrical gas holdup distributions over the cross-section area CSA of the bubble columns without vertical internals; however, the columns equipped densely with vertical internals did not have symmetrical gas holdup distributions. The presence of an extra central tube in the circular configuration played a key role in the gas-liquid distribution over the cross-section area

CSA of the bubble column. The hexagonal configuration had the advantage of providing the best spread of the gas phase over the entire cross-section area CSA of the column. Furthermore, the bubble column equipped with 1-inch vertical internals exhibited more uniform gas holdup distribution than the column with 0.5-in. Internals. Also, the visualization of the gas-liquid distributions for bubble columns with and without internals reveal that the well-known phenomenon of the core-annular liquid circulation pattern that observed in the bubble column without internals still exists in bubble column packed densely with vertical internals.

Based on investigations mentioned and listed in Table 1, the presence of internals, the solid loading, and the bubble column dimension have significant effects on the local gas holdup and the hydrodynamics parameters, embedded the bubble chord length, bubble rise velocity, bubble passage frequency, and the gas-liquid interfacial area. However, the most investigations mentioned above have been accomplished at lab scale and high dynamic liquid level (aspect ratio, $H/D \geq 9$), further, all the knowledge for the effect of the solids loading was conducted in bubble column without internals. Therefore, those results may have a high uncertainty regarding scale-up and design, particular the practical applications for the bubble/slurry bubble column reactors have a low dynamic liquid level (i.e., $H/D \leq 5$) for cost and thermohydraulic reasons [26]. Based on that, for the first time, the effects of low aspect ratio (H/D = 3, 4 and 5) and solid loading (C_s = 0.0, 9.1 and 25 vol. %) on the bubble dynamics and fully developed region in an industrial-sized bubble column with the presence of heat exchanger internal structure has been investigated. Data obtained in this work, aims to assess the bubble dynamics quantivly a slurry bubble column that used in Fischer-Tropsch (F-T) synthesis process, used to validate the simulations

results in terms of using the population balance model (PBM), particularly the simulation at high superficial gas velocity by utilizing the bubble chord length distribution, and validate the simulation result with the experiment results.

2. EXPERIMENTAL SETUP

Impact of solids loading on the bubble properties were investigated in the sparger region (close to distributor plate), and the fully developed flow region, that after demarcate the axial location for the transition from developed flow to fully developed flow region. The experiments were accomplished in an industrial pilot plant scale slurry bubble column of a height 152.5 in. (3.9 m) and an inner diameter of 24 inches (0.6 m) as shown in the schematic diagram in Figure 1(a-b). The gas phase is compressed air, while the liquid phase is deionized water in batch mode conditions. Glass beads of particle size d_p= 150 μm and density 2500 kg/m^3 were the solids phase. The solids loading (C_s = 0%, 9.1 and 25 vol.%) is calculated based on the volume of liquid phase. The gas phase was sparged from the bottom of the bubble column reactor through the gas distributor. The gas distributor plate, which was designed in our laboratory based on previous work using perforated plate with open area 1.09% [39], consists of 600 holes with hole diameter of d_0 = 3 mm diameter. These holes are organized in a triangular arrangement with 20 mm pitch as shown in Figure 2(c). A screen of stainless steel with size 400 mesh has been mounted on the distributor to prevent solid particles from the dropping underneath the distributor plate through the holes during shutdown and when operating at low gas velocity U_g. Gas velocity U_g, is calculated based on the free cross-sectional area (CSA) of the column for the flow and varied from

0.2 to 0.45 m/s. Gas velocity was measured and controlled by using two parallel rotometers (Omega). The experiments were carried out under ambient temperature and pressure, and the dynamic liquid level was varied from *H/D* = 3 to *H/D* = 5. Recently, Sultan et al. [23] studied the effect of internal tubes with different configurations (circular and hexagonal) on the gas holdup profile. They revealed that the bubble column with internals arranged in a hexagonal configuration provides higher cross-sectional gas holdup distribution. Therefore, a heat exchanging internals with hexagonal lattice, as shown Figure 3, was used. The heat exchanging internals occupies 24% of the CSA of the column, and consists of 12 closed loop PVC tubes of 0.06 m diameter as shown in Figure 1(e). The bubble dynamics have been measured by utilizing our advanced four-point fiber optical probe to assess the local gas holdup, bubble chord length, bubble frequency, bubble rise velocity, and interfacial area. These properties have been assessed at axial positions starting from 0.3 m above the distributor plate and moving upward with increment of 12 in. (0.3 m). At each axial position, five dimensionless radius locations (r/R) were measured as shown in Figure 2(a-b). However, advanced four-point optical fiber optical probe was inserted vertically from the top of the column to prevent the effect of the presence of probe on the bubble properties and the liquid flow pattern, in case of, inserted horizontally. Therefore, two holders probe have constructed as shown in Figure 1(f-g), the top one has been used to hold the probe at the desired axial position, while the middle one has been used to prevent the fluctuation of the probe inside the slurry bubble column during the operation. ANOVA test, which is a statistical method, has been used to demarcate the axial location for the transition from developed flow to fully developed flow region.

Table 1. A summary of the previous studies of bubble dynamics in SBCR at ambient and severe operating conditions

Authors	Setup dimension and internals arrangement	Solids loading (C_s) and particles dimeter (d_p)	Technique of measurement	Operation condition	Findings
Tyagi and Buwa [27]	H = 1.4 m W = 0.2 m D = 0.05 m $H/D \approx 7$ No internals used	• Glass beads • C_s = 0.0-40 vol% • d_p= 250 µm	Dual-tip voidage (conductivity) probes	Batch mode operation for liquid phase U_g= 0.05-0.3 m/s Pressure = 1 bar Temperature = ambient	• An increase in solid loading tend to decrease the gas volume fraction of the small bubble size and increase the volum fraction of the large bubble size. • The number of large bubble size increased, and small size decreased with increases the solid loading. • With increase the gas velocity the large bubble size was increased, therefore, no longer effect for the solids loading was observed. • At low gas velocity, the gas volume fraction profile of the small bubble size was uniform profile. • In wall region was indicated, small gas volume fraction of large bubble size and high gas fraction of the small bubble size. Contrary, in the central region of the bubble column. • At low gas velocity, the bubble size distribution exhibited a narrow size distribution. While at high gas velocity, the fraction of the large bubble was increased
Manjrekar and Dudukovic [28]	H = 2 m D = 0.2 m $H/D \approx 9$ No internals used	• aluminum oxide catalyst d_p= 60 µm. • glass spheres d_p= 300-350 µm. • Solid loading C_s= 10 wt.%.	Four-point fiber optical probe technique	Batch mode operation for liquid phase U_g= 0.1-0.45 m/s Pressure = 1 bar Temperature = ambient	• The local gas holdup and bubble frequency were reduced with increases the solid loading. • While the bubble size and bubble rise velocity increased with increase the solids loading. • Increase the particles size led to reduce the solids effect on the bubble dynamic.
Kumar and Khanna [29]	H = 2.72 m D = 0.154 m $H/D \approx 18$ No internals used	• Glass beads • C_s = 1-9 wt.% • d_p= was not noted	Differential Pressure Transducer (DPT)	Batch and co-current flow mode of liquid U_g= 0.01-0.4 m/s, U_l= 0.0-0.16 m/s. Pressure = 0.1-0.7 MPa Temperature = ambient	• The local gas holdup significantly was decreased with increasing the solids loading and increasing the liquid velocity. • Whereas, an increase the operating pressure and gas velocity tend to increase the local gas holdup.
Rabha et al. [30]	H = 1.5 m D = 0.07 m $H/D \geq 15$ No internals used	• Glass beads • C_s = 0.0-20 wt.% • d_p= 50, 100, and 150 µm.	Ultrafast electron beam X-ray tomography technique	Batch mode operation for liquid phase U_g= 0.02-0.05 m/s Pressure = 1 bar Temperature = ambient	• The cross-section gas holdup decreased with an increase the solid loading C_s • While, the high solid concentration led to creates large bubble size, in turn, breakup and increase the gas holdup at high solid loading
Rabha et al. [31]	H = 1.5 m D = 0.07 m $H/D \geq 15$ No internals used	• Glass beads • C_s = 0.0-36 wt.% • d_p= 100 µm.	Ultrafast electron beam X-ray tomography technique	Batch mode operation for liquid phase U_g= 0.02-0.05 m/s Pressure = 1 bar Temperature = ambient	• Adding the solid particles reduces the cross-sectional gas holdup due to promoting the bubble coalescence. • At low gas velocity $U_g \leq 2$ m/s and high solids loading C_s= 36 wt.% the break-up increased for the large bubbles, and hence, the radial gas holdup stat to enhanced. • After the solid loading C_s>1 wt.%, the bubble size distribution depends on the gas velocity and the solids loading. • Increasing the gas velocity increases the bubble size. • The gas holdup increased linearly with increase the gas velocity; whereas, the average gas holdup reduced less with increase the solids loading.

Table 1. A summary of the previous studies of bubble dynamics in SBCR at ambient and severe operating conditions (cont.)

Wu et al. [4]	H = 1.05 m D = 0.1 m $H/D \approx 9$ No internals used	• Alumina based catalyst skeleton • C_s = 0.0-25 vol% • d_p = 100 µm.	Four-point fiber optical probe technique	Batch mode operation for liquid phase U_g = 0.013-0.13 m/s Pressure = 1 bar Temperature = ambient	• Applicable of the four-point fiber optical probe to measure the bubble dynamic • An increase in solid loading tend to decrease the local gas holdup and bubble pass frequency which results an increase the bubble size and bubble rise velocity.
Behkish et al. [32]	H = 3 m D = 0.29 m $H/D \approx 10$ No internals used	• Alumina powder • C_s = 0.0-20 vol% • d_p = 32.33 and 42.37 µm.	Differential Pressure Transducer (DPT) High-speed camera	Batch mode operation for liquid phase U_g = 0.07-0.39 m/s Pressure = 0.67-3 MPa Temperature = 300-473K	• Total gas holdup increased significantly with increasing the operating pressure and temperature. • While, an increase the solid loading tends to decrease the total gas holdup.
Rados et al. [12]	H = 2.5 m D = 0.162 m $H/D \approx 11$ No internals used	• Glass beads • C_s = 9.1 vol% • d_p = 150 µm	Single source gamma ray Computed Tomography (CT)	Batch mode operation for liquid phase U_g = 0.08 and 0.45 m/s Pressure = 0.1 and 1.0 MPa Temperature = ambient	• The solids holdup decreased along with increase the axial location in the bubble column • The solids holdup in wall region greater than in the central region of the bubble column due to low gas holdup in the wall region • The increase in the gas velocity led to increase the overall and local gas holdup • an increase in operating pressure at the same superficial gas velocity results in a higher gas holdup profile • The effect of operating pressure on the gas holdup profile is as strong as the effect of superficial gas velocity • the effect of pressure on the solid's holdup profile was found to be less significant than on the gas holdup profile • an increase in pressure leads to the formation of smaller bubbles, which could indicate a delay in the flow regime transition from bubbly to churn-turbulent flow
Li and Prakash [33]	H = 2.4 m D = 0.28 m $H/D \geq$ 5-7 No internals used	• Glass beads • C_s = 0.0-0.4 vol% • d_p = 35 µm	Fast response pressure transducers The dynamic gas disengagement DGD technique	Batch mode operation for liquid phase U_g = 0.05 and 0.3 m/s Pressure = 1 bar Temperature = ambient	• The gas holdup due to small bubbles decreased with increasing the slurry concentration up to $C_s \geq$ 25 vol%, but increased slightly at higher slurry concentrations • For a given gas velocity, the rise velocity of the large bubble fraction increased slightly with increasing slurry concentration up to a slurry concentration of about 20 vol% and reached an asymptotic value for higher slurry concentrations
Krishna et al. [34]	H = 4 m D = 0.1, 0.19 and 0.38 m H/D was not noted No internals used	• Porous silica particles • C_s = 0.0-36 vol% • d_p = 27-47 µm	Pressure Transducer	Batch mode operation for liquid phase U_g = churn turbulent flow Pressure = 1 bar Temperature = ambient	• Total gas holdup decreased with increasing the solids loading and bubble column diameter.
Swart et al. [35]	H = 2.5 m W = 0.3 m D = 0.005 m No internals used	• Porous silica particles • C_s = 0.0-38.6 vol% • d_p = 38 µm	Video camera	Batch mode operation for liquid phase U_g = churn turbulent flow Pressure = 1 bar Temperature = ambient	• An increase the solid loading led to increase the bubble size and size distribution which in turn decreases the total gas holdup
S. Sasaki et al. [36]	$0.16 \leq D \geq 2$ m $0.4 \leq H_0 \geq 4$ m H/D was not noted No internals used	• No solids used	Image processing method, high-speed video camera (IDT, Motion Pro X-3)	Batch mode operation for liquid phase U_g = 0.025-0.35 m/s Pressure = 1 bar Temperature = ambient	• The ratio of H_0 to D is useless to evaluate the critical height • The overall gas holdup decreased with increasing the D and decreasing the H_0 • Insignificant effect for the D and H_0 on the overall gas holdup as long the bubble column scaled up

Table 1. A summary of the previous studies of bubble dynamics in SBCR at ambient and severe operating conditions (cont.)

G. Besagni et al. [16]	D = 0.24 m H = 5.3 m H/D = 5 to 10 No internals used	• No solids used	Expansion bed technique	Batch mode operation for liquid phase U_g = 0.004-0.23 m/s Pressure = 1 bar Temperature = ambient	• In batch bubble column model, the changing in the aspect ratio has turned out to decrease the gas holdup and destabilize the homogeneous flow regime. While, in the counter-current bubble column model, has turned out to increase the gas holdup and destabilize the homogeneous flow regime • Three flow regimes are available in the bubble column (batch model) • The critical value of the aspect ratio H/D ranged between 5 and 10, based on the bubble column operating model (batch or counter-current)
Jasim et al. [37]	H = 1.83m D = 0.14 m H/D = 11.25 Vertical internals • 30-tubes • Cover 25% of CSA • 0.5-inch tube diameter • Hexagonal and circular arrangement	• No solids used	Four-point fiber optical probe technique	Batch mode operation for liquid phase U_g = 0.02-0.45 m/s Pressure = 1 bar Temperature = ambient	• The presence of internals and the variation in the internals configurations significantly effect on the bubble hydrodynamics • Internals with circular arrangement increases significantly the local gas holdup in the central region of the bubble column, whereas, inhibits the local gas holdup in the wall region. • The presences of internals with hexagonal arrangement providing asymmetrical radial profiles for the local gas holdup.
Jasim et al. [38]	H = 1.83m D = 0.14 m H/D = 11.25 Vertical internals • 8-30-tubes • Cover 25% of CSA • 0.5-inch and 1-inch tube diameter • Circular arrangement	• No solids used	Four-point fiber optical probe technique	Batch mode operation for liquid phase U_g = 0.2-0.45 m/s Pressure = 1 bar Temperature = ambient	• The presence of internals and the variation in the tube diameter significantly impact on the bubble dynamics • Using internals of 0.5-inch tube diameter increases the local gas holdup in the center region and decreases the local gas holdup in the wall region comparing with bubble column without internals • Using internals of 1-inch tube diameter enhances the local gas holdup in the wall region (i.e., reduces the gap in gas holdup between the center and the wall regions).

The principle of this method is depending on the evaluating of the variance of the mean variable for the radial profile of local gas holdup in specific axial location with the radial profile of local gas holdup of the next axial position. When the variance in the radial profile of local gas holdup of these two axial positions are insignificant, that indicates the fully developed flow region [40].

3. MEASURMENT TECHNIQUE

3.1. FOUR-POINT OPTICAL PROBE

The measurement of the bubble properties were carried out using in-house manufactured four-point optical fiber probe technique, which developed by Frijlink [41], as shown in Figure 4. This technique was applied for the first time in a three-phase system by Wu et al. [4]. Later, Kagumba [42] and Manjrekar and Dudukovic [28] utilized the method for solid loading of C_s = 10 vol.%, and C_s = 25 vol.%, respectively. The probe was manufactured in our mFReal (Multiphase Flows and Multiphase Reactors Engineering and Applications Laboratory) in the Chemical and Biochemical Engineering Department at Missouri University of Science and Technology. The data processing algorithm employed for the output signal of optical probe was updated by Xue [43] in the Chemical Reaction Engineering Laboratory (CREL) at Washington University. The updated algorithm is able to modify the probe coordinates and increases the number of accepted bubbles improving the probe reliability. Additional information about the validation and the data processing algorithm are variable in Xue et al. [43]–[45].

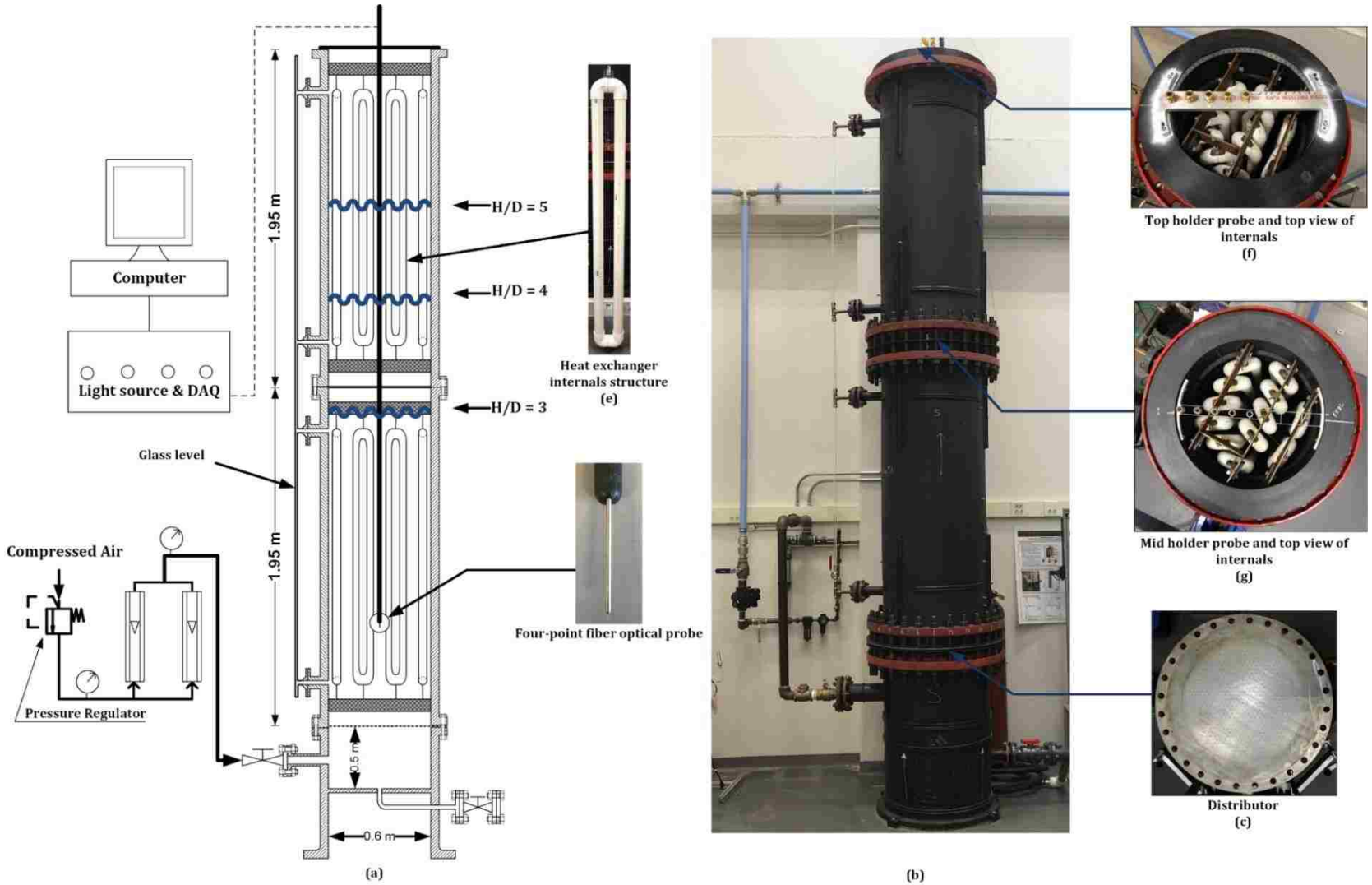

Figure 1. Schematics of the experimental setup of the pilot plant industrial size column with heat exchanging internals configuration

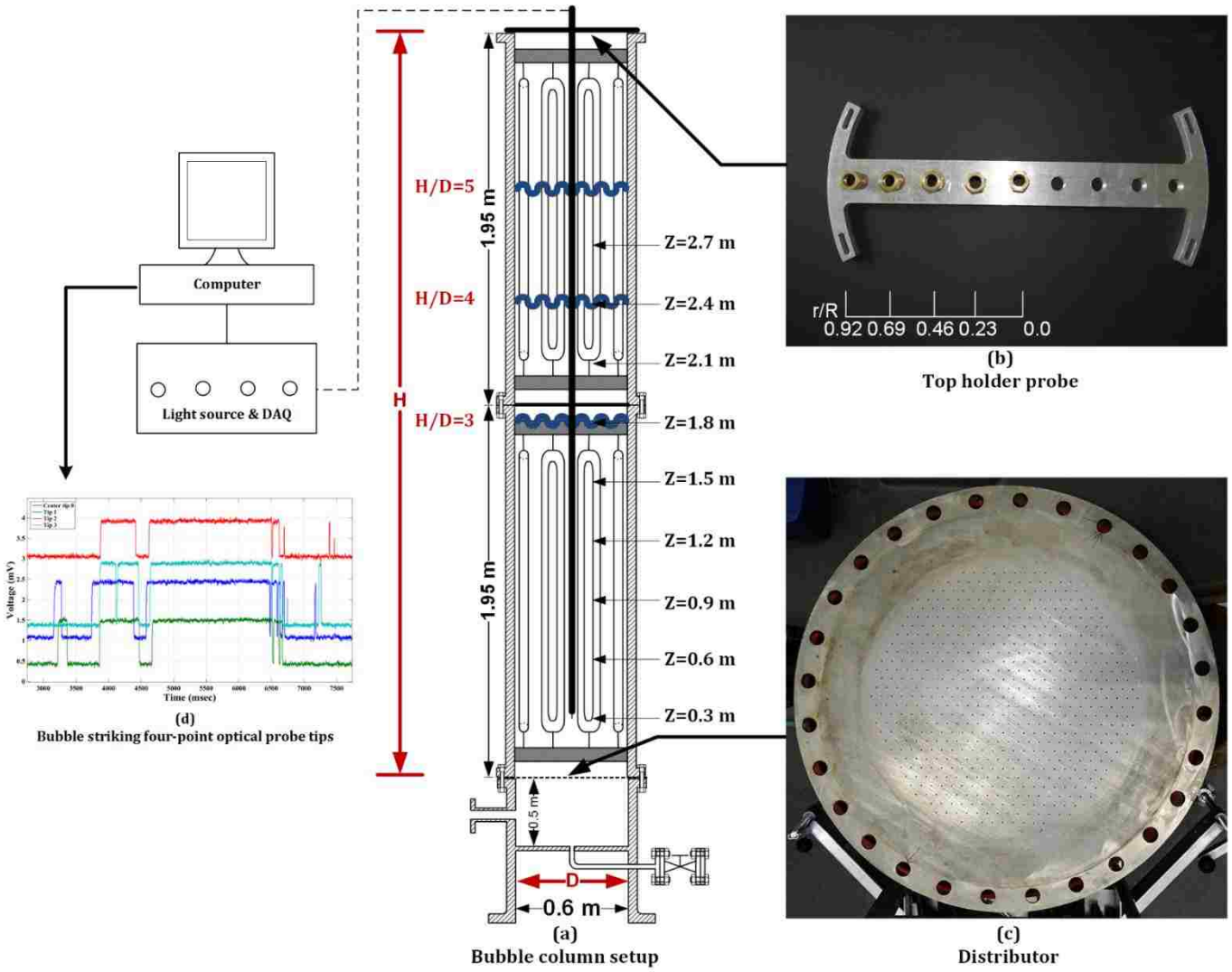

Figure 2. Schematic for the axial and radial locations for the four-point fiber optical probe

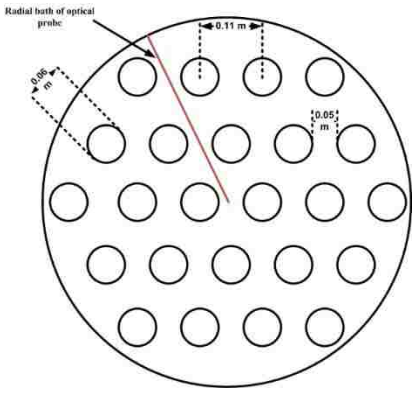

Figure 3. Internals of the hexagonal configuration covering 24% of the (CSA) of bubble column

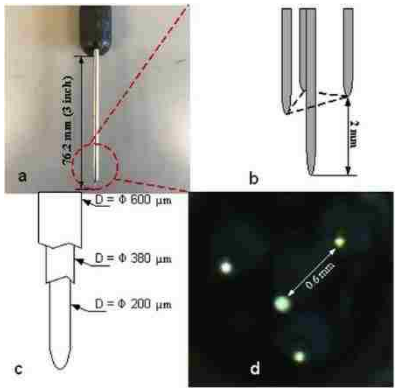

Figure 4. The advanced four-point optical fiber probe structure, (a) Optical probe (b) Side view with dimension (c) Finishing tip (d) Top view with distance space

4. METHODS AND DATA PROCESSING

4.1. OVERALL GAS HOLDUP

Overall (global) gas holdup was measured by using expansion bed technique as shown in equation (1):

$$\varepsilon_G = \frac{H_D - H_S}{H_D} \quad (1)$$

where H_D and H_S are the heights of the dynamic and static liquid level, respectively. The static liquid level, measured by utilizing a side arm glass level, was adjusted to keep the dynamic liquid level at the desired height aspect ratio (*H/D* = 5, 4 and 3) for each experiment of varying gas velocity.

5. RESULTS AND DISCUSSION

5.1. THE EFFECT OF THE SOLIDS LOADING AND ASPECT RATIO ON THE FULLY DEVELOPED FLOW REGION

Bubble column consists of three regions: sparger, fully developed flow, and disengagement regions [11], [46]. Through these regions, the bubble size develops depending on the bubble coalescence and breakup rates, which varied with the axial location. When those two rates are in equilibrium, the bubbles reach a stable bubble size [6], [18], [32]. As the aspect ratios used in this study (*H/*D = 5, 4, and 3) are lower than those used in previous studies demarcating the fully developed flow region is crucial. According to the design and scale-up of bubble/slurry bubble columns needs, the local gas holdup is a key parameter in the SCBR [1], [2], [25], [47]–[51]. Recently Guan et al. [52] succeed in using the radial profiles of local gas holdup to investigate the effect of bubble column diameter, superficial gas velocity, and the distributor design on the flow development region. Furthermore, for the first time, Shaikh and Al-Dahhan [53] used the gas holdup radial profile to demarcate the flow regime in the bubble/slurry bubble column. Therefore, in this work, the radial profiles for the local gas holdup have been used to demarcate the full development flow region by evaluating the variation in the radial profile in between two axial locations sequentially. Figure 5 illustrates the demarcation and the

effect of solid loading on the fully developed flow region at H/D = 4, and U_g = 0.45 m/s, while, Table 2 summarizes the impacts of gas velocity, aspect ratio, and solids loading on the fully developed flow region.

Figure 5(a), (b), and (c) illustrate the radial profiles of local gas holdup in different axial locations for the slurry bubble column with internals operated at the dynamic liquid level H/D = 4, solids loading C_s =0.0, 9.1, and 25 vol% and the superficial gas velocity U_g = 0.45 m/s, which is calculated based on the free CSA of the bubble column. Meanwhile, the impact of superficial gas velocity, solids loading, and aspect ratios on the fully developed flow region has been listed in Table 2. Results in Figure 5(a-c) exhibit that the radial profiles of the local gas holdup have no significant variance at Z = 1.2 m, 1.2 m, and Z = 0.9 m above the distributor for solids loading C_s = 0.0, 9.1, and 25 vol%, respectively, however, the effect of the solids loading was significent just in high concentration C_s = 25 vol.%. This phenomenon can be attributed to the increase the viscosity of the slurry (liquid and solid) with increase the solids loading, which in turn, reduces the liquid turbulent eddies that inhibit the chaotic in the bubble column, thereby, adding the solids prompt to appearing the fully developed flow regime. Simellar effect for the solid was pronounced in other aspect ratios, particulary in H/D = 3, as listed in Table 1. Data obtained in Table 2 indicate that the variation in the aspect ratio exhibit a significant impact on creating the fully developed flow region, where increase the aspect ratio was providing an enough axial distance to create the fully developed region due to reaching to stable bubble size, however, this finding agrees with the results that reported by Al-Naseri et al. [2]. Further, a decrease in superficial gas velocity in the absence of solids enhances the fully developed flow region to appear early at a lower axial postion. In the absence of solids, the increasing in the

superficial gas velocity enhances the chaotic behavior in the bubble columns by increasing the turbulent kinetic energy (TKE) and the eddy [5], [22]. Whereas, adding the solids inhibits the effect of the gas velocity, therefore, the gas velocity exhibits a slight impact, at low solids loading, and no impact mentioned on the fully developed flow at C_s = 25 vol.%. Accordingly, the fully developed flow and the sparger regions have been demarcated at different axial levels depending on the variation in the aspect ratio, solid loading and the gas velocities. Hence, the fully developed flow and the sparger regions for all different operation conditions were defined at *H/D* = 2.5 (H = 1.5 m), and *H/D* = 1 (H = 0.6 m), respectively. In this work, therefore, the effects of solid loading (C_s), superficial gas velocities (U_g) and aspect ratios (*H/D*) on the bubble properties have been illustrated in these levels.

Table 2. The effect of solids loading C_s, and aspect ratio *H/D* effect on the transition level of the sparger region to the fully developed flow region under different operating conditions

U_g (m/s)	Axial location of the fully developed flow in bubble column with internals, Z (m), C_s = 0.0 vol. %			Axial location of the fully developed flow in slurry column with internals, *Z* (m), C_s = 9.1 vol. %			Axial location of the fully developed flow in slurry column with internals, *Z* (m), C_s = 25 vol. %		
	H/D=5	*H/D*=4	*H/D*=3	*H/D*=5	*H/D*=4	*H/D*=3	*H/D*=5	*H/D*=4	*H/D*=3
0.2	0.9 m	0.9 m	0.9 m	0.9 m	0.9 m	0.9 m	1.2 m	0.9 m	0.9 m
0.3	1.2 m	1.2 m	N/A	1.2 m	1.2 m	0.9 m	1.2 m	0.9 m	0.9 m
0.45	1.2 m	1.2 m	N/A	1.2 m	1.2 m	0.9 m	1.2 m	0.9 m	0.9 m

5.2. OVERALL GAS HOLDUP

Figure 6 (a-c) exhibits the effect of solids loading and gas velocity, based on the free CSA for the flow column, on the overall gas holdup at different aspect ratios. As shown, the increasing in the gas velocity would enhances the overall gas holdup which can be attributed to increase the bubbles breakup rate which leads to increase the bubble

population (i.e. increasing the volume which is occupied by gas phase). While, increasing the solids loading has a slight impact toward decrease the overall gas holdup ranged by (3-12 %), and this influence decreased with the increase in the gas velocity progressively.

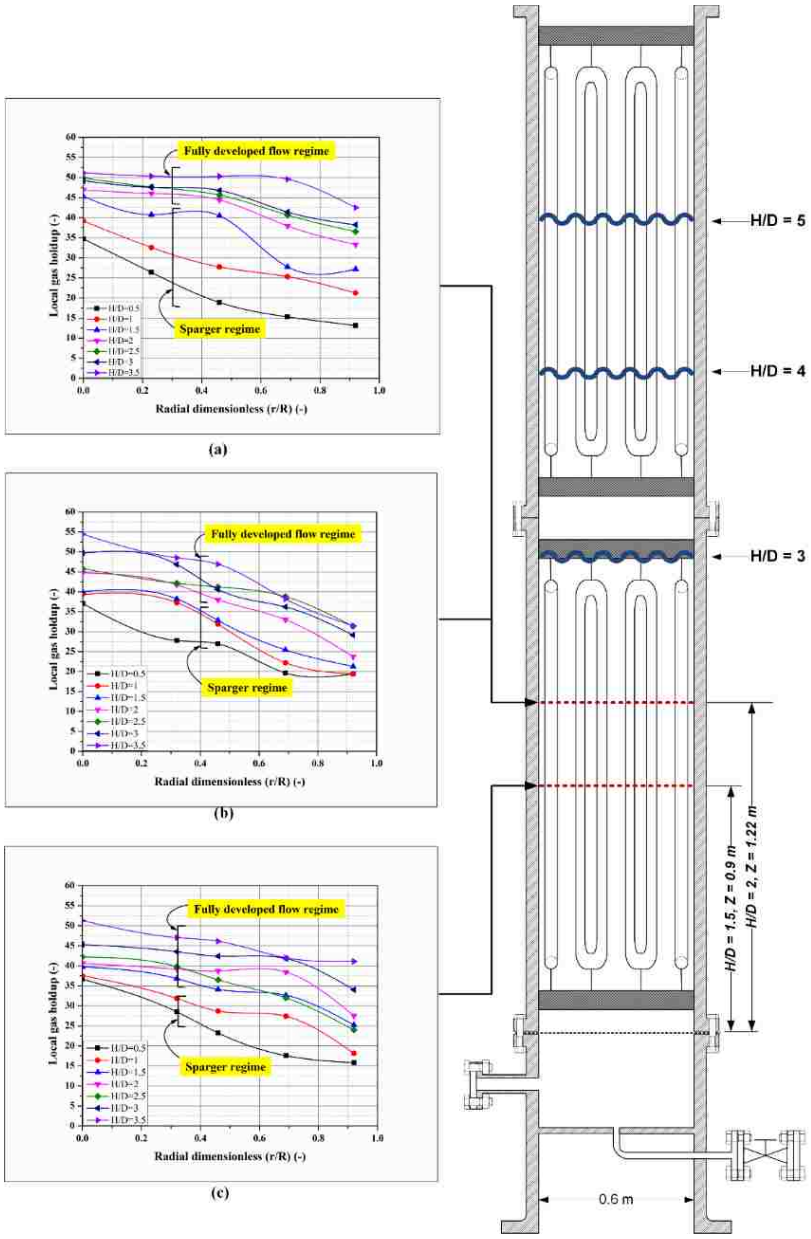

Figure 5. Fully developed flow region in the slurry bubble column with internals at aspect ratio H/D=4, and U_g=0.45 m/s (a); C_s = 0.0 vol. % (b); C_s = 9.1 vol. % (c); C_s = 25 vol. %

This percentage of decrease is lower than what was reported in the previous investigations conducted in the absent of internals. Thus, this can be the reason to enhance the bubble break-up rate, which in turn, causing increasing the local gas holdup. This phenomenon attributed to increase the bubble size as a result of solids loading, and then increase the bubble rise velocity, which means reducing the residence time of the gas-phase in the slurry bubble column, and hence, reducing the local gas holdup. Whereas, the variation in the aspect ratio has an insignificant effect on the overall gas holdup. However, the studied parameters, including the presence of internals, gas velocity, and solids loading, appear different levels of influence on the overall gas holdup. Therefore, we expected that the superficial gas velocity has the most effect on the bubble properties, while, the presence of internals would decrease the solids loading effect.

5.3. LOCAL GAS HOLDUP

Figure 7(a-c) present the solids loading impact on the radial profiles of the local gas holdup in the fully developed flow and the sparger regions. In the fully developed flow region, the magnitude of the local gas holdup decreases significantly with the increase of the solids loading particularly, in the wall region of column at all aspect ratios. The results obtained in the fully developed flow region are consistent with the previous works [1], [4], [27], [28], [31], [42], [51], [54]. However, this phenomenon was attributed by an increase the slurry phase viscosity due to the presence of solids which results to enhances the bubble coalescence rate [19], [32]. Whilst, data obtained in the sparger region illustrate, that the radial profiles and the magnitude value of the local gas holdup exhibit a slight changing with solids loading.

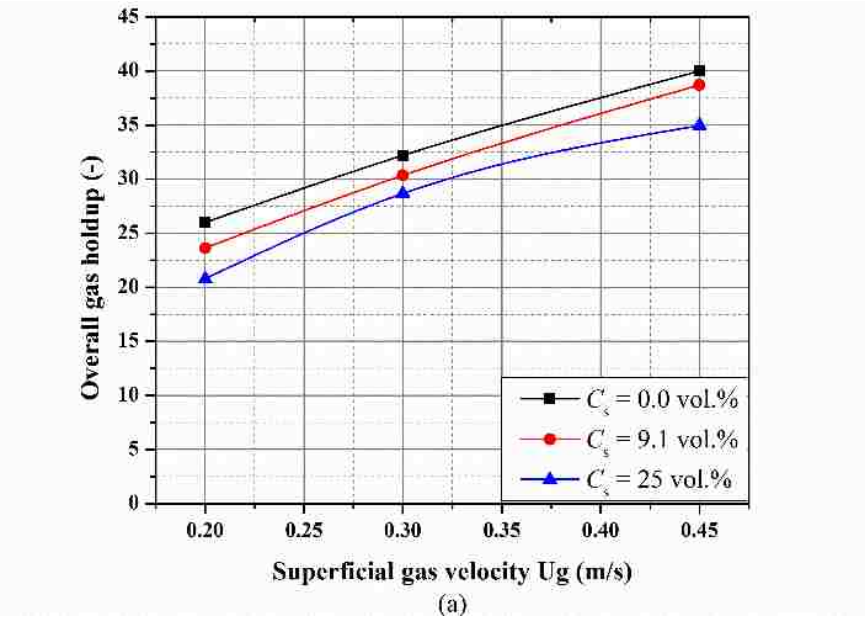

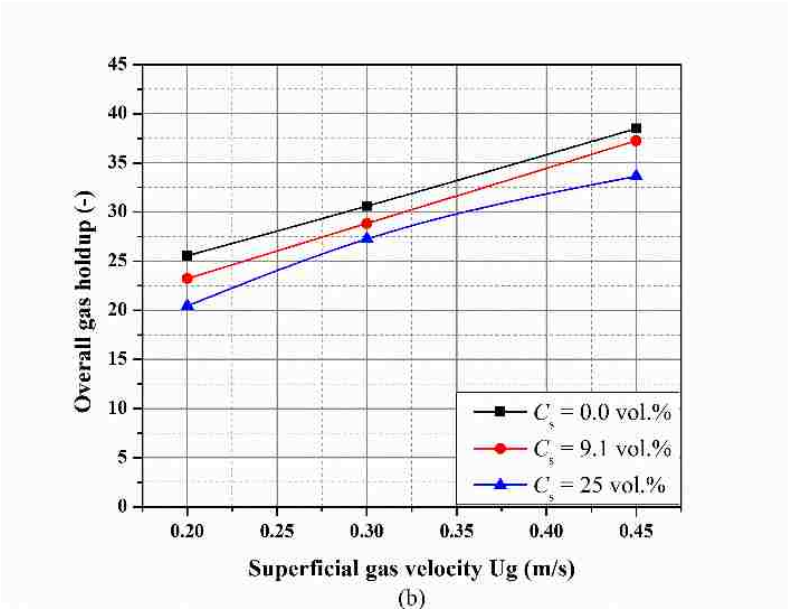

Figure 6. The effect of gas velocity based on the free CSA for the flow and the solids loading on the overall gas holdup; (a) *H/D* = 5; (b) *H/D* = 4; (c) *H/D* = 3

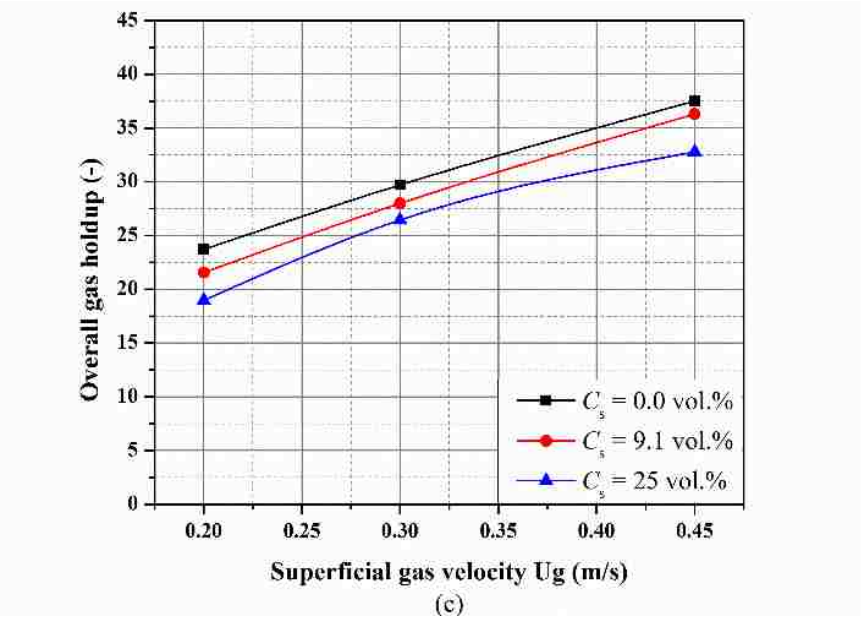

Figure 6. The effect of gas velocity based on the free CSA for the flow and the solids loading on the overall gas holdup; (a) *H/D* = 5; (b) *H/D* = 4; (c) *H/D* = 3 (cont.)

Ojima et al. [19] studied the impact of particles size and solids loading on the time required for bubble coalescence after bubble contact and reveals that the time decreases with increasing the solids loading (i.e. enhancing the bubble coalescence rate). According to Ojima et al. [19] attribution, this required time probably is greater than the residual time for the bubble in the sparger region, and hence, solids loading exhibits a slight effect on the local gas holdup.

The effect of the superficial gas velocity on the local gas holdup in the center and wall region of the bubble column has been illustrated in Figure 9(a-c). Results show that the local gas holdup increased with increasing the gas velocity at all solids loadings and in both the wall and center regions. Although solids loading increases the bubble chord length which results to concentrate the gas phase of large bubble size in the center of the column, internals existence ruptures these large bubbles to maintain the local gas holdup in same

profile at different solids loadings. Worth to mention, the most experimental studies addressed to investigate the effect of solids loading on the bubble dynamics have been conducted in the absent of internals, and hence, the effect of the solids loading in this study will quite different comparing with what have revealed by Wu et al. [4]. Therefore, comparing the current data obtained in slurry bubble column with internals has been conducted with data obtained in slurry bubble column without internals that reported by Manjrekar and Dudukovic [28]. Figure 8 illustrates that presence of internals exhibit a significant effect towards reducing the solids loading effect on the local gas holdup, particularly in the wall region of the column due to promoting the internals for the breaking-up the bubbles, specially the large bubbles, and hence, the local gas holdup has been increased. Accordingly, these findings represent new knowledge that have not been known before and have not been reported both in open and patent literature in terms the effect of solids loading on the local gas holdup with the presence of internals.

5.4. BUBBLE CHORD LENGTH DISTRIBUTION

Bubble chord length distribution provides a better understanding and physical attribution about the impact of solids loading on the bubble dynamics, particularly, in the presence of internals where the radial profiles and distributions of the bubble properties controlled by the interfacial forces distribution and the internals hindering. However, the effect of solids loading at different aspect ratios on the bubble chord length distribution in the fully developed flow and the sparger regions are illustrated in Figure 10(a-c) and Figure 11(a-c), respectively.

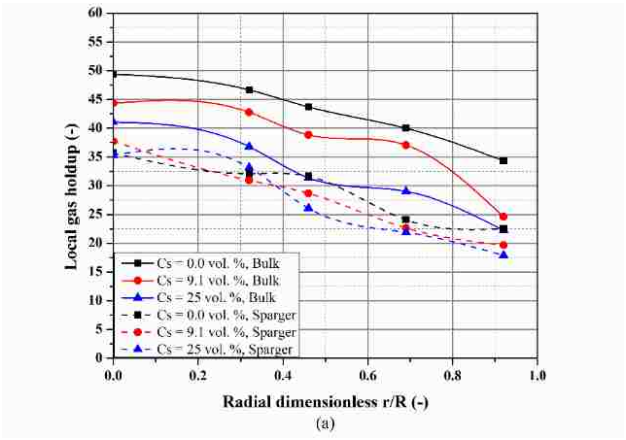

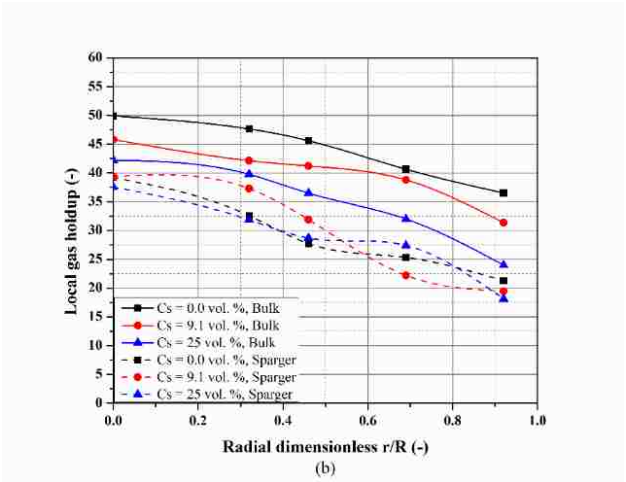

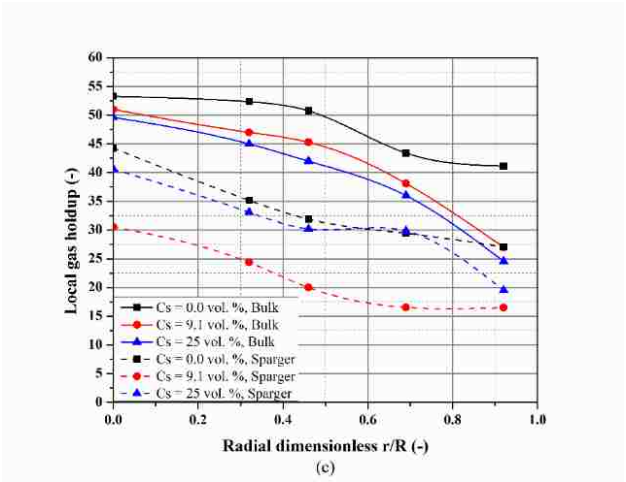

Figure 7. The effect of solids loading on the radial profiles of the local gas holdup in the fully developed region and the sparger regions, U_g = 0.45 (m/s); (a) *H/D* = 5, (b) *H/D* = 4, (c) *H/D* = 3

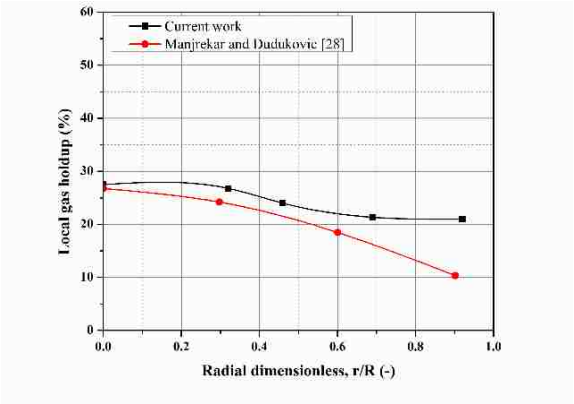

Figure 8. Comparing the local gas holdup in slurry bubble column at H/D = 5 and C_s = 9.1 vol. % with data reported by Manjrekar and Dudukovic [28]

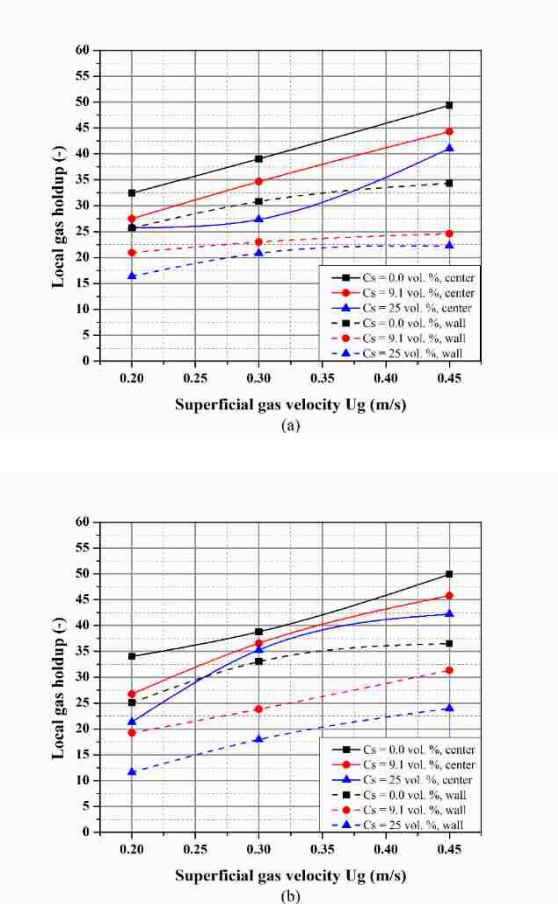

Figure 9. The effect of gas velocity in the fully developed region on the local gas holdup in the center and the wall regions; (a) *H/D* = 5, (b) *H/D* = 4, *H/D* = 3

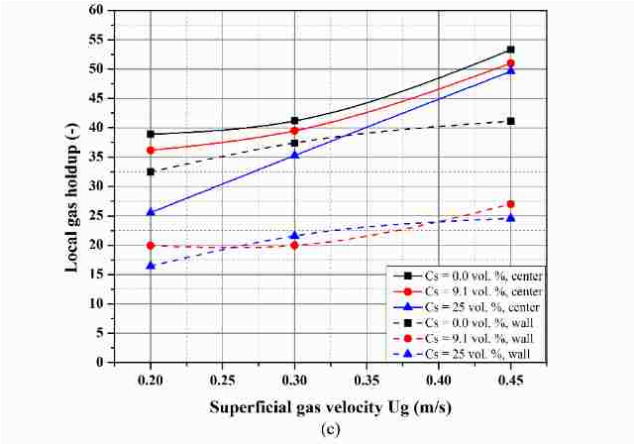

Figure 9. The effect of gas velocity in the fully developed region on the local gas holdup in the center and the wall regions; (a) *H/D* = 5, (b) *H/D* = 4, (c) *H/D* = 3 (cont.)

The bubble chord length presented in the forms of probability density function (pdf) in the center and wall regions of bubble column. Figures show that chord length has been increased with increasing the solid loading under all operating conditions, which is in alignment with the most investigations [4], [27], [28], [31], [32], [54], [55]. This behavior is due to the increase of the slurry viscosity with the solids loading, which increases the bubbles coalescence [56], tending to format large bubbles size. Further, Table 3 summarizes the statistical parameters in terms of mean and variance of the chord length in the fully developed flow and the sparger regions at the studied gas velocities. In fully developed flow region, the mean chord length decreases with increasing the superficial gas velocity, which is a result of enhancing the bubble breakup rate with increasing the superficial gas velocity U_g. This result is in contrast with the results that reported by Wu et al. [4], and Hooshyar et al. [54], in terms that the bubble chord length enhanced with increase the gas velocity. The reason is these works were conducted at gas velocity varied to covers the bubbly and churn turbulent flow regimes, therefore, the effect of gas velocity on the chord length was exhibited comparing between these two regims.

Recently, Al-Naseri et al. [57] studied the effect of low aspect ratios on the flow regime transtion in bubble column reactor using the same setup that used in this work, and revealed that the bubble chord length in the churn turbulent flow regime decreases progressively with increase the gas velocity from U_g=0.15 to 0.45 m/s. Hence, that attributes the contrast with results of Wu et al. [4], and Hooshyar et al. [54] due to the current work has been accomplished in churn turbulent flow regime. Adding solids, which causing increasing in the bubble size, rises the number of liquid eddies that can break up the bubbles based on the Weber number (W_e) [58]. As well, the presence of internals also reduces the liquid eddies length [5], [22]. All that, in turn, explain the reason for increase the influence of gas velocity on the chord length progressively with increase the solids loading. Moreover, similar impact for the solids loading has been indicated in the sparger region, which seldom exhibits changing in the hydrodynamics by other parameters (i.e., the presence of internals and bubble column dimension) except the distributor design. The impact of solids loading in the center and the wall regions on the bubble chord length is listed in Table 4. The results obtained appear that bubble size in the wall region is lower than in the center region at all operating conditions. This difference in bubble size for both regions was not affected by the solids loading, which is an evidence to the presence of internals that controls the bubble size radially depending on the internal structure as well. Worth to mention, in similar studies Manjrekar and Dudukovic [28], Wu et al. [4], and Hooshyar et al. [54] reported that the maximum increase in the bubble size was 40-75% (based on the studied solids concentration). While in the current study, the maximum increase in the chord length reaches 22% either in the fully developed flow region or in the sparger region, which is attributed to the presence of internals that reduces the solid loading

influence on the bubble chord length. However, the enhancement in the bubble size and the bubble velocity, in turn, induce the liquid eddies and the wake region, which is located a distance behind the bubble and enhanced by increasing the bubble size[51], therefore, that heat transfer coefficient increased by the solid adding [42], [59]–[61].

Table 3. The statistical parameters of the effect of the gas velocity and solid loading on the bubble chord length in the center of the column

H/D=3												
Ug m/s	C_s = 0.0 vol.%				C_s = 9.1 vol.%				C_s = 25 vol.%			
	Fully developed flow		Sparger		Fully developed flow		Sparger		Fully developed flow		Sparger	
	Mean	Var	Mean	Var	Mean	Var	Mean	Var	Mean	Var	Mean	Var
0.2	0.61	0.86	0.52	0.36	0.81	0.83	0.77	0.47	0.89	1.98	0.83	1.27
0.3	0.69	1.07	0.50	0.46	0.78	0.95	0.73	0.85	0.79	1.02	0.76	1.2
0.45	0.53	0.75	0.50	0.43	0.70	0.83	0.67	1.04	0.73	0.97	0.70	0.72
H/D=4												
Ug m/s	C_s = 0.0 vol.%				C_s = 9.1 vol.%				C_s = 25 vol.%			
	Fully developed flow		Sparger		Fully developed flow		Sparger		Fully developed flow		Sparger	
	Mean	Var	Mean	Var	Mean	Var	Mean	Var	Mean	Var	Mean	Var
0.2	0.74	0.66	0.72	0.24	0.86	1.13	0.81	1.02	0.91	1.4	0.86	0.85
0.3	0.67	1.04	0.50	0.81	0.74	0.763	0.66	0.8	0.83	0.6	0.73	0.66
0.45	0.60	0.62	0.46	0.46	0.66	0.65	0.65	0.61	0.76	0.66	0.71	0.49
H/D=5												
Ug m/s	C_s = 0.0 vol.%				C_s = 9.1 vol.%				C_s = 25 vol.%			
	Fully developed flow		Sparger		Fully developed flow		Sparger		Fully developed flow		Sparger	
	Mean	Var	Mean	Var	Mean	Var	Mean	Var	Mean	Var	Mean	Var
0.2	0.75	0.82	0.66	0.38	0.90	1.22	0.89	1.22	1.01	1.31	1.10	1.14
0.3	0.70	0.95	0.52	0.73	0.78	0.77	0.74	0.98	0.92	1.06	0.89	0.77
0.45	0.63	0.47	0.51	0.61	0.70	0.81	0.69	0.67	0.84	0.65	0.78	0.72

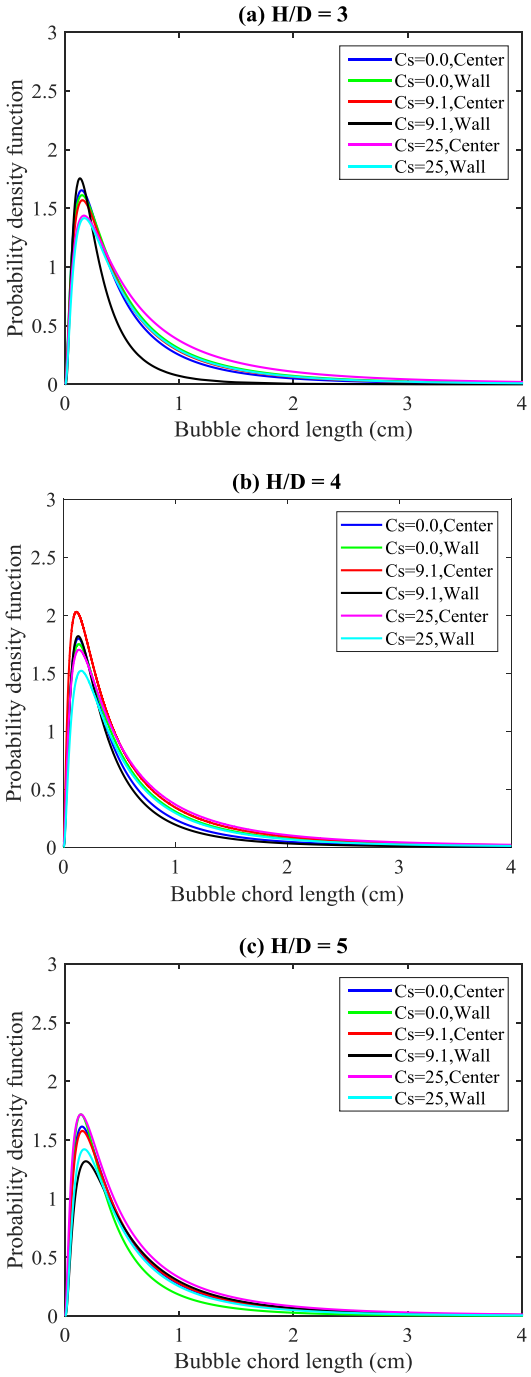

Figure 10. The effect of solids loading on the bubble chord length in the fully developed flow region; (a) *H/D* = 3, (b) *H/D* = 4, (c) *H/D* = 5

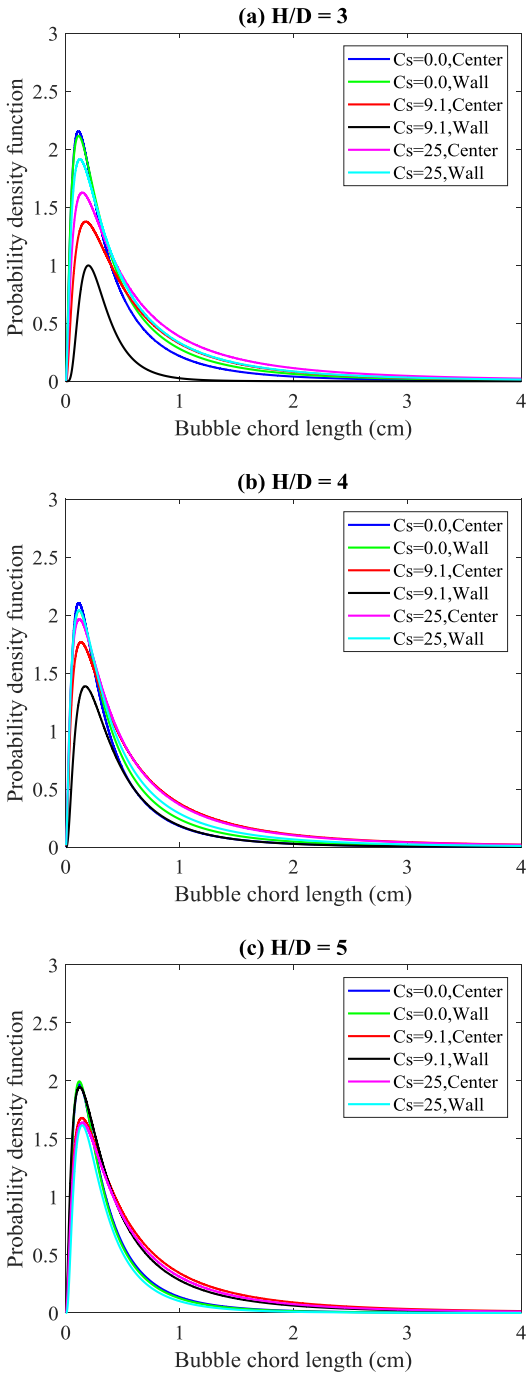

Figure 11. The effect solids loading on the bubble chord length in the sparger region; (a) *H/D* = 3, (b) *H/D* = 4, (c) *H/D* =

Table 4. The statistical parameters of the effect of the solids loading on the bubble chord length in the center and wall regions of the column, Ug = 0.45 m/s

H/D=3												
measurements	Fully developed flow region						Sparger region					
	C_s = 0.0 vol.%		C_s = 9.1 vol.%		C_s = 25 vol.%		C_s = 0.0 vol.%		C_s = 9.1 vol.%		C_s = 25 vol.%	
	Center	Wall	Center	Wall	Center	Wall	Center	Wall	Center	Wall	Center	Wall
Mean (cm)	0.53	0.50	0.70	0.55	0.73	0.72	0.50	0.56	0.67	0.60	0.69	0.65
Varince (cm^2)	0.75	1.15	0.83	1.13	0.97	1.02	0.43	0.48	1.04	0.21	0.72	0.52
H/D=4												
measurements	Fully developed flow region						Sparger region					
	C_s = 0.0 vol.%		C_s = 9.1 vol.%		C_s = 25 vol.%		C_s = 0.0 vol.%		C_s = 9.1 vol.%		C_s = 25 vol.%	
	Center	Wall	Center	Wall	Center	Wall	Center	Wall	Center	Wall	Center	Wall
Mean (cm)	0.60	051	0.66	0.57	0.76	0.72	0.46	0.55	0.65	0.71	0.71	0.58
Varince (cm^2)	0.62	0.82	0.65	0.66	0.66	0.86	0.46	0.5	0.61	1.35	0.49	0.46
H/D=5												
measurements	Fully developed flow region						Sparger region					
	C_s = 0.0 vol.%		C_s = 9.1 vol.%		C_s = 25 vol.%		C_s = 0.0 vol.%		C_s = 9.1 vol.%		C_s = 25 vol.%	
	Center	Wall	Center	Wall	Center	Wall	Center	Wall	Center	Wall	Center	Wall
Mean (cm)	0.63	0.59	0.81	0.70	0.84	0.73	0.51	0.50	0.69	0.60	0.78	0.60
Varince (cm^2)	0.47	0.7	0.81	1.19	0.65	1.07	0.61	0.36	0.67	0.51	0.72	1.21

5.5. BUBBLE RISE VELOCITY

As pointed earlier, the four-point optical fiber probe, inserted vertically, was oriented to down due to the setup limitation reason. Thus, in all experiments, the bubble properties were measured based on the bubble that moves in the upward direction, thereby, the bubble rise velocity concept has been used in this work. Youssef et al. [58], Kagumba and Al-Dahhan [1], and Jasim et al. [37], [38] studied the influence of internals on the bubble dynamics of bubble column, while, Wu et al. [4] and Manjrekar and Dudukovic [28] studied the solids loading effect on the bubble dynamics. They measured the bubble properties in two orientations upward and downward. According to their data obtained, that most bubbles in the center region of the bubble column have moved in an upward direction. Hence, in this study, the solids loading and gas velocity effects on the bubble rise velocity

distribution have been demarcated in the center of the bubble column. Figure 12(a-c) and Figure 12(a-c) illustrate the solids loading effect on the bubble rise velocity distribution in histogram forms with normal distribution in the fully developed flow and the sparger regions, respectively, and for all aspect ratios (H/D = 5, 4 and 3). The results show that the mean bubble rise velocity increased with increasing the solids loading by ~ 7 to 30 vol.% and this enhancement is stronger with solids loading of 25 vol. %. A similar effect has been shown in the sparger region with less influence. The increase could be partly due to an increase in the viscosity of the slurry phase due to the solids loading. As the slurry phase viscosity increases, the bubble coalescence is promoted, which increases the bubble buoyancy. Thereby, that would also attribute the reduction in the local gas holdup as a result to the increase in the bubble rise velocity, which means reducing the residual time for the bubble inside the column. On the other hand, the impact of gas velocity on the bubble rise velocity at different solids loading levels (C_s = 0.0, 9.1 and 25 vol. %) in the fully developed flow and the sparger regions are illustrated in Figure 14(a-c) and Figure 15(a-c), respectively. The results exhibit a remarkable increasing in the mean bubble rise velocity with increasing the gas velocity in both regions by ~ 6 to 67 %. This phenomenon (i.e., the enhancement in the bubble rise velocity) increased with adding the solids due to the dual enhancement by the solids loading and the gas velocity on the bubble rise velocity. As shown in Figure 14 and Figure 15, as the solids loading increases from C_s = 0.0 to C_s = 25 vol.%, the mean bubble rise velocity increases by 25% at U_g = 0.2 m/s, and this enhancement is increased progressively with increasing the gas velocity to reach 45%. This is because the large bubble size has been indicated in low gas velocity, as mention earlier, and adding solids would increase the bubble size significantly. Hooshyar et al. [54]

explained this phenomenon by studying the effect of solid loading on the bubble dynamics utilizing the four-optical probe and conducted a simple force balance over a single bubble. They proposed that the increase in the bubble size could not explain the increase in the bubble velocity with increase the superficial gas velocity.

5.6. BUBBLE PASSING FREQUENCY

The effect of superficial gas velocity on the bubble passing frequency in fully developed flow and the sparger regions has been illustrated in Figure 16(a-c) and Figure 17(a-c), respectively, for different solids loading (C_s = 0.0, 9.1 and 25 vol. %) and for the center and the wall region of the bubble column. As shown in the figures, in the absence of solids loading case (C_s = 0.0 vol. %), the center and wall regions exhibit a similar behavior where the bubble passing frequency increased with increasing the gas velocity and the difference between these two regions is a negligent. When adding the solids (C_s = 9.1 and 25 vol. %), the bubble passing frequency in the center region exhibits increase with the increase of the gas velocity, whereas, the wall region appears a slight increase. Furthermore, the solids loading decreases the bubble passing frequency for all the velocities (U_g = 0.2, 0.3 and 0.45 m/s), and increases the gap in bubble passing frequency between the center and wall region progressively with increasing the gas velocity. To explain that, with the presence of the solids there are two mechanical parameters affect this variation in the bubble passing frequency. Second, increasing the obstruction by the internals structure against the large bubbles that leads to accumulate in the center region. Therefore, the reduction in the bubble passing frequency in the wall is much more than the center region.

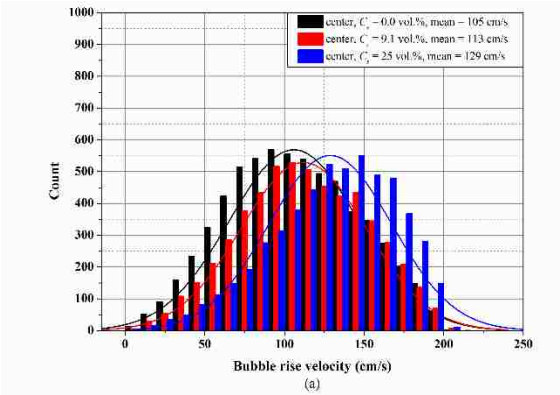

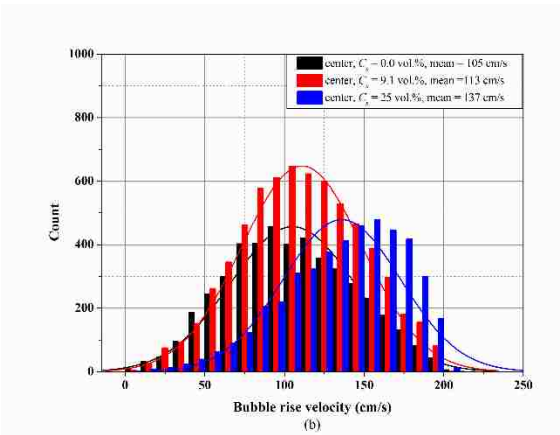

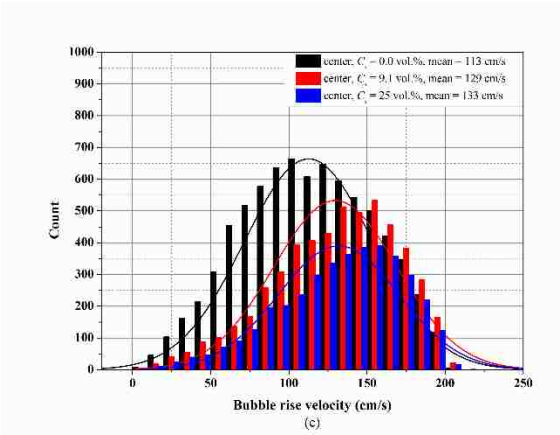

Figure 12. The effect of solids loading on the bubble rise velocity in fully developed flow region and U_g = 0.45 m/s; (a) H/D = 5; (b) H/D = 4; (c) H/D = 3

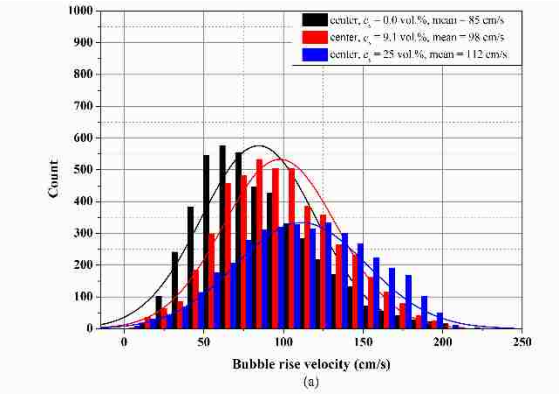

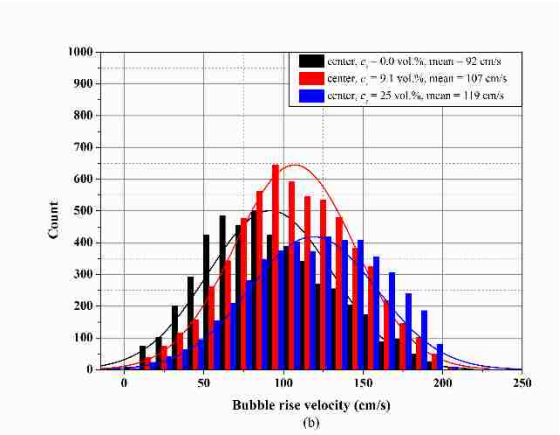

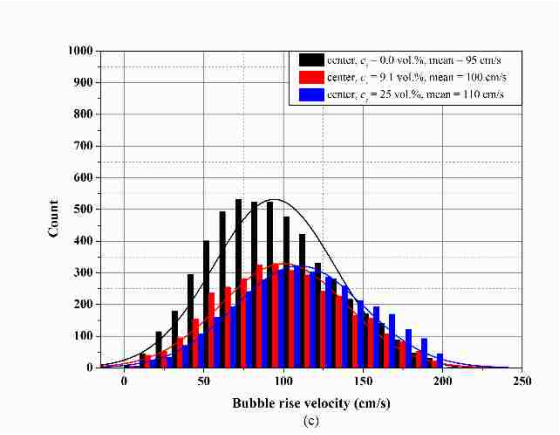

Figure 13. The effect of solids loading on the bubble rise velocity in sparger region and U_g = 0.45 m/s; (a) H/D = 5; (b) H/D = 4; (c) H/D = 3

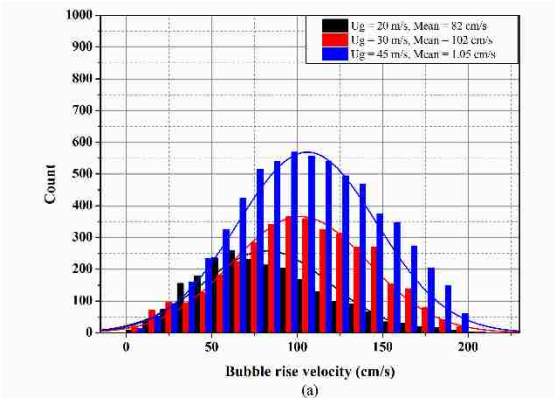

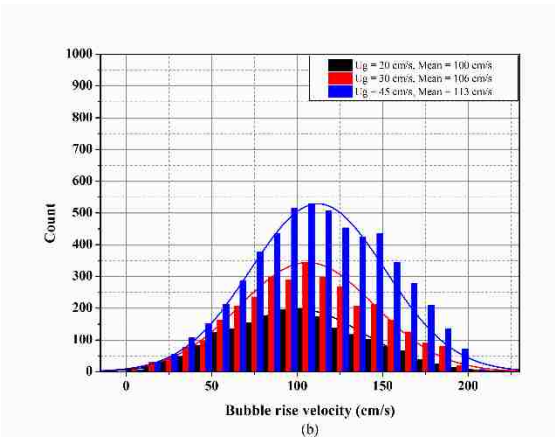

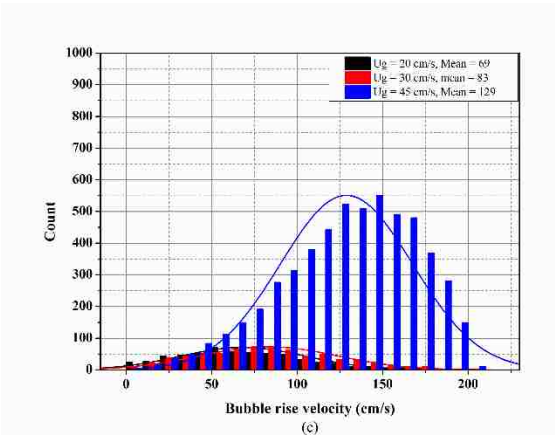

Figure 14. Gas velocity effect on the bubble rise velocity in fully developed flow region and *H/D* = 5; (a) C_s = 0.0 vol. %; (b) C_s = 9.1 vol. %; (c) C_s = 25 vol. %

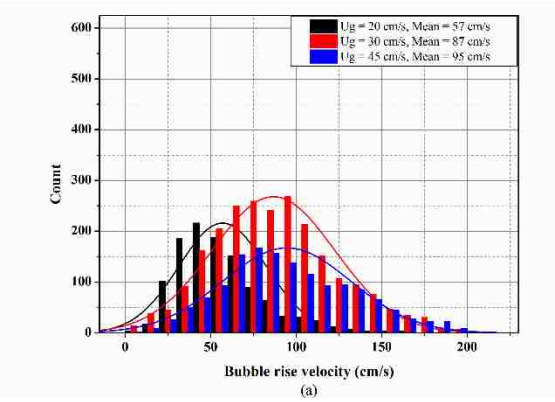

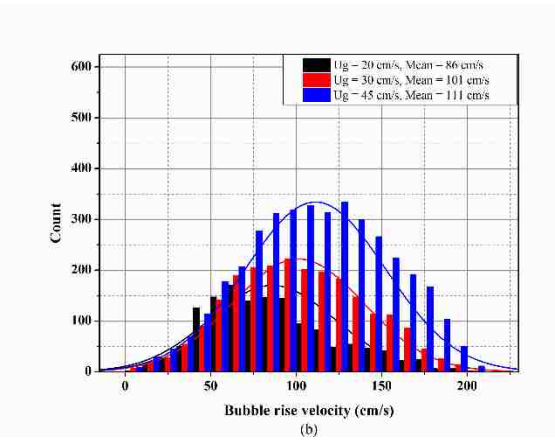

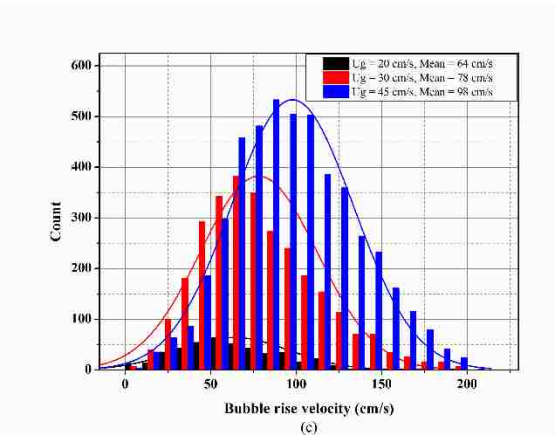

Figure 15. Gas velocity effect on the bubble rise velocity in sparger region and *H/D* = 5; (a) C_s = 0.0 vol. %; (b) C_s = 9.1 vol. %; (c) C_s = 25 vol.

Meanwhile, the figures exhibit a slight impact of the aspect ratio on the bubble passing frequency where the increase in the aspect ratio decreases the bubble passing frequency. The results provide an evidence for the increase of bubble coalescence rate and the reason of the reduction in the local gas holdup in SBCR, which would be responsible for increased bubble velocity. The radial bubble passing frequency is controlled by the bubble slip velocity created by the turbulent dispersion and the net radial force, therefore like gas holdup, adding solids would affect the radial profile of bubble passing frequency as well [1]. According to Choi and Lee [62], the bubble passing frequency is a function for the bubble size, and bubble rise velocity as well as the intensity of the liquid turbulence. Therefore, bubble passing frequency affects the transport phenomena (both mass and heat transfer), and hence, the conversion and selectivity will be affected. Worth to mention, the reduction in the numbers of bubbles in the wall region (i.e., the bubbles that rise upward), indicates to that the existence of solids enhances the liquid circulation.

5.7. BUBBLE SPECIFIC INTERFACIAL AREA

The bubble specific interfacial area is bubble surface area per unit volume of liquid/slurry-phase. It is a key parameter for the mass transfer phenomenon in the multiphase system, where the transfer of the species occur cross it from gas to liquid/slurry phase and vice versa [63]. Behkish [64] investigated the bubble properties and the volumetric liquid-side mass transfer coefficient ($k_\ell a$) in bubble and slurry bubble column operated under pressure (0.1-2.7 MPa) and temperature (323-453 K). He revealed that the liquid-side mass transfer coefficient was varied with the changing of the bubble interfacial area.

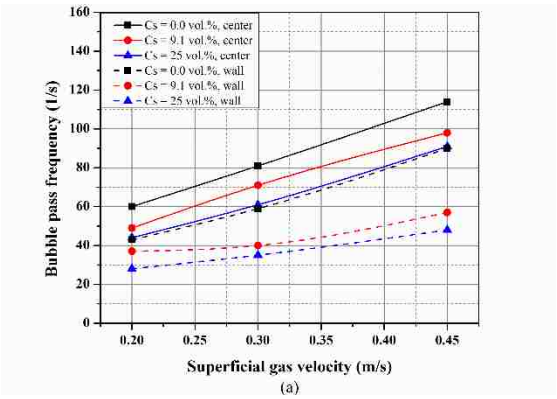

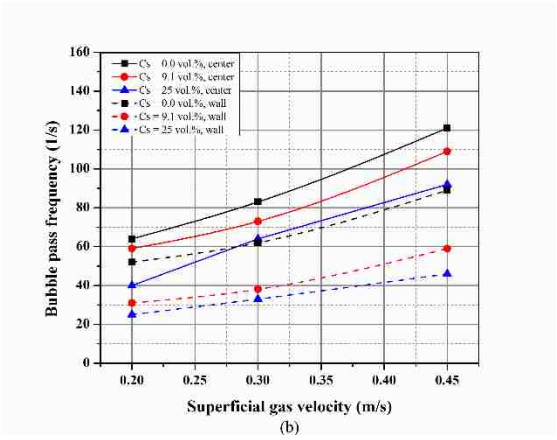

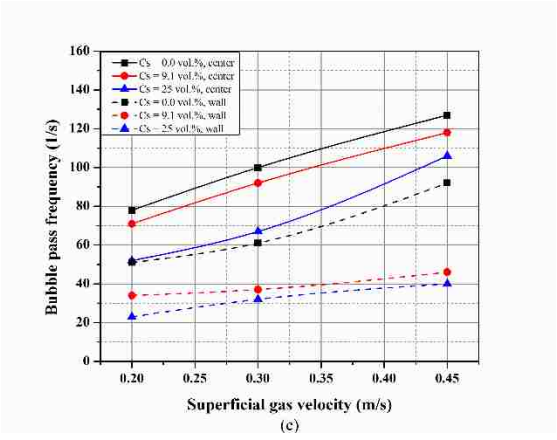

Figure 16. The effect of gas velocity and solids loading on the bubble passing frequency in the fully developed flow region; (a) *H/D* = 5; (b) *H/D* = 4; (c) *H/D* = 3

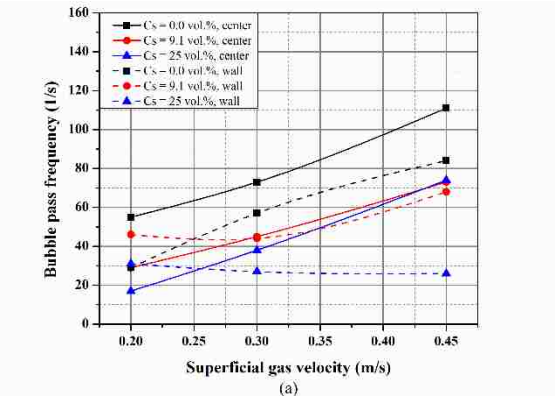

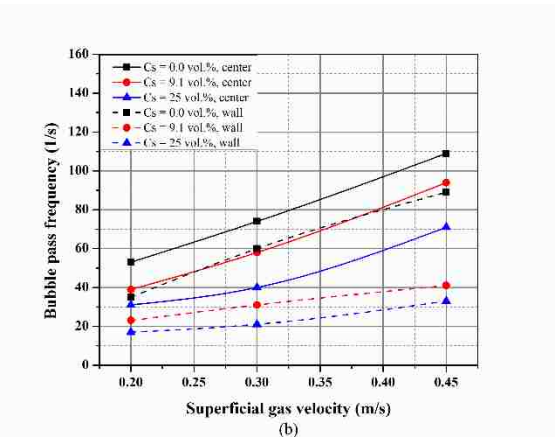

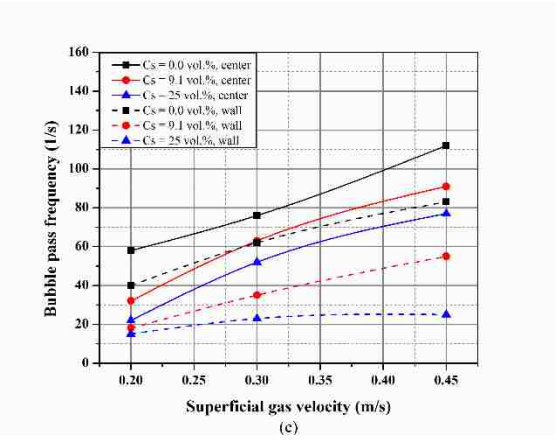

Figure 17. The effect of gas velocity and solids loading on the bubble passing frequency in the sparger region; (a) *H/D* = 5; (b) *H/D* = 4; (c) *H/D* = 3

Further, the bubble interfacial area is a characteristic to the degree of mixing in the multiphase. Kagumba and Al-Dahhan [1] reported that the profile of the bubble interfacial area was increased with gas velocity in a low range of U_g (0-0.1 m/s), while, at a high range of U_g (0.1-0.45 m/s) being less or slightly increased.. Their attribution was that the flow regime was transited from the transition to the churn turbulent regime. According to Kagumba and Al-Dahhan [1], the bubble interfacial area could be used as a parameter to demarcate the flow regime transition. Therefore, introducing the influence of the solids loading with the presence of internals and the gas velocity on the bubble interfacial area is essential to improve the SBCR performance, particularly, that the transfer coefficients are related significantly to the rate of reaction.

The effect of gas velocity and solids loading on the specific interfacial bubble area for the fully developed flow and the sparger regions has been exhibited in Figure 18 (a-c) and Figure 19 (a-c), respectively. The figures show a significant increase in the bubble interfacial area with the increase the superficial gas velocity in both regions the fully developed flow and the sparger. In the fact of matter, the spherical bubbles have a low surface area per unit volume. Meanwhile, as the superficial gas velocity increases, the shape of bubbles deforme and be more irregular. Thus, that could be the reason to attribute the increase in the bubble interfacial area with increase the superficial gas velocity. According to Kagumba and Al-Dahhan [1], and Al-Naseri et al. [2], reported that the interfacial area mainly relates to the bubble passage frequency, and hence, the trends of bubble interfacial area in the center and wall regions of the bubble column, and for both regions the fully developed flow and the sparger are similar to that in the in Figure 16 and Figure 17. While, the solids loading appears a significant impact toward decrease the

interfacial bubble area, which could be explanted to increase the bubble size and reduce the bubble passing frequency. However, the wall region exhibits a low value for the bubble interfacial area by adding the solids, which is confirmation of the reducing in the numbers of the rising bubbles and low bubble size concertation.

6. REMARKS

For the first time, the effects of solids loading (C_s = 0.0, 9.1 and 25 vol.%), gas velocity (U_g = 0.2, 0.3 and 0.45 m/s) calculated based on the free CSA for flow column, and different low aspect ratios (H/D = 3, 4 and 5) on the bubble properties with presence of industrial heat exchanging internals have been investigated in an industrial-size pilot-plant bubble/slurry bubble column. Bubble properties, including the local gas holdup, bubble chord length, bubble rise velocity, bubble pass frequency, and bubble interfacial are, have been measured by utilizing advanced four-point optical fiber probe. The data obtained reveal the following.

Increased the solids loading exhibits earlier transition to fully developed region. This effect is suppressed by increasing the aspect ratio. The superficial gas velocity has only slight impact on the transition to the fully developed region at low solids loading and insignificant at C_s = 25 vol. %.

The overall gas holdup increased remarkably by increasing the superficial gas velocity with the presence of internals and the solids. While, a slightly decreased was observed with increased solids loading and increased aspect ratio.

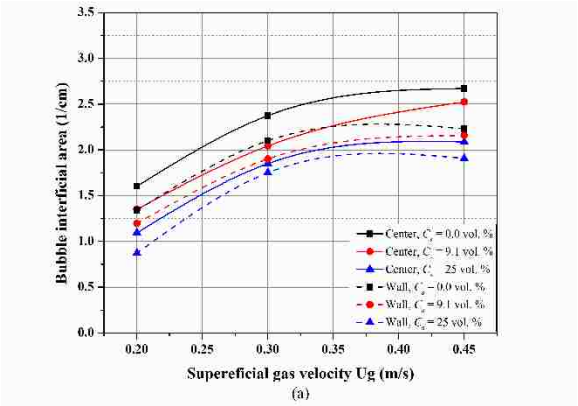

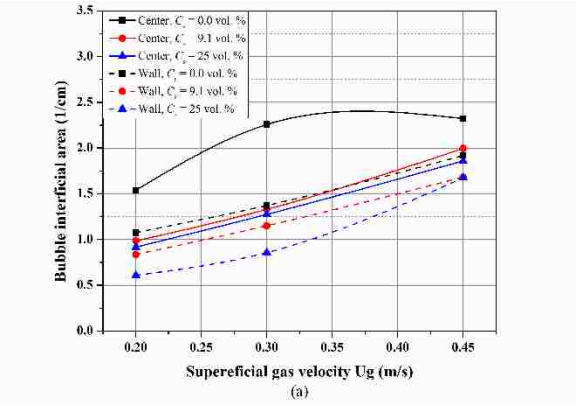

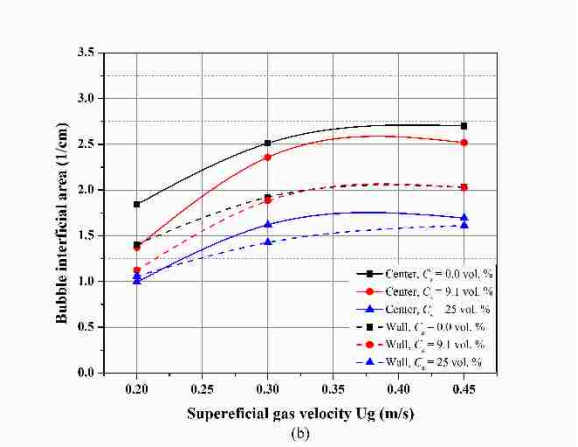

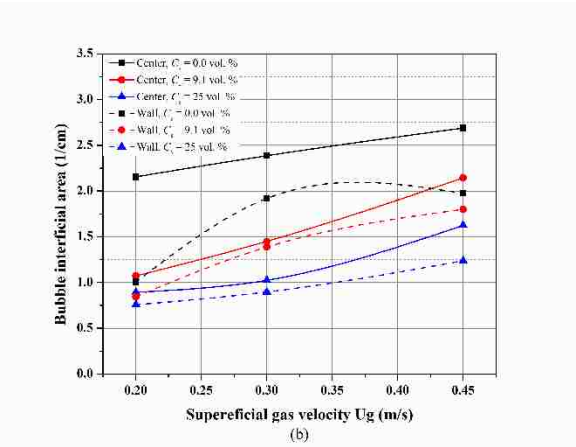

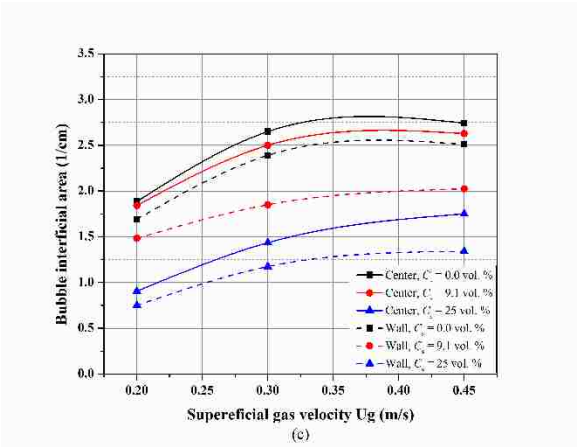

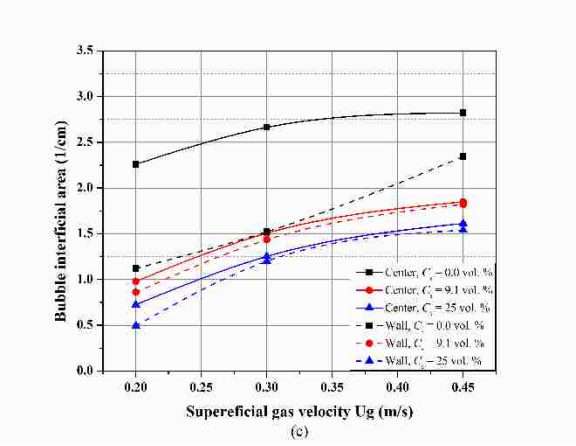

Figure 18. The effect of the gas velocity and solids loading on the specific bubble interfacial area in the fully developed flow region; (a) *H/D* = 5; (b) *H/D* = 4; (c) *H/D* = 3

Figure 19. The effect of the gas velocity and solids loading on the specific bubble interfacial area in the sparger region; (a) *H/D* = 5; (b) *H/D* = 4; (c) *H/D* = 3

Increase in the gas velocity and the presence of internals reduced the influence of the solids loading on the overall gas holdup, which is expected that this can be extended to the entire bubble properties. This phenomenon attributed due to the enhancement the bubble breakup rate. Whereas, the solids loading reduces the influence of the variation of the aspect ratio on the bubble properties and the overall gas holdup.

Adding solids significantly affects the radial distribution of bubble properties. This effect is due to increased pseudo-slurry phase viscosity, which promotes coalescence of the large bubbles. Consequently, the bubble rise velocity increases and gas holdup, bubble frequency, and interfacial area decrease.

The presence of internals changes the radial profiles and distribution of the bubble properties in the sparger and fully developed flow regions for all the gas velocities studied. In comparison with the previous studies, it can be seen that internals reduce the effect of solids loading on the local radial profiles, particularly, reducing the difference in the local gas holdup in the center and the wall regions of the bubble column.

The bubble rise velocity has exhibited a strong dependency toward the gas velocity, solids loading, and the bubble size that promoted by increasing the solids loading. While, the bubble chord length has shown a sensitivity toward the gas velocity, thereby, it could be utilized as a feature to demarcate the flow regime transition.

NOMENCLATURE

CSA = cross section area (m^2)

H/D = aspect ratio, ratio of height of dynamic liquid level to bubble column diameter (-)

d_p = solid particle diameter (μm)

GTL = industrial process to convert the gas to liquid fuel

SBCR = slurry bubble column reactor

BC = bubble column

C_s = solid loading (concertation) volume percentage (%)

CT = gamma-ray Computed Tomography

CARPT = radioactive particle tracking

DPT = differential pressure transducer

d_0 = hole diameter in distributor (mm)

U_g = superficial gas velocity (m/s)

H = height bubble column (m)

H_D = dynamic liquid level (m)

H_S = statistic liquid level (m)

ε_G = overall gas holdup (-)

TKE = turbulent kinetic energy (m^2/s^2)

W_e = Weber number = $\left(\tau d_{b,max}\right)/\sigma$

$\tau = \frac{1}{2}\rho_l \bar{u}_e^2$

$\bar{u}_e^2$ = average value of the fluctuating = $2\left(l_e \rho_l \frac{P}{V}\right)^{2/3}$

$k_\ell a$ = liquid mass transfer coefficient

REFERENCES

[1] M. Kagumba and M. H. Al-Dahhan, "Impact of internals size and configuration on bubble dynamics in bubble columns for alternative clean fuels production," *Industrial and Engineering Chemistry Research*, vol. 54, no. 4, pp. 1359–1372, 2015.

[2] H. Al-Naseri, J. P. Schlegel, and M. H. Al-Dahhan, "The Effects of Internals and Low Aspect Ratio on The Flow Development and Bubble Dynamics in Pilot-Plant Bubble Column for Fischer-Tropsch synthesis," *Experimental Thermal and Fluid Science*, vol. 104, no. October 2018, pp. 284–301, 2019.

[3] R. Krishna and S. T. Sie, "Design and scale-up of the Fischer – Tropsch bubble column slurry reactor," *Fuel Processing Technology*, vol. 64, pp. 73–105, 2000.

[4] C. Wu, K. Suddard, and M. H. Al-Dahhan, "Bubble Dynamics Investigation in a Slurry Bubble Column," *AIChE Journal*, vol. 54, no. 5, pp. 1203–1212, Jan. 2008.

[5] J. Chen, F. Li, S. Degaleesan, P. Gupta, M. H. Al-Dahhan, M. P. Duduković, B. A. Toseland, M. P. Dudukovic, and B. A. Toseland, "Fluid dynamic parameters in bubble columns with internals," *Chemical Engineering Science*, vol. 54, no. 13–14, pp. 2187–2197, 1999.

[6] R. Schäfer, C. Merten, and G. Eigenberger, "Bubble size distributions in a bubble column reactor under industrial conditions," *Experimental Thermal and Fluid Science*, vol. 26, no. 6–7, pp. 595–604, 2002.

[7] G. Besagni and F. Inzoli, "The effect of liquid phase properties on bubble column fluid dynamics: Gas holdup, flow regime transition, bubble size distributions and shapes, interfacial areas and foaming phenomena," *Chemical Engineering Science*, vol. 170, pp. 270–296, 2016.

[8] U. P. Veera, J. B. B. Joshi, U. Parasu Veera, and J. B. B. Joshi, "Measurement of gas hold-up profiles in bubble column by gamma ray tomography Effect of liquid phase properties," *Chemical Engineering Research and Design*, vol. 78, no. 3, 2000.

[9] P. Rollbusch, M. Becker, M. Ludwig, A. Bieberle, M. Grünewald, U. Hampel, and R. Franke, "Experimental investigation of the influence of column scale, gas density and liquid properties on gas holdup in bubble columns," *International Journal of Multiphase Flow*, vol. 75, pp. 88–106, 2015.

[10] I. S. Shin, S. M. Son, U. Y. Kim, Y. Kang, S. D. Kim, H. Jung, I. Sang Shin, S. M. Son, U. Y. Kim, Y. Kang, D. Kim, and H. Jung, "Multiple effects of operating variables on the bubble properties in three-phase slurry bubble columns," *Korean Journal of Chemical Engineering*, vol. 26, no. 2, pp. 587–591, 2009.

[11] A. Esmaeili, S. Farag, C. Guy, and J. Chaouki, "Effect of elevated pressure on the hydrodynamic aspects of a pilot-scale bubble column reactor operating with non-Newtonian liquids," *Chemical Engineering Journal*, vol. 288, pp. 377–389, 2016.

[12] N. Rados, A. Shaikh, and M. H. Al-Dahhan, "Phase Distribution in a High Pressure Slurry Bubble Column via a Single Source Computed Tomography," *The Canadian Journal of Chemical Engineering*, vol. 83, no. February, 2005.

[13] P. M. Wilkinson, A. P. Spek, and L. L. van Dierendonck, "Design parameters estimation for scale- up of high- pressure bubble columns," *AIChE Journal*, vol. 38, no. 4, pp. 544–554, 1992.

[14] A. Forret, J. M. Schweitzer, T. Gauthier, R. Krishna, and D. Schweich, "Influence of scale on the hydrodynamics of bubble column reactors: An experimental study in columns of 0.1, 0.4 and 1 m diameters," *Chemical Engineering Science*, vol. 58, no. 3–6, pp. 719–724, 2003.

[15] S. Sasaki, K. Uchida, K. Hayashi, and A. Tomiyama, "Effects of column diameter and liquid height on gas holdup in air-water bubble columns," *Experimental Thermal and Fluid Science*, vol. 72, pp. 67–74, 2017.

[16] G. Besagni, A. Di Pasquali, L. Gallazzini, E. Gottardi, L. P. M. Colombo, and F. Inzoli, "The effect of aspect ratio in counter-current gas-liquid bubble columns: Experimental results and gas holdup correlations," *International Journal of Multiphase Flow*, vol. 94, pp. 53–78, 2017.

[17] S. Sasaki, K. Hayashi, and A. Tomiyama, "Effects of liquid height on gas holdup in air–water bubble column," *Experimental Thermal and Fluid Science*, vol. 72, pp. 67–74, 2016.

[18] H. Li, A. Prakash, A. Margaritis, and M. A. Bergougnou, "Effects of micron-sized particles on hydrodynamics and local heat transfer in a slurry bubble column," *Powder Technology*, vol. 133, no. 1–3, pp. 171–184, 2003.

[19] S. Ojima, S. Sasahi, K. Hayashi, A. Tomiyama, S. Sasaki, K. Hayashi, A. Tomiyama, and and A. T. Shimpei Ojima, Shohei Sasaki, Kosuke Hayashi, "Effects of particle diameter on bubble coalescence in a slurry bubble column," *Journal of chemical engineering of Japan*, vol. 48, no. 3, pp. 181–189, 2015.

[20] N. Rados, A. Shaikh, and M. H. Al-Dahhan, "Solids flow mapping in a high pressure slurry bubble column," *Chemical Engineering Science*, vol. 60, no. 22, pp. 6067–6072, 2005.

[21] M. K. Al Mesfer, A. J. Sultan, and M. H. Al-Dahhan, "Impacts of dense heat exchanging internals on gas holdup cross-sectional distributions and profiles of bubble column using gamma ray Computed Tomography (CT) for FT synthesis," *Chemical Engineering Journal*, vol. 300, pp. 317–333, 2016.

[22] M. K. Al Mesfer, A. J. Sultan, and M. H. Al-Dahhan, "Study the Effect of Dense Internals on the Liquid Velocity Field and Turbulent Parameters in Bubble Column for Fischer–Tropsch (FT) Synthesis by Using Radioactive Particle Tracking (RPT) Technique," *Chemical Engineering Science*, vol. 161, pp. 228–248, 2017.

[23] A. J. Sultan, L. S. Sabri, and M. H. Al-Dahhan, "Investigating the influence of the configuration of the bundle of heat exchanging tubes and column size on the gas holdup distributions in bubble columns via gamma-ray computed tomography," *Experimental Thermal and Fluid Science*, vol. 98, no. February, pp. 68–85, 2018.

[24] A. J. Sultan, L. S. Sabri, and M. H. Al-Dahhan, "Impact of heat-exchanging tube configurations on the gas holdup distribution in bubble columns using gamma-ray computed tomography," *International Journal of Multiphase Flow*, vol. 106, pp. 202–219, 2018.

[25] A. J. Sultan, L. S. Sabri, and M. H. Al-Dahhan, "Influence of the size of heat exchanging internals on the gas holdup distribution in a bubble column using gamma-ray computed tomography," *Chemical Engineering Science*, vol. 186, pp. 1–25, 2018.

[26] G. Bloch, "Axial and Radial Dispersion in a Large-Diameter Bubble Column Reactor at Low Height-to- Diameter Ratios," *Chemical Ingenier Technik*, vol. 87, no. No. 6, pp. 756–761, 2015.

[27] P. Tyagi and V. V. Buwa, "Dense gas–liquid–solid flow in a slurry bubble column: Measurements of dynamic characteristics, gas volume fraction and bubble size distribution," *Chemical Engineering Science*, vol. 173, pp. 346–362, 2017.

[28] O. N. Manjrekar and M. P. Dudukovic, "Application of a 4-point optical probe to a Slurry Bubble Column Reactor," *Chemical Engineering Science*, vol. 131, pp. 313–322, 2015.

[29] S. Kumar and A. Khanna, "Experimental analysis and development of correlations for gas holdup in high pressure slurry co-current bubble columns," *Korean Journal of Chemical Engineering*, vol. 31, no. 11, pp. 1964–1972, 2014.

[30] S. Rabha, M. Schubert, and U. Hampel, “Intrinsic flow behavior in a slurry bubble column: A study on the effect of particle size,” *Chemical Engineering Science*, vol. 93, pp. 401–411, 2013.

[31] S. Rabha, M. Schubert, M. Wagner, D. Lucas, and U. Hampel, “Bubble Size and Radial Gas Hold-Up Distributions in a Slurry Bubble Column Using Ultrafast Electron Beam X-Ray Tomography,” *AIChE Journal*, vol. 59, no. 5, pp. 1709–1722, 2013.

[32] A. Behkish, R. Lemoine, L. Sehabiague, R. Oukaci, and B. I. Morsi, “Gas holdup and bubble size behavior in a large-scale slurry bubble column reactor operating with an organic liquid under elevated pressures and temperatures,” *Chemical Engineering Journal*, vol. 128, no. 2–3, pp. 69–84, 2007.

[33] H. Li and A. Prakash, “Influence of slurry concentrations on bubble population and their rise velocities in a three-phase slurry bubble column,” *Powder Technology*, vol. 113, no. 1–2, pp. 158–167, 2000.

[34] R. Krishna, J. W. A. de Swart, J. Ellenberg, G. B. Martina, and C. Maretto, “Gas holdup in slurry bubble columns: Effect of column diameter and slurry concentrations,” *A.I.Ch.E. Journal*, vol. 43, p. 311, 1997.

[35] J. W. A. De Swart, R. E. Van Vliet, and R. Krishna, “Size, structure and dynamics of ‘large’ bubbles in a two-dimensional slurry bubble column,” *Chemical Engineering Science*, vol. 51, no. 20, pp. 4619–4629, 1996.

[36] S. Sasaki, K. Uchida, K. Hayashi, and A. Tomiyama, “Effects of column diameter and liquid height on gas holdup in air-water bubble columns,” *Experimental Thermal and Fluid Science*, vol. 72, pp. 67–74, 2017.

[37] A. A. Jasim, A. J. Sultan, and M. H. Al-Dahhan, “Impact of heat exchanging internals configurations on the gas holdup and bubble properties in a bubble column,” *International journal of multiphase flow*, vol. 112, pp. 63–82, 2019.

[38] A. A. Jasim, A. J. Sultan, and M. H. Al-Dahhan, “Influence of heat-exchanging tubes diameter on the gas holdup and bubble dynamics in a bubble column,” *Fuel*, vol. 236, no. March 2018, pp. 1191–1203, 2019.

[39] B. C. Ong, P. Gupta, A. Youssef, M. Al-Dahhan, and M. P. Duduković, “Computed Tomographic Investigation of the Influence of Gas Sparger Design on Gas Holdup Distribution in a Bubble Column,” *Industrial & Engineering Chemistry Research*, vol. 48, no. 1, pp. 58–68, 2009.

[40] G. E. P. Box, W. G. Hunter, and J. S. Hunter, *Statistics for Experimenters An Introduction to Design, Data Analysis, and Model Bulding*. Wiley, 1978.

[41] J. J. Frijlink, “Physical aspects of gassed suspension reactors,” Delft University of Technology, 1987.

[42] M. Kagumba, “Heat transfer and bubble dynamics in bubble and slurry bubble columns with internals for Fischer-Tropsch synthesis of clean alternative fuels and chemicals,” Missouri University of Science and Technology, 2013.

[43] J. Xue, “Bubble Velocity, Size and Interfacial Area Measurements in Bubble columns,” Washington Univeristy, Saint Louis, 2004.

[44] J. Xue, M. Al-Dahhan, M. P. Dudukovic, and R. F. Mudde, “Four-point optical probe for measurement of bubble dynamics: Validation of the technique,” *Flow Measurement and Instrumentation*, vol. 19, no. 5, pp. 293–300, 2008.

[45] J. Xue, M. Al-dahhan, M. P. Dudukovic, and R. F. Mudde, “Bubble Dynamics Measurements Using Four-Point Optical Probe,” *The Canadian Journal of Chemical Engineering*, vol. 81, no. August, pp. 375–381, 2003.

[46] A. B. Pandit and Y. K. Doshi, “Mixing time studies in bubble column reactor with and without internals,” *International Journal of Chemical Reactor Engineering*, vol. 3, pp. 1–23, 2005.

[47] R. Krishna, J. Ellenberger, D. E. Hennophof, D. E. Hennephof, and D. E. Hennophof, “Analogous description of the hydrodynamics of gas-solid fluidized beds and bubble columns,” *The Chemical Engineering Journal*, vol. 53, no. 1, pp. 89–101, 1993.

[48] R. Krishna and J. Ellenberger, “Gas holdup in bubble column reactors operating in the churn-turbulent flow regime,” *AIChE Journal*, vol. 42, no. 9, pp. 2627–2634, 1996.

[49] V. P. Chilekar, C. Singh, J. Van Der Schaaf, B. F. M. Kuster, and J. C. Schouten, “A Gas Hold-Up Model for Slurry Bubble Columns,” *AIChE Journal*, vol. 53, no. 7, pp. 1687–1702, 2007.

[50] A. Shaikh and M. Al-Dahhan, “Scale-up of bubble column reactors: A review of current state-of-the-art,” *Industrial and Engineering Chemistry Research*, vol. 52, no. 24, pp. 8091–8108, 2013.

[51] M. Kagumba, H. Al-Naseri, and M. H. Al-Dahhan, “A new contact time model for the mechanistic assessment of local heat transfer coefficients in bubble column using both the four-optical fiber probe and the fast heat transfer probe-simultaneously,” *Chemical Engineering Journal*, vol. 361, no. December 2018, pp. 67–79, 2019.

[52] X. Guan, N. Yang, Z. Li, L. Wang, Y. Cheng, and X. Li, "Experimental Investigation of Flow Development in Large-Scale Bubble Columns in the Churn-Turbulent Regime," *Industrial and Engineering Chemistry Research*, vol. 55, no.

[53] A. Shaikh and M. Al-Dahhan, "Characterization of the hydrodynamic flow regime in bubble columns via computed tomography," *Flow Measurement and Instrumentation*, vol. 16, pp. 91–98, 2005.

[54] N. Hooshyar, P. J. Hamersma, R. F. Mudde, and J. R. Van Ommen, "Gas fraction and bubble dynamics in structured slurry bubble columns," *Industrial and Engineering Chemistry Research*, vol. 49, no. 21, pp. 10689–10697, 2010.

[55] A. Yasunishi, M. Fukuma, and K. Muroyama, "Measurement Of Behavior Of Gas Bubbles And Gas Holdup In A Slurry Bubble Column By A Dual Electroresistivity Probe Method," *Journal of Chemical Engineering of Japan*, vol. 19, no. 5, pp. 444–449, 1986.

[56] J. R. Crabtree and J. Bridgwater, "Bubble coalescence in viscous liquids," *Chemical Engineering Science*, vol. 26, no. 6, pp. 839–851, Jun. 1971.

[57] H. Al-Naseri, J. P. Schlegel, and M. H. Al-Dahhan, "The Impact of Low Aspect Ratio on Flow Regime Transition in Industrial-Sized Pilot Plant Bubble Column Reactor," *Chemical Engineering Journal*, vol. submitted, 2018.

[58] A. A. Youssef, M. E. Hamed, J. T. Grimes, M. H. Al-Dahhan, and M. P. Duduković, "Hydrodynamics of pilot-scale bubble columns: Effect of internals," *Industrial and Engineering Chemistry Research*, vol. 52, no. 1, pp. 43–55, 2013.

[59] H. Li and A. Prakash, "Survey of heat transfer mechanisms in a slurry bubble column," *The Canadian Journal of Chemical Engineering*, vol. 79, no. 5, pp. 717–725, 2001.

[60] S. Kumar, K. Kusakabe, K. Raghunathan, and L. - S. Fan, "Mechanism of heat transfer in bubbly liquid and liquid-solid systems: Single bubble injection," *AIChE Journal*, vol. 38, no. 5, pp. 733–741, 1992.

[61] G. Q. G. Yang, X. Luo, R. Lau, and L. S. Fan, "Heat-Transfer Characteristics in Slurry Bubble Columns at Elevated Pressures and Temperatures," *Industrial & Engineering Chemistry Research*, vol. 39, no. 7, pp. 2568–2577, 2000.

[62] K. H. Choi and W. K. Lee, "Behavior of Bubble in a Concentric Cylindrical Airlift Column," *Korean Journal of Chemical Engineering*, vol. 9, no. 2, pp. 66–73, 1992.

[63] L. Sehabiague, “Modeling, Scaleup and Optimization of Slurry Bubble Column,” University of Pittsburgh, Sanson School of Engineering, 2012, 2012.

[64] A. Behkish, “Hydrodynamic and Mass Transfer Parameters in Large-Scale Slurry Bubble Column Reactors,” Chemical Engineering, University of Pittsburgh, 2004,

III. THE IMPACT OF LOW ASPECT RATIO ON FLOW REGIME TRANSITION IN INDUSTRIAL-SIZED PILOT PLANT BUBBLE COLUMN REACTOR

ABSTRACT

Numerous studies on flow regime were executed in lab scale bubble columns with high dynamic liquid level (aspect ratio, $H/D \geq 5$), while in the industry the typical dimension is $H/D \leq 5$. Therefore, the purpose of this paper is to study the effect of low aspect ratio ($H/D \leq 5$) on the flow regime transitions in an industrial-sized bubble column. The flow regime at three aspect ratios (H/D = 3, 4, and 5) was demarcated experimentally using linear and non-linear methods, which are represented by the drift-flux and Kolmogorov Entropy (KE), respectively. The four-point optical fiber probe technique has been used to quantify the bubble properties at different regimes and to infer the flow pattern. The experiments were conducted in industrial-sized bubble column of 0.6 m I.D. and 3.89 m height. The superficial gas velocity varies from 0.005 m/s to 0.45 m/s. The results display that the variation in the aspect ratio has a significant impact on the transition velocity to the churn turbulent regime, while the overall gas holdup in the churn turbulent regime increases with increase the aspect ratio. Three mean regimes were indicated by the linear method: bubbly, transition, and churn turbulent. Four regimes are demarcated by the nonlinear method: gas maldistribution, bubbly, transition, and churn turbulent. The results for transition velocity show disagreement with data in the literature. While the empirical correlations of Ribeiro [1], and Şal et al. [2], which are validated with experimental results,

introduce a good agreement with percentage errors of 8.6-17.3% and 8.26-25.69%, respectively.

1. INTRODUCTION

Bubble columns are a type of multiphase reactor characterized by excellent thermal control, high heat/mass transfer rate, high selectivity and conversion, and low operation and maintenance costs. They are widely utilized in chemical, petrochemical, metallurgical, and biochemical industries. Specific examples include Fischer-Tropsch (F-T) synthesis, water treatment, liquid phase methanol synthesis, and dimethyl ether synthesis. The disadvantages of this reactor are the difficulty in scale-up and design due to the complex interactions between the gas and liquid phase, and the liquid circulation and back mixing which negatively affects the selectivity and conversion [3].

In spite of the wide industrial uses of bubble columns, still there is difficulty in their design and scale-up because of a lack of knowledge on the flow structure and dynamics. Numerous investigations have been conducted in improving their understanding; however, the convoluted hydrodynamic characteristics and the inherent unsteadiness of the flow complicate the design and operation of the bubble columns [4]. A stronger fundamental understanding of the liquid flow structure and hydrodynamic parameters will promote the modeling, design, and scale-up properly [5]. The variation in these design parameters, which included the dimension of the bubble column, gas and liquid phase properties, and the operating conditions, divide the bubble column behavior into different regimes referred to as the flow regimes or flow patterns [6]. Different gas and liquid dynamic behaviors characterize each flow regime. Consequently identifying the flow regime at which a bubble

column will be operated is essential for reliable modeling, design, and scale-up. Often, models formed for a particular flow regime are not valid for other flow regimes because of the differences in mixing [7] and mass/heat transfer characteristics [8].

Most studies on the sensitivity of the flow regime to the bubble column dimensions have been conducted in facilities that were not similar to those utilized in the field (aspect ratio $H/D \geq 9$, an inner diameter ID = 6-18 inches). While, the actual aspect ratio for the bubble column reactor that used in the industry is $H/D \leq 5$, because of the limitation in the column manufacturing and constructor, cost, and exothermic reasons [9]. Therefore, the results of these studies are not qualified for scale up to industrial size without error in design. Based on this, this work aims to investigate the effect of the low dynamic liquid level (aspect ratio, H/D) on the flow regime by using the overall gas holdup and the pressure transducer signal to demarcate the transition velocities and measuring the bubble properties to characterize the different regimes. The results will be compared with previous experimental work and with empirical correlations.

2. FLOW REGIMES IN BUBBLE COLUMN

In general, there are three flow regimes of interest in chemical processing as shown in the schematic of Figure 1: (1) the bubbly or homogeneous flow regime, (2) the transition regime, and (3) the churn turbulent or heterogeneous flow regime. The boundaries that separate these regimes are usually not sharp but are named by transition velocities as represented by points A and B in Figure 1 [5]. In the homogenous regime, as shown in Figure 2(a), the bubbles are characterized by relatively small and uniform spherical shape,

low number density, bubbles traveling rectilinearly with minor lateral variation, and gentle gas-liquid agitation. Bubbles are widely spaced, reducing interactions and leading to insignificant bubble coalescence and breakup. The bubble size distribution is narrow and depends strongly on the liquid properties and design of the gas distributor.

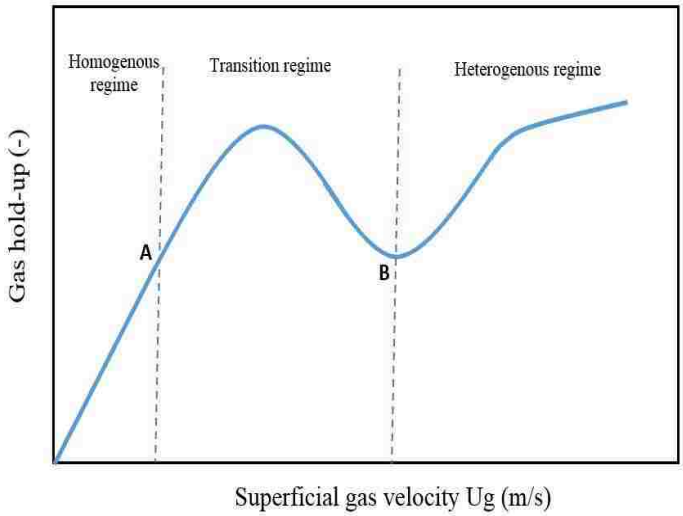

Figure 1. Flow regime transition in bubble column

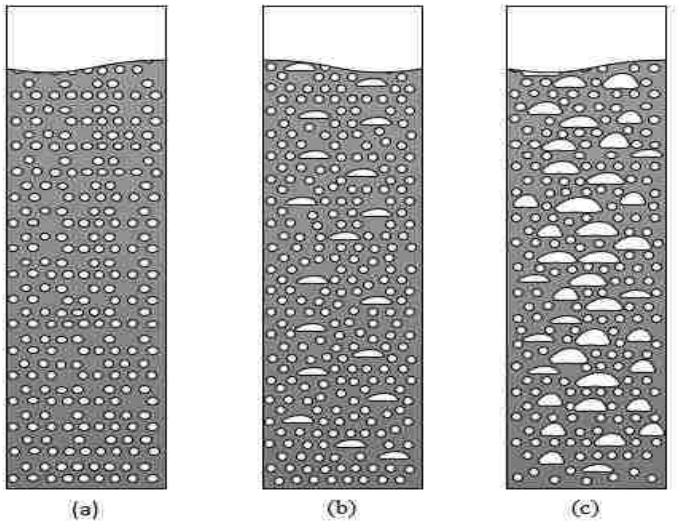

Figure 2. Visual observations of the three flow regimes in bubble column

Relatively flat radial profiles for the gas holdup and liquid velocity are present in the entire cross-section of the bubble column.

As the superficial gas velocity increases, the transition flow regime is encountered where the flow pattern transits gradually from bubbly to the churn regime. This regime is shown in Figure 2(b). The bubble population increases, which leads to decreasing space between bubbles and enhances the coalescence significantly. Therefore a wider bubble size distribution and larger eddies and flow macrostructure exist due to the onset of bubble coalescence [10]. The existence of two sub-regime transitions, first and second sub-regimes, have been revealed by E. Olmos et al. [11-12], and Barghi et al.[13]. In the first sub-regime transition, the bubble coalescence occurs only in the distributor region, whereas in the second sub-regime transition the bubble coalescence and breakup begin to dominate in the bulk region, together with the development of gross liquid circulation effects.

The heterogeneous regime, which occurs at high superficial gas velocity, is shown in Figure 2(c). It is characterized by disturbing the bubbly flow regime due to enhancement in the turbulent motion of gas bubbles and liquid recirculation. As a result unsteady flow regimes and large bubbles with short residence times are formed by coalescence. Because of the increase in the bubble coalescence and breakup, various bubble sizes appear in this regime, leading to a wide bubble size distribution. The bubble number density becomes so large that the bubbles begin to interact with each other directly or indirectly through collisions or the effects of wakes. With a further increase in bubble number density, the bubbles tend to coalesce to form aspherical cap bubbles and the flow changes to interacting churn-turbulent bubbly flow. The flow contains cap bubbles formed in this way as well as smaller bubbles and is highly agitated because of the interactions between bubble motions

and turbulent flow. The large bubbles churn through the liquid; thus, it is called churn-turbulent flow. The large bubbles can form a cluster of bubbles which behaves like a single gastropod. They sometimes coalesce to form a gas slug and sometimes separate into individual bubbles particularly in the small diameter column. This flow regime is thus a transition from bubbly flow to slug or churn flow. Churn-turbulent flow frequently is observed in industrial-size, large-diameter columns [14].

Extensive studies have been conducted to investigate the flow regime transitions are listed with more detail in Table 1. Different aspects of the experiments that may affect the flow regime transitions have been listed: the bubble column dimension, gas distributor design, gas/liquid flow rate, and operating conditions (pressure, temperature, solid concentration and particle diameter, and gas/liquid physical properties). The impact of operating pressure on the flow regime transition has been studied by Shaikh and Al-Dahhan [5] using the radial profile of gas holdup, which was measured by gamma-ray computed tomography (CT) technique. The results reported that the increase in pressure leads to a delay in the transition velocity. Furthermore, the transition in flow regime was demarcated clearly under ambient pressure, in contrast to high pressure where the transition occurs gradually. Nedeltchev et al. [15] identified the flow regime transition by utilizing the pressure transducer technique and used two types of organic liquids, 1-Butanol and gasoline, at different pressures. The study revealed that the pressure influence on flow regime transition varied according to the liquid properties. Moreover, the second and fourth transition velocities under ambient pressure occur earlier in 1-butanol than in gasoline.

Mena et al. [16] experimentally investigated the impact of solids concentration on the homogeneous/heterogeneous flow regime transition and homogenous stability using

particle diameter d_p = 2.1 mm. The critical condition for stability was expressed by the values of gas holdup and gas flow rate. The study showed that for low solids concentration (C_s < 3 Vol%) the homogeneous regime is stabilized and the transition velocity for the homogeneous regime increases, whereas high solid concentration (C_s > 3 Vol%) destabilized the homogeneous regime and decreased the transition velocity. Furthermore, Kumar et al. [17] studied the solid effect by using different particle diameter, d_p=35 μm. The results were compatible with Mena et al. [16], except, the velocity transition for the homogenous regime increased with increased solids concentration until C_s = 1 Vol%. This difference could be attributed to an increase in the bubble coalescence rate for smaller particle diameters. The sparger geometry effect had been studied by Şal et al. [2]. The flow regime transition was indicated experimentally by measuring the global gas hold-up and calculating the drift-flux, and predictively by using linear stability theory and correlations based on dimensionless numbers. The results reported that the transition velocity for the homogeneous and heterogeneous regimes decreased with increasing sparger hole diameter. The effect of bubble column dimensions (height and diameter) on flow regime transition were investigated experimentally by Nedeltchev and Schubert [18] and extensively by Ruzicka et al. [19]. The results of Ruzicka, Drahos, et al. [19] showed that increasing size in height or diameter decreases the stability of the homogenous regime.

A local measurement technique has been used to demarcate the flow regime transition as well. Zhang et al. [20] used the bubble properties as a criterion to identify the flow regime transition and developed an empirical correlation to predict the flow regime boundaries. The bubble properties were measured using a two-element conductivity probe that placed at the center of a bubble column at the height of H/D = 7.87 above the

distributor. The regimes have been identified locally by bubble properties since each regime has an individual dynamic. According to the data obtained, reported the capability of the bubble properties to demarcate the flow regime transition, whereas, the experimental results exhibit alignment with the prediction results. Similarly, Shiea et al. [21] proved the applicability of bubble properties to detect the transition regimes. They reported that the transition occurred throughout the bubble column at nearly the same superficial gas velocity and emphasized that probe should be located in the center of the column and far from the distributor.

Various algorithm methods have been used to analyze the signals of the techniques that used to identify the transition. The time series signal from the multiphase system can be analyzed by nonlinear methods such as chaos analysis using the Kolmogorov Entropy (KE) or statistical analysis using standard deviation, fractal analysis, power spectral density, etc. [7], [10], [11], [13], and [17]. Recently, Medjiade et al. [22] conducted a flow regime transition study to compare different techniques and pressure impact. Their results sho wed that the KE method was the most reliable analysis method.

Numerous studies [23-27] developed correlations, were formulated based on bubble properties, to predict the flow regime transition. Mishima et al. [23] formulated predictive correlations postulating the gas hold-up as the criteria to identify the flow regime transition and applicability at different temperatures and pressures. Subsequently, these correlations have been validated by Schlegel et al. [28]. Furthermore, Simonnet et al. [29], Lin et al. [30], Das et al. [31], and Baten and Krishna [32] utilized CFD simulation to predict the flow regime transition. Das et al. [31] successfully identified the transition from bubbly to slug regime by utilizing CFD simulation using the population bubble model to

account for the bubble size, bubble frequency, and bubble coalesce and break up rate. Coalescence and breakup rate were used as new criteria to indicate flow regime transition. The results exhibit a good agreement with the experiments and the strength of the CFD simulation to define the bubbly flow boundaries.

3. EXPERIMENTAL SETUP AND MEASUREMENT TECHNIQUES

3.1. EXPERIMENTAL SETUP

The experimental work, which conducted by using a bubble column of an inside diameter of 0.6 m and a height of 3.9 m, have been carried out at ambient pressure and temperature. The schematic diagram of the bubble column illustrated in Figure 3 that shows the dimension and the locations of the techniques (advanced four-point fiber optical probe and the pressure transducer). The oil-free compressed air was used as the gas phase, where the air flow rate was adjusted by using two parallel rotometers. Meanwhile, the superficial gas velocity has been calculated based on the net cross-section area (CSA) of the bubble column and varied from 0.005 m/s to 0.45 m/s. Tap water constituted the liquid phase. An air-water system was used since the bulk of the published data and knowledge are based on a system that is easy and cost effective to use, and in order to have a basis for the comparison. The air was sparged into the bubble column from the bottom through the distributor, which consisted of 600 holes with a diameter of 3 mm arranged in a triangular pattern with 20 mm pitch and 1.451% open area. The superficial gas velocity was incremented by 0.005 m/s, when measuring pressure fluctuations, whereas, the increment was 0.01 m/s when measuring the overall and local gas holdup.

Table 1. Previous studies in flow regime in bubble column

Author	Setup Dimension (m)	System and flow direction	Operation condition	Technique	Method of data analysis	Investigation goals and results
Medjiade et al. [22]	D=0.102 H=2.4	Two Phases (Nitrogen-Water) Poll condition	Temperature:298 K Pressure: 0.1, 0.25, 0.5, 1.0, 2.0 MPa	Differential pressure sensor	Standard deviation, fractal analysis, Power spectral density, Chaos analysis (Kolmogorov Entropy KE)	Investigate the operating pressures impact on the flow regime transition by using different analysis techniques.
Nedeltchev and Schubert [18]	D=0.15, 0.4 H=2	Two phases (air-water)	Ambient temperature and pressure	Wire Mesh Sensor	New statistical parameter, Chaos analysis (Kolmogorov Entropies KE)	Demarcate the transition regime in two bubble columns of different diameter size by using new parameter.
Sal et al. [2]	D=0.33 H=3	Two phases (air-water) counterflow	Ambient temperature and pressure	Measurement overall gas holdup	Drift-flux, Linear stability	Investigate the effect of sparger geometry (hole diameter) on flow regime transition by measuring the global gas holdup.
Shiea et al. [21]	D=0.09 H=1.8	Two phases (air-water) up flow	Ambient temperature and pressure	Resistivity Probe (double-needle)	Bubble properties	Using bubble properties as criteria to detect the flow regime transition, wherein three different axial- locations detected.
Li et al. [33]	H=0.8 Depth=0.01 Width=0.1	Three-phase: (air-water-glass beads), pool condition	Ambient temperature and pressure	Pressure transducer	Statistical, Hurst, Hilbert-Huang transfer, Shannon entropy analysis	Investigate the flow regime and transition velocity by using different techniques analysis in three phases system.
Nedeltchev et al. [34]	D=0.14 H=1.33	Two phases (air-water) pool condition	Ambient temperature and pressure	Pressure transducer	Chaos analysis (Kolmogorov Entropies KE)	Identify the flow regime in three types of reactors (bubble column, spouted bed, and fluidized bed) by using the pressure transducer and analyze the time series signal by (Kolmogorov Entropies KE).
Schlegel et al. [28]	D=0.15 H=4.4	Two phases (air-water) up flow	Ambient temperature and pressure	Electrical Impedance Void Meters	Cumulative Probability Density Function (CPDF)	Characterize the flow regime in different axial locations, the cumulative probability density function (CPDF) is analysis technique used to analyze the time sires signal, which extruded from the Electrical Impedance Void Meters technique.

Table 1. Previous studies in flow regime in bubble column (cont.)

Vandenberghe et al. [35]	D=0.062 H=1.62	Two phases (air-water) counterflow	Ambient temperature and pressure	Manometer pressure	Drift-flux	Improve the empirical correlation (Drift Flux) by finding a new correlation to relate the characteristic (exponent m) $j_{GL} = U_t \varepsilon_g (1-\alpha_g)^m$ to bubble Reynolds number.
Wu et al. [7]	D=0.15 H=1.5	Two phases (air-water) pool condition	Ambient temperature and pressure	Pressure transducer, Measurement overall gas holdup	Linear analysis (global gas holdup), Nonlinear analysis (Cross-Correlation Function CCF) and Chaos analysis	Identify the flow regime by using new nonlinear analysis technique, called (CCF), and investigate the effect of hole diameter of sparger; the results have been validated with chaos analysis (K) and linear analysis global gas holdup technique.
Barghi et al. [13]	D=0.15 H=2.4	Three phases (air-water-glass beads 35 μm) pool condition	Ambient temperature and pressure	Pressure transducer	Stander deviation, Skewness, Kurtosis, Probability	Investigate the solid particle effect in bubble column on the flow regime transition, utilizing the global gas holdup and different analyzing techniques for pressure fluctuation signal.
Olmos et al. [12]	H=1.2 Depth=0.04 Width=0.2	Two phases (air-water) pool condition	Ambient temperature and pressure	Visual method, Laser Doppler velocimetry (LDV)	Frequency analysis, Chaos analysis, Fractal analysis	Investigate the transition and structure of flow regime in 2D bubble column by utilizing various analysis techniques for Leaser Doppler Velocimeter (LDV).
Ruzicka et al. [19]	D=0.14, 0.29, 0.4 H=0.1-1.2	Two phases (air-water) pool condition	Ambient temperature and pressure	Pressure transducer, Measurement overall gas holdup	Drift-flux, Voidage	The bubble column dimension (Height, Diameter, Aspect ratio) impact on the regime transition has been studied; this study included validation for the results with theoretical prediction models [24] and [36].
Zhang et al. [20]	D=0.0826 H=2	Three phases (air-water-glass beads) up flow	Ambient temperature and pressure	Conductivity Probe	Bubble Properties	This study used the bubble properties (bubble frequency, sauter mean, bubble chord length and time needed for a bubble pass a specific point) as criteria to investigate the impact of particle size and density on flow transition.
Mishima and Ishii [23]		Two phases, upward	Ambient temperature and pressure	Modeling	Gas holdup	In this study, the gas holdup, which derived based on that four regimes bubbly, slug, churn and annual exist, used as criteria to predict the flow regime in two-phase upward flow in vertical tube.

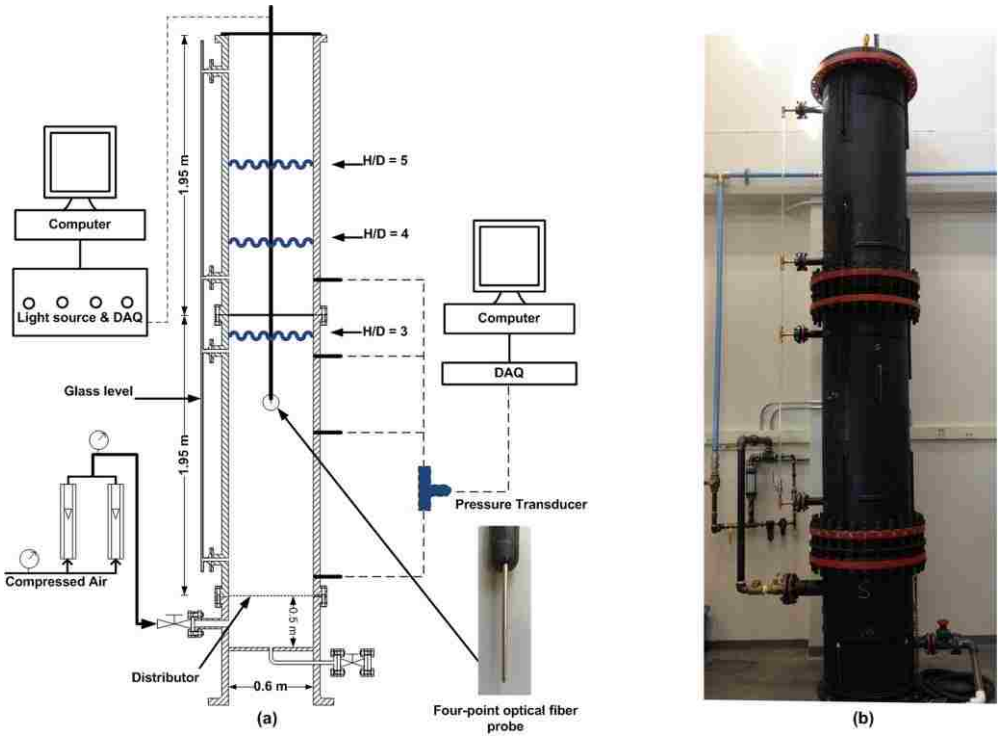

Figure 3. A schematic diagram of the experimental setup

3.2. MEASUREMENT TECHNIQUES

3.2.1. Differential Pressure Transducer. The differential pressure transducer (Omega Inc. PX409-005DWUI), which consisted of two ports, was used to obtain the pressure drop fluctuation signal. The first port of the pressure transducer was placed at the bottom of the bubble column, 0.15 m above the distributor. Because of using different dynamic liquid levels (*H/D* = 3, 4, and 5) in this work, the second port was placed at axial positions of 1.2, 1.7, and 2 m above the distributor, respectively, to prevent the errors in the measurement of pressure due to the disengagement region. Thereby, the pressure drop variations in the sparger and bulk regions were evaluated in this work. The 4-20 mA signal from the pressure transducer was collected by an OMB-DAQ-56 data acquisition board (Omega Inc.) with a sampling rate of 66.7 Hz. The durability, low price, installation, and

sensitivity for flow regime transition are the features of the pressure transducer, and hence, it has been used extensively in industry to monitor the operation. In addition, it is easy to indicate the flow regime and its transition through analyzing the pressure fluctuations signal whether the absolute or pressure drop signals, especially, when operating in severe conditions (high pressure), where the visual observation is impossible.

3.3. FOUR-POINT OPTICAL PROBE TECHNIQUE

An advanced four-point optical fiber probe, developed at Delft University [37], with data processing software developed at the mFReaL laboratory [38], has been used to measure the chord length, local gas holdup, interfacial area, bubble rise velocity and bubble frequency. Previous researchers Hebrard et al. [39], Zhang et al. [20], and Shiea et al. [21], employed the properties of bubble chord length and the bubble frequency to identify the flow regime transition. Schlegel et al. [21], and Shiea et al. [28] reported that the center region of the bubble column is the best position for the probe to prevent the wall effect on the probe measurement. Further, the flow regime transition occurs in the bulk and sparger region simultaneously [20, 28]. The fully developed region is affected by the superficial gas velocity, the presence of internals, and the variation in the aspect ratio [40]. Therefore, the flow regime that tested under different dynamic liquid levels (H/D = 3, 4, and 5) has been examined in the fully developed flow regime that demarcated by Al-Naseri et al. [40]. Hence, the optical probe was fixed in the center of the bubble column at axial location H = 5 ft, 6 ft, and 6 ft, to prevent the distributor effect on the data.

3.3.1. Overall Gas Holdup. The overall gas hold-up was measured by using equation (1) to demarcate the flow regime transition by linear method. The $\boldsymbol{H_D}$ and $\boldsymbol{H_S}$

represent the dynamic liquid level and the static liquid level, respectively. During the experiment, the static level was adjusted in order to keep the dynamic liquid level equal to the aspect ratios *H/D* = 3, 4, or 5. It has been found that height variation does not affect the hydrodynamics of the bed [41], [42].

$$\varepsilon_G = \frac{H_D - H_S}{H_D} \tag{1}$$

3.4. ANALYSIS METHODS

3.4.1. The Kolmogorov Entropy (KE). Multiphase system has been classified as a chaotic system [42-43]. Therefore, using the non-linear analysis method for the time-series signals of the pressure fluctuation will be a powerful technique to indicate the flow regime transition, especially as the systems are very sensitive to small variation in the initial conditions [8]. The Kolmogorov Entropy (KE), which is defined as a time series analysis approach that is utilized to quantify the level of disorder and non-linear features in a hydrodynamics system [45], is one of the chaos parameters that was used previously to quantify the chaos degree of the bubble column [8, 22, 34]. Large and small value of KE indicates disorder and order, respectively. The algorithm to calculate the KE have been developed by Schouten [46], and Toukan et al. [45] as expressed in equation (2).

$$KE = -f_s \ln\left(1 - \frac{1}{\bar{b}}\right) \tag{2}$$

where: f_s is the sampling frequency, and $\bar{b}$ defined by equation (3)

$$\bar{b} = \frac{1}{M}\sum_{i=1}^{M} b_i \tag{3}$$

More detail can be found in the work of Letzel et al. [8], and Nedeltchev [46] were drawing the KE with the superficial velocity and who used the minimum KE as a transition between two regimes.

3.4.2. The Drift Flux. The drift-flux method is a linear analysis method based on the volumetric flux of a component phase relative to a surface moving at the volume-averaged velocity [48], as defined by equation (4). Plotting the drift-flux versus the superficial gas velocity has been utilized to characterize the flow regime transition from the change in the slope of the curve.

$$j_{GL} = U_g(1 - \varepsilon_G) \mp U_l \varepsilon_G \tag{4}$$

where $\varepsilon_G, U_g,$ and U_l are overall gas hold-up, superficial gas velocity, and superficial liquid velocity, respectively. In this work, the superficial liquid velocity is zero since the liquid phase is not flowing through the bubble column during the operating (i.e., batch process).

3.4.3. Bubble Properties. The bubble properties that include the local gas holdup, bubble chord length, bubble frequency, interfacial area, and bubble rise velocity have been utilized to demarcate the flow regime transition and characterize the dynamic properties in each regime. Kagumba and Al-Dahhan [41] measured the bubble properties in the bubbly and churn-turbulent flow regimes in two sizes of bubble columns of diameter 6, and 18 inches, utilizing the advanced four-point optical probe technique with a sample rate of 40 kHz and time sampling of 138 sec, and the measurement was repeated three times. Accordingly, the bubble properties in this work have been obtained by using the same sample rate and the sampling time for Kagumba and Al-Dahhan [42].

4. RESULTS AND DISCUSSION

4.1. OVERALL GAS HOLDUP

Flow regime transition in bubble column operated with aspect ratio *H/D* = 3 has been illustrated in Figure 4. The change in the slope of the trend indicates the transition from one regime to another. Three regimes have been demarcated, bubbly (homogenous) regime from point A to B, transition regime from point B to C, and heterogeneous (churn turbulent) regime from point C to D. In the bubbly flow regime, the overall gas holdup is growing rapidly with the superficial gas velocity, while, in the transition flow regime exhibits a slight increasing with the gas velocity increases. In the churn-turbulent flow regime the overall gas holdup increases with the superficial gas velocity again, but with a different slope than in the bubbly regime. In similar approach, the results for aspect ratio *H/D* = 4 and 5 have been indicated in Figure 5. The transition regime in both *H/D* = 4 and 5 begins at U_g = 0.08 m/s, and ends at U_g = 0.13 and 0.11 m/s, respectively.

Furthermore, Figure 5 illustrates the effect of the dynamic liquid level on the overall gas holdup and the flow regime transition. The increase in the dynamic liquid levels exhibits an insignificant impact on the first transition velocity from the bubbly to the transition regime, and a significant effect on the second transition from the transition to the churn turbulent regime, which occurs at U_g = 0.15, 0.13, and 0.11 m/s for *H/D* = 3, 4, and 5, respectively, therefore, the decreasing in the aspect ratio would delay the second transition. Moreover, the influence of the dynamic liquid level seems obvious on the overall gas holdup, which is increased with dynamic liquid level increasing. The physical attribution for the impact of the dynamic liquid levels on the overall gas holdup and the flow regime transition is the aspect ratio increasing leads to increasing the bubble

coalescence rate and then increases the bubble size, thereby accelerates the transition to churn turbulent regime early and decreases the overall gas holdup. This effect has not been detected in the homogenous regime because this regime is characterized by uniform bubble size and low bubble population, hence the bubble coalescence rate is low.

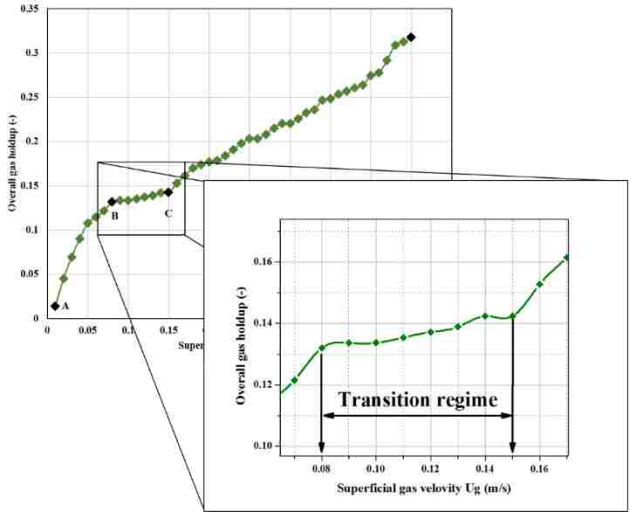

Figure 4. Flow regime transition in bubble column H/D = 3

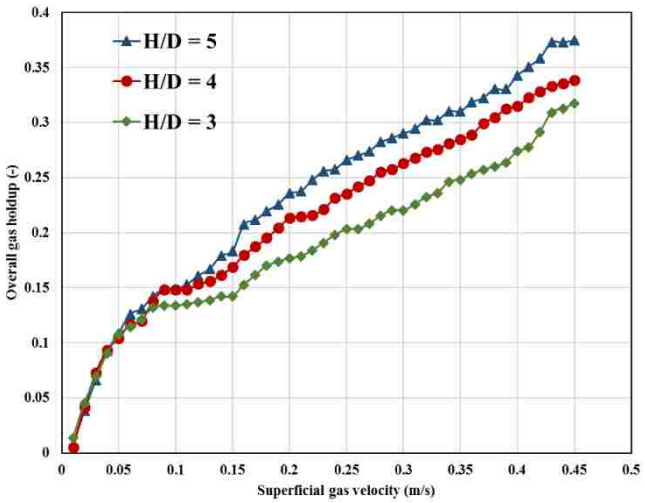

Figure 5. The effect of dynamic liquid levels on the flow regime transition by gas holdup method

4.2. THE DRIFT DLUX

The slope of the overall gas holdup curve in Figures 4 and 5 changes gradually, which may limit the accuracy of the flow regime transition identification. Therefore, the drift flux method has been used for this purpose as well. Drift-flux was plotted as a function of the overall gas holdup by using equation (4) in Figure 6 and Figure 7. The flow regime transition in the bubble column operated with aspect ratio *H/D* = 3 has been illustrated in Figure 6. The drift-flux exhibits three segments with different slopes. The change in the slope represents the transition from one regime to another. Bubbly flow regime starts from point (A) and ends at point (B) at gas holdup = 0.132, which is equivalent to superficial gas velocity U_g = 0.08 m/s. The churn turbulent regime begins from point (C) and ends in a point (D) at gas holdup = 0.142, which is equivalent to superficial gas velocity U_g = 0.14 m/s. Using drift-flux method provides easy demarcation for the regime transitions.

The impact of the dynamic liquid levels on the flow regime transition has been illustrated in Figure 7. The first part of this curve shows an insignificant effect for the dynamic liquid levels with a good agreement with the gas holdup method. While, the second part of the trend of drift flux shows a significant influence for the dynamic liquid levels, where the transition occurs at gas holdup of 0.14, 0.11, and 0.1 m/s for aspect ratio *H/D* = 3, 4, and 5, respectively.

From both methods, increasing the aspect ratio leads to the transition between the transition regime to churn turbulent regime to occur earlier at lower superficial gas velocity as illustrated in Figure 8. The transition in the drift-flux method is clearer and it is easy to identify the transition for all regimes.

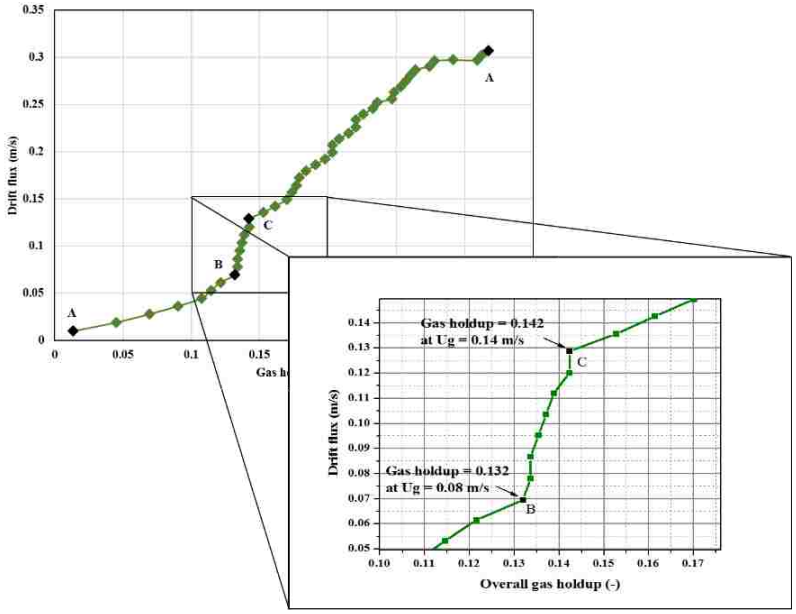

Figure 6. Flow regime transition using drift flux in bubble column H/D = 3

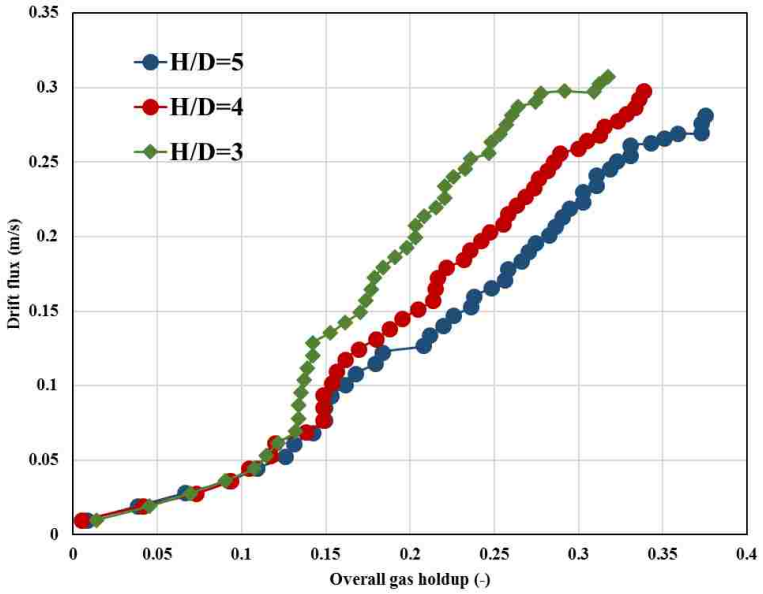

Figure 7. The effect of dynamic liquid levels on the flow regime transition by the drift-flux method

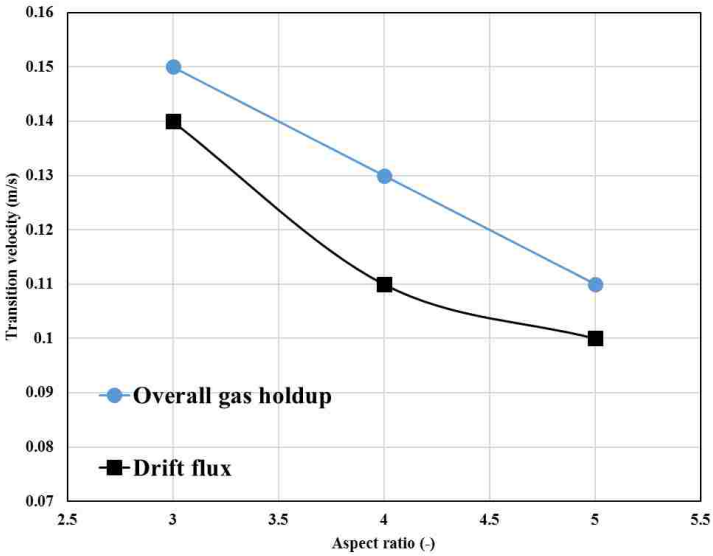

Figure 8. The effect of the dynamic liquid levels on the velocity transition on churn turbulent regime

4.3. THE KOLMOGOROV ENTROPY METHOD (KE)

The linear methods have demonstrated the impact of the dynamic liquid level on the transition between flow regimes, especially the churn turbulent regime. However, the multiphase system in the bubble column still anonymous with more information about the sub-regime if it exists in this size of bubble column "regarding this work investigates the flow regime in industrial-sized bubble column" or not, and how far it is affected. Therefore, utilizing the nonlinear method is imperative to demarcate the sub-regimes in the transition regime. Figure 9-11 show the Kolmogorov Entropy (KE) as a function of the superficial gas velocity by using equation (2). The principle used to identify the flow regime by Kolmogorov Entropies (KE) is the same that used by previous researchers Nedeltchev et al. [8], and Letzel et al. [34], where the sharp minimum value of the curve is the threshold

of the new regime. Figure 9-11 exhibit the four previously identified regimes: gas maldistribution, bubbly, transition, and the churn turbulent regime.

Gas maldistribution is the first flow regime has been indicated, which is determined by the sparger design. Usually, it is prevailing as long as the bubble column is operated with a superficial gas velocity under the Weber number (W_e). The bubbly flow regime begins at U_g = 0.04 m/s for aspect ratios *H/D* = 3 and 4, but U_g = 0.03 m/s when the *H/D* = 5. At U_g = 0.08 m/s and in all *H/D* the transition regime starts. At *H/D* = 3 and as shown in Figure 9, the transition regime consists of two sub-regimes and ends at U_g = 0.14 m/s where the churn turbulent regime starts. While for *H/D* = 4 and 5 there are no sub-regimes, and the transition regime ends at U_g = 0.11 and 0.105 m/s, respectively, where the churn turbulent begins as in Figure 10-11. Although the nonlinear method introduces more details about the flow regimes and points to transition regimes clearly, both methods emphasize the effect of dynamic liquid levels on the flow regimes.

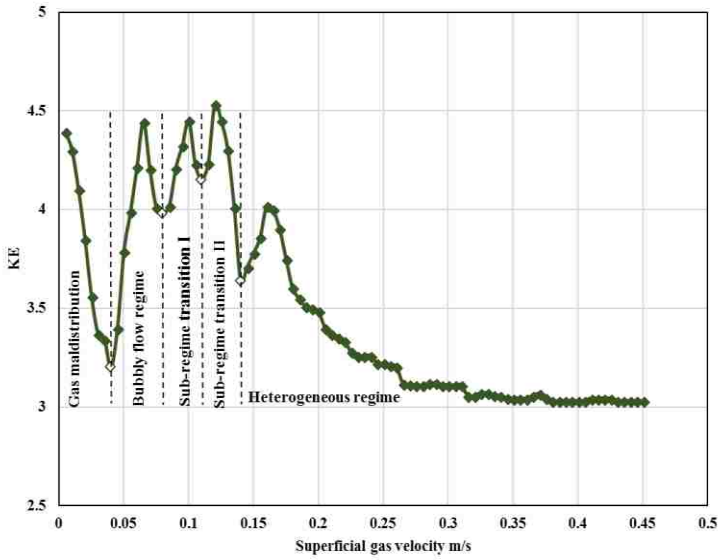

Figure 9. Flow regime transition in aspect ratio *H/D* = 3

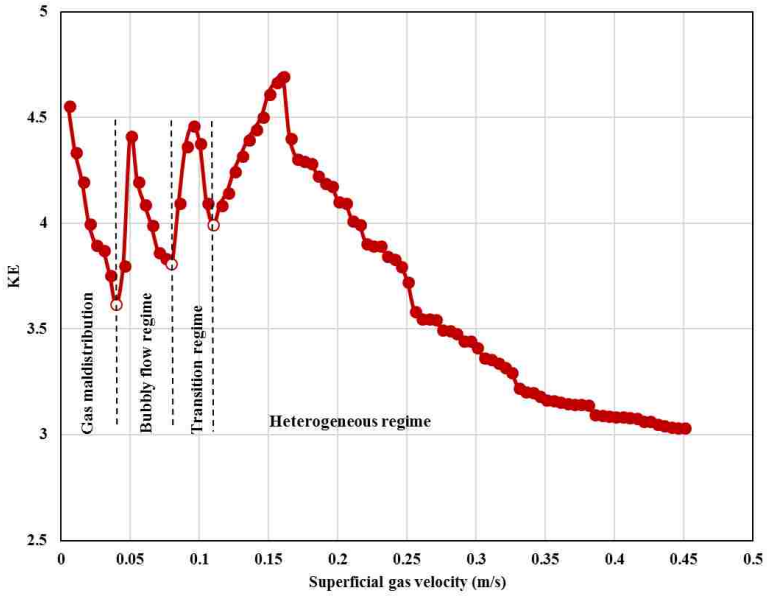

Figure 10. Flow regime transition in aspect ratio *H/D* = 4

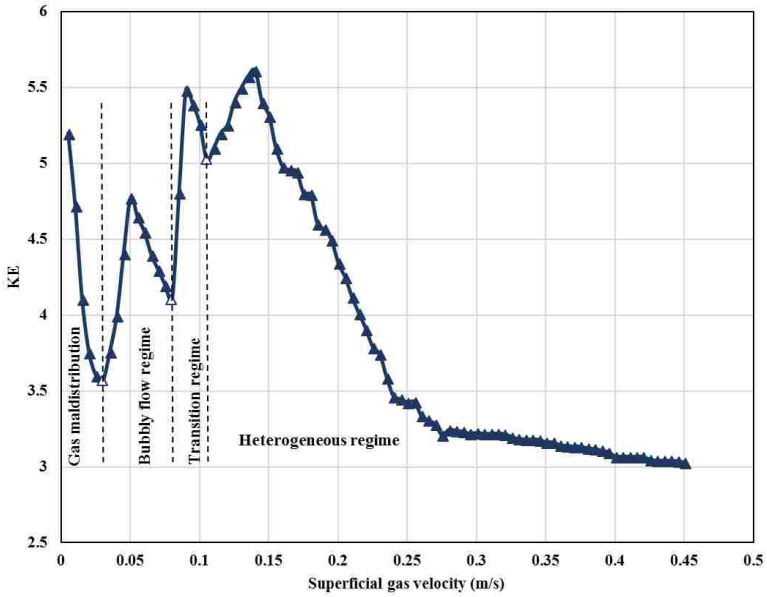

Figure 11. Flow regime transition in aspect ratio *H/D* = 5

4.4. CHARACTERIZING AND DEMARCATION OF FLOW REGIMES BY BUBBLE PROPERTIES

Based on the physical phenomena, the changes in holdup, drift-flux, and KE associated with flow regime transitions are a result of changes in bubble properties. Therefore, the local bubble properties have been used to delineate the flow regime boundaries and describe how these properties change from one regime to another. Zhang et al. [20], Shiea et al. [21] utilized the bubble chord length and the bubble frequency to demarcate the flow regime transitions in a bubble column of two phases (air-water) up flow. According to this work, the experiments were conducted in pool conditions (liquid phase is stagnant), and the bubble properties may not have the same trend depicted in the results of Zhang et al. [20], Shiea et al. [21]. Figure 12 depicts the mean bubble chord length versus the superficial gas velocity U_g to demarcate the flow regime transition in aspect ratio *H/D* = 3. As shown in this figure, the trend is divided into three parts: (A-B), (B-C), and (C-D), which represent the bubbly, transition, and churn turbulent regime, respectively. In the first segment (A-B) the mean bubble chord length increases rapidly with the increasing of superficial gas velocity. This indicates an increase in the rate of the bubble coalescence, attributed to growing the bubble population as shown in Figure 13 in part (A-B), which shows the local bubble frequency plotted versus the superficial gas velocity. As this regime predominates at low superficial gas velocity, the turbulent liquid eddies will be weak and reducing the bubble breakup rate. At U_g = 0.08 m/s, which is the critical velocity for the transition regime, the magnitude of the mean bubble chord length increases slowly with the increase in superficial gas velocity U_g. This could be attributed to increasing the strength of turbuluent eddies, thereby enhencing the bubble breakup rate.

At U_g = 0.14 m/s the churn turbulent regime begins. The enhancement in the turbulent motion of gas bubbles and liquid eddies are features of this regime. Therefore, in contrast with other regimes, the bubble size decreases sharply with the increasing of superficial gas velocity in this regime, as a result of the increasing of bubble breakup due to the turbulent eddies. In symmetrically, part (C-D) in Figure 13 exhibits the bubble numbers are rapidly increased with the increasing of superficial gas velocity that would confirm the enhancement in the bubble breakup in this regime. Furthermore, the variation in the bubble size and bubble population in the three regimes have been illustrated in Figure 14. However, the bubbly flow regime (U_g= 0.04 m/s) is characterized by uniform bubble size in which the bubbles population are concentrated, and a tight variance. As the superficial gas velocity increases, the flow structure in the bubble column enters to transition regime and then churn turbulent flow regime where the bubble population that relates to a wider range of bubbles size is increased, and hence, the flow pattern is characterized by non-uniform bubbles size. Thereby, simulating the bubble column reactor at high superficial gas velocity (transition and turbulent flow regime) with assuming that bubbles are one size is not related to the physical phenomena and implement the population balance model PBM would be critical to accurate the numerical solution. The local gas holdup, interfacial area, and bubble rise velocity illustrated in Figure 15, Figure 16, and Figure 17, respectively, show a similar trend to the bubble frequency but do not show a clear changing allows to identify the boundaries of the flow regime transition. Results are consistent and aligned with the mean context of these regimes identification. Data obtained for the entire aspect ratios (*H/D* = 4 and 5) exhibit the same trend of bubble properties, and hence, have not illustrated in this work.

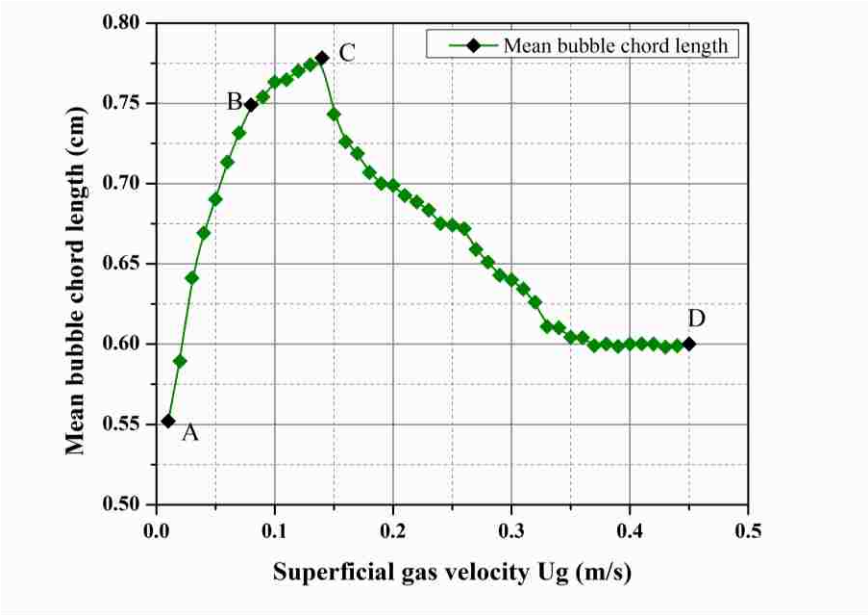

Figure 12. The mean bubble mean chord length (cm) at *H/D* = 3

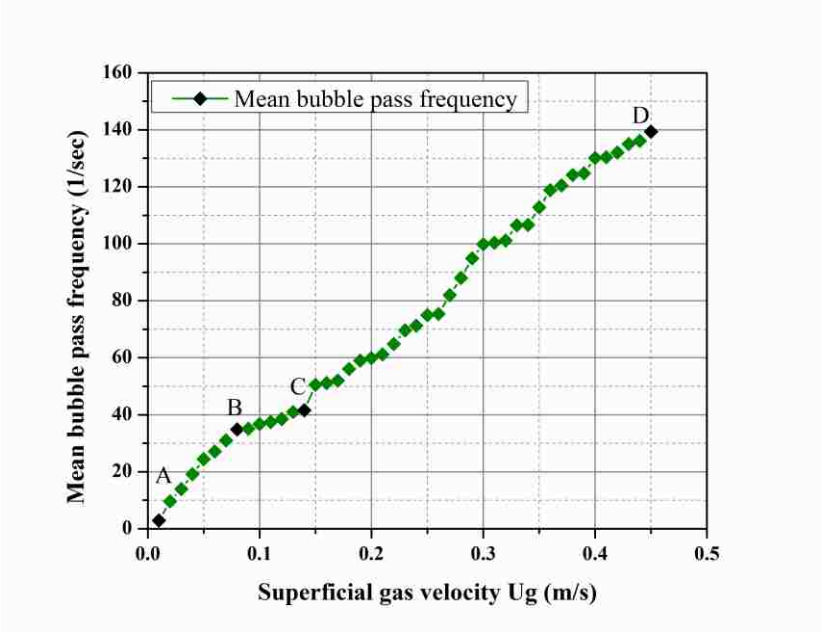

Figure 13. The mean bubble pass frequency (1/s) at *H/D* = 3

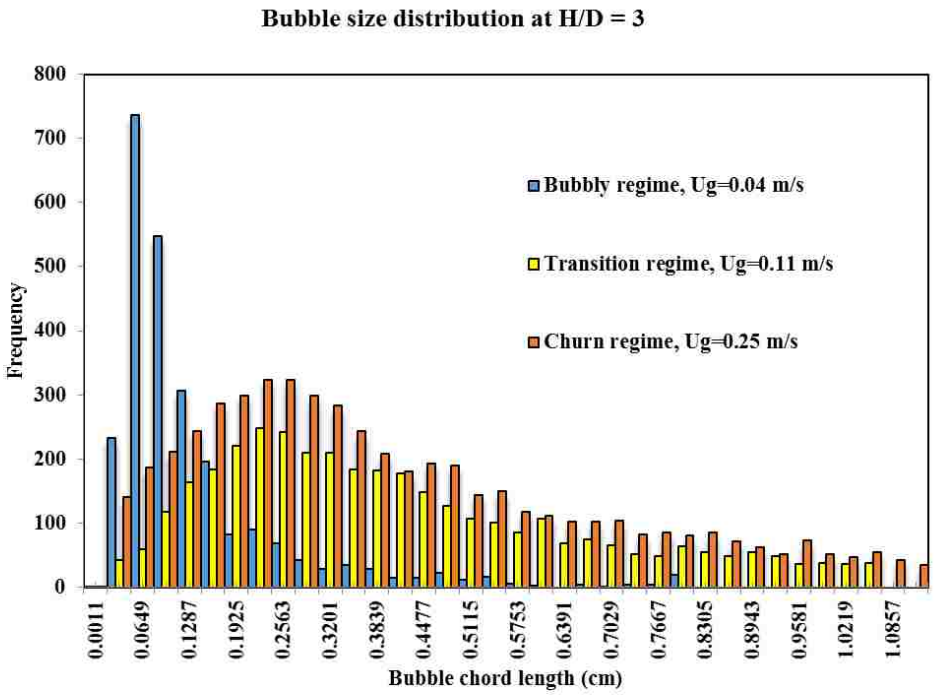

Figure 14. Bubble size distribution at *H/D* = 3

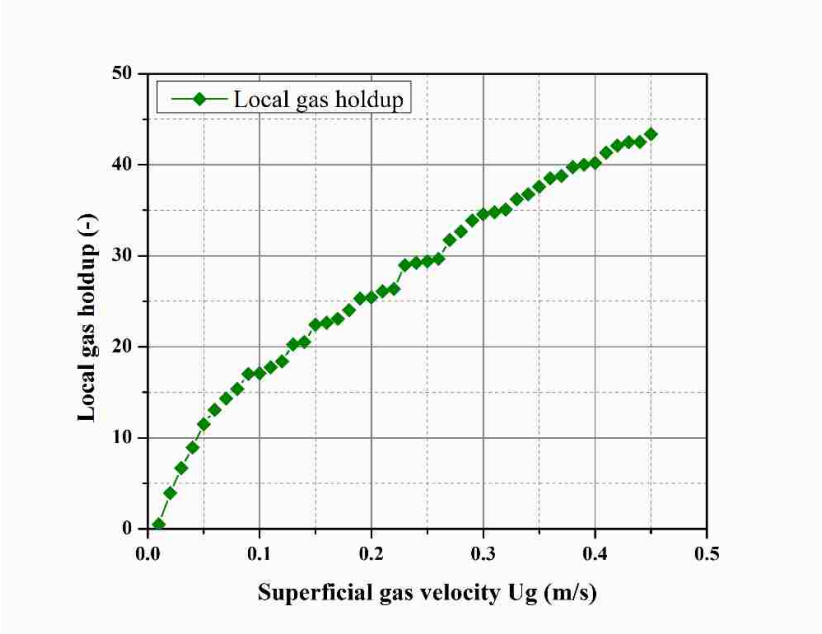

Figure 15. Local gas holdup profile in bubble column H/D = 3

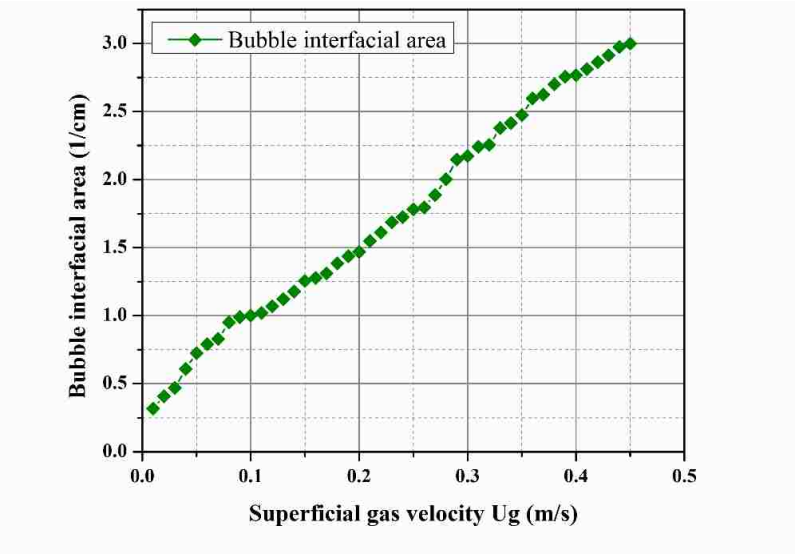

Figure 16. Bubble interfacial area in bubble column H/D = 3

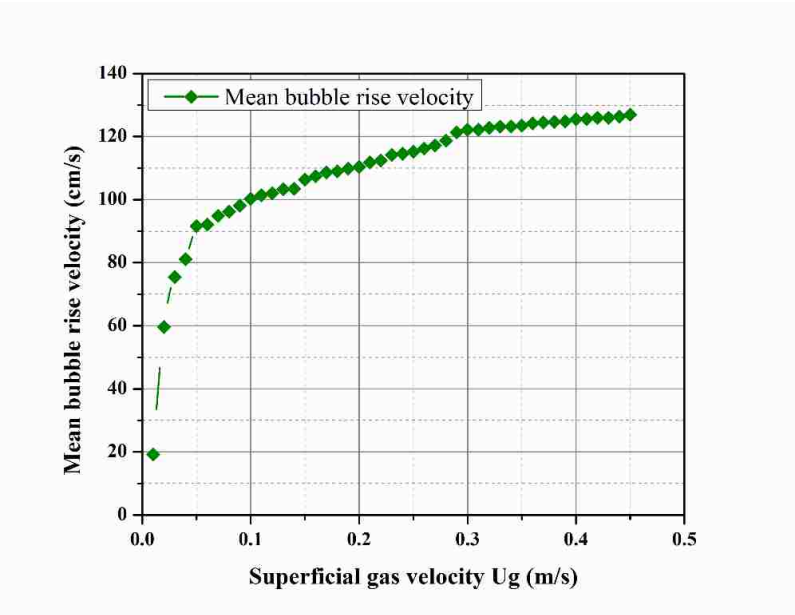

Figure 17. Bubble rise velocity in bubble column H/D = 3

In order to attribute the aspect ratio effect on the flow regime transition, Figure 18 shows the effect of the variation of aspect ratio (*H/D* = 5, 4 and 3) on the local gas holdup. In the bubbly flow regime, there is insignificant effect of the aspect ratio. The transition

and churn turbulent flow regimes exhibit that decreasing the aspect ratio promotes the local gas holdup. Previous research Shaikh and Al-Dahhan [5] revealed that increasing the pressure would promote the local gas holdup and delays the transition to the churn turbulent regime and that solid loading inhibits the local gas holdup and promotes the flow regime transition. Accordingly, the parameters, which in turn, enhance, or inhibit the local gas holdup would increase or decrease the transition velocity, respectively. Hence the effect of increasing aspect ratio (*H*/D) delays the flow regime transition and promotes the local gas holdup.

Furthermore, data obtained of bubble properties reveal that the bubble dynamics are varied according to the superficial gas velocity, which in turn, explain the reason for the existence of the different flow regimes in two-phase systems. Therefore, in terms of the simulation, the considering to the local bubble dynamics and combine the population bubble model (PBM) are essential for the simulation in the transition and churn turbulent flow regimes.

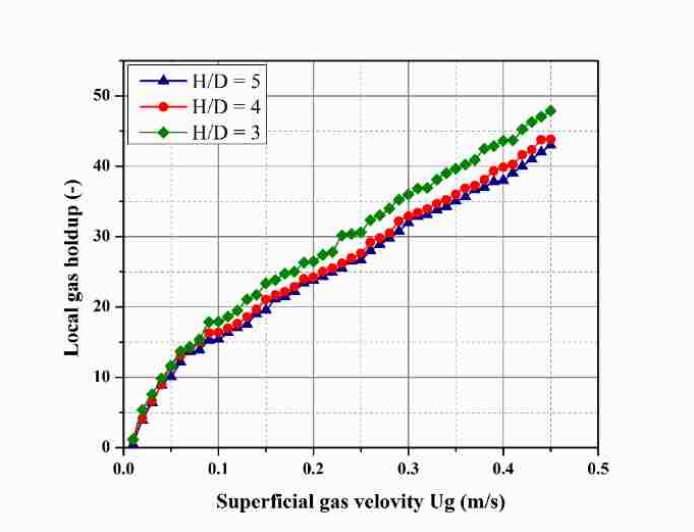

Figure 18. Aspect ratio effect on the local gas holdup

4.5. THE VALIDATION OF EMPIRICAL CORRELATION RESULTS

4.5.1. Empirical Correlations. Empirical correlations to estimate the flow regime transition are a subject of many studies that included the effect of physical properties of the fluids or the impact of the operation and geometric parameters such as the superficial gas velocity, the sparger design, and the diameter and height of the bubble column. Among these correlations, the following have been used to estimate the transition velocity.

4.5.1.1. Ribeiro [1]. Recently, a new empirical correlation has been proposed by Ribeiro [1] to predict the transition velocity. This study investigated the impact of the diameter and height of the bubble column, and the geometric dimension of the sparger in the proposed correlation as well as the physical properties of the fluids. Therefore, from the point of view of this work, this correlation would be more precision in the transition estimation.

$$\ln We_{trans} = f_1(d_{eq}, Mo) + f_2(d_{eq}, Mo, H_b, D_c) \ln Re_{ref} \tag{5}$$

$$f_1(d_{eq}, Mo) = a_0 + a_1 d_{eq}^{a_2} + a_3 \ln Mo \tag{6}$$

$$f_2(d_{eq}, Mo, H_b, D_c) = b_0 + b_1 \left(\frac{d_{eq} H_b}{D_c}\right)^{b_2} + b_3 \ln Mo \tag{7}$$

Where;

$$We_{trans} = \frac{U_{trans}^2 d_{eq} (\rho_L - \rho_G)}{\sigma} \tag{8}$$

$$Mo = \frac{g \mu_L^4 (\rho_L - \rho_G)}{\rho_L^2 \sigma^3} \tag{9}$$

$$Re_{ref} = \frac{u_{ref} d_{eq} (\rho_L - \rho_G)}{\mu_L} \tag{10}$$

$$u_{ref} = 0.352 \in_{ref} \left(1 - \in_{ref}\right)\sigma^{0.12}\rho_G^{-0.04} \quad (11)$$

$$\in_{ref} = min(4.72\rho_G^{0.48}\sigma^{0.06}\rho_L^{-0.5}, 0.5) \quad (12)$$

4.5.1.2. Şal et al. [2]. The experimental results for the sparger impact on the flow regime transition have been compared with the linear stability theory proposed by Şal et al. [2]. The correlation has been formed by using dimensionless analysis (Buckingham-π theorem). In addition, to make a general formula that could to display the sparger impact in the correlation, the dimensionless diameter ratio (d_0/D_c) was implemented with other dimensionless groups. The correlation estimates the gas holdup at which the transition regime occurs, as function of the superficial gas velocity as shown in equation (13).

$$\varepsilon_G = 0.2278\left[\frac{Fr^{0.7767}Ar^{0.3649}(d_0/D_c)^{0.478}}{Eo^{0.3916}We^{0.2402}}\right] \quad (13)$$

4.5.1.3. Wilkinson [27]. Wilkinson [27] developed a relationship to predict the velocity at which the regime transition happens, by utilizing two bubble columns with I.D. 0.15 and 0.23 m and various gases such as air, SF_6, N_2, CO_2, H_2, He, and different liquids such as water, mono-ethylene glycol, and n-heptane and operated under pressure up to 1.5 MPa. The correlations that given in equations (14)-(15) has been validated with the experimental results of Wilkinson [27].

$$U_{s,b} = 2.25\left[\frac{\sigma}{\mu_L}\right]\left[\frac{\sigma^3\rho_L}{g\mu_L^4}\right]^{-0.273}\left[\frac{\rho_L}{\rho_G}\right]^{0.03} \quad (14)$$

$$\frac{U_{trans}}{U_{s,b}} = \varepsilon_{trans} = 0.5\, exp(-193\rho_G^{-0.61}\mu_L^{0.5}\sigma^{0.11}) \quad (15)$$

The flow regime, as mentioned before, is a function for various parameters such as physical properties of the fluid, operation pressure, and the geometric dimension of the bubble column. Therefore, the correlations, which are considering to all these parameters,

will have the more accurate predicted transition value both either velocity transition or gas holdup transition.

However, Table 2 shows the comparison between the experimental transition and the predicted transitions, utilizing the empirical correlations in equations (5), (13) and (15), at different operating dynamic liquid levels. The correlations of Ribeiro [1] and Şal et al. [2] show minimum error percentage 8.26-25.69 % and 8.6-17.3 %, respectively, at all aspect ratios *H/D*. While the maximum percentage error given by Wilkinson [27] correlation gives 96-104 %. Within the range of operating conditions studied, clearly the empirical correlations formulated based on the physical properties, and geometric parameters give better predictions compared to the Wilkinson [27] correlation which is formulated based on just the physical properties.

Table 2. Validation of the empirical correlations with current work results

Aspect ratio H/D	Experimental U_{trans} (m/s)	Experimental Gas holdup (-)	Ribeiro [1]		Wilkinson [27]		Sal et al. [2]	
			U_{trans} (m/s)	Error %	U_{trans} (m/s)	Error %	Gas holdup (-)	Error %
3	0.14	0.14	0.15	8.6	0.004	104	0.16	8.26
4	0.11	0.16	0.13	17.3	0.004	96.4	0.14	12.82
5	0.1	0.15	0.11	13	0.004	96	0.12	25.69

5. EXPERIMENTAL RESULTS COMPARISON

The comparison of the current data with that available in the open literature is also conducted. Nedeltchev et al. [48], and [49] studied the flow regime transition in two different bubble columns diameters of 0.15 m and 0.4 m I.D. and $H/D \geq 5$. The transition velocities from this work that detected by the KE method will be used in the comparison.

Table 3 displays the difference in the transition velocities of both regimes. Increase in the bubble column diameter causes delayed transition, while the regular trend for the impact of the diameter increasing is to decrease the second transition velocity. That could be attributed to influence of low aspect ratio on the coalescence and breakup rates of bubbles. Based on that, the low aspect ratio parameter may be more significant than the height and diameter of the bubble column.

Table 3. The comparison between the experimental results and the open literature

H/D	The transition from bubbly to transition regime			The transition from transition to churn turbulent regime		
	Current work D = 0.6 m	Nedeltchev et al. [49]		Current work D = 0.6 m	Nedeltchev et al. [49]	
		D = 0.15 m	D = 0.4 m		D = 0.15 m	D = 0.4 m
3	0.08	0.034	0.034	0.14	0.089	0.078
4	0.08	0.034	0.034	0.11	0.089	0.078
5	0.08	0.034	0.034	0.1	0.089	0.078

6. CONCLUSIONS

In this study, the influence of the different dynamic liquid levels on the flow regime transition is investigated in an industrial size bubble column by utilizing the overall gas holdup, drift flux, and pressure transducer techniques. The experiment results were validated with the empirical correlation. In addition, an advanced four-point optical fiber probe has been used to measure the bubble chord length, frequency, local holdup, velocity, and interfacial area of different regimes.

The aspect ratio (*H/D*) has a significant impact on the transition between the churn regime and transition regime. Increase in the aspect ratio led to a decrease in the transition

velocity. No insignificant impact has been observed for the aspect ratio on the transition between the bubbly and transition regimes.

The magnitude of the overall gas holdup increases with decrease in the aspect ratio (*H/D*) in the churn turbulent regime, while no change has been monitored for the overall gas holdup in both bubbly and transition regimes.

Although the linear and non-linear methods are able to identify key transitions, the linear method identified three main regimes (bubbly, transition, and churn regime) while the non-linear method delineates four regimes (gas maldistribution, bubbly, transition, churn regime).

The experimental results for this work have been compared with data from the literature. The comparison has revealed a disagreement with other studies, namely Nedelthchev et al. [49], in all aspect ratio (*H/D*) tested. Therefore, further study of bubble columns at industrial size operated with low aspect ratios is highly recommended.

Based on the validation of the predicted value with the experimental result the predictive correlations which is embedded the bubble column dimension and the fluids physical properties most precisely anticipate the flow regime transition.

The applicability of the bubble properties in detecting the regime transition by the mean bubble chord length and bubble pass frequency. The transitions in the flow pattern as a function for the superficial gas velocity is a result of that changing in the bubble properties. Therefore, any parameter, that can influent in the bubbles, is worth to investigate its impact on the flow pattern.

NOMENCLATURE

d_p = particle diameter

C_s = solid concentration %Vol

H_D = bubbling height of bubble column (m)

H_S = static liquid level (m)

D = bubble column diameter (m)

L = axial location in bubble column (ft.)

f_s = sample frequency (s^{-1})

$\bar{b}$ = mean of all b values (-)

b_i = number of sequential pair of points on the attractor (-)

M = sample size of b values (-)

U_g = superficial gas velocity (m/s)

U_l = superficial liquid velocity (m/s)

j_{GL} = drift flux (m/s)

We_{trans} = Weber number transition

We = Weber number

d_{eq} = equivalent diameter of the bubble column (m)

Mo = Morton number

Re_{ref} = Reynolds number

$a_0, a_1, a_2, b_0, b_1, b_2, b_3$ = constant coefficients available in [1]

g = gravity m/s^2

U_{trans} = velocity transition (m/s)

u_{trans} = reference gas velocity (m/s)

$\in_{ref}$ = reference gas holdup (-)

Fr = Froude number

Ar = Archimedes number

Eo = Eotvos number

U_{sb} = mean bubble rise velocity of small bubble (m/s)

Greek letters

ε_G = overall gas holdup (-)

ε_g = local gas holdup (-)

ρ = density (kg/m^3)

σ = liquid surface tension

μ_L = liquid viscosity

Subscripts

s = solid (slurry)

p = particle solid (slurry)

g, G = gas phase

l, L = liquid phase

$trans$ = transition point

ref = reference value

sb = small bubble diameter

REFERENCES

[1] C. P. Ribeiro, "On the estimation of the regime transition point in bubble columns," *Chem. Eng. J.*, vol. 140, no. 1–3, pp. 473–482, 2008.

[2] S. Şal, Ömer F. Gül, Mustafa Özdemir, Ö. F. Gül, and M. Özdemir, "The effect of sparger geometry on gas holdup and regime transition points in a bubble column equipped with perforated plate spargers," *Chem. Eng. Process. Process Intensif.*, vol. 70, pp. 259–266, 2013.

[3] L.-S. Fan, *Gas-Liquid-Solid Fluidization Engineering. Butterworth Serise in Chemical Engineering*. Boston, MA, 1989.

[4] M. Elena Díaz, F. J. Montes, and M. A. Galán, "Influence of aspect ratio and superficial gas velocity on the evolution of unsteady flow structures and flow transitions in a rectangular two-dimensional bubble column," *Ind. Eng. Chem. Res.*, vol. 45, no. 21, pp. 7301–7312, 2006.

[5] A. Shaikh and M. Al-Dahhan, "Characterization of the hydrodynamic flow regime in bubble columns via computed tomography," *Flow Meas. Instrum.*, vol. 16, pp. 91–98, 2005.

[6] S. K. Majumder, *Hydrodynamics and Transport Processes of Inverse Bubble Flow*. 2016.

[7] J. J. Wu, D. Wang, L. hua Li, and J. T. Zhou, "Characterization of Flow Regimes in Bubble Columns through CCF Analysis of Pressure Fluctuations," *Chem. Eng. Technol.*, vol. 28, no. 10, pp. 1109–1113, 2005.

[8] H. M. Letzel *et al.*, "Characterization of regimes and regime transitions in bubble columns by chaos analysis of pressure signals," *Chem. Eng. Sci.*, vol. 52, no. 24, pp. 4447–4459, 1997.

[9] G. Bloch, H. J. Zander, B. Wunderlich, and T. Acher, "Axial and radial dispersion in a large-diameter bubble column reactor at low height-to-diameter ratios," *Chemie-Ingenieur-Technik*, vol. 87, no. 6, pp. 756–761, 2015.

[10] S. Nedeltchev, A. Shaikh, and M. Al-Dahhan, "Flow regime identification in a bubble column based on both statistical and chaotic parameters applied to computed tomography data," *Chem. Eng. Technol.*, vol. 29, no. 9, pp. 1054–1060, 2006.

[11] E. Olmos, C. Gentric, S. Poncin, and N. Midoux, “Description of flow regime transitions in bubble columns via laser Doppler anemometry signals processing,” *Chem. Eng. Sci.*, vol. 58, no. 9, pp. 1731–1742, 2003.

[12] E. Olmos, C. Gentric, and N. Midoux, “Identification of Flow Regimes in a Flat Gas-liquid Bubble Column via Wavelet Transform,” *Can. J. Chem. Eng.*, vol. 81, no. August, pp. 382–388, 2003.

[13] S. Barghi, A. Prakash, A. Margaritis, and M. A. Bergougnou, “Flow Regime Identification in a Slurry Bubble Column from Gas Holdup and Pressure Fluctuations Analysis,” *Can. J. Chem. Eng.*, vol. 82, no. October, pp. 865–870, 2004.

[14] C. L. Hyndman, F.Larachi, and C. Guy, “Understanding gas-phase hydrodyamics in bubble columns: a convective model based on kinetic theory,” *Chem. Eng. Sci.*, vol. 52, no. 1, pp. 63–77, 1997.

[15] S. Nedeltchev, U. Jordan, O. Lorenz, and A. Schumpe, “Identification of various transition velocities in a bubble column based on Kolmogorov entropy,” *Chem. Eng. Technol.*, vol. 30, no. 4, pp. 534–539, 2007.

[16] P. C. Mena, M. C. Ruzicka, F. A. Rocha, J. A. Teixeira, and J. Drahoš, “Effect of solids on homogeneous-heterogeneous flow regime transition in bubble columns,” *Chem. Eng. Sci.*, vol. 60, no. 22, pp. 6013–6026, 2005.

[17] S. Kumar, N. Srinivasulu, P. Munshi, and A. Khanna, “Flow regime transition identification in three phase co-current bubble columns,” *Can. J. Chem. Eng.*, vol. 91, no. 3, pp. 516–523, 2013.

[18] S. Nedeltchev and M. Schubert, “Statistical validation of the mixing length concept in bubble columns operated in the transition flow regime,” *J. Chem. Eng. Japan*, vol. 48, no. 2, pp. 107–111, 2015.

[19] M. C. Ruzicka, J. Drahos, M. Fialova, and N. H. Thomasb, “Effect of bubble column dimensions on flow regime transition,” *Chem. Eng. Sci.*, vol. 56, pp. 6117–6124, 2001.

[20] J. P. Zhang, J. R. Grace, N. Epstein, and K. S. Lim, “Flow regime identification in gas-liquid flow and three-phase fluidized beds,” *Chem. Eng. Sci.*, vol. 52, pp. 3979–3992, 1997.

[21] M. Shiea, N. Mostoufi, and R. Sotudeh-Gharebagh, “Comprehensive study of regime transitions throughout a bubble column using resistivity probe,” *Chem. Eng. Sci.*, vol. 100, pp. 15–22, 2013.

[22] W. T. Medjiade, A. R. Alvaro, and A. Schumpe, “Flow regime transitions in a bubble column,” *Chem. Eng. Sci.*, vol. 170, pp. 263–269, 2017.

[23] K. Mishima *et al.*, “Flow regime transition for upward two-phase flow in vertical tubes,” *Int. J. Heat Mass Transf.*, vol. 27, no. 5, pp. 723–737, 1984.

[24] A. I. . Shnip, R. V. Kolhatkar, D. Swamy, and J. B. Joshi, “Criteria for the transition from the homogeneous to the heterogeneous regime in two-dimensional bubble column reactors,” *Int. J. Multiph. Flow*, vol. 18, no. 5, pp. 705–726, 1992.

[25] S. V. Ghatage, M. R. Bhole, N. Padhiyar, J. B. Joshi, and G. M. Evans, “Prediction of regime transition in three-phase sparged reactors using linear stability analysis,” *Chem. Eng. J.*, vol. 235, pp. 307–330, 2014.

[26] I. G. Reilly, D. S. Scott, D. E. Bruijn, and D. Macintyre, “The Role of Gas Phase Momentum in Determining Gas Holdup and Hydrodynamic Flow Regimes in Bubble Column Operations,” vol. 72, no. 1961. 1994.

[27] P. M. Wilkinson, “Physical Aspects and Scale-up of High Pressure Bubble Columns,” Dept. of Chemical Engineering, University of Groningen, NL, 1991.

[28] J. P. Schlegel, P. Sawant, S. Paranjape, B. Ozar, T. Hibiki, and M. Ishii, “Void fraction and flow regime in adiabatic upward two-phase flow in large diameter vertical pipes,” *Nucl. Eng. Des.*, vol. 239, no. 12, pp. 2864–2874, 2009.

[29] M. Simonnet, C. Gentric, E. Olmos, and N. Midoux, “CFD simulation of the flow field in a bubble column reactor: Importance of the drag force formulation to describe regime transitions,” *Chem. Eng. Process. Process Intensif.*, vol. 47, no. 9–10, pp. 1726–1737, 2008.

[30] T.-J. Lin, J. Reese, T. Hong, and L.-S. Fan, “Quantitative analysis and computation of two-dimensional bubble columns,” *AIChE J.*, vol. 42, no. 2, pp. 301–318, 1996.

[31] A. K. Das, P. K. Das, and J. R. Thome, “Transition of Bubbly Flow in Vertical Tubes: New Criteria Through CFD Simulation,” *J. Fluids Eng.*, vol. 131, no. 9, p. 091304, 2009.

[32] J. M. van Baten and R. Krishna, “CFD Simulations of a Bubble Column Operating in the Homogeneous and Heterogeneous Flow Regimes,” *Chem. Eng. Technol.*, vol. 25, no. 11, pp. 1081–1086, 2002.

[33] W. L. Li, W. Q. Zhong, B. S. Jin, R. Xiao, and T. T. He, “Flow regime identification in a three-phase bubble column based on statistical, Hurst, Hilbert-Huang transform and Shannon entropy analysis,” *Chem. Eng. Sci.*, vol. 102, pp. 474–485, 2013.

[34] S. Nedeltchev, S. Aradhya, F. Zaid, and M. Al-Dahhan, “Flow Regime Identification in Three Multiphase Reactors Based on Kolmogorov Entropies Devived from gauge Pressure Fluctuations,” *J. Chem. Eng. Japan*, vol. 45, no. 9, pp. 757–764, 2012.

[35] J. Vandenberghe, J. Choung, Z. Xu, and J. Masliyah, “Drift Flux Modelling for a Two-Phase System in a Flotation Column,” *Can. J. Chem. Eng.*, vol. 83, no. 1969, pp. 169–176, 2005.

[36] M. C. Ruzicka, J. Zahradnik, J. Drahoš, and N. H. Thomas, “Homogeneous – heterogeneous regime transition in bubble columns,” *Chem. Eng. Sci.*, vol. 56, pp. 4609–4626, 2001.

[37] J. J. Frijlink, “Physical aspects of gassed suspension reactors,” Delft University of Technology, 1987.

[38] J. Xue, “Bubble Velocity, Size and Interfacial Area Measurements in Bubble columns,” Washington Univeristy, Saint Louis, 2004.

[39] G. Hebrard, D. Bastoul, and M. Roustan, “Influence of the gas sparger on the hydrodynamic behavior of bubble columns,” *Chem. Eng. Res. Des.*, vol. 74, no. 3, pp. 406–414, 1996.

[40] H. Al-Naseri, J. P. Schlegel, and M. H. Al-Dahhan, “The Effects of Internals and Low Aspect Ratio on The Flow Development and Bubble Dynamics in Pilot-Plant Bubble Column for Fischer-Tropsch synthesis,” *Exp. Therm. Fluid Sci.*, vol. submitted, 2018.

[41] M. Kagumba, “Heat transfer and bubble dynamics in bubble and slurry bubble columns with internals for Fischer-Tropsch synthesis of clean alternative fuels and chemicals,” Missouri University of Science and Technology, 2013.

[42] M. Kagumba and M. H. Al-Dahhan, “Impact of internals size and configuration on bubble dynamics in bubble columns for alternative clean fuels production,” *Ind. Eng. Chem. Res.*, vol. 54, no. 4, pp. 1359–1372, 2015.

[43] R. Krishna, J. Ellenberger, D. E. Hennophof, D. E. Hennephof, and D. E. Hennophof, “Analogous description of the hydrodynamics of gas-solid fluidized beds and bubble columns,” *Chem. Eng. J.*, vol. 53, no. 1, pp. 89–101, 1993.

[44] J. Ellenberger and R. Krishna, “A unified approach to the scale-up of gas-solid fluidized bed and gas-liquid bubble column reactors,” *Chem. Eng. Sci.*, vol. 49, no. 24, pp. 5391–5411, 1994.

[45] A. Toukan, V. Alexander, H. AlBazzaz, and M. H. Al-Dahhan, "Identification of flow regime in a cocurrent gas – Liquid upflow moving packed bed reactor using gamma ray densitometry," *Chem. Eng. Sci.*, vol. 168, pp. 380–390, 2017.

[46] J. C. Schouten, F. Takens, and C. M. Van Den Bleek, "Maximum-likelihood estimation of the entropy of an attractor," *phys. Rev. E Stat. Phys. Plasmas Fluids Relat. Interdiscip. Top.*, vol. 49, no. 1, pp. 126–129, 1994.

[47] S. Nedeltchev, "Application of chaos analysis for the investigation of turbulence in heterogeneous bubble columns," *Chem. Eng. Technol.*, vol. 32, no. 12, pp. 1974–1983, 2009.

[48] G. B. Wallis, *One-Dimensional Two-Phase Flow*. 1969.

[49] S. Nedeltchev, S. Rabha, U. Hampel, and M. Schubert, "A New Statistical Parameter for Identifying the Main Transition Velocities in Bubble Columns," *Chem. Eng. Technol.*, vol. 38, no. 11, pp. 1940–1946, 2015.

[50] S. Nedeltchev, "New methods for flow regime identification in bubble columns and fluidized beds," *Chem. Eng. Sci.*, vol. 137, pp. 436–446, 2015.

IV. THE EFFECT OF HEAT EXCHANGING INTERNALS ON THE FLOW REGIME TRANSITION IN INDUSTRIAL SCALE PILOT PLANT BUBBLE COLUMN REACTOR

ABSTRACT

In this work, for the first time, the effects of the variation in the low aspect ratio and the presence of heat exchanging internals on the flow regime transition in an industrial-scale pilot- plant bubble column have been investigated. The flow regime transition has been demarcated experimentally by the linear method (overall gas holdup and drift flux), and the non-linear method (Kolmogorov Entropy (KE)) using the liquid extension technique and the differential pressure technique, respectively. While, an advanced four-point optical fiber probe has been utilized to demarcate the transition velocities and characterize the bubble properties, which are the local gas holdup, bubble chord length, and bubble passing frequency, of each flow regime. The experiments were executed in an industrial-scale bubble column of I.D. 0.6 m and 3.96 m height that occupied by a heat exchanging internals covering 24 % of the total cross-sectional area of the bubble column. The superficial gas velocity varied from 0.005 m/s to 0.45 m/s. The experiment results exhibit that the presence of internals and a decrease in the aspect ratio (*H/D*) led to delays in the transition velocities from bubbly to transition regime and from the transition to churn turbulent flow regime. Furthermore, the measurements of the bubble properties exhibit the capability of bubble mean chord length and the bubble frequency to identify the flow regime transition.

1. INTRODUCTION

Bubble column, one type of multiphase reactor, is characterized by high selectivity and conversion, good in mixing, desirable thermal control, and low cost of maintenance. The disadvantages of this reactor are the back mixing, intense liquid circulation and difficulty in design and scale up as a result of the complex interactions between the phases. Bubble column reactors have been utilized widely in industries in various processes such as biochemical, metallurgical, and petrochemical processes. Among these processes is the Fischer-Tropsch (F-T) process, which uses the slurry bubble column reactor that is considered as a bubble column of gas-slurry phase. The reaction that takes place in this reactor for Fischer-Tropsch (F-T) synthesis process is an exothermic reaction, and hence, using a heat exchanging internals is essential to operating the reactor at the desired temperature. The hydrodynamics of the bubble column reactor is characterized by high sensitivity to the superficial gas velocity because of its effect on the bubble properties [1]–[10], thereby, the liquid flow structure that is including the liquid velocities, the shear and normal stresses, the turbulent kinetic energy, and the turbulent eddy diffusivity, is varied based on the operating gas velocity. Therefore, the variation in the superficial gas velocity would divide the hydrodynamics in the bubble column to so-called flow regimes (pattern), and each regime is characterizing in different bubble dynamics[8], [11]–[14].

There are three main regimes in the bubble column: (1) the bubbly or homogeneous flow regime which is prevalent at low superficial gas velocity (U_g) and characterized by a narrow bubble size distribution, and relatively uniform radial profile of the gas holdup and axial liquid velocity [8], [15]; (2) the transition regime, which consists of two sub regimes

[2-4]. The first transition sub regime is characterized by irregular flow pattern of bubble plume and bubble coalescence [18]. As the superficial gas velocity increases, the flow structure is established (fully developed) in the second transition regime. This regime specifies that the bubble coalescence and break up rates dominate the bulk region and the distributor impacts are omitted; (3) the churn turbulent or heterogeneous regime which also consists of two regime. The methods for the flow regime detection are two including the linear, and the non-linear methods. Each method offers different features, where the linear method is easy and direct to analyze, but it is limited to lab scale. While, the non-linear method is preferred to be used for the industrial scale as it is based on chaotic analysis, although the capability of this method to demarcate the flow regime transition is controversial in most recent investigations that utilized different techniques in the multiphase flow system. Usually, the type of the method to detect flow regimes was chosen depending on the operation conditions (pressure and temperature) and the type of technique used.

Flow regime transition and demarcation in bubble column reactors are subjected to numerous studies that aim to identify the flow regime, optimize the bubble column performance, and improve the scale-up and design. Table 1 summarizes some studies that were conducted to quantify considering the effect of various parameters on the flow pattern utilizing different techniques and operation conditions.

Shaikh and Al-Dahhan [19] investigated the effect of the pressure operation (0.4 and 1 MPa) on the flow regime transition in a bubble column of 0.162 m inner diameter and a height 2.5 m, using gamma ray computed tomography (CT) technique. The steepness of the gas holdup radial profiles over the cross-section of the bubble column was used to

demarcate the velocity of flow regime transition. They reported that increasing the operation pressure would increase the transition velocity and increase the gas holdup, further, the change in the flow regime exhibited a noticeable change at ambient conditions, while at higher pressure, a gradual change occurs over a region of superficial gas velocities.

The effect of the physical properties of the fluid (gas-phase and liquid-phase) on the flow regime transition have been conducted by Reilly et al. [20], Gourich et al. [21], and Kim et al. [22]. According to Reilly et al. [20] investigated the effect gas density (air, helium, nitrogen, carbon dioxide, and argon) on the gas holdup and flow regime transition in bubble column of 0.15 m inner diameter and a height 2.7 m using manometric pressure. Their results revealed that the transition velocity increased with increasing the gas density, further, the gas density exhibited a greater effect on the gas holdup (in terms the gas holdup increased with increasing the gas density) in the churn turbulent flow regime comparing with the bubbly flow regime. Meanwhile, Kim et al. [22] studied the effects of the gas density (using air, helium, and carbon dioxide) and the liquid density (using water, aqueous ethanol solutions, and aqueous glycerol solutions) on the flow regime transition and the gas holdup. Data obtained reported that the gas density increased, the gas holdup increased at all studied gas velocities, which in turn delays the flow regime transition (i.e., increase the transition velocity), while the gas holdup in the liquid mixtures were higher than those for tap water. The transition gas holdup for the ethanol solutions increased to a sharp maximum and then decreased as the surface tension increased.

The effect of the presence of solids particles, in regards to the effects the solids loading and the particles diameter (d_p), on the flow regime transition have been conducted in terms that the presence of solids decreases the gas holdup in bubble column [13], [16],

[23]–[27]. Li et al. [24] studied the effect of the solids loading (3-30 vol.%), average particle size (d_p= 48 µm- 270 µm), and particle density (ρ_p= 2500 kg/m^3 – 4800 kg/m^3) on the flow regime transitions in a rectangular bubble column (Height (*H*)= 0.8 m, Long (*L*)= 0.1 m and wide (*W*) = 0.01 m) using the differential pressure signal technique. Their results revealed that the increase in the solids loading and the particle density led to decrease in the transition velocities in all regimes. While, the particle size exhibited dual effect; when shifted from 48 µm to 150 µm, it had a little effect on the operation ranges of flow regimes, whereas, the particle size increased from 150 µm to 270 µm, the values of the second and the third transitional gas velocities decreased.

Furthermore, the impacts of the bubble column geometry, including the diameter and the height of bubble column, and sparger geometry on the flow regime transition in two-three-phase system were conducted [14], [28]–[31]. Hebrard et al. [14], Krishna and Ellenberger [28], and Sal et al. [29] investigated the effect of the sparger design on the flow regime transition in different bubble column diameters using different techniques. They reported that increase the hole diameter of the perforated plates in turn sharply decreases the transition velocity and decreases the overall gas holdup, particularly in the homogenous flow regime. Ruzicka et al. [31], and Besagni et al. [30] reported that the variation in the diameter, the height, and the aspect ratio of the bubble column destabilize the homogenous regime and advance the transition. However, experimental data reviewed indicate that the investigated parameters (operation condition, solids loading, bubble column geometry, and the sparger design), which influence the flow regime transition, the hydrodynamics are affected by these parameters as well.

Recently our research group works extensively on the impact of the vertical bundle internals on the liquid structure [7], gas holdup radial profile [5], [6], [32], [33], and bubble properties [2], [3], [34]–[37] by utilizing the RPT technique, the CT technique, and the four-point optical fiber probe, respectively. The most critical parameters that influence flow regime transition are the internals and the bubble column dimensions as they impact the liquid structure and the bubble properties (bubble chord length, bubble pass frequency, local gas holdup, interfacial area, and the bubble velocity). Accordingly, all investigations that are reviewed have proved the significant effect for the presence of internals on the bubble dynamics and the liquid flow pattern, and hence, it is unquestionable that the impact of the internals will reflect on the flow regimes behaver. Furthermore, the most the studies that addressed the flow regime transition in the bubble column were conducted in the absence of internals and in high aspect ration ($H/D \geq 9$).

This work aims to investigate, for the first time, the effects of the presence of internals and the variation of low aspect ratio ($H/$D = 3, 4, and 5) on the flow regime transition at low aspect ratio in industrial-sized pilot-plant scale bubble column. The linear methods (overall gas holdup and drift flux), and the non-linear method (chaotic) have been used to demarcate the flow regime transition utilizing liquid extinction level technique, and pressure transducer technique, respectively. Meanwhile, an advanced four-point fiber optical probe technique has been used to characterize the bubble properties, which included the local gas holdup, interfacial area, bubble frequency, bubble velocity, and the mean bubble chord length, in different regimes and to determined the transition regime velocity.

Table 1. Summary of selected reported studies on the flow regime transition

Author	Setup Dimension (m)	Operation condition	Technique	Method of data analysis	Investigation goals and results
Medjiade et al. [38]	D=0.102 H=2.4 *H/D* > 15	• Batch mode operation for liquid phase (Nitrogen-Water) • Temperature:298 K • Pressure: 0.1, 0.25, 0.5, 1.0, 2.0 MPa	Differential pressure sensor	Standard deviation, fractal analysis, Power spectral density, Chaos analysis (Kolmogorov Entropy KE)	Goals; • Investigate the operating pressures impact on the flow regime transition by using different analysis techniques. Results; • The increase in the pressure led to increases the transition velocity.
Olmos et al. [17]	H=1.2 Depth=0.04 Width=0.2	Batch mode operation for liquid phase (air-water) Ambient temperature and pressure	Visual method, Laser Doppler velocimetry (LDV)	Frequency analysis, Chaos analysis, Fractal analysis	Goals; • Investigate the transition and structure of flow regime in 2D bubble column by utilizing various analysis techniques for Leaser Doppler Velocimetry (LDV). Results; • The capability of chaos analysis to demarcate the flow regime transition.
Barghi et al. [16]	D=0.15 H=2.4 *H/D* = 9	• Batch mode operation for liquid phase (air-water-glass beads 35 µm) • Ambient temperature and pressure	Pressure transducer	Stander deviation, Skewness, Kurtosis, Probability	Goals; • Investigate the solid particle effect in bubble column on the flow regime transition. Results; • The increase in the solids loading led to decreases the transition velocity.
Schlegel et al. [39]	D=0.15 H=4.4 *H/D* = 29	• Co-current flow of both phase (air-water) • Ambient temperature and pressure	Electrical Impedance Void Meters	Cumulative Probability Density Function (CPDF)	Goals; • Characterize the flow regime in different axial locations, the cumulative probability density function (CPDF). Results; • The flow regime transition occur simultaneously in the whole the bubble column.
Nedelthev et al. [15]	D=0.14 H=1.33 *H/D* > 9	• Batch mode operation for liquid phase (air-water) • Ambient temperature and pressure	Pressure transducer	Chaos analysis (Kolmogorov Entropies KE)	Goals; • Identify the flow regime in three types of reactors (bubble column, spouted bed, and fluidized bed) by using the pressure transducer and analyze the time series signal by (Kolmogorov Entropies KE). Results; • The capability of the Kolmogorov Entropies KE method to demarcate the flow regime transition in the three types of multiphase reactors (bubble column, spouted bed, and fluidized bed).
Sal et al. [29]	D=0.33 H=3 *H/D* = 9	• Counter-courrent flow of both (air-water) • Ambient temperature and pressure	Measurement overall gas holdup	Drift-flux, Linear stability	Goals; • Investigate the effect of sparger geometry (hole diameter) on flow regime transition by measuring the global gas holdup. Results; • The increase the hole diameter of the sparger in turn decreases the transition velocity.

Table 1. Summary of selected reported studies on the flow regime transition (cont.)

Shiea et al. [12]	D=0.09 H=1.8 *H/D* = 20	• Co-current flow of both phase (air-water) • Ambient temperature and pressure	Resistivity Probe (double-needle)	Bubble properties	Goals; • Using bubble properties as criteria to detect the flow regime transition, wherein three axial different locations detected. Results; • The capability of the bubble chord length and the bubble passing frequency to demarcate the flow regime transition.
Nedeltchev and Schubert [40]	D=0.15, 0.4 H=2 *H/D* > 9	• Batch mode operation for liquid phase (air-water) • Ambient temperature and pressure	Wire Mesh Sensor	New statistical parameter, Chaos analysis (Kolmogorov Entropies KE)	Goals; • Demarcate the transition regime in two bubble columns of different diameter size by using new parameter. Results; • It was found that the first transition velocity increases with column diameter, whereas, the second value decreases slightly. • It was possible to correlate the new parameter Φ to the mixing length *L* only in the transition flow regime. This limitation of the range of applicability of the mixing length concept has not been described in the literature so far.
Wu et al. [41]	D=0.15 H=1.5 *H/D* = 10	• Batch mode operation for liquid phase (air-water) • Ambient temperature and pressure	Pressure transducer, Measurement overall gas holdup	Linear analysis (global gas holdup), Nonlinear analysis (Cross-Correlation Function CCF) and Chaos analysis	Goals; • Identify the flow regime by using new nonlinear analysis method, called cross-correlation function (CCF). • Investigate the effect of hole diameter of sparger; the Results; • Data obtained have been validated with chaos analysis (K) and linear analysis global gas holdup technique.
Ruzicka et al. [31]	D=0.14, 0.29, 0.4 H=0.1-1.2	• Batch mode operation for liquid phase (air-water) • Ambient temperature and pressure	Pressure transducer, Measurement overall gas holdup	Drift-flux, Voidage	Goals; • The bubble column dimension (height, diameter and aspect ratio) impact on the regime transition. Results; • This study included validation for the results with theoretical prediction models [42] and [43]. • The results show that both the column height and width destabilize the homogeneous regime and advance the transition
Zhang et al. [13]	D=0.0826 H=2 *H/D* = 24	• Co-current flow of both phase (air-water-glass beads) • Ambient temperature and pressure	Conductivity Probe	Bubble Properties	Goals; • The impact of particle size and density on flow transition. Results; • Increasing the particles size led to increases the break-up, which in turn delays the transition in the coalescence regime.
Li et al. [27]	H=0.8 Depth=0.01 Width=0.1	• Batch mode operation for liquid phase (air-water-glass beads) • Ambient temperature and pressure	Pressure transducer	Statistical, Hurst, Hilbert-Huang transfer, Shannon entropy analysis	Goals; • Investigate the flow regime and transition velocity by using different techniques analysis in three phases system. Results; • The Hilbert–Huang transform and Shannon entropy analysis methods offer very high resolution in identifying the different flow regimes.

2. EXPERIMENTAL SETUP

The effect of the presence of internals on the flow regime transition velocities has been conducted by utilizing industrial-size pilot plant bubble column of inside diameter ID = 0.6 m and a height H = 3.9 m. Figure 1 shows a schematic diagram of the bubble column. Air was used as a gas phase where the superficial gas velocity U_g, which calculated based on the free cross section CSA of the bubble column and ranged from 0.05-0.45 (m/s), has been controlled and measured by using two rotameters connected in parallel (Omega). While the tap water was used as a liquid phase. The experiments have been executed in three low dynamic liquid levels (H_D) to the column diameter (D_c) (aspect ratio *H/D* = 3, 4, and 5), where the static liquid level H_S was adjusted to verify the needed aspect ratio (*H/D*) at different superficial gas velocities U_g. Industrial-size heat exchanger internals structure, which consists of 12 dual PVC pipe of 0.06 m diameter with the hexagonal arrangement and covers 24% of cross section area CSA of the bubble column, mimics the heat exchanger in Fischer-Tropsch synthesis (F-T).

The gas distribution, which has been utilized, was a fine perforated stainless-steel plate contains 600 holes of 3 mm diameter arranged in a triangular pattern with 20 mm pitch and 1.451% open area. In this work, two method have been used to demarcate the flow regime transition the linear method and the non-linear method by employing the extension liquid level technique, and differential pressure transducer technique, respectively. In addition, the advanced four-point fiber optical probe was used to characterize the bubble dynamics in different flow regimes and to apply the bubble properties, which are including the local gas holdup, bubble chord length, bubble rise

velocity, bubble pass frequency, and the interfacial area, to investigate effects of the presence of internals and the variation in the aspect ratio on the flow regime transition. Next section more detail information related to the techniques that used.

3. MEASURMENT TECHNIQUE

3.1. DIFFERENTIAL PRESSURE TRANSUDER

The pressure drop fluctuation signal is measured by using the differential pressure transducer (Omega Inc. PX409-005DWUI). However, The durability, the low price, the easy installation, and the sensitivity for flow regime transition are the features of the pressure transducer, and hence, the pressure transducer has been equipped extensively in industry to monitor the operation. In addition, it is easy to indicate the flow regime and its transition through analyzing the pressure fluctuations signal whether the absolute or pressure drop signals, in particular, when operating in severe conditions (high pressure), where the visual observation is impossible. The ports of the pressure transducer have been connected to the wall of the bubble column to void the wall effect on the pressure fluctuation signals.

Furthermore, the bubble column connected in two locations with the pressure transducer to evaluate the pressure drop variations in the sparger and bulk regions. The first port was placed at the bottom of the bubble column with a distance of 0.15 m above the perforated plate distributor. Whereas the second port was connected in three different axial locations 1.2, 1.7, and 2 m above due to that experiments were conducted in three aspect ratio H/D = 3, 4, and 5, respectively, and to prevent the disengagement region impact.

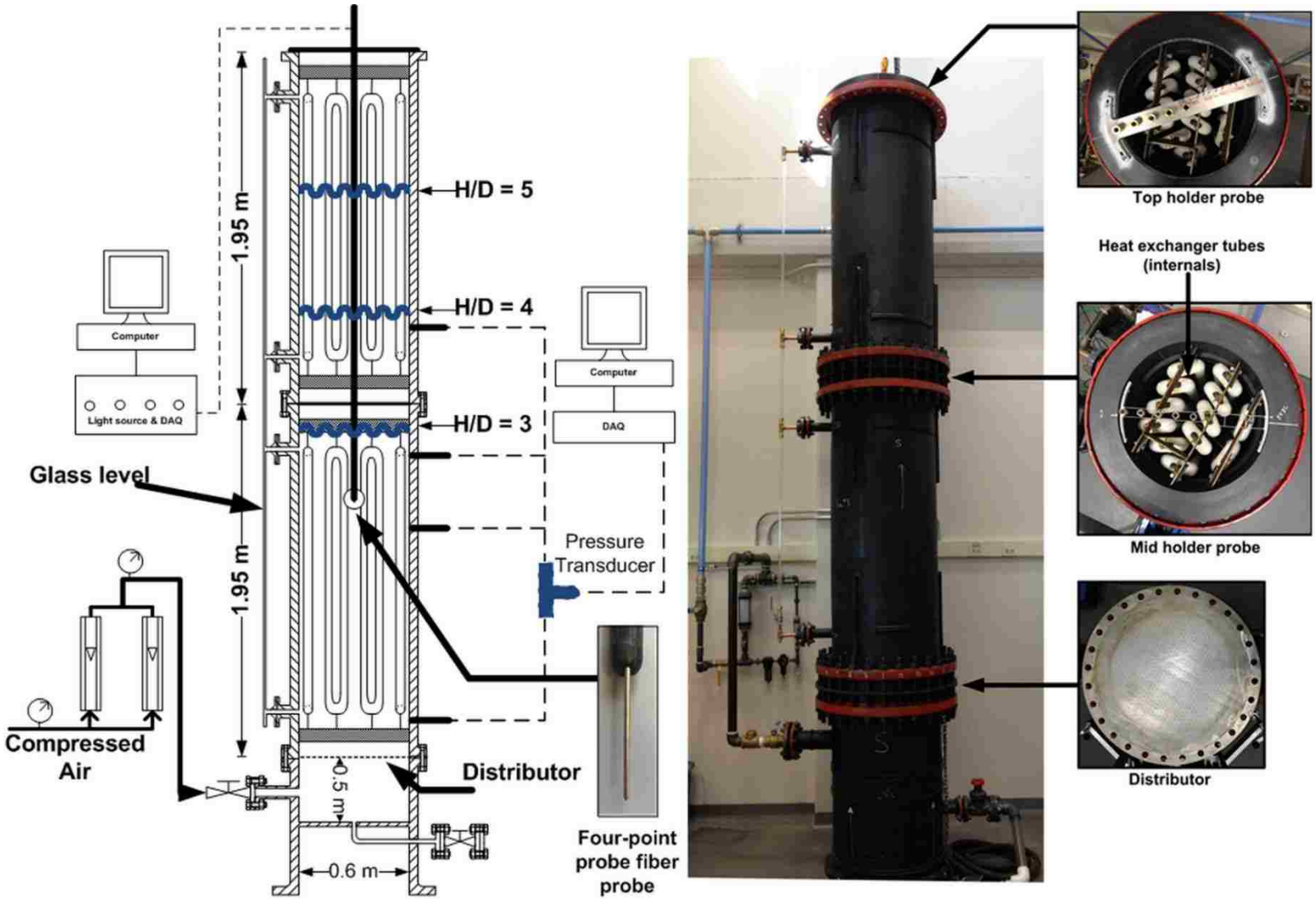

Figure 1. A schematic diagram of the experimental setup

Furthermore, the signal of the fluctuation of pressure was first converted to an electric signal (4-20 mA) by the pressure transducer and then collected by an OMB-DAQ-56 data acquisition board (Omega Inc.) with a sampling rate of 66.7 Hz.

3.2. FOUR-POINT OPTICAL PROBE TECHNIQUE

The bubble properties assessment including the local gas holdup, bubble rise velocity, chord length, interfacial area, frequency, were carried out by using the in-house four-point fiber optical probe. The optical probe, which manufactured in mFReal (Multiphase Flow and Multiphase Reactors Engineering Laboratory) in the Chemical and Biochemical Engineering Department at Missouri University of Science and Technology, has been first developed by Frijlink [44]. Subsequently, Xue [45] updated the algorithm data processing and validated the measurement of the bubble properties that found by using the new algorithm with data obtained by video imaging, thus, the updated algorithm version was applied in this work. However, the new algorithm of data processing has proved the capability to increase the precision of the optical probe by counts more number of bubbles with different angles and adjusts the error in-house manufacturing, more details can be found in the work of Xue et al. [46], Xue [45], and Xue et al. [47].

Furthermore, the data collected of the bubble properties with the sample rate and the time sampling are 40 kHz, and 138 sec, respectively. The advanced four-point fiber optical probe has been applied in two-three-phase bubble column reactor [48], and in different bubble column setup instruction (with and without internals) [7-8], [34-35]. In the most of these investigations, the optical probe was inserted from the side of bubble column wall, horizontally, whereas in this work, the optical probe has been inserted vertically from

the top of the bubble column reactor to void the effect of optical probe structure on the hydrodynamics of bubble column. And fixed at the fully development region that was demarcated by Al-Naseri et al. [2] to prevent the effect of the distributor and the disengagement region. Hence, the flow regime has been tested under different dynamic liquid levels (*H/D* = 3, 4, and 5) in the fully developed flow regime, and the optical probe was fixed in center of the bubble column at axial location H = 5 ft, 6 ft., and 6 ft. to prevent the distributor effect on the data.

3.3. OVERALL GAS HOLDUP AND DRIFT FLUX

The linear method, which utilized to indicate the flow regime transition, has been applied by two approaches measuring the overall gas holdup, and the drift-flux using equations (1), and (2), respectively.

$$\varepsilon_G = \frac{H_D - H_S}{H_D} \tag{1}$$

$$j_{GL} = U_g(1 - \varepsilon_G) \mp U_l \varepsilon_G \tag{2}$$

where; the $\varepsilon_G, H_D, H_S, j_{GL}, U_g, and\ U_l$ are the overall gas holdup (-), dynamic liquid level (m), static liquid level (m), drift flux (m/s), superficial gas velocity (m/s), and superficial liquid velocity (m/s) (which is zero due to the liquid phase is not flowing through the bubble column), respectively. The dynamic liquid level was maintained in the desired height during the variation in the superficial gas velocity (0.05-0.45 m/s) to demarcate the flow regime transition for the three aspect ratios (*H/D* = 3, 4, and 5). Meanwhile, the drift flux that defined as the volumetric flux of a component phase relative to a surface moving at the volume-averaged velocity [52] was emploied to demaricate the flow regime transition

as well. Accourding to Sal et al. [29] the drift flux method exhibites better distinguation for the regime transition than the overall gas holdup.

3.4. DEFINITION OF THE KOLMOGOROV ENTROPY (KE)

The Kolmogorov entropy (KE) is a quantitative measure of the disorder and non-linear characteristic in a chaotic system. Meanwhile, the flow in the bubble column has been classified as a chaotic system due to the high sensitivity to small changes in the initial condition [37-39]. Therefore, using the KE exhibits the capability to demarcate the flow regime transition in various types of multiphase flow [12], [37], and [40]. According to Nedeltchev et al. [57] and Toukan et al. [53] the large value of KE represents very disorder (irregular dynamic behavior), small value when the system is more regular, periodic like behavior, and zero for completely periodic systems. This parameter has been employed for flow regime identification, due to it is sensitive to changes in operating conditions. Hence, in current work, the KE that calculated from the non-linear chaos analysis to the pressure transducer time series as expressed in equation (3) was utilized to identify the mean flow regime boundaries in the bubble column.

$$KE = -f_s \ln\left(1 - \frac{1}{\bar{b}}\right) \tag{3}$$

where; $\bar{b}$ is the sequential pairs of points that defined by equation (4), while f_s is the sampling frequency (1/s).

$$\bar{b} = \frac{1}{M}\sum_{i=1}^{M} b_i \tag{4}$$

It is worth noting, the mFReal lab computational MATLAB program that formatted and updated by Toukan et al. [53] was used in this work to calculate all the pairs vectors

and the KE. Further information is related to the likelihood estimation method to the KE can be found in Toukan et al. [53], and Schouten et al. [58].

4. RESULTS AND DISCUSSION

4.1. CHARACTERIZING AND DEMARCTION OF FLOW REGIMES BY BUBBLE PROPERTIES

First using for the bubble properties including the bubble pass frequency and the mean bubble chord length to delineate the flow regime transition was successfully executed by Zhang et al. [13], and Shiea et al. [12]. Subsequently, Al-Naseri et al. [8] investigated the impact of the law aspect ratios on the flow regime transition in the bubble column without internals utilizing the same setup of this work. Data obtained revealed the capability of the bubble frequency and the mean chord length to demarcate the regime transition, whereas, the local gas holdup, interfacial area, and the bubble rise velocity did not exhibit a clear transition for the flow regime. Hence, demarcating the flow pattern by using the bubble frequency and mean chord length in this work was satisfying. Furthermore, measuring the bubble properties would provide a better understanding for the influence of the variation in the aspect ratio, and the presence of the internals on the flow regime boundaries.

Figure 2 illustrates the mean bubble chord length versus the superficial gas velocity U_g for the cases of bubble column with and without internals. The trends for both cases consist of three segments (A-B), (B-C), and (C-D) that represent the bubbly, transition, and the churn turbulent flow regimes, respectively. However, the results are aligning with the data revealed by Shiea et al. [16], Al-naseri et al. [43], and Zhang et al. [13] where in the

first part of trend (A-B) the size of chord length increased rapidly with the superficial gas velocity due to promoting the coalesce rate as result to the increase the bubble population with increasing the superficial gas velocity. In similarity, part (A-B) in Figure 3 that shows the bubble pass frequency versus the superficial gas velocity, the bubble frequency increase rapidly with the superficial gas velocity as well. That would confirm the increase in the bubble population, which in turn, enhances the bubble coalesce rate. Meanwhile, in case of the bubble column with internals, part (B-C) in Figure 2 and Figure 3, the rate of increasing in the mean chord length, and bubble frequency, respectively, was observed that started at U_g= 0.11 m/s as transition from the bubbly flow to transition flow regime and ended at U_g= 0.17 m/s as transit from transition to churn turbulent flow regime. In this part (B-C), the mean chord length and the bubble frequency exhibit slightly increasing with the superficial gas velocity U_g which attributed to promoting the turbulent eddies with the gas velocity, and hence, that would enhance the bubble break-up rate, which in turn, inhibits the accelerated growth in the bubble size and the bubble frequency. At U_g= 0.17 m/s, where the mean chord length reaches the maximum value, the churn turbulent flow regime starts where the liquid turbulent eddies significantly promoted in this regime [7]. Consequently, the both of bubble size decreased gradually and the bubble frequency increased with the increase the superficial gas velocity U_g due to increasing the bubble break-up rate [59]. However, the transition velocities in the bubble column with internals for aspect ratios *H/D* = 3, 4, and 5 have occurred in (0.11-0.17 m/s), (0.11-0.16 m/s), and (0.11-0.135 m/s), respectively. Meanwhile, the transition velocities in the bubble column without internals for aspect ratios *H/D* = 3, 4, and 5 have occurred in (0.08-0.14 m/s), (0.08-

0.11 m/s), and (0.08-0.1 m/s). Data obtained show that the presence of internals, and decrease the aspect ratio impact toward shifting (delaying) the transition velocities.

Accordingly, Figure 2 and Figure 3 illustrate the effect of the internals on the mean chord length and the bubble frequency, respectively. As shown, the presence of internals has decreased the bubble mean chord length and increased the bubble frequency significantly, and hence, the local gas holdup was increased as illustrated in Figure 4. This phenomenon could be attributed that the presence of internals promotes the population of small turbulent liquid eddies [7], which in turn, increase the bubble break-up rate, consequently, decreases the mean bubble chord length and increases the bubble frequency [59]. The bubble gas phase generates the liquid turbulent eddies, thereby, the bubble size and the population would administrate the chaotic degree.

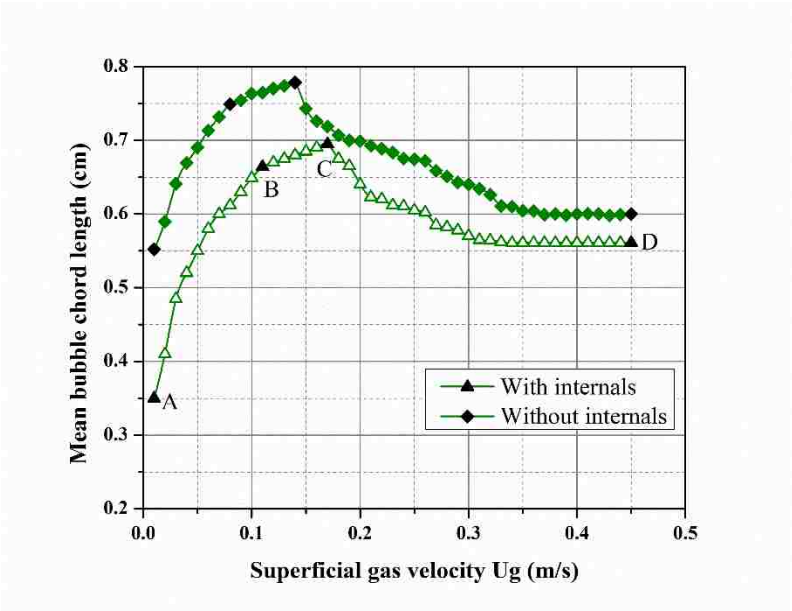

Figure 2. Flow regime demarcation by the mean bubble chord length (cm) in a bubble column with and without internals and *H/D* = 3

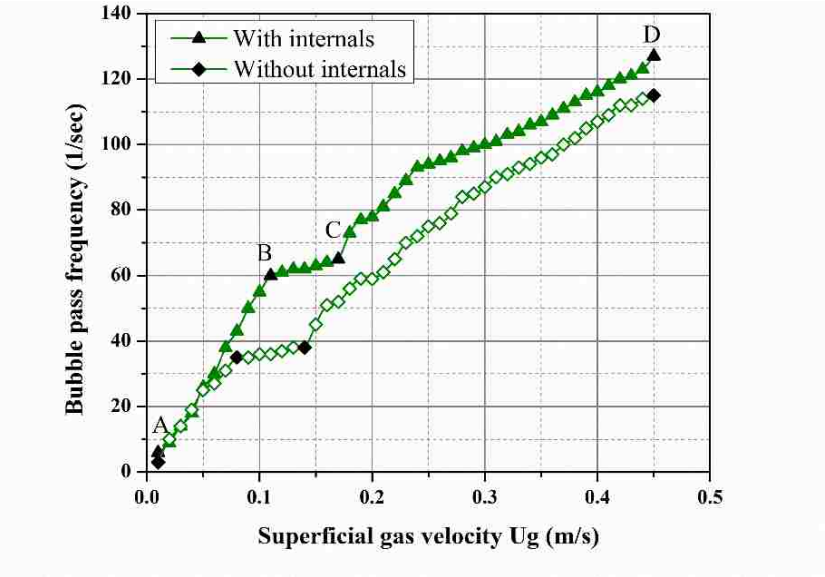

Figure 3. Flow regime demarcation by the bubble frequency (1/s) in a bubble column with and without internals and *H/D* = 3

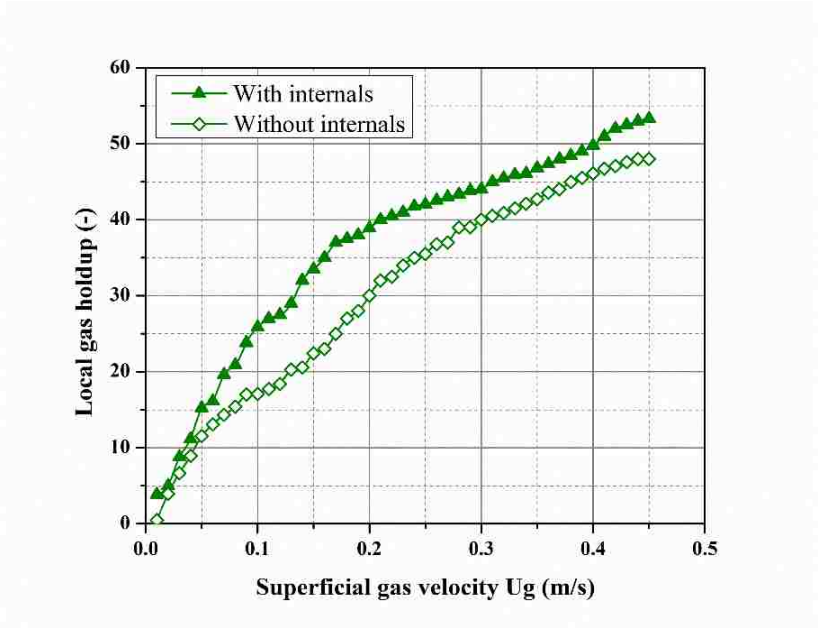

Figure 4. Internals effect on the local gas holdup (-) at aspect ratio *H/D* = 3

4.2. IDENTIFY THE FLOW REGIME TRANSITION BY LINEAR METHODS (OVERALL GAS HOLDUP AND DRIFT FLUX)

Demarcating the flow regime by using the linear method, based on the overall gas holdup, has been illustrated in Figure 5 for the bubble column with internals *H/D* = 3.

The overall gas holdup observes semi-constant trend with increasing the superficial gas velocity U_g, in this regime the rate of break-up starts growing with growing the liquid turbulent eddies, therefore, no significant variation in the bubble dynamics with increasing the superficial gas velocity as illustrated in Figure 3, and hence, that would reflect on the overall gas holdup. In the part (C-D), the overall gas holdup re-increased with increase the superficial gas velocity.

This regime is characterizing in the changing the bubble properties significantly due to increasing the population of the liquid turbulent eddies increased significantly, in particular, the small ones [7]. However, data obtained for the overall gas holdup in different aspect ratios exhibit similar trend with superficial gas velocity. The effect of aspect ratio and the presence of internals on the transition velocities have been illustrated in Figure 6, and Figure 7, respectively. As shown in Figure 6, the increase in the aspect ratio led to accelerating the transition from the bubbly flow to churn turbulent flow regime. Meanwhile, the presence of internals delays the transition. In the previous study conducted by Al-Naseri et al. [2] revealed that the bubble size was increased by increasing the aspect ratio and decreased with the presence of internals. Therefore, that probably attributes the transition occurred early at high aspect ratio, where the liquid turbulent eddies that are introduced by the gas phase are related to the bubble size, and hence, increasing the big bubbles population would increase the chaotic degree in the multiphase flow pattern and the vice versa with the existence of internals.

Figure 8 exhibits the drift-flux versus the overall gas holdup using the equation (2). In this method, the transition in the flow regime was demarcated clearly as shown in Figure 8. The drift-flux exhibits three segments with different slopes. The change in the slope represents the transition from one regime to another. Bubbly flow starts from point (A) and ends at point (B) at gas holdup = 0.203, which is equivalent to superficial gas velocity U_g = 0.115 m/s. The churn turbulent regime begins from point (C) and ends in point (D) at gas holdup = 0.211, which is equivalent to superficial gas velocity U_g = 0.17 m/s. Using drift flux method provides easy demarcation for the regime transitions.

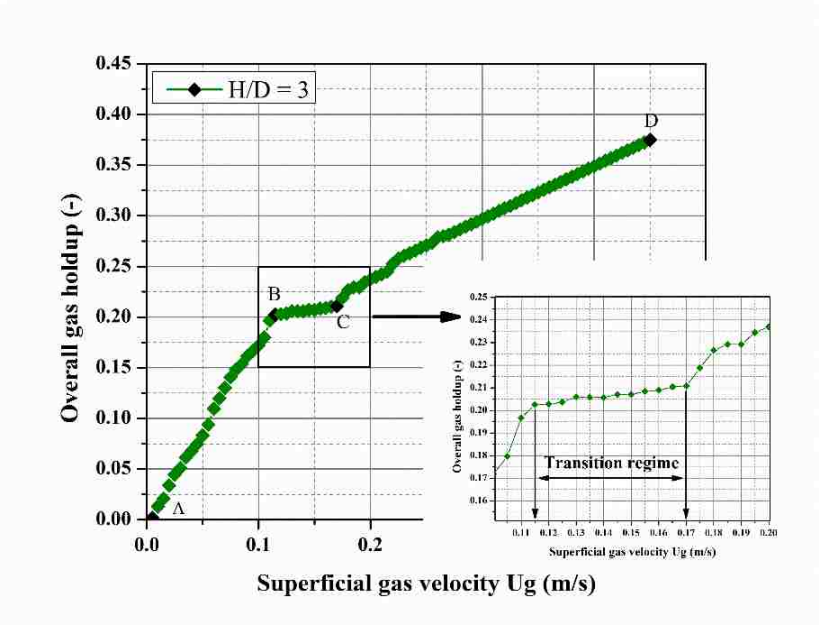

Figure 5. Flow regime transition in bubble column *H/D* = 3

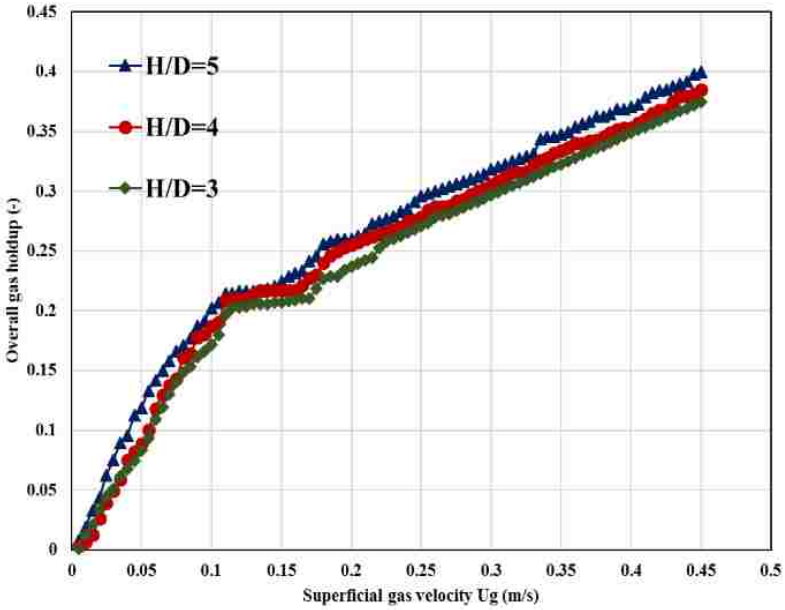

Figure 6. The aspect ratio effect on the flow regime transition velocities

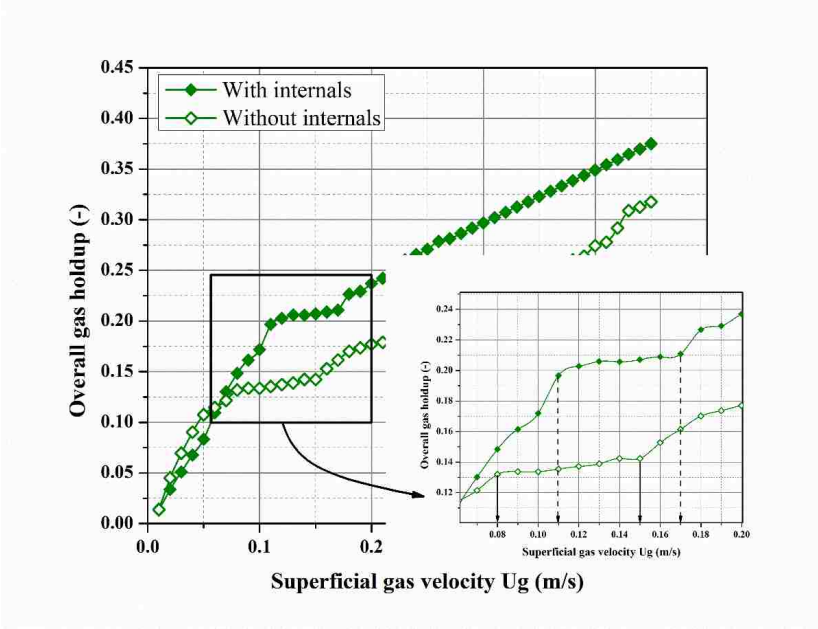

Figure 7. Internals effect on the flow regime transition in bubble column *H/D* = 3

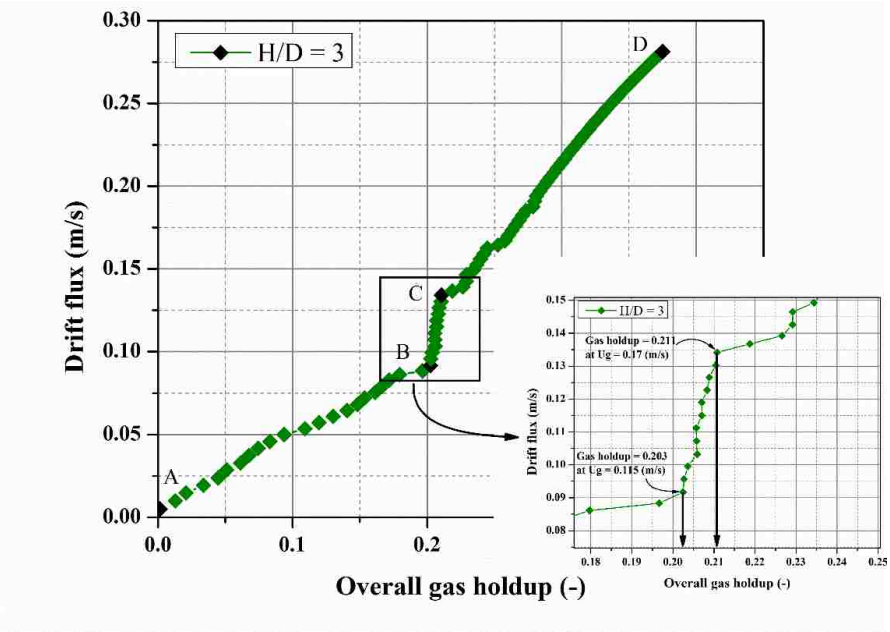

Figure 8. Flow regime transition using drift flux in bubble column *H/D* = 3

The next regime is the bubbly flow, which is ending at U_g = 0.115 m/s for bubble column operated in aspect ratio *H/D* = 3, and U_g = 0.11 m/s for aspect ratio *H/D* = 4 and 5. In this regime the bubble dynamic continues in change with growing for the coalescence rate, thereby, the bubble size and the frequency increased significantly in this regime. The transition regime follows the bubbly flow regime, which consists of two sub-regimes for aspect ratio *H/D* = 3 and 4, and ending at U_g = 0.155, and 0.135 m/s for aspect ratios (both *H/D* = 3 and 4), and 5, respectively. In the transition regime flow, the bubble break-up rate starts in increasing to the limit that being equal to the coalescence rate as result to promoting the liquid turbulent eddies, which is increasing significantly with an increase the superficial gas velocity. Hence, the increasing in the bubble frequency and the mean bubble chord length be slower until the threshold of the churn turbulent flow regime as shown in Figure 2 and Figure 3. In the turbulent flow regime, where the turbulent eddies

be predominant, the bubble break-up rate overcomes the coalescence rate. Thereby, the mean bubble chord length significantly decreased in this regime tile reach so-called stable bubble size, in which the bubble coalescence and break-up rates in equally. Furthermore, the changing in the KE value in significant fluctuation that could be attributed to the variation in the bubble size, in particular, the liquid eddies are introduced by the bubble gas phase. Therefore, the KE magnitude in Figure (9), Figure (10), and Figure (11) exhibits stability in value at U_g = 0.35 m/s, where at the same superficial gas velocity in Figure 2 the mean bubble chord length appears same behavior.

4.3. IDENTIFY THE FLOW REGIME TRANSITION BY NON-LINEAR METHOD (KOLMOGOROV ENTROPIES (KE))

Utilizing Kolmogorov Entropies (KE) approach contributes to the quantum assessment of the disorder of the multiphase system, and the bubble properties that examined could introduce the physical attribution for the changing in the chaotic behavior degree in the bubble column with the presence of internals at different aspect ratios. Therefore, the Kolmogorov Entropies (KE) that calculated by using equation (3) based on the pressure fluctuation signal has been plotted versus the superficial gas velocity U_g. In order to demarcate the flow regime transition the Figure (9), Figure (10) and Figure (11) illustrate the (KE) for the bubble column with internals operated in aspect ratios *H/D* = 3, 4, and 5, respectively. It is worth mentioning, the fluctuation in the trend of the (KE) was explained regarding previous investigations Al-Naseri et al. [8] where each minimum value of KE represents transfer point from regime to another one. However, the chaotic analysis method shows that there are four-flow regimes maldistribution, bubbly, transition, and churn turbulent flow regime. Accordingly, the maldistribution regime, which is ending at

U_g= 0.02, and 0.025 m/s for both (*H/D* = 3, and 4), and *H/D* = 5, respectively, is predominating in as long the low superficial gas velocities value is lower than Weber number (W_e), and hence, it characterizes that is administrated by the sparger design, bubbles size are small, and non-uniform bubble population distribution.

4.4. EXPERIMENTAL RESULTS COMPARISON

As we mentioned, the flow regime transition in bubble column has been addressed in many studies. Therefore, the experimental results for current work were compared with these previous investigations. Sal et al. [29] studied the effect of sparger design (with three holes diameter d_0 = 1, 2, and 3 mm) on the flow regime transition in bubble column of a diameter = 0.3 m and a height = 3 m using the linear method (gas holdup and drift flux) to demarcate the regime transition.

Their results that listed in Table 2 shows that the transition velocities decrease sharply as the hole diameter of the sparger increases. Meanwhile, increasing the hole diameter of the perforated plate led to decrease the overall holdup in the homogeneous flow regime, while no significant difference in the heterogenous regime was observed, and hence, the sparger effect on the flow transition velocities could be attributed to increasing the overall gas holdup.

Table 3 lists the data obtained from the comparison between the current data and Sal et al. [29] results of sparger type (P3) due to using the same hole diameter of the perforated plate.

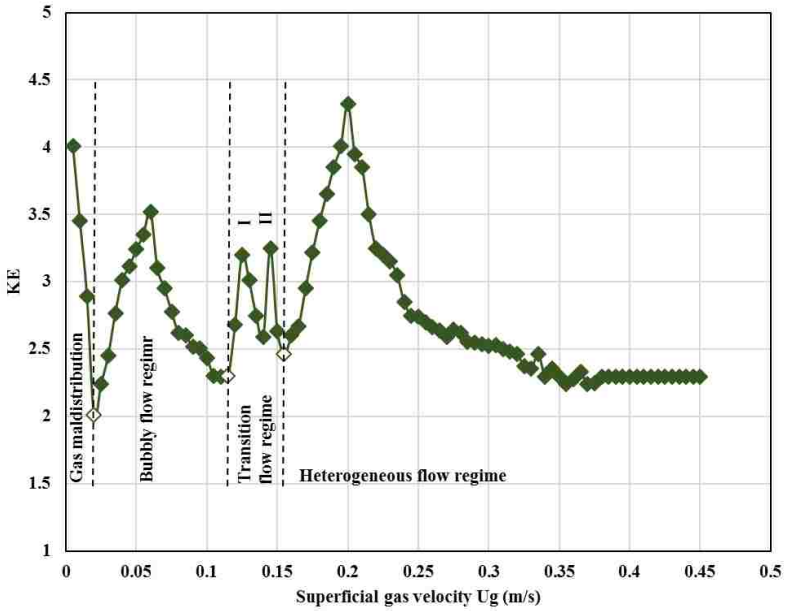

Figure 9. Identify the flow regime transition in a bubble column with aspect ratio *H/D* = 3 by Kolmogorov Entropy (KE) method

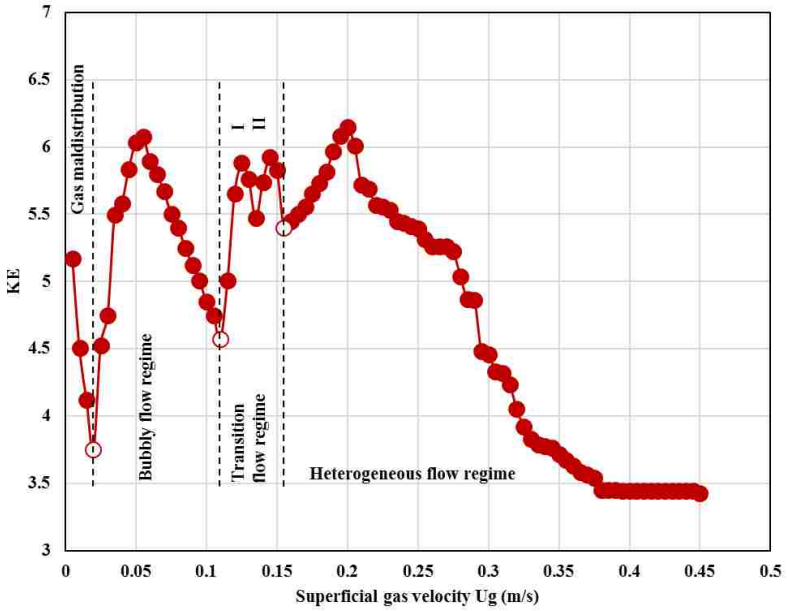

Figure 10. Identify the flow regime transition in a bubble column with aspect ratio *H/D* = 4 by Kolmogorov Entropy (KE) method

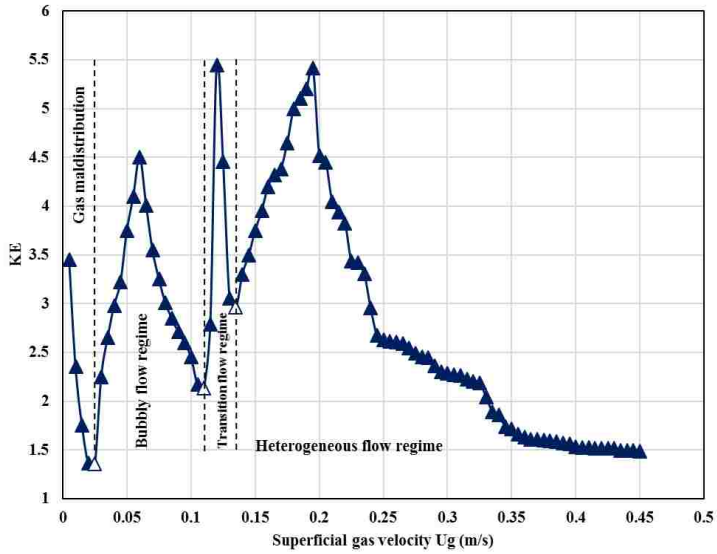

Figure 11. Identify the flow regime transition in a bubble column with aspect ratio *H/D* = 5 by Kolmogorov Entropy (KE) method

Table 3 reveals the difference between the transition velocities of the two studies whether in the first transition or in the second one and that was attributed to the effects of the presence of internals, the bubble column diameter, and the height of aspect ratio on the bubble dynamics. Hence, that reflected on the entire data obtained in the previous studies, and the industrial-sized bubble column must be considered in the future works. Another comparing has been executed with the results of Nedeltchev et al. [15] where the flow regime transition was demarcated in bubble column of a diameter 0.15 m by utilizing the chaotic analysis KE method. Figure 12 illustrates the transition velocities in the bubble column without internals that used by Nedeltchev et al. [15], the minimum values of KE indicates to a threshold of new regime, and hence, there are four transitions located in U_g = 0.016, 0.03, 0.04, and 0.046 m/s that represents the maldistribution, bubbly, sub-regime transition (I and II), and churn turbulent flow regimes, respectively. Regarding to the data

obtained in Figure (9), Figure (10), and Figure (11) of the transition velocities for aspect ratios *H/D* = 3, 4, and 5, there is agreement about four regimes existence in the bubble column and there is no effect for the presence of internals to eliminate any flow pattern. Whereas, increasing the aspect ratio lead to eliminate the second sub-transition regime in particular *H/D* = 4, and 5.

Table 2. Design details of perforated plate spargers and experimental values of transition velocity reported by Sal et al. [29]

Sparger type	Hole diameter, d_0 mm	Number of holes *N*	First transition U_g (m/s)	Second transition U_g (m/s)
P1	1	817	0.074	0.099
P2	2	217	0.71	0.094
P3	3	91	0.168	0.09

Table 3. The comparison between the experimental results and Sal et al. [29]

Bubble column	First transition U_g (m/s)	Second transition U_g (m/s)
Sal et al. [29], bubble column of (P3)	0.168	0.09
H/D = 3	0.11	0.17
H/D = 4	0.11	0.16
H/D = 5	0.11	0.135

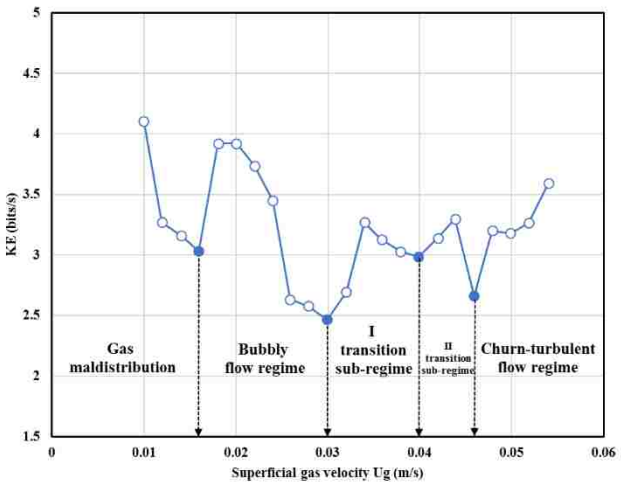

Figure 12. Flow regime transition using KE in bubble column of 0.14 m ID as adapted by Nedeltchev et al. [15]

5. CONCLUSION

In this study, for the first time, the effects of the presence of internals and the variation in the aspect ratio (*H/D* = 3, 4, and 5) on the flow regime transition have been studied in an industrial size bubble column by utilizing the overall gas holdup, and differential pressure transducer techniques. Meanwhile, an advanced four-point optical fiber probe has been used to measure the bubble chord length, frequency, local holdup, velocity, and interfacial area of different regimes. However, data obtained exhibit the following remake points.

Data obtained show that the existence of internals delays the transition flow regime. While, the increase in the aspect ratio led to accelerate the occurring of transition at lower velocities. The explanation for this phenomenon was attributed that bubble size was impacted where the parameter that promotes the bubble size would enhance the transition occurs early such as the increase of aspect ratio, and the vice versa with the parameters that decreases the bubble size such as the presence of internals.

The mean bubble chord length and the bubble frequency exhibit the capability to demarcate the transition flow regime with existence the internals at different aspect ratio.

The Kolmogorov entropy (KE) results exhibit a significant fluctuation in the magnitude value of the KE through the transition regimes (sub-regime I and II). Simultaneously in these regimes, bubbles exhibit a significant variation in the mean bubble chord length (bubble size). While, the KE exhibits semi-constant value at U_g= 0.35 m/s, where the bubble size has shown a constant value.

The comparison data obtained, exhibits an alignment with Sal et al. [29], and Nedeltchev et al. [15] about the capability of linear and non-linear methods, respectively, to identify the regime transition, although, the difference in the magnitude value of the transition velocities that attributed to the presence of internals and the low aspect ratio.

NOMENCLATURE

CT = gamma-ray computed tomography

RPT = radioactive particle tracking

d_p = particle diameter

d_0 = hole diameter of the perforated plate

C_s = solid concentration %Vol

H_D = bubbling height of bubble column (m)

H_S = static liquid level (m)

CSA = cross-section area (m^2)

D, D_c = bubble column diameter (m)

H = bubble column height (m)

H/D = aspect ratio (-)

L = axial location in bubble column (ft.)

KE = Kolmogorov Entropy (bit/s)

f_s = sample frequency (s^{-1})

$\bar{b}$ = mean of all b values (-)

b_i = number of sequential pair of points on the attractor (-)

M = sample size of b values (-)

U_g = superficial gas velocity (m/s)

U_l = superficial liquid velocity (m/s)

j_{GL} = drift flux (m/s)

We = Weber number

Greek letters

ε_G = overall gas holdup (-)

ε_g = local gas holdup (-)

Subscripts

s = solid (slurry)

p = particle solid (slurry)

g, G = gas phase

l, L = liquid phase

REFERENCES

[1] M. Kagumba, H. Al-Naseri, and M. H. Al-Dahhan, "A new contact time model for the mechanistic assessment of local heat transfer coefficients in bubble column using both the four-optical fiber probe and the fast heat transfer probe-simultaneously," *Chem. Eng. J.*, vol. 361, no. December 2018, pp. 67–79, 2019.

[2] H. Al-Naseri, J. P. Schlegel, and M. H. Al-Dahhan, "The Effects of Internals and Low Aspect Ratio on The Flow Development and Bubble Dynamics in Pilot-Plant Bubble Column for Fischer-Tropsch synthesis," *Exp. Therm. Fluid Sci.*, vol. submitted, 2018.

[3] A. A. Youssef, M. E. Hamed, J. T. Grimes, M. H. Al-Dahhan, and M. P. Duduković, "Hydrodynamics of pilot-scale bubble columns: Effect of internals," *Ind. Eng. Chem. Res.*, vol. 52, no. 1, pp. 43–55, 2013.

[4] A. A. Youssef, M. E. Hamed, M. H. Al-Dahhan, and M. P. Duduković, "A new approach for scale-up of bubble column reactors," *Chem. Eng. Res. Des.*, vol. 92, no. 9, pp. 1637–1646, 2014.

[5] M. K. Al Mesfer, A. J. Sultan, and M. H. Al-Dahhan, "Impacts of dense heat exchanging internals on gas holdup cross-sectional distributions and profiles of bubble column using gamma ray Computed Tomography (CT) for FT synthesis," *Chem. Eng. J.*, vol. 300, pp. 317–333, 2016.

[6] A. J. Sultan, L. S. Sabri, and M. H. Al-Dahhan, "Investigating the influence of the configuration of the bundle of heat exchanging tubes and column size on the gas holdup distributions in bubble columns via gamma-ray computed tomography," *Exp. Therm. Fluid Sci.*, vol. 98, no. February, pp. 68–85, 2018.

[7] M. K. Al Mesfer, A. J. Sultan, and M. H. Al-Dahhan, "Study the Effect of Dense Internals on the Liquid Velocity Field and Turbulent Parameters in Bubble Column for Fischer–Tropsch (FT) Synthesis by Using Radioactive Particle Tracking (RPT) Technique," *Chem. Eng. Sci.*, vol. 161, pp. 228–248, 2017.

[8] H. Al-Naseri, J. P. Schlegel, and M. H. Al-Dahhan, "The Impact of Low Aspect Ratio on Flow Regime Transition in Industrial-Sized Pilot Plant Bubble Column Reactor," *Chem. Eng. J.*, vol. submitted, 2018.

[9] J. Chen *et al.*, "Fluid dynamic parameters in bubble columns with internals," *Chem. Eng. Sci.*, vol. 54, no. 13–14, pp. 2187–2197, 1999.

[10] J. J. J. Chen, M. Jamialahmadi, and S. M. Li, "Effect of liquid depth on circulation in bubble columns: a visual study," *Chem. Eng. Res. Des.*, vol. 67, no. 2, pp. 203–207, 1989.

[11] J. P. P. Schlegel, S. Sharma, R. M. M. Cuenca, T. Hibiki, and M. Ishii, "Local flow structure beyond bubbly flow in large diameter channels," *Int. J. Heat Fluid Flow*, vol. 47, pp. 42–56, 2014.

[12] M. Shiea, N. Mostoufi, and R. Sotudeh-Gharebagh, "Comprehensive study of regime transitions throughout a bubble column using resistivity probe," *Chem. Eng. Sci.*, vol. 100, pp. 15–22, 2013.

[13] J. P. Zhang, J. R. Grace, N. Epstein, and K. S. Lim, "Flow regime identification in gas-liquid flow and three-phase fluidized beds," *Chem. Eng. Sci.*, vol. 52, pp. 3979–3992, 1997.

[14] G. Hebrard, D. Bastoul, and M. Roustan, "Influence of the gas sparger on the hydrodynamic behavior of bubble columns," *Chem. Eng. Res. Des.*, vol. 74, no. 3, pp. 406–414, 1996.

[15] S. Nedeltchev, S. Aradhya, F. Zaid, and M. Al-Dahhan, "Flow Regime Identification in Three Multiphase Reactors Based on Kolmogorov Entropies Devived from gauge Pressure Fluctuations," *J. Chem. Eng. Japan*, vol. 45, no. 9, pp. 757–764, 2012.

[16] S. Barghi, A. Prakash, A. Margaritis, and M. A. Bergougnou, "Flow Regime Identification in a Slurry Bubble Column from Gas Holdup and Pressure Fluctuations Analysis," *Can. J. Chem. Eng.*, vol. 82, no. October, pp. 865–870, 2004.

[17] E. Olmos, C. Gentric, S. Poncin, and N. Midoux, "Description of flow regime transitions in bubble columns via laser Doppler anemometry signals processing," *Chem. Eng. Sci.*, vol. 58, no. 9, pp. 1731–1742, 2003.

[18] E. Olmos, C. Gentric, and N. Midoux, "Identification of Flow Regimes in a Flat Gas-liquid Bubble Column via Wavelet Transform," *Can. J. Chem. Eng.*, vol. 81, no. August, pp. 382–388, 2003.

[19] A. Shaikh and M. Al-Dahhan, "Characterization of the hydrodynamic flow regime in bubble columns via computed tomography," *Flow Meas. Instrum.*, vol. 16, pp. 91–98, 2005.

[20] I. G. Reilly, D. S. Scott, D. E. Bruijn, and D. Macintyre, "The Role of Gas Phase Momentum in Determining Gas Holdup and Hydrodynamic Flow Regimes in Bubble Column Operations," vol. 72, no. 1961. 1994.

[21] B. Gourich, C. Vial, A. H. Essadki, F. Allam, M. B. Soulami, and M. Ziyad, "Identification of flow regimes and transition points in a bubble column through analysis of differential pressure signal - Influence of the coalescence behavior of the liquid phase," *Chem. Eng. Process. Process Intensif.*, vol. 45, no. 3, pp. 214–223, 2006.

[22] J. Y. Kim *et al.*, "Gas holdup and hydrodynamic flow regime transition in bubble columns," *J. Ind. Eng. Chem.*, vol. 56, pp. 450–462, 2017.

[23] S. Kumar, N. Srinivasulu, P. Munshi, and A. Khanna, "Flow regime transition identification in three phase co-current bubble columns," *Can. J. Chem. Eng.*, vol. 91, no. 3, pp. 516–523, 2013.

[24] W. Li, W. Zhong, B. Jin, Y. Lu, and T. He, "Flow patterns and transitions in a rectangular three-phase bubble column," *Powder Technol.*, vol. 260, pp. 27–35, 2014.

[25] P. C. Mena, M. C. Ruzicka, F. A. Rocha, J. A. Teixeira, and J. Drahoš, "Effect of solids on homogeneous-heterogeneous flow regime transition in bubble columns," *Chem. Eng. Sci.*, vol. 60, no. 22, pp. 6013–6026, 2005.

[26] S. Orvalho *et al.*, "Flow regimes in slurry bubble column: Effect of column height and particle concentration," *Chem. Eng. J.*, vol. 351, no. February, pp. 799–815, 2018.

[27] W. L. Li, W. Q. Zhong, B. S. Jin, R. Xiao, and T. T. He, "Flow regime identification in a three-phase bubble column based on statistical, Hurst, Hilbert-Huang transform and Shannon entropy analysis," *Chem. Eng. Sci.*, vol. 102, pp. 474–485, 2013.

[28] R. Krishna and J. Ellenberger, "Gas holdup in bubble column reactors operating in the churn-turbulent flow regime," *AIChE J.*, vol. 42, no. 9, pp. 2627–2634, 1996.

[29] S. Şal, Ömer F. Gül, Mustafa Özdemir, Ö. F. Gül, and M. Özdemir, "The effect of sparger geometry on gas holdup and regime transition points in a bubble column equipped with perforated plate spargers," *Chem. Eng. Process. Process Intensif.*, vol. 70, pp. 259–266, 2013.

[30] G. Besagni, A. Di Pasquali, L. Gallazzini, E. Gottardi, L. P. M. Colombo, and F. Inzoli, "The effect of aspect ratio in counter-current gas-liquid bubble columns: Experimental results and gas holdup correlations," *Int. J. Multiph. Flow*, vol. 94, pp. 53–78, 2017.

[31] M. C. Ruzicka, J. Drahos, M. Fialova, and N. H. Thomasb, "Effect of bubble column dimensions on flow regime transition," *Chem. Eng. Sci.*, vol. 56, pp. 6117–6124, 2001.

[32] A. J. Sultan, L. S. Sabri, and M. H. Al-Dahhan, "Impact of heat-exchanging tube configurations on the gas holdup distribution in bubble columns using gamma-ray computed tomography," *Int. J. Multiph. Flow*, vol. 106, pp. 202–219, 2018.

[33] A. J. Sultan, L. S. Sabri, and M. H. Al-Dahhan, "Influence of the size of heat exchanging internals on the gas holdup distribution in a bubble column using gamma-ray computed tomography," *Chem. Eng. Sci.*, vol. 186, pp. 1–25, 2018.

[34] M. Kagumba and M. H. Al-Dahhan, "Impact of internals size and configuration on bubble dynamics in bubble columns for alternative clean fuels production," *Ind. Eng. Chem. Res.*, vol. 54, no. 4, pp. 1359–1372, 2015.

[35] A. A. Jasim, A. J. Sultan, and M. H. Al-Dahhan, "Influence of heat-exchanging tubes diameter on the gas holdup and bubble dynamics in a bubble column," *Fuel*, vol. 236, no. March 2018, pp. 1191–1203, 2019.

[36] A. A. Jasim, A. J. Sultan, and M. H. Al-Dahhan, "Impact of heat exchanging internals configurations on the gas holdup and bubble properties in a bubble column," *Int. J. Multiph. flow*, vol. 112, pp. 63–82, 2019.

[37] A. Youssef, “Fluid Dynamics And Scale-Up Of Bubble Columns With Internals,” Washington University in St. Louis, 2010, 2010.

[38] W. T. Medjiade, A. R. Alvaro, and A. Schumpe, “Flow regime transitions in a bubble column,” *Chem. Eng. Sci.*, vol. 170, pp. 263–269, 2017.

[39] J. P. Schlegel, P. Sawant, S. Paranjape, B. Ozar, T. Hibiki, and M. Ishii, “Void fraction and flow regime in adiabatic upward two-phase flow in large diameter vertical pipes,” *Nucl. Eng. Des.*, vol. 239, no. 12, pp. 2864–2874, 2009.

[40] S. Nedeltchev and M. Schubert, “Statistical validation of the mixing length concept in bubble columns operated in the transition flow regime,” *J. Chem. Eng. Japan*, vol. 48, no. 2, pp. 107–111, 2015.

[41] J. J. Wu, D. Wang, L. hua Li, and J. T. Zhou, “Characterization of Flow Regimes in Bubble Columns through CCF Analysis of Pressure Fluctuations,” *Chem. Eng. Technol.*, vol. 28, no. 10, pp. 1109–1113, 2005.

[42] A. I. . Shnip, R. V. Kolhatkar, D. Swamy, and J. B. Joshi, “Criteria for the transition from the homogeneous to the heterogeneous regime in two-dimensional bubble column reactors,” *Int. J. Multiph. Flow*, vol. 18, no. 5, pp. 705–726, 1992.

[43] M. C. Ruzicka, J. Zahradnik, J. Drahoš, and N. H. Thomas, “Homogeneous – heterogeneous regime transition in bubble columns,” *Chem. Eng. Sci.*, vol. 56, pp. 4609–4626, 2001.

[44] J. J. Frijlink, “Physical aspects of gassed suspension reactors,” Delft University of Technology, 1987.

[45] J. Xue, “Bubble Velocity, Size and Interfacial Area Measurements in Bubble columns,” Washington Univeristy, Saint Louis, 2004.

[46] J. Xue, M. Al-Dahhan, M. P. Dudukovic, and R. F. Mudde, “Four-point optical probe for measurement of bubble dynamics: Validation of the technique,” *Flow Meas. Instrum.*, vol. 19, no. 5, pp. 293–300, 2008.

[47] J. Xue, M. Al-dahhan, M. P. Dudukovic, and R. F. Mudde, “Bubble Dynamics Measurements Using Four-Point Optical Probe,” *Can. J. Chem. Eng.*, vol. 81, no. August, pp. 375–381, 2003.

[48] C. Wu, K. Suddard, and M. H. Al-Dahhan, “Bubble Dynamics Investigation in a Slurry Bubble Column,” *AIChE J.*, vol. 54, no. 5, pp. 1203–1212, Jan. 2008.

[49] M. Kagumba, “Heat transfer and bubble dynamics in bubble and slurry bubble columns with internals for Fischer-Tropsch synthesis of clean alternative fuels and chemicals,” Missouri University of Science and Technology, 2013.

[50] A. Youssef, “Fluid Dynamics and Scale-up of Bubble Columns with Internals,” Washington University in St. Louis, 2010.

[51] A. A. Youssef and M. H. Al-Dahhan, “Impact of internals on the gas holdup and bubble properties of a bubble column,” *Ind. Eng. Chem. Res.*, vol. 48, no. 17, pp. 8007–8013, 2009.

[52] G. B. Wallis, *One-Dimensional Two-Phase Flow*. 1969.

[53] A. Toukan, V. Alexander, H. AlBazzaz, and M. H. Al-Dahhan, “Identification of flow regime in a cocurrent gas – Liquid upflow moving packed bed reactor using gamma ray densitometry,” *Chem. Eng. Sci.*, vol. 168, pp. 380–390, 2017.

[54] R. Krishna, J. Ellenberger, D. E. Hennophof, D. E. Hennephof, and D. E. Hennophof, “Analogous description of the hydrodynamics of gas-solid fluidized beds and bubble columns,” *Chem. Eng. J.*, vol. 53, no. 1, pp. 89–101, 1993.

[55] J. Ellenberger and R. Krishna, “A unified approach to the scale-up of gas-solid fluidized bed and gas-liquid bubble column reactors,” *Chem. Eng. Sci.*, vol. 49, no. 24, pp. 5391–5411, 1994.

[56] H. M. Letzel *et al.*, “Characterization of regimes and regime transitions in bubble columns by chaos analysis of pressure signals,” *Chem. Eng. Sci.*, vol. 52, no. 24, pp. 4447–4459, 1997.

[57] S. Nedeltchev, A. Shaikh, and M. Al-Dahhan, “Flow regime identification in a bubble column based on both statistical and chaotic parameters applied to computed tomography data,” *Chem. Eng. Technol.*, vol. 29, no. 9, pp. 1054–1060, 2006.

[58] J. C. Schouten, F. Takens, and C. M. Van Den Bleek, “Maximum-likelihood estimation of the entropy of an attractor,” *phys. Rev. E Stat. Phys. Plasmas Fluids Relat. Interdiscip. Top.*, vol. 49, no. 1, pp. 126–129, 1994.

[59] A. Serizawa and I. Kataoka, “Turbulence suppression in bubbly two-phase flow,” *Nucl. Eng. Des.*, vol. 122, pp. 1–16, 1990.

V. 3D CFD SIMULATION OF BUBBLE COLUMN REACTOR; VALIDATION OF INTERFACIAL FORCES AND INTERNALS EFFECT

ABSTRACT

Bubble column with and without internals have been simulated in 3D time-dependent using Eulerian-Eulerian approach incorporated with the population balance model PBM to address the effects of the presence of internals, the internals configurations (hexagonal and circular), and the internals diameter (tube diameter 0.5-inch and 1-inch) on the time-averaged gas holdup distribution. The used superficial gas velocities are U_g = 0.05, 0.2, and 0.45 m/s to cover the bubbly flow and the churn turbulent flow regimes. In the first part, the turbulent models and the interfacial forces, embedding drag, lift, wall lubricated, and turbulent dispersion, have been validated azimuthally with the experimental results of the gas holdup and liquid velocity that reported by Al Mesfer et al. [1-2], and Sultan et al. [3-4]. In the second part, the validated CFD closures are utilized to simulate the bubble column equipped with different internals configurations and different internals tubes diameters. The validated closures exhibit the capability to predict the hydrodynamics of the bubble column in the used gas velocities and various internals configurations and diameters, further, incorporate the population balance model, in turn, promotes the prediction of simulation in high superficial gas velocity. However, the simulation results for the effect of internals revealed that the time-averaged of the gas holdup was enhanced significantly in the wall region of the bubble column. The gas holdup profiles in the presence of internals in different configurations provide a uniform gas holdup profile. While, the results of the effect of internals diameter exhibit that the gas holdup was

increased remarkably in the center and the wall regions of the bubble column equipped by internals of 1-inch diameter more than in using internals of 0.5-inch. However, the effect of internals configurations reported that the internals with hexagonal arrangement increases the gas holdup in the center region more than the circular arrangement, and less in the wall region comparing with the circular arrangement.

1. INTRODUCTION

Bubble column reactors (bubble and slurry bubble column with and without internals) have been utilized widely in different fields such as chemical, petrochemical, wastewater treatment, bioprocess, and metallurgical industries, because of their good features that regard to the high mass and heat transfer coefficient, good in the mixing and the thermal control, the low in cost and the movable parts, and high conversion [5]–[9]. Among these processes are Fischer-Tropsch (F-T) synthesis and methanol synthesis that typically used with the presence of internals. In spite of the competitive features, the disadvantages of bubble column reactors are complex in design due to the interaction between the phases, back-mixing, and the liquid circulation [10]–[14]. Hence, numerous studies that addressed to investigate the effects of physics properties of gas-liquid phase, the presence of internals, bubble column dimension, and the sparger design have been conducted either experimentally [6], [9], [13], [15]–[20] or theoretically [14], [21]–[29] to optimize the bubble column reactor performance.

Experimentally, Al Mesfer et al. [1] studied the effect of the presence of heat exchanging internals on the gas holdup profiles in the bubble column utilizing gamma ray computed tomography (CT). The experiments were conducted in a Plexiglas bubble

column of 5.5 inches (0.14m) inner diameter and a height 72 inches (1.83m) operated at ambient temperature and pressure. The superficial gas velocity that calculated based on the free and total cross-sectional area (CSA) for flow column was varied 0.05-0.45 m/s to covers the bubbly flow and the churn turbulent flow regime. Heat exchanging internals consists of thirty vertical Plexiglas tubes of 0.5 inch, which cover ~25% of the total cross-sectional area of the column, were arranged hexagonally in a triangular pitch of 0.84 inch (2.14 cm). They reported that the gas holdup distribution over the cross-sectional area of the column exhibited a symmetrical shape during operating the bubble column with internals at low superficial gas velocity. Furthermore, the overall gas holdup and the profile of the gas holdup of the bubble column without internals, at churn turbulent flow regime, can be extrapolated to those in the center region of the bubble column with internals. However, the present of internals significantly prompted the overall gas holdup and the profile of gas holdup in case the superficial gas velocity is based on the total (CSA) for flow column, whereas, the present of internals insignificantly effects on the overall gas holdup and the profile of gas holdup when the superficial gas velocity is based on the free (CSA) for flow column. However, the gas holdup profile in the bubble column with internals exhibited less steeper profile at high superficial gas velocity comparing with the gas holdup in the bubble column without internals. Subsequently, using the same setup of bubble column and internals that used by Al Mesfer et al. [1] and superficial gas velocity was ranged 0.05-0.45 m/s based free and total cross-sectional area (CSA) for flow column, Al Mesfer et al. [2] investigated the effect of internals on the liquid velocity and the turbulent parameters including the Reynolds stresses, turbulent kinetic energy, and turbulent eddy diffusivities. Their experiments were conducted utilizing the advanced

radioactive particle tracking (RPT) technique. The results revealed that the presence of internals increases the axial centerline liquid velocity and decreases significantly the turbulent parameters, while, increasing the superficial gas velocity would increase the axial centerline liquid velocity and the turbulent parameters.

The impact of the configuration of internals on the gas holdup distribution in a bubble column was investigated by Sultan et al. [4] using gamma ray tomography (CT) technique. Three configurations of internals, arranged in a hexagonal, circular, and circular with central tube that cover ~25% of the cross-sectional area (CSA) of column, were used. They revealed that the presence of internals, for all the configurations, enhanced the gas holdup in the wall region. While, the variation in the configuration of internals significantly controlled the gas holdup distribution over the cross-sectional of column, further, the internals with hexagonal arrangement provided higher and uniform gas phase distribution. Consequently, the impact of the size of internals tube on the gas holdup up distribution was investigated by Sultan et al. [3] using gamma ray tomography (CT) technique, while, the experiments were executed in a bubble column of 5.5 inched (0.14 m) diameter and a height 72 inches (1.83 m). Two sizes of heat exchanging internals that arranged in circular configuration 0.5, and 1 inch. Data obtained shown that the gas holdup profile exhibited a wave shape in the bubble column with internals, whereas, the internals with size of 1 inch provided a uniform gas holdup profile over the cross-sectional of the column.

In the same context, Kagumba and Al-Dahhan [30] investigated the effects of the presence of internals with different configurations and the size of internals tube on the bubble properties, which are included the local gas holdup, bubble chord length, interfacial area, bubble velocity, and bubble passing frequency, using the four-point optical probe.

The investigation utilized two configurations of internals hexagonal, and circular with tube size 0.5 inch, and 1 inch, respectively, have occupied ~25% of the cross-sectional of column. The superficial gas velocity based on the free and total cross-sectional area (CSA) for flow column was varied 0.03-0.45 m/s to covers the bubbly flow and churn turbulent flow regimes. They reported that although the presence of internals in the bubble column has insignificant effect on the local gas holdup during the operating in superficial gas velocity based on the total cross-sectional (CSA) for flow column, but it significantly effects on the bubble properties, in particular, the bubble chord length distribution, where the presence of internals decreases the bubble chord length which is reflected that to increase the bubble passing frequency and the interfacial area. However, the measurements of the bubble chord length exhibited that the bubbles in the low superficial gas velocity are small size, whereas, the bubbles size were increased and be in wide range of sizes with increasing the superficial gas velocity.

Recently, the effect of the configurations of heat exchanging internals and tube dimeter, mimicking the F−T process, on the bubble properties was reported by Jasim et al. [31], [32]. The studies were conducted in a bubble columns of diameter 5.5 inches (0.14 m) and 72 inches (1.83 m) with superficial gas velocity, based on free cross-sectional area (CSA) for flow column, varied between 0.02 and 0.45 m/s. The internals used were of different configurations with cross-sectional areas covering 25% of the cross-sectional area (CSA) of column. They reported the presence of internals led to enhance the bubble breakup rate, giving rise to smaller bubble chord lengths. Thus, increased specific interfacial area between the gas and liquid phases was higher in the bubble column with

internals. However, obtained results agree with Sultan et al. [3], [4] in terms the effect of internals configurations and tube size on the gas holdup profile.

Despite there are a relative agreement among these studies in terms of the effect of studied parameters on the hydrodynamics of the bubble column reactor, but the most of these studies have been conducted at ambient temperature and pressure and utilizing the water and the air as a liquid phase and gas phase, respectively. Hence, that is contrast with the practical applications for the bubble/slurry bubble column in regards the operating conditions and the physical properties of the fluids. Thereby, still, there are errors between the experimental results and the design regarding the scale-up. However, the data obtained by the previous studies still provide a huge benchmark data that can be used for validation computational fluid dynamics (CFD). Consequently, using the numerical methods introduces an excellent offer to improve the design and the scale-up tasks, and a full-scale experimentation in bubble columns is expensive; a more cost-effective approach to exploring these reactions is by using validated computational fluid dynamics models [33], particularly, the recent development that conducted in the capability of the computer and the simulation codes.

Three approaches the VOF approache, Eulerian-Lagranging approache [34]–[36], and Eulerian-Eulerian models [37]–[41] are primarily employed to the CFD simulation. In the Eulerian-Lagrangian model, the continuous phase is described in an Eulerian representation while the dispersed phase is treated as discrete bubbles and each bubble is tracked by solving the equations of motion for individual bubbles, wich requires tracking the dynamics of each bubble, therefore, is usully applied to cases with low superficial gas velocity due to computer limitations. The VOF method solves the instantaneous Navier-

Stokes equations to obtain the gas and liquid flow field with an extremely high spatial resolution. The evoluation of the gas-liquid interface is tracked using a volum-tracking scheme. However, the VOF method is limited to a small number of bubbles, such as less than 10 bubbles in the flow field, due to computational limitations. The Eulerian-Eulerian model treats dispersed (gas bubbles) and continuous (liquid) phases as interpenetrating continua, and describes the motion for gas and liquid phases in an Eulerian frame of reference. The Eulerian-Eulerian method is often used because memory storage requirements and demand of computer power depend only on the number of computational cells considered intead of the number of bubbles. The Eulerian-Eulerian approach can be applied to cases for low and high superficial gas velocities. In most industrial applications, high superficial gas velocity is used and therefore the Eulerian-Eulerian method is preferred [40].

Larachi et al. [42] simulated, for the first time, the impacts of liquid circulation in bubble column with the presence of internals using two-fluid Euler approach continuum transient 3D simulations. Bubble column with five internals configurations and without internals have been simulated and performed at a superficial gas velocity U_g=0.12 m/s. While, the simulation results of the bubble column without internals have been validated with the experimental results that reported by Sanyal et al. [43] using the radioactive particle tracking (RPT), and computerized gamma-ray tomography (CT) to validate the liquid velocity, and the gas holdup, respectively. However, the numerical results revealed that the presence. Subsequently, Guo and Chen [44] investigated the impacts of vertical internals with circular configuration on the hydrodynamics of the bubble column using the Eulerian two fluid model coupled with a population balance model (TFM-PBM), and

applying interfacial forces that including the drag force, lift force, and wall lubrication force. Results of the local gas holdup were validated with the benchmark experimental data of Kagumba and Al-Dahhan [30] where they investigated the effects of internals with different sizes and two configurations (hexagonal and circular) on the bubble dynamics using the advance four-point optical fiber probe. However, the numerical data revealed that the radial wall lubrication force greatly affects the radial distribution of time-averaged gas holdup, especially in the internals affecting region. When the internals were present, the turbulent dissipation rates increased significantly in the gaps between the internal walls, and more bubbles with smaller bubble size were predicted in the bubble column. Meanwhile, the gas holdup increased with dense internals insertion, especially in r/R equal to 0.6–0.9 region. The internals and the configurations influence the overall liquid circulation.

Guan and Yang [45] studied the influence of the interfacial forces, including drag force, lift force, turbulent dispersion force, and wall force on the hydrodynamics in pilot-scale bubble columns with internals, which covers 5% of the cross-sectional area of the bubble column with hexagonal configuration. While, the numerical results of the local gas holdup and the axial liquid velocity were validated experimental data reported by Shang Yu et al. [46]. The CFD results revealed that the lift force, turbulent dispersion force, and wall force are optional interfacial forces in the simulation of the bubble column without internals, in contrasts to simulation case of bubble column with internals where they are significant to predict flow characteristics accurately. Furthermore, despite the insignificant effect on gas holdup, the presence of internals gives rise to an enhancement of large-scale liquid circulation due to the remarkable decrease of turbulent viscosity. Bhusare et al. [26]

performed a numerical simulation for a bubble column with and without internals by using the OpenFOAM CFD tool to study the capability of the OpenFOAM CFD tool to simulate the bubble column and address the effect of the presence of internals on the hydrodynamics of the bubble column. The OpenFOAM CFD tool results have been validated locally regarding gas holdup and axial liquid velocity with the experimental works. However, the results obtained show that the OpenFOAM simulations are in a good agreement with the experimental data. In addition, it is observed that the overall flow pattern in the column remains unaffected with the insertion of the internals in the column. While, with increasing the number of internals the averaged gas hold-up was increased and the axial liquid velocity was decreased, which attributed to reducing the fluctuations in the column with internals as compared to that of the open column.

Recently, Agahzamin and Pakzad [47] investigated the effects of internals with three circular arrangements on the hydrodynamics of the bubble column by utilizing the Eulerian-Eulerian model incorporated with population balance model (PBM) and interfacial forces including the lift force and wall force (applying different models). Validating the interfacial forces and the simulation code was executed by comparing the local gas holdup of the numerical work with the experimental work of Youssef [48]. The results reported that by choosing the appropriate interfacial forces, the simulation model would agree with the experimental data.

In this study, the interfacial forces that embedded the drag, lift, wall lubricated, and turbulent dispersion (using different models) have been validated azimuthally with experimental data obtained by Al Mesfer et al. [1-2], and Sultan et al. [3-4] that conducted in a bubble column with and without internals by using gamma-ray computed tomography

(CT) technique. Meanwhile, the standard $(k-\varepsilon)$ turbulence model and the renormalization group RNG $(k-\varepsilon)$ model have been validated with the experimental data obtained by Al Mesfer et al. [2] performed in the same setup that used by Al Mesfer et al. [1], and Sultan et al. [3-4] utilizing the Radioactive Particle Tracking (RPT) technique. As well, the effects of internals using different configurations and diameters of the tube on the gas holdup profiles have been simulated using 3D CFD simulation. Eulerian-Eulerian approach coupled with population bubble model (PBM) has been utilized for the simulation purposes. Therefore, this work has been accomplished through three steps. First-step; investigate the sensitivity of the numerical solution regarding the grid size effect, the time-collection effect, and the time steady-state effect. Second-step; validation the interfacial forces, and the turbulence models. Third-step; investigate the effects of the presence of internals, the configurations of internals, and the size of the internals rod. The simulation has been accomplished in the same setup that utilized by Al Mesfer et al. [1-2], and Sultan et al. [3-4] using the Eulerian-Eulerian approach coupling with the population balance model (PBM).

1.1. GOVERNING EQUATIONS OF EULERIAN-EULERIAN APPROACH

As mentioned earlier, in this work the Eulerian-Eulerian approach has been used in the numerical simulation. The Eulerian modelling framework is based on ensemble-averaged mass and momentum transport equations governing each phase [49]. The continues phase in the approach is the liquid phase ($q = L$) and the gas phase (bubble) as disperse phase ($q = G$).

Continuity equation; for a flow with equally sized bubbles of diameter d_B, and without mass transfer between the phases, these equations can be written as shown in Eq. (1):

$$\frac{\partial(\rho_q \alpha_q)}{\partial t} + \nabla(\rho_q \alpha_q \boldsymbol{u}_q) = 0 \tag{1}$$

Momentum equation; the momentum conservation for the control volume of multiphase flows is described by the Navier-Stokes as shown in Eq. (2).

$$\begin{aligned} &\frac{\partial}{\partial t}(\alpha_q \rho_q \boldsymbol{u}_q) + \nabla.(\alpha_q \rho_q \boldsymbol{u}_q \boldsymbol{u}_q) \\ &= \underbrace{-\alpha_q \nabla p}_{I} + \underbrace{\nabla.(\alpha_q \tau_q)}_{II} + \underbrace{\alpha_q \rho_q \vec{g}}_{III} + \underbrace{F_{pq}}_{IV} \end{aligned} \tag{2}$$

The terms I, II, III, and IV on the right-hand side of Eq. (2) are the pressure gradient (∇p), the stress tensor (τ_q), the gravitational force ($\vec{g}$) and the interfacial forces (F_{pq}), respectively, which are describe the all forces that acting on the phase q in the control volume. The stress tensor τ_q for q phase as shown in Eq. (3), where μ_{eff} is the effective viscosity. However, $\mu_{eff,L}$ is the effective viscosity for the liquid phase, which is a result of three contributions as given in Eq. (4); $\mu_{L,L}$, $\mu_{T,L}$ and $\mu_{B,L}$ represent the molecular viscosity, the shear induced turbulence viscosity and the bubble induced turbulence, respectively. Sato et al. [50] proposed an exertion for the viscosity due to the turbulence induced by the movement of the bubbles as shown in Eq. (5), where the $C_{\mu,B}$ is a constant model equal to 0.6 as reported in previous studies [51], [52]. The effective gas viscosity $\mu_{eff,G}$ depends on the effective liquid viscosity and can be expressed as given in Eq. (6).

$$\tau_q = \mu_{eff,q}\left(\nabla \boldsymbol{u}_q + (\nabla \boldsymbol{u}_q)^T - \frac{2}{3} I(\nabla. \boldsymbol{u}_q)\right) \tag{3}$$

$$\mu_{eff,L} = \mu_{L,L} + \mu_{T,L} + \mu_{B,L} \tag{4}$$

$$\mu_{B,L} = \rho_L C_{\mu,B} \alpha_G d_B |\boldsymbol{u}_G - \boldsymbol{u}_L| \tag{5}$$

$$\mu_{eff,G} = \frac{\rho_G}{\rho_L} \mu_{eff,L} \tag{6}$$

1.2. TURBULENT CLOSURE MODELS

Although, the two equation models like the $k - \varepsilon$ model suffer from the assumption of isotropic eddy viscosity, they still score over the high-fidelity models like the Reynolds stress model, as they are simple and less computationally demanding. For gas-liquid systems, the mixture $k - \varepsilon$ model [53], [54] proves to be more reliable for a wide range of dispersed phase fraction, when compared to earlier works that considered only the turbulent kinetic energy in the continuous phase. As $k - \varepsilon$ is employed for turbulence modelling, the turbulent eddy viscosity is calculated using the $k - \varepsilon$ turbulence model, where k represents the turbulent kinetic energy and ε its dissipation rate in the liquid phase. k and ε determine the energy in turbulence and the scale of the turbulence, respectively. The turbulent eddy viscosity $\mu_{T,L}$, the turbulent kinetic energy k and the energy dissipation rate ε can be shown by the following equations:

$$\mu_{T,L} = C_\mu \rho_L \frac{k^2}{\varepsilon} \tag{7}$$

$$\frac{\partial(\alpha_L \rho_L k_L)}{\partial t} + \nabla(\alpha_L \rho_L k_L \boldsymbol{u}_L) = \nabla\left(\alpha_L \frac{\mu_{T,L}}{\sigma_k} \nabla k_L\right) + \alpha_L\left(G_{k,L} - \rho_L \varepsilon_L\right) + S_k \tag{8}$$

$$\frac{\partial(\alpha_L \rho_L \varepsilon_L)}{\partial t} + \nabla(\alpha_L \rho_L \varepsilon_L \boldsymbol{u}_L) = \nabla\left(\alpha_L \frac{\mu_{T,L}}{\sigma_\varepsilon} \nabla \varepsilon_L\right) + \alpha_L \frac{\varepsilon_L}{k_L}\left(C_{\varepsilon 1} G_{k,L} - C_{\varepsilon 2} \rho_L \varepsilon_L\right) + S_\varepsilon \tag{9}$$

with standard model constants $C_{\varepsilon 1}$= 1.44, $C_{\varepsilon 2}$= 1.92, C_{μ} = 0.09, σ_k= 1, σ_{ε} = 1.3. The term G in equations (8-9) is the production of turbulent kinetic energy which is described by

$$G = \tau_L = \nabla \boldsymbol{u}_L \tag{10}$$

1.3. INTERFACIAL FORECES (MOMENTUM TRANSFER)

Interfacial forces, which is the momentum transfer between the dispersion phase (bubbles), and the continuing phase (liquid), is essential to the modeling of the gas-liquid flows due to significantly administrating the distribution of gas and liquid phases in the flow volume. The fourth term (F_{pq}) on the RSH of the momentum Eq. (2) represents the interfacial forces, including the drag force (F_{drag}), lift force (F_{lift}), wall lubrication force ($F_{wall\ lub.}$), turbulent dispersion force ($F_{turbulent\ dis.}$), and virtual force ($F_{virtual}$) as shown in Eq. (11) [55].

$$F_{pq} = F_{drag} + F_{lift} + F_{turbulent\ dis.} + F_{wall\ lub.} + F_{virtual} \tag{11}$$

1.3.1. Drag Models. The drag force is the resistance that experienced by a bubble moving within the continuous phase, due to the shear stress and the pressure distribution around the moving bubble surface, thereby, it is the mean reason to deform the bubble shape [55], [56]. Hence, Eq. (12) has been formulated to calculate the drag force, where $\boldsymbol{C_D}$ is the drag coefficient that is a function of bubble's Reynolds number $\boldsymbol{C_D(Re_B)}$, known as the drag curve, can be correlated for individual bubbles for different flow regions based on the $\boldsymbol{Re_B}$ as given in Eq. (13):

$$F_{drag} = \frac{2}{3}\alpha_G \rho_L \frac{C_D}{d_B}(\boldsymbol{u}_G - \boldsymbol{u}_L)|\boldsymbol{u}_G - \boldsymbol{u}_L| \tag{12}$$

$$Re_B = \frac{\rho_L d_B (\boldsymbol{u}_G - \boldsymbol{u}_L)}{\mu_L} \tag{12}$$

In this work, different models formulated to calculate the drag coefficient (C_D) have been applied like Grace et al. [57], Tomiyama [58], Morsi and Alexander [59], and Schiller and Naumann [60].

1.3.1.1. Grace et al. [57] model. Grace et al. [57] model classified the calculation of the drag coefficient based on the shape of a bubble that is related to the flow regime. Therefore, Grace et al. [57] model is properly fit to the gas-liquid system flow through off three drag coefficients $C_{D_{sphere}}$, $C_{D_{cap}}$ and $C_{D_{ellipse}}$, which represent the bubbly, transition, and churn turbulent flow regimes, respectively.

$$C_D = max\left(min\left(C_{D_{ellipse}}, C_{D_{cap}}\right), C_{D_{sphere}}\right) \tag{14}$$

$$C_{D_{sphere}} = \begin{cases} 24/Re_B & Re_B < 0.01 \\ 24(1 + 0.15Re_B^{0.687}) & Re_B \geq 0.01 \end{cases} \tag{15}$$

$$C_{cap} = \frac{8}{3} \tag{16}$$

$$C_{ellipse} = \frac{4}{3}\frac{g d_B}{U_t^2}\frac{(\rho_L - \rho_G)}{\rho_L} \tag{17}$$

where U_t is the terminal velocity of bubble that was correlated as in Eq. (18)

$$U_t = \frac{\mu_L}{\rho_L d_B} M_o^{-0.149}(J - 0.857) \tag{18}$$

where M_o is the Morton number given by Eq. (19), and J is given by piecewise function as in Eq. (20).

$$M_o = \frac{\mu_L^4 g(\rho_L - \rho_G)}{\rho_L^2 \sigma^3} \tag{19}$$

$$J = \begin{cases} 0.94\,H^{0.757} & 2 < H \leq 59.3 \\ 3.42H^{0.441} & H > 59.3 \end{cases} \quad (20)$$

$$H = \frac{3}{4} E_o M_o^{-0.149} \left(\frac{\mu_L}{\mu_{ref}}\right)^{-0.14} \quad (21)$$

where E_o is Eötvös number:

$$E_o = \frac{g(\rho_L - \rho_G) d_B^2}{\sigma}$$

1.3.1.2. Tomiyama [58] model. Tomiyama [58] developed a drag coefficient model, which is considering the fluid properties, as given in Eq. (23), and hence, the degree of contamination of the continuing phase was taken into account.

$$C_D = max\left(min\left(\frac{24}{Re}(1 + 0.15Re^{0.687}), \frac{72}{Re}\right), \frac{8}{3}\frac{E_o}{E_o + 4}\right) \quad (22)$$

1.3.1.3. Morsi-Alexander [59] model. Morsi and Alexander [59] model calculates the drag coefficient C_D by the given Eq. (23), while Re_B is the bubble's Reynolds number as defined by Eq. (13) and the constants a_i are coefficients that calculated based on the Reynolds number, more details in Fluent [61].

$$C_D = a_1 + \frac{a_2}{Re_B} + \frac{a_3}{Re_B^2} \quad (23)$$

1.3.1.4. Schiller and Naumann [60] model. Schiller and Naumann [60] as given in Eq. (24)

$$C_D = \begin{cases} 24(0.15Re_B^{0.687})/Re_B & Re_B \leq 1000 \\ 0.44 & Re_B \geq 1000 \end{cases} \quad (24)$$

1.3.2. Lift Models. The lift force is a lateral force that a bubble experiences and being perpendicular to the direction of bubble's motion a result of the horizontal velocity gradient, thereby, the lift force correlated with the local liquid velocity and the slip velocity as shown in Eq. (25).

$$F_{lift} = C_l \rho_L \alpha_G (\boldsymbol{u}_L - \boldsymbol{u}_G) \times (\nabla \times \boldsymbol{u}_L) \tag{25}$$

According to Bothe et al. [62] and Lucas et al. [63], they suggested that the lift force is sensitive to the bubble size, therefore, small bubble size driven by positive lift forces, whereas, the large bubble size driven by negative lift force with opposite direction, which migrates toward the center region of the bubble column. Meanwhile, Tomiyama [58] quantified and classified the small bubble size and large bubble size by $d_B \leq 5.8\, mm$ and $d_B \geq 5.8\, mm$, respectively. Therefore, the lift force significantly effects on the radial profiles of gas holdup and on the liquid velocity.

1.3.3. Wall lubrication Models. Wall lubrication force is a force that is responsible for pushing the bubbles away from the vicinity of the wall area and generated as a result to the surface tension of bubbles, which in turn reduce the gas holdup in the wall area [64]. However, the general model for the wall lubrication force as given in Eq. (26):

$$F_{wall\ lub} = C_W \rho_L \alpha_G \left|(\boldsymbol{u}_L - \boldsymbol{u}_G)_{\parallel}\right|^2 \vec{\boldsymbol{n}}_W \tag{26}$$

where $\left|(\boldsymbol{u}_L - \boldsymbol{u}_G)_{\parallel}\right|$ is the phase relative velocity component tangential to the wall surface, and $\vec{\boldsymbol{n}}_W$ is the unit normal pointing away from the wall. There are different models to assess the wall lubrication coefficient C_W:

1.3.3.1. Antal et al. [65] model. Antal et al. [65] proposed a model as given in Eq. (27) to compute the wall lubrication coefficient C_W:

$$C_W = max\left(0, \frac{C_{W1}}{d_B} + \frac{C_{W2}}{y_W}\right) \tag{27}$$

where C_{W1}=-0.01and C_{W2}=0.05 are non-dimensional coefficient, $d_B$is the bubble diameter, and y_W is the distance to the nearest wall. Noting, $C_w$has non-zero value only within a thin layer adjacent to the wall that satisfies to $y_W \leq -(C_{W2}/C_{W1})d_B$.

1.3.3.2. Tomiyama [58] model. Tomiyama [58] has modified the wall lubrication coefficient formulated by Antal et al. [65] based on the data obtained of experiments with the flow of air bubbles in glycerin in a pipe. Tomiyama model, as given in Eq. (28), considers to the bubble column diameter and the fluid properties. However, although this model is superior to the Antal's model, it is restricted to flow in column geometries because of the dependence on column diameter D [66].

$$C_W = C_o \frac{d_B}{2}\left(\frac{1}{y_W^2} - \frac{1}{(D - y_W)^2}\right) \tag{28}$$

where D is the column diameter, C_o is a coefficient depends on the Eötvös number E_o as given in Eq. (29):

$$C_o = \begin{cases} 0.47 & E_o < 1 \\ e^{10.933E_o + 0.179} & 1 \leq E_o \leq 5 \\ 0.00599E_o - 0.0187 & 5 < E_o \leq 33 \\ 0.179\ 33 & 33 \leq E_o \end{cases} \tag{29}$$

1.3.3.3. Frank et al. [66] model. Frank et al. [66] proposed a model calculates the wall lubrication coefficient independently from the column diameter, as given in Eq. (30), in contrast, Tomiyama [58] model.

$$C_W = C_o max\left(0, \frac{1}{C_{Wd}} . \frac{1 - y_W/C_{WC}d_B}{y_W(y_W/C_{WC}d_B)^{m-1}}\right) \quad (30)$$

where C_o is determined as in Eq. (29), C_{Wd} is the damping coefficient, by default C_{Wd}=6.8, determines the relative magnitude of the force. While, m is the constant of the power law, m=1.5 and 2, and C_{WC} is the cut-off coefficient and determines the distance to the wall within which the force is active [61].

1.3.4. Turbulent Dispersion Models. Turbulent dispersion force is a turbulent interphase transfer which induces the turbulent diffusion in the dispersed phase (the gas phase in this study), and hence, it is taken as a function of turbulent kinetic energy in the continuous phase (the liquid phase in this study) [55], [64], the general formula as given in Eq. (31):

$$F_{T,L} = -F_{T,G} = -f_{T,limiting} K_{GL} \boldsymbol{u_{dr}} \quad (31)$$

where $F_{T,L}$, and , $F_{T,G}$ are the turbulent dispersion of the liquid phase, and the gas phase, receptively. While, $f_{T,limiting}$ is a factor that can be used to impose a limiting function on the turbulent dispersion force, K_{GL} is the exchange coefficient ($K_{GL} = \rho_G f d_B a_G / 6\tau_G$), and $\boldsymbol{u_{dr}}$ is the drift velocity and accounts for the dispersion of the gas phase due to transport by turbulent fluid motion.

1.3.4.1. Simonin [67] model. Simonin and Viollet [67] formulated a new model to calculate the turbulent dispersion force as given in Eq. (32):

$$F_{T,L} = -F_{T,G} = C_{TD} K_{GL} \frac{\boldsymbol{D}_{T_{GL}}}{\sigma_{GL}} \left(\frac{\nabla \alpha_G}{\alpha_G} - \frac{\nabla \alpha_L}{\alpha_L} \right) \tag{32}$$

where C_{TD}, and σ_{GL} are a user-modifiable constant that are set to 1, and 0.75 by default, respectively, and $\boldsymbol{D}_{T_{GL}}$ is the fluid-particulate dispersion tensor.

1.3.4.2. Burns et al. [68] model. Burns et al. [68] derived a model based on Favre averaging of the drag term. The final expression is similar to Simonin's model. For the Burns et al. [68] model, the dispersion scalar is estimated by the turbulent viscosity of the continuous phase as shown in Eq. (33):

$$\boldsymbol{D}_L = \boldsymbol{D}_G = \boldsymbol{D}_{T_{GL}} = \mu_{TL} / \mu_{TG} \tag{33}$$

and

$$F_{T,L} = -F_{T,G} = C_{TD} K_{GL} \frac{\boldsymbol{D}_L}{\sigma_{GL}} \left(\frac{\nabla \alpha_G}{\alpha_G} - \frac{\nabla \alpha_L}{\alpha_L} \right) \tag{34}$$

Here, C_{TD}=1 and σ_{GL}=0.9 by default.

1.4. POPULATION BALANCE MODEL (PBM)

According to what mentioned, the interfacial forces and the turbulent model are depended in their calculations on the bubble diameter. Hence, an assumption that the bubbles have one diameter, in turn, significantly influences the simulation results of the momentum transfer between two phases, particularly the simulation in the transition and the churn turbulent flow regimes, where the bubbles are existing in a wide spectrum of bubble sizes [10], [30], [69]. Therefore, since the bubble breakup and coalescence exist in bubble columns within the heterogeneous, transition, churn turbulent flow regimes, these

phenomena should be considered in the simulation. The usual approach is to use population balance models, which describe the variation in a given population property over space and time in a velocity field. In bubble column modeling, the application of population balance models is to determine the bubble size distribution over space and time, and how this distribution develops due to the breakup and coalescence processes. The general form of the PBM equation for the gas–liquid bubbly flow can be expressed as follows in Eq. (35):

$$\underbrace{\frac{\partial n(v,t)}{\partial t}}_{I} + \underbrace{\nabla.[U_b n(v,t)]}_{II} = \underbrace{S_i}_{III} \tag{35}$$

where the bracketed terms represent time variation (I), and convection (II), while, term (III) is the sources term of i-th bubble group generated by bubble coalescence and breakup as expressed in Eq. (36)

$$S_{\boldsymbol{B}} = B_{c,i} - D_{c,i} + B_{b,i} - D_{b,i} \tag{36}$$

Here, $B_{c,i}$, $D_{c,i}$, $B_{b,i}$, and $D_{b,i}$ are the source terms of birth due to coalescence, death due to coalescence, birth due to breakage, and death due to breakup, resistively. The population balance equation (PBE) can be solved by different methods, such as the discrete method, the standard method of moments (SMM), the quadrature method of moments (QMOM), etc. The discrete method developed by Ramkrishna [70] is applied in this work. It is based on the continuous particle size distribution with a set of discrete size classes and each class is represented by a pivot size x_i, showing the outstanding characteristics on robust numerics and directly giving the particle size distribution (PSD). Eq. (35) is integrated over each size interval $[v_i, v_{i+1}]$, resulting in Eq. (36):

$$\frac{\partial N_i(t)}{\partial t} + \nabla.[U_b N_i(t)]$$

$$= \frac{1}{2}\int_{v_i}^{v_{i+1}} dv \int_0^v n(v-\acute{v},t)n(\acute{v},t)a(v-\acute{v},\acute{v})\,d\acute{v}$$

$$- \int_{v_i}^{v_{i+1}} n(v,t)\,dv \int_0^{\infty} n(\acute{v},t)a(v,\acute{v})\,d\acute{v}$$

$$+ \int_{v_i}^{v_{i+1}} dv \int_0^{\infty} \beta(v,\acute{v})b(\acute{v})n(\acute{v},t)\,d\acute{v} - \int_{v_i}^{v_{i+1}} b(v)n(v,t)\,dv \quad (37)$$

The population in a representative volume x_i has a fraction of bubbles born in the size range (x_i, x_{i+1}) or (x_{i-1}, x_i). For bubbles born in the size range (x_i, x_{i+1}), bubbles with a percentage of $\lambda_1(v, x_i)$ are assigned to x_i, and for those born in the range (x_{i-1}, x_i), bubbles with a percentage of $\lambda_2(v, x_{i+1})$ are assigned to x_{i+1}. The values of $\lambda_1(v, x_i)$ and $\lambda_2(v, x_i)$ are given by the following equations.

$$\lambda_1(v, x_i)x_i + \lambda_2(v, x_{i+1})x_{i+1} = v \quad (38)$$

$$\lambda_1(v, x_i) + \lambda_2(v, x_{i+1}) = 1 \quad (39)$$

The final discrete PBM after all terms in Eq. (37) are reconstructed is expressed as in Eq. (40):

$$\frac{\partial N_i(t)}{\partial t} + \nabla.[U_b N_i(t)]$$

$$= \sum_{g_{i-1} \le (g_j + g_k) \le g_{i+1}}^{j \ge k} \left(1 - \frac{1}{2}\delta_{j,k}\right)\omega_{i,jk}N_j(t)N_k(t)$$

$$- N_i(t)\sum_{k=1}^{M} a_{j,k}N_k(t) + \sum_{k=i}^{M} \psi_{i,k}b(g_k)N_k(t)$$

$$- b(g_i)N_i(t) \quad (40)$$

$$\omega_{i,jk} = \begin{cases} (x_{i+1} - v)/(x_{i+1} - x_i), & x_i < v \leq x_{i+1} \\ (v - x_{i-1})/(x_i - x_{i-1}), & x_{i-1} < v \leq x_i \end{cases} \tag{41}$$

$$\psi_{i,k} = \int_{x_i}^{x_{i+1}} \frac{x_{i+1} - v}{x_{i+1} - x_i} \beta(v, x_k) dv + \int_{x_{i-1}}^{x_i} \frac{v - x_{i-1}}{x_i - x_{i-1}} \beta(v, x_k) dv \tag{42}$$

Here, the breakup rate $b(v)$ proposed by Luo and Svendsen [71] and the aggregation rate $a_{i,j}$ of Luo [72] are used, respectively. The formulas are described briefly as follows:

$$b(v) = 0.9238\big(1 - \alpha_g\big)^n \left(\frac{\varepsilon}{d^2}\right)^{1/3} \int_{\xi_{min}}^{1} \frac{(1+\xi)^2}{\xi^{11/3}} exp\big\{-12\big[f^{2/3} + (1-f)^{1/3} - 1\big]\sigma\rho^{-1}\varepsilon^{-2/3}d^{-5/3}\xi^{-11/3}\big\} d\xi \tag{43}$$

$$a_{i,j} = \frac{1.43\pi}{4}\big(d_i^2 + d_j^2\big)\big(d_i^{3/2} + d_j^{3/2}\big)^{1/2}\, \varepsilon\, exp\big(-t_{drainage}/t_{contact}\big) \tag{44}$$

where f is the volume fraction of one daughter bubble, and ξ is the ratio of eddy size to parent bubble. The bubbles with different sizes are classified into 10 groups for simulation at churn turbulent flow regime, and 4 groups for the bubbly flow regime.

2. NUMERICAL DETAILS

The numerical solutions have been accomplished using the commercial computational fluid dynamics code FLUENT (Ansys-15). Pressure-outlet boundary condition is used for the outlet surface of the bubble column (with and without internals). While the velocity condition has been applied for the inlet surface of the bubble column

with gas volume fraction equal to 1 due to that the liquid phase in the bubble column operated in batch mode. Along the walls, including the bubble column wall and the outside surface of internals, the no-slip boundary conditions are adapted. Worth to mention, the bubble column simulations during high gas velocities (U_g= 0.2 and 0.45 m/s) encounters serious numerical problem represented in that the dynamic liquid level was spilled out from the bubble column due to the large gas volume fraction gradient in the dynamic liquid level, where the same phenomenon was observed by Liang et al. [73]. Thereby, used-defined function (UDF) was implemented to increase the superficial gas velocity slowly and linearly with time of the simulation in the inlet surface to avoid the gas volume fraction increases rapidly, and this (UDF) is a function for the time, when the superficial gas velocity reaches the needed velocity (0.2 or 0.45 m/s), this (UDF) will be inactive. The SIMPLE scheme has been used to solve pressure-velocity coupling, while, second upwind scheme is used for the momentum, volume fraction. However, type of grid that used for the bubble column with and without internals is hexahedral grid throughout the bubble column with internals, whereas, the grid of the bubble column without internals was generated by a commercial grid-generation tool, ICEM (Ansys-15) as shown in Figure 1. The numbers of the final grid numbers for the bubble with and without internals are 694,930 and 430,331 cells, respectively. Furthermore, due to the simulation has been conducted using the Eulerian-Eulerian approach, demarcating the magnitude of the time step is essential to prevent encounter some stability or convergence problems in the numerical solution. Therefore, the Courant-Friederichs-Levy (CFL) condition, as given in Eq. (45), was applied to calculate the time step

$$C = \frac{u_y \, \Delta t}{\Delta y} \leq 0.125 \quad (45)$$

where C, u_y, Δy, and Δt are Courant number, superficial gas velocity in a y-axial direction (m/s), cell size in a y-axial direction (m), and time step (s), respectively, and hence, the time step was varied according to superficial gas velocity. However, in this study, the time step of 0.001 (s) has been used for all CFD simulations.

3. EXPERIMENTAL SETUP AND VALIDATION METHOD

The bubble column with and without internals that simulated in this work is 1.83 m in height and 0.14 m in inner diameter. While, three types of internals have been used to simulated the internals effect; type (b) is internals of hexagonal arrangement, type (c) is circular arrangement of 0.5-ich tube diameter, and type (d) is internals of circular arrangement of 1-ich tube diameter as illustrated in Figure 1(b, c, and d), respectively, more details about the bubble column and the internals arrangements were explained in Sultan et al. [3], [4], and Al Mesfer et al. [1].

However, the superficial gas velocity calculated based on the free cross-sectional area (CSA) for flow column was varied from 0.05 to 0.45 m/s, therefore, the initial liquid level was adapted with time of simulation t=0.0 (s) to maintain the dynamic liquid level at desired height. Al Mesfer et al. [1] investigated the impact of the internals on the gas holdup profiles using the CT technique. The gas holdup measurements were conducted at level *L/D*=5.2, the scan cross-sectional was divided into 80×80 pixels, therefore, the gas holdup profiles exhibited using two methods local profile (line A-A and B-B as shown in Figure

2), and lines averaged of the horizontal pixels and the vertical pixels (the green lines in Figure).

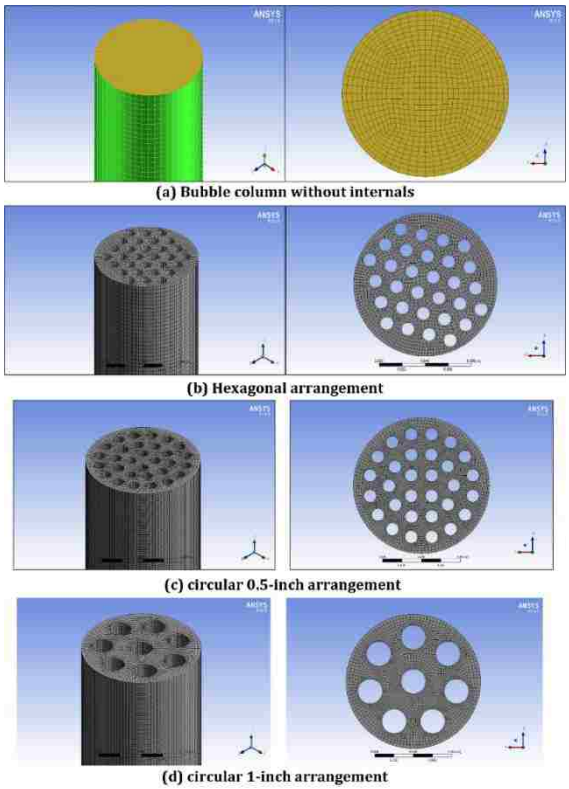

Figure 1. Grid setup used in CFD simulation (a) bubble column without internals (b) bubble column with internals of hexagonal arrangement (c) bubble column with internals of circular 1-inch arrangement (d) bubble column with internals circular 1-inch arrangement

According to Al Mesfer et al. [1], results of these different methods of the gas holdup distribution exhibited a significant difference in the gas holdup profiles for the same operation condition. Thereby, Sultan et al. [3], [4], [74] suggested that demonstrating the time-averaged cross-sectional gas holdup distribution azimuthally would provide quantifiable and easy to understand the results. Furthermore, to determine the azimuthally

averaged profiles, a method was developed to divide the reconstructed image (80×80 pixels) in half (left and right; 40×40 pixels) and then averaged them separately not to smooth it out and to achieve a more precise representation of the results. Therefore, simulation data obtained in this study have been collected using the same method of azimuthally, which in turn would conduct the validation precisely.

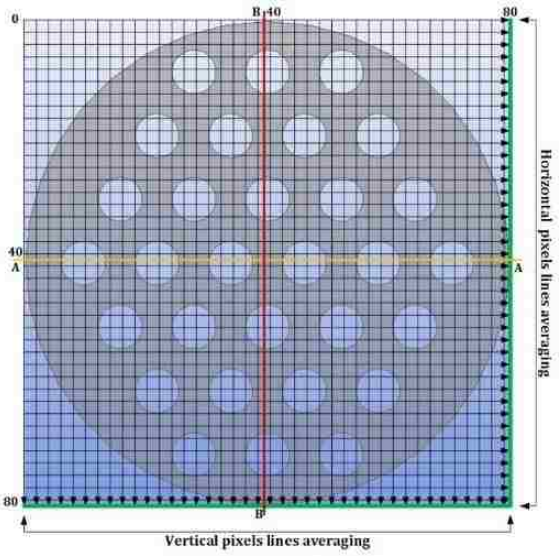

Figure 2. Imposing the bubble column with internals on 80×80 pixels used for image reconstruction (for clarity it is plotted 40×40 pixels where each pixel contains two pixels). The horizontal line (A–A) and vertical line (B–B) are for presenting of local gas. Figure adapted from [1]

4. RESULTS AND DISCUSSION

4.1. NUMERICAL SIMULATION SENSITIVITY

The grid size is a critical factor in solving the governing equations of CFD simulation. A well orthogonal of grid will reflect to influence on the numerical solution in

regards to the instability and lack of convergence [55]. Therefore, testing five different sizes of grid that their specifications are listed in Table 1, have been accomplished as first step. Figure 3 illustrates the effect of grid size on the time-averaged cross-sectional of gas holdup distribution was obtained in *L/D* = 5.2. The variation in the time-averaged cross-sectional gas holdup affected by the grid size was demarcated by calculating the average absolute relative difference (AARD) comparing to the experimental results as given in Eq. (13);

$$AARD = \frac{1}{N}\sum_{N}^{i=1}\left|\frac{\epsilon_{i,experiment} - \epsilon_{i,grid}}{\epsilon_{i,experiment}}\right| \quad (13)$$

Thereby, the variations in the AARD between the experiment data of Al Mesfer et al. [1] and the five sizes of grids type A, B, C, D and E are 30.2, 19.5, 20.3, and 19.9 and 20.1. Accordingly, the average absolute relative difference (AARD) between grid types (B to E) are insignificant, therefore, type B has been utilized in whole the simulations of validation and internals effect study.

Table 1. The grid size specifications

Type	Dimensions	Type	No. of cells
A	$\Delta y = 0.01$	Sweep /O-grid	47223
B	$\Delta y = 0.0067$	Sweep /O-grid	167300
C	$\Delta y = 0.005$	Sweep /O-grid	430331
D	$\Delta y = 0.004$	Sweep /O-grid	880992
E	$\Delta y = 0.0033$	Sweep /O-grid	1569683

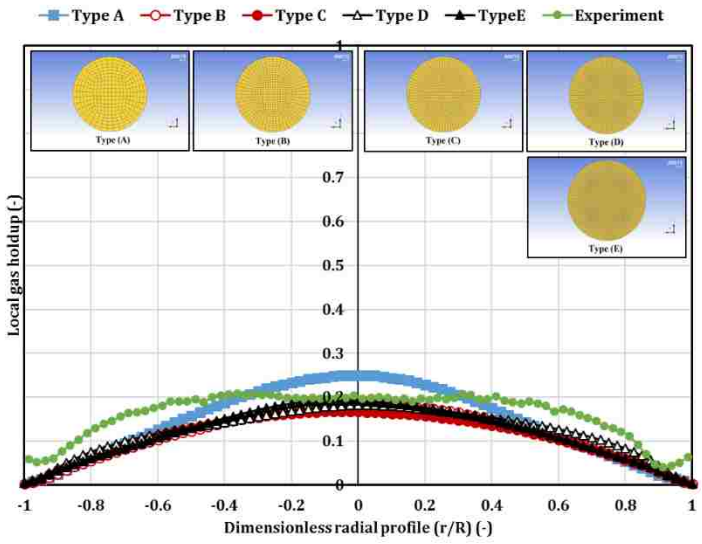

Figure 3. The effect of the grid size on the azimuthally gas holdup profile, U_g=0.05 m/s

As long the numerical simulation for the multiphase flow in the bubble column have utilized the Eulerian-Eulerian approach, solving the governing equations in time-dependent is essential to avoid the instability and the divergence. Consequently, demarcating the steady-state or the pseudo-steady state condition of the system is important to start the time-averaged solution. Figure 4 illustrates the area weighted averaged of the local gas holdup in the central region and *L/D* = 5.2 as a function of the time. As shown in Figure 4, the time-averaged of the local gas holdup no longer varies with time significantly after 30, 60 and 100 (s) for superficial gas velocity 0.05, 0.2 and 0.45 m/s, respectively. The difference in the time needed to reach the steady-state for each superficial gas velocity used attributed to the using the (UDF) in the high superficial gas velocity (0.2 and 0.45 m/s), and hence, the numerical solution keeps unsteady till the (UDF) reaches the needed superficial gas velocity value. Therefore, it can be concluded that after initial transition of

about 30, 60 and 100 (s) for superficial gas velocity 0.05, 0.2 and 0.45 m/s, respectively, the pseudo-steady state condition has been established.

The flow in bubble column is classified as chaotic system [13], [75], [76]. Hence, the numerical results, were extracted after 30, 60 and 100 (s) for superficial gas velocity 0.05, 0.2 and 0.45 m/s, respectively, after the start of the simulation, have been exhibited in the time-averaged sense. Accordingly, in this study, the period of time that needed to collect data in time-averaged sense has been defined as duration-time-averaged. The effect of duration-time-averaged on the time-averaged gas holdup distribution is worth to consider. Figure 5 shows the time-averaged cross-sectional gas holdup distribution for different duration-time-averaged for the simulation of bubble column without internals at U_g=0.2 m/s. The variation in the duration-time-averaged exhibits slightly effect on the time-averaged gas holdup distribution, where the (AARD) varied in a rang (1.02-2.9), which is attributed to avoiding the unsteady-state time zone. However, in this work the duration-time averaged of 60 (s) has been used.

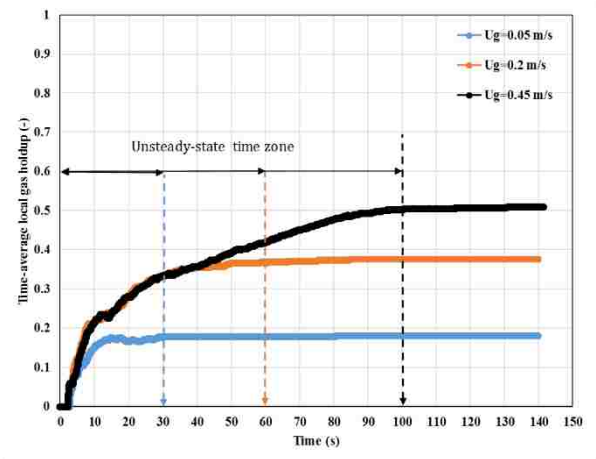

Figure 4. The variation of area weighted averages of local gas holdup with time in bubble column without internals

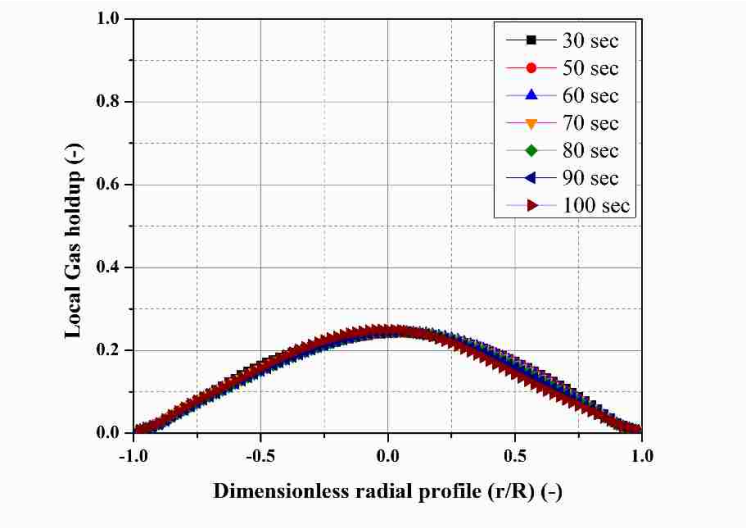

Figure 5. The effect of time collection on the time-averaged cross-sectional gas holdup distribution, Ug=0.2 m/s

4.2. VALIDATION THE INTERFACIAL FORCES AND THE POPULATION BUBBLE MODEL PBM

The gas holdup distribution is a key parameter in the bubble column reactors, where the radial variation in the gas holdup leads to the liquid circulation, which results in demonstrating the mixing rate and the heat and mass transfer [16], [73], [77]. Thereby, gas holdup has been used to validate the simulation results of this study.

4.2.1. Drag Force. The drag force, among all the interfacial forces, is dominant the predicting of the hydrodynamics in the bubble column [78], [79], and if validated properly the entire interfacial forces would be validated correctly. The effect of different models of drag force on the time-averaged gas holdup distribution comparing with experimental results of Al Mesfer et al. [1] under the condition of superficial gas velocity U_g=0.08 m/s has been illustrated in Figure 6 and Figure 7. The simulation results in Figure

6 show that the time-averaged of gas holdup profile for all different models exhibits a semi-flat distribution, which attributed to that the drag force is the only interfacial force that used in Figure 6, particularly, in the wall region (r/R= 0.66-1). Therefore, the simulation results, by using the (AARD), has been validated based on avoiding the wall region, and hence, the (AARD) for the models Morsi-Alexander, Schiller-Naumann, Grace, and Tomiyama with the experimental results are 30.4, 28.2, 20.8, and 18, respectively. Accordingly, the Grace and Tomiyama models, present the closest profile to the experiment results, have been established for the next validation. Furthermore, the CFD scan images for the time-averaged cross-sectional gas holdup distribution in *H*/D = 5.2 that illustrated in Figure 7 depicts significant different flow pattern in the bubble column for each drag models comparing with the experimental results, therefore, applying only the drag force was not adequate to simulating the hydrodynamics in the bubble column, particularly, in the wall region.

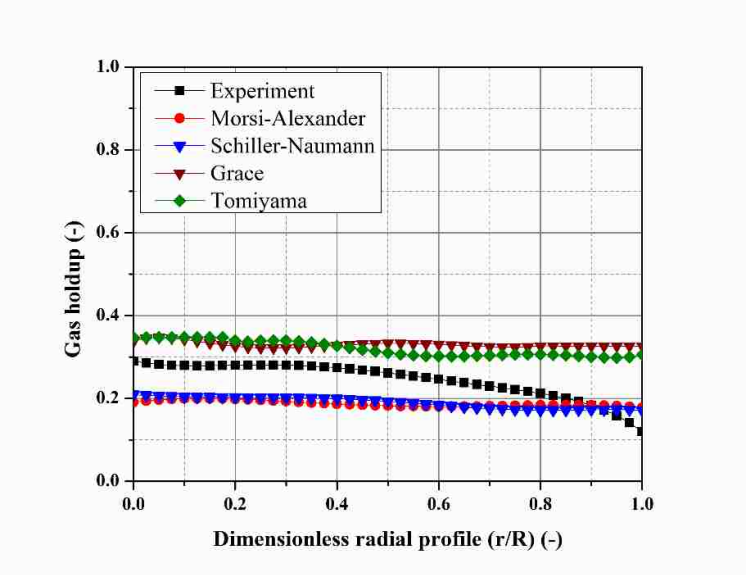

Figure 6. Drag forces effect on the simulation results of bubble column without internals

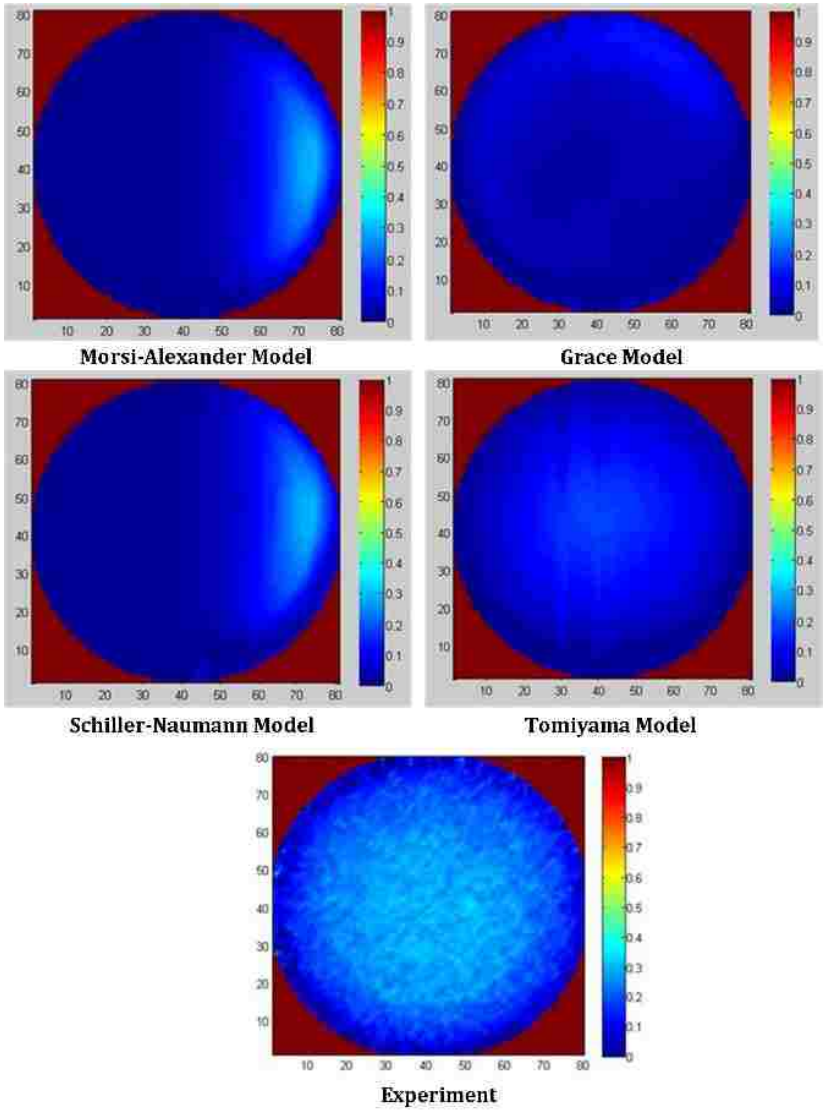

Figure 7. The CFD simulation scan images obtained for cross-sectional time averaged of gas holdup, bubble column without internals, Ug=0.08 m/s

4.2.2. Wall Lubrication. In this part, the drag force, Grace and Tomiyama models, was combined with the wall lubrication force to validate the wall force that performed using three models. The three models are Antal et al. [65], Tomiyama [58] and Frank et al. [66] with default set value of that coefficients that given in equations (27-30). The simulation results with all wall lubrication models investigated are shown in Figure 8

to illustrate the effect of wall lubrication force on the time-averaged gas holdup for different models. As can be seen from Figure 8 the effect of the wall lubrication with different models is significant both in the enhancing the drag force performance and the prediction of the wall region. Although, the prediction of this region was not satisfying due to using constant bubble size $\boldsymbol{d_B}$= 5 mm. The validating of wall lubrication models was by (AARD) for Grace/Antal et al. [65], Grace/Tomiyama [58], Grace/Frank et al. [66], Tomiyama/Antal et al. [65], Tomiyama/Tomiyama [58] and Tomiyama/Frank et al. [66] models are 17. 29.6, 35,3, 42.2, 39.1, and 37.3, respectively. Therefore, drag force of Grace model and wall lubrication of Antal et al. [65] proved a better validation in terms of (AARD), and hence, these models have been applied in current study.

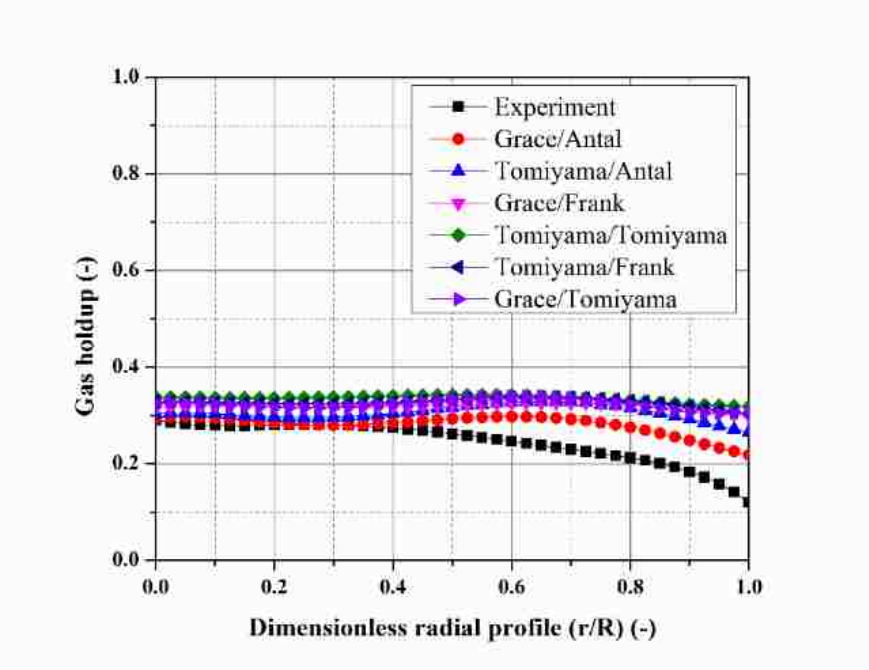

Figure 8. Wall Lubrication forces on the simulation results of bubble column without internals

4.2.3. Turbulent Dispersion. Two turbulent dispersion force models described in equations (32 and 34) were compared with the experimental results. The two models have been tested with default coefficients. The effect of the different models of the turbulent dispersion force is illustrated in Figure 9. The simulation results of Simonin and Viollet [67] is in good agreement with the experimental data comparing with Burns et al. [68] model, which appears an underestimated prediction. While, close to the wall region a significant difference between Simonin Viollet [67] model. However, the simulation trends, applied Simonin and Viollet [67] and Burns et al. [68] models with their default coefficients value, the time-averaged gas holdup profile in the wall region of the bubble column is still less than the experimental results, which could be attributed to absent of the effect of lift force.

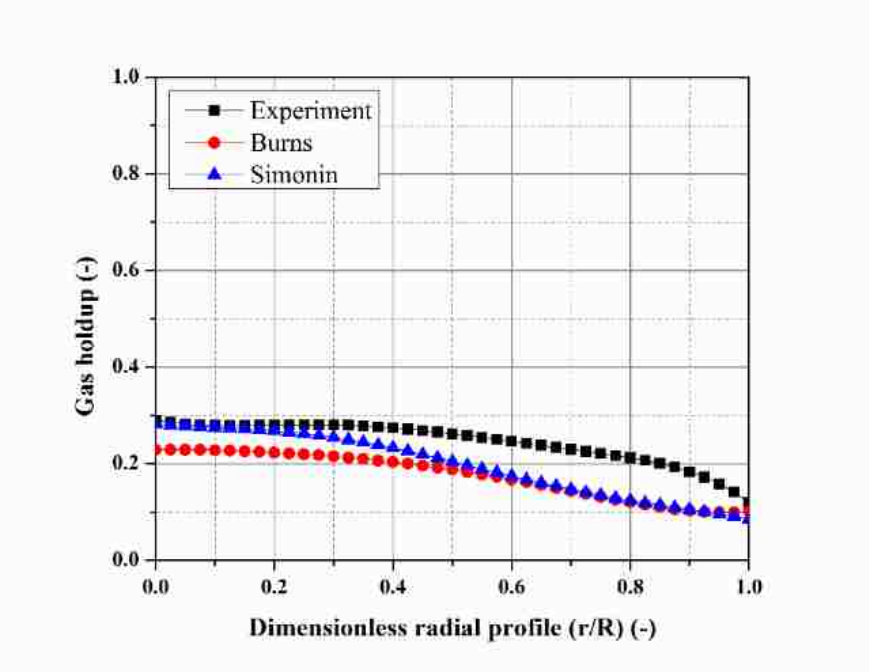

Figure 9. Turbulent Dispersion forces on the simulation results of bubble column without internals

4.2.4. Lift Force. Tabib et al. [80] concluded during analyzing the interfacial forces and turbulent models in 3D simulation bubble column that the positive value of lift force coefficient C_l would makes the bubbles concentrate towards the wall region of bubble column (i.e., leads to a flatter gas holdup profile), therefore, the magnitude of the coefficient will depend on the bubble size. Tabib et al. [80] reported that C_l=-0.2 gives a good agreement with the experimental results. In this work the experimental results that used show the gas holdup in a parabolic profile (i.e., high gas holdup in the central region of the bubble column, and hence, C_l= -0.2 has been used in this study. Figure 10 illustrates the effect of the lift force on the simulation results of the time-averaged gas holdup profile. However, the trends in Figure 10 show that using a constant lift force coefficient improves the simulation results with diversion (AARD = 17%), although, it is underestimate the experimental results, particularly, the wall region. Since lateral lift force presents the migration of bubbles towards the bubble column center or wall regions based on the bubbles size, it becomes the administrating force to control the gas holdup distribution [81]. Thereby, as long assuming one bubble size in the simulation, the prediction results is hard to converge with the experimental results.

4.2.5. Population Bubble Model (BPM). As shown in validating interfacial forces, the performance of these forces is governed by the bubbles size. The flow in the bubble column is complex as a result to the interaction between the phases and the momentum transferring cross the gas-liquid interface surface, which is controlled by the bubble size. Therefore, using the population bubble model PBM to predict the bubble size will improve the numerical solution in capturing the hydrodynamics of the bubble column, especially, in the turbulent flow regime, where the bubbles prevail in wide range sizes.

In this study, Luo-Luo models have been used for the coalescence rate and the break-up rate, respectively. Figure 11 illustrates the effect of using the population bubble model PBM on the simulation results of the time-averaged gas holdup distribution.

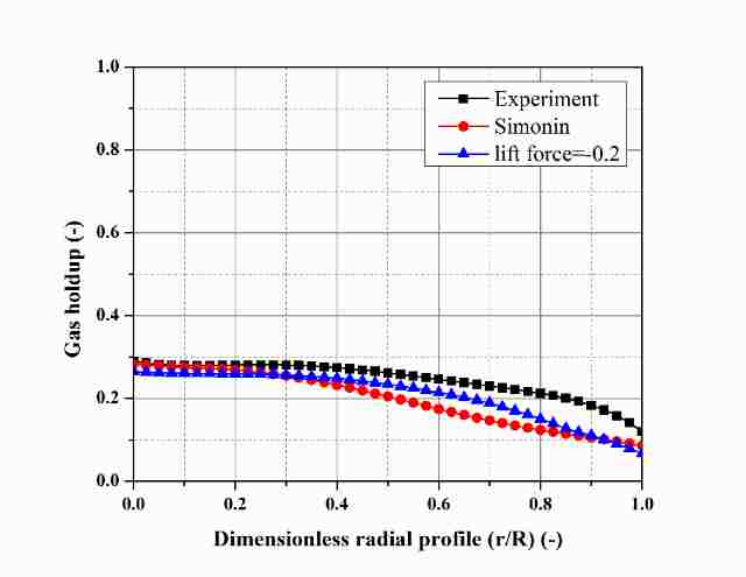

Figure 10. Lift force effect on the simulation results of bubble column without internals

The simulation results appear a good agreement comparing with the experimental data with a percentage of averaged absolute relative difference about (AARD = 5.8%), which reflect the capability of the PBM improve the simulation in terms to increase the matching between the simulation results from the experimental data. Chen et al. [82] implemented the bubble population balance equation (BPBE) using two numbers of bubble groups (9 and 16 classes) to simulate the bubble column in two and three dimensions operated over a range of superficial gas velocity (U_g=0.08 to 0.2 m/s). Their results revealed that the incorporation of the BPBE is critical to capture the gas holdup profile faithfully, and using nine groups of bubble size are sufficient. Recently, Kagumba and Al-Dahhan [30] measured the bubble properties in experimental setup of a bubble column with

and without internals, which is the same that used in this simulation study. Accordingly, data obtained by Kagumba and Al-Dahhan [30] in regards to the bubble size has been utilized in this study to optimizing the numbers of the bubble groups.

Five numbers of bubble groups (5, 10, 15, 20, and 25), listed in Table 2, have been used to solve the population bubble model PBM. The simulation results of the effect different numbers of bubble groups on the time-averaged gas holdup are illustrated in Figure 12. Data obtained show that the variation in the numbers of bubble groups significantly effect on the simulation results with a percentage of averaged absolute relative difference with the experimental results about (AARD = 39.45%, 33.62%, 37.1%, 16.8%, and 16.6%) for the used bubble groups 5, 10, 15, 20, and 25, respectively, accordingly, it seems there is no significant variation in the numerical solution between the group number 20 and 25. Therefore, the group number 20 has been applied for the simulation operated in superficial gas velocity U_g=0.2 and 0.45 m/s (churn turbulent flow regime), whereas, bubble group number 10 has been used for the simulation under operating condition of superficial gas velocity U_g= 0.05 m/s (bubbly flow regime).

4.3. TURBULENT MODEL VALIDATION

Two models of turbulent kinetic, which are stander ($k-\varepsilon$) and RNG ($k-\varepsilon$), have been investigated Figure 13 and validated with the experimental results of al Mesfer et al. [2] to predict the liquid velocity. The simulation results of two models are illustrated in Figure 13. As shown, RNG ($k-\varepsilon$) model exhibits a good matching to the experimental results for the liquid velocity with diversion (AARD = 17.6%), in particular, in the central and the wall regions of the bubble column and the reflecting point that is located at r/R

~0.69, whereas, stander $(k-\varepsilon)$ model lost the prediction in these regions. The renormalization group (RNG) model represents the effect of the small-scale turbulence by means of a random forcing function in the momentum equation, and hence, renormalization group (RNG) model procedure systematically removes scales of motion from the governing equations by expressing their effects in terms of larger scale motions and a modified viscosity.

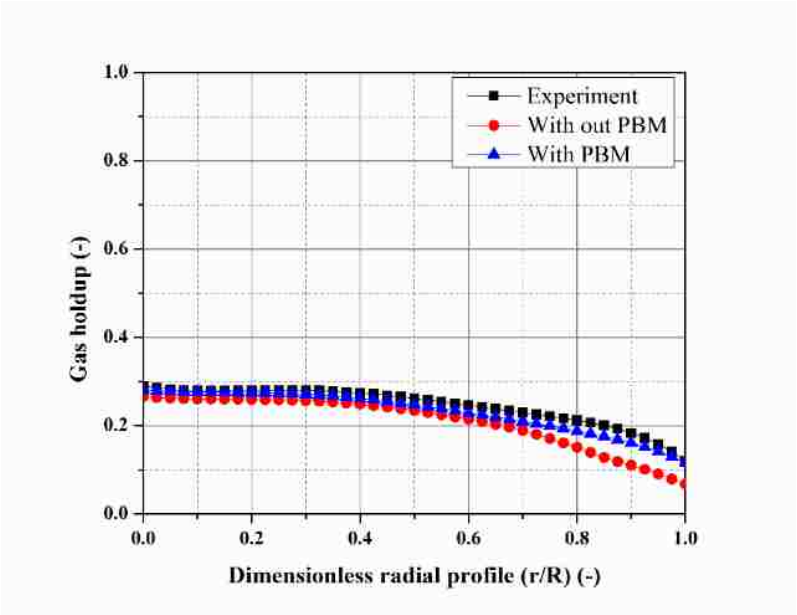

Figure 11. Population Bubble Model (PBM) effect on the simulation results of bubble column without internals

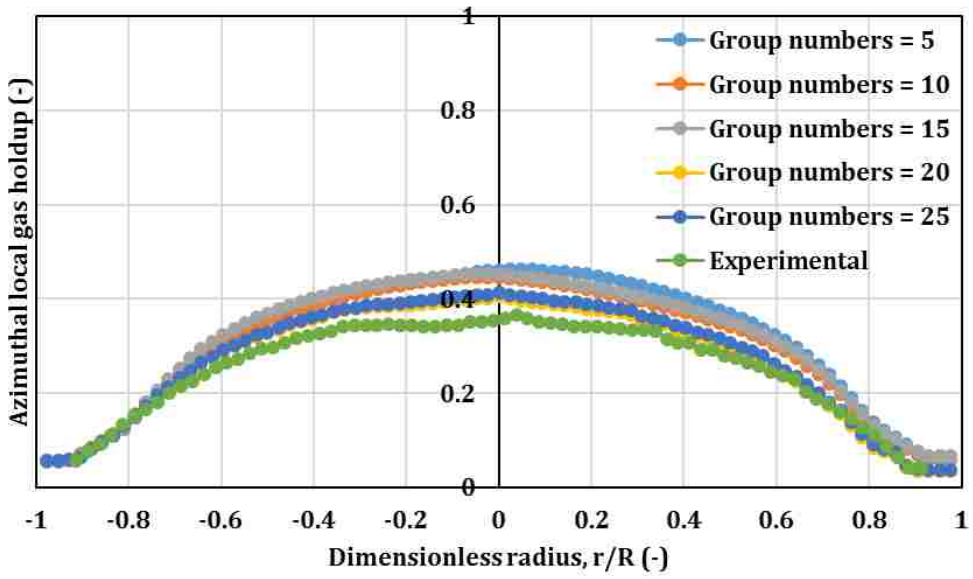

Figure 12. The effect of the group numbers of bubbles on the simulation results of gas holdup in bubble column without internals, Ug=0.2 m/s

Table 2. Bubble groups numbers

5 groups															
Classes index	**1**	**2**	**3**	**4**	**5**										
d_B **mm**	**1.3**	**2.6**	**5.1**	**10.2**	**20.2**										
10 groups															
Classes index	**1**	**2**	**3**	**4**	**5**	**6**	**7**	**8**	**9**	**10**					
d_B **mm**	**1.3**	**1.76**	**2.4**	**3.3**	**4.4**	**5.97**	**8.1**	**11**	**14.9**	**20.2**					
15 groups															
Classes index	**1**	**2**	**3**	**4**	**5**	**6**	**7**	**8**	**9**	**10**	**11**	**12**	**13**	**14**	**15**
d_B **mm**	**1.3**	**1.6**	**1.9**	**2.3**	**2.9**	**3.5**	**4.2**	**5.2**	**6.3**	**7.6**	**9.3**	**11.3**	**13.7**	**16.7**	**20.3**
25 groups															
Classes index	**1**	**2**	**3**	**4**	**5**	**6**	**7**	**8**	**9**	**10**	**11**	**12**	**13**	**14**	**15**
d_B **mm**	**1.3**	**1.5**	**1.74**	**2**	**2.3**	**2.67**	**3.1**	**3.57**	**4.13**	**4.8**	**5.5**	**6.36**	**7.35**	**8.5**	**9.81**
Classes index	**16**	**17**	**18**	**19**	**20**										
d_B **mm**	**11.3**	**13.1**	**15.1**	**17.5**	**20.2**										
25 groups															
Classes index	**1**	**2**	**3**	**4**	**5**	**6**	**7**	**8**	**9**	**10**	**11**	**12**	**13**	**14**	**15**
d_B **mm**	**1.3**	**1.46**	**1.64**	**1.84**	**2.06**	**2.3**	**2.6**	**2.92**	**3.3**	**3.67**	**4.13**	**4.6**	**5.2**	**5.83**	**6.55**
Classes index	**16**	**17**	**18**	**19**	**20**	**21**	**22**	**23**	**24**	**25**					
d_B **mm**	**7.35**	**8.3**	**9.26**	**10.4**	**11.7**	**13.1**	**14.7**	**16.5**	**18.5**	**20.8**					

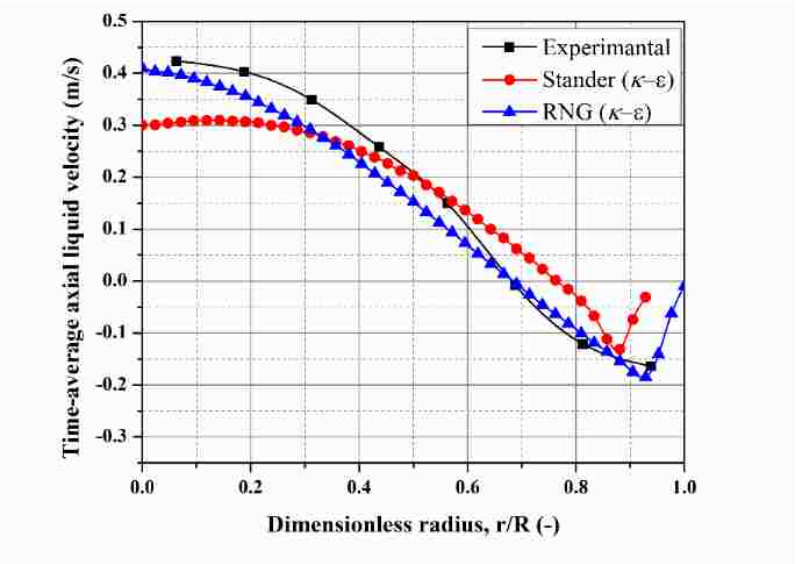

Figure 13. The effect of turbulent kinetic energy models on the time-averaged axial liquid velocity (m/s) validated with the experimental results

While, the stander ($k-\varepsilon$) model uses the small eddies in defining the large eddies scale, which in turn, reduces the efficiency of this model at high Reynolds numbers (i.e., high superficial gas velocity) [51], [83], and hence, stander ($k-\varepsilon$) model is restricted in flow without internals geometric inside the simulated field. Accordingly, using the RNG ($k-\varepsilon$) model is critical as long the current work aims to study the effect of internals at churn turbulent flow regime.

4.4. THE EFFECT OF SUPERFIFICAL GAS VELOCITY ON THE VALIDATION OF SIMULATION RESULTS

Figure 14(a-c) and Figure 15(a-c) illustrate the simulation results of the time-averaged gas holdup distribution validated azimuthally with the experimental results that reported by Sultan et al. [4] in bubble column without internals and bubble column with internals, respectively. The validation results in bubble column without internals show that

the percentage of averaged absolute relative difference (AARD) between the time-averaged gas holdup distributions of the simulation and experimental results in gas velocities of 0.05, 0.2 and 0.45 m/s are about 14.6%, 16.8% and 16.2%, respectively. While, in the case of bubble column with internals the absolute relative difference (AARD) between the time-averaged gas holdup distributions of the simulation and experimental results in gas velocities of 0.05, 0.2 and 0.45 m/s are about 29.5%, 24.8% and 15.9%, respectively. However, the good agreement between the simulation results and the experimental data confirms the capability of the used validated CFD closures in predict the hydrodynamics of bubble column in the bubbly flow and the churn turbulent flow regimes, which attributed to two reasons; first, coupling the Eulerian-Eulerian approach with the population bubble model (PBM); second, the group numbers that used have covered the all the bubbles sizes that measured in the experiment.

4.5. THE EFFECT OF SUPERFICIAL GAS VELOCITY ON THE TIME-AVERAGED GAS HOLDUP DISTRIBUTION

The simulation results for the effect of the superficial gas velocity on the time-averaged gas holdup distribution in bubble column without internals is illustrated in Figure 16. As shown, as the superficial gas velocity increases, the magnitude value of the time-averaged gas holdup increases along the radial position. However, the gas holdup magnitude value at the central region of the bubble column is about 0.2 at 0.05 m/s and with increasing the superficial gas velocity from 0.05 m/s to 0.2 m/s, and 0.45 m/s, the gas holdup increases by 51%, and 63%, respectively.

It is worth noting that the simulation at low superficial gas velocity U_g=0.05 m/s in the bubbly flow regime, the simulation results of the gas holdup at the region close to the

wall is larger than that obtained at higher velocities. However, data obtained qualitatively agree with the results reported by Kagumba and Al-Dahhan [30], Kumar [84], Rados et al. [85], and Nedeltchev and Shaikh [86]. Figure 16 clearly exhibits that the time-averaged gas holdup has smooth profile with parabolic shape and the maximum magnitude value has been obtained in the central region of the bubble column and progressively decreased towards the walls. This phenomenon can be attributed to that gas bubbles tend to accumulate at the core of the column where there is less shear stress than near the walls, which leads to gross liquid circulation throughout the column, with liquid flowing up in the center and down near the walls [87].

Meanwhile, the effect of superficial gas velocity, based on free cross section area (CSA) for flow column, on the time-averaged gas holdup distribution in the bubble column with the presence of internals has been illustrated in Figure 17. The gas holdup magnitude value at the central region of the bubble column is about 0.19 at 0.05 m/s and with increasing the superficial gas velocity from 0.05 m/s to 0.2 m/s, and 0.45 m/s, the gas holdup increases by 66%, and 78%, respectively, while, the magnitude value of the gas holdup in the wall region exhibits insignificantly affected by the increase the superficial gas velocity.

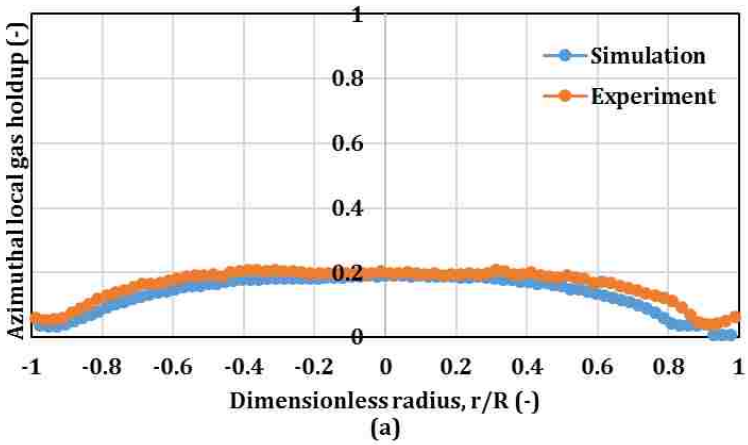

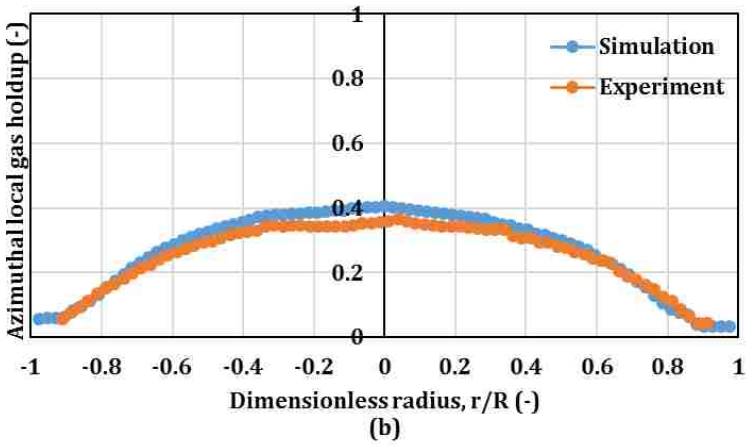

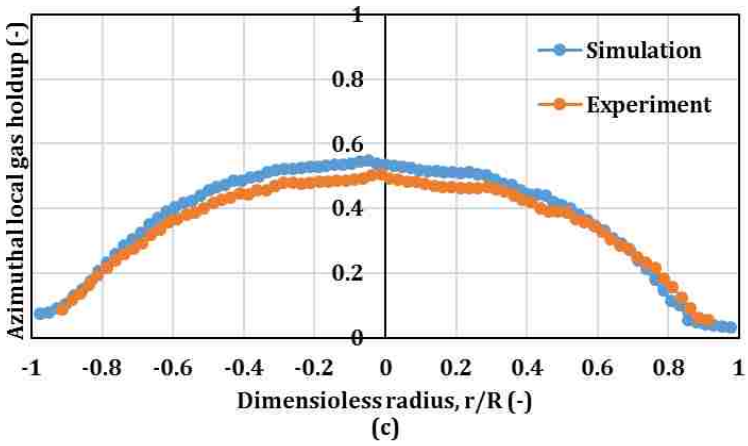

Figure 14. Validating the CFD simulation results azimuthally in bubble column without internals (a) Ug=0.05 m/s, (b) Ug=0.2 m/s, (C) Ug=0.45 m/s

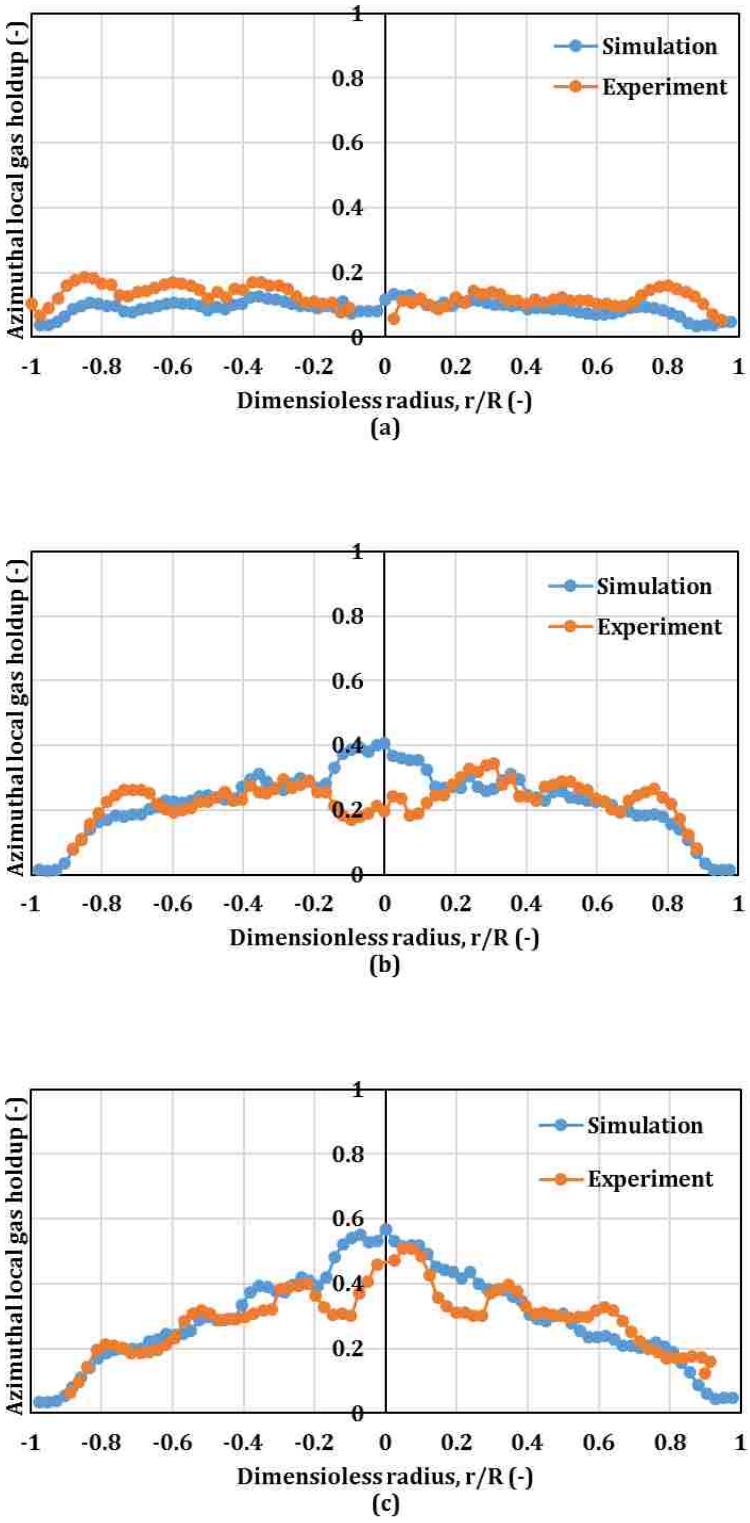

Figure 15. Validating the CFD simulation results azimuthally in bubble column with internals (a) Ug=0.05 m/s, (b) Ug=0.2 m/s, (C) Ug=0.45 m/s

4.6. THE EFFECT OF THE PRESENCE OF INTERNALS ON THE TIME-AVERAGED GAS HOLDUP DISTRIBUTION

Figure 18 illustrates the effect of the presence of internals with hexagonal configuration on the time-averaged gas holdup distributions in various gas velocities U_g=0.05 m/s, and U_g=0.2 m/s, which calculated based on the free (CSA) for flow column, corresponding to the bubbly flow and the churn turbulent flow regimes, respectively.

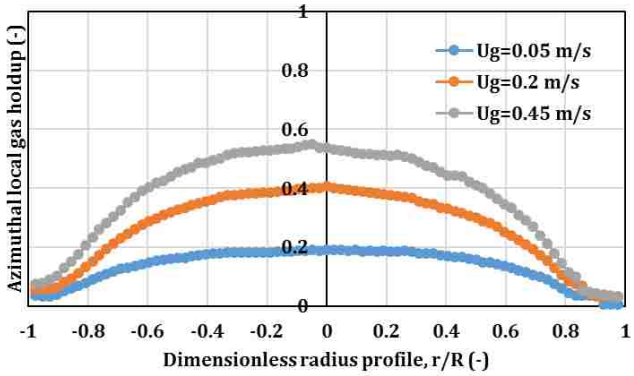

Figure 16. The effect of superficial gas velocity on the time-averaged gas holdup distribution in bubble column without internals

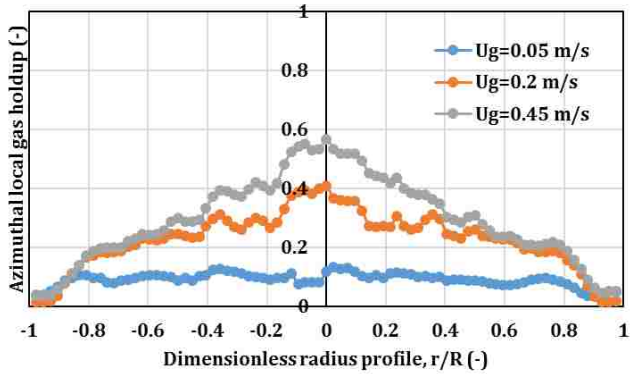

Figure 17. The effect of superficial gas velocity on the time-averaged gas holdup distribution in bubble column with internals

As shown, the gas holdup profiles in the bubble column with internals a slightly effected by the presence of internals, which is attributed to that the gas velocities have been calculated based on the free cross-section (CSA) for flow column that in turn subtracts the mass flow rate of the gas-phase, which occupies the total cross-section area of the internals tubes. This finding agrees with the results reported by Al Mesfer et al. [1], Kagumba and Al-Dahhan [30], and Sultan et al. [3].

Furthermore, as shown in Figure 18 that the presence of internals significantly alters the gas holdup profiles from a parabolic shape and smooth curve, in case of bubble column without internals, to wavy line profiles in bubble column with the presence of internals. This phenomenon could be attributed to occupying the cross-section of bubble column by the internals, and hence, the bubbles distribution along the cross-section of the bubble column will be controlled by the internals tube. Therefore, the different curvatures in the gas holdup profiles have been related to the numbers of internals tubes, the gaps between the tubes, and the size of the internals tubes.

It is worth noting that in Figure 17 and Figure 18, as the superficial gas velocity increases, the gas holdup profiles be steeper and the most of the gas fraction concentrates in the central region of the bubble column, while, there is no change in the wall region. The enhancement in the gas holdup in the central region could be attributed to that bubbles in the absent of internals move towards the low shear stress region (i.e., in the center of bubble column and away from the wall of the bubble column), and hence, the large bubbles sizes accumulate in the central region of the bubble column. While, in the presence of internals the bubbles movement is controlled via the internals due to the hindrance that offer by the tubes against the bubble movement. Figure 19(a-f) depicts the CFD scan images for the

time-averaged cross-section gas holdup distributions in bubble column with and without internals at different boundary conditions (i.e., at superficial gas velocity U_g=0.05, 0.2, and 0.45 m/s). However, the variations in the color indicate to the alteration in the magnitude value of the time-averaged local gas holdup. In Figure 19 clearly illustrates that the variation in the gas holdup distribution over the cross-section of the bubble column is significantly controlled by the presence of internals and the superficial gas velocity. The same phenomenon has been reported by Al Mesfer et al. [1], Sultan et al. [4], Agahzamin and Pakzad [47].

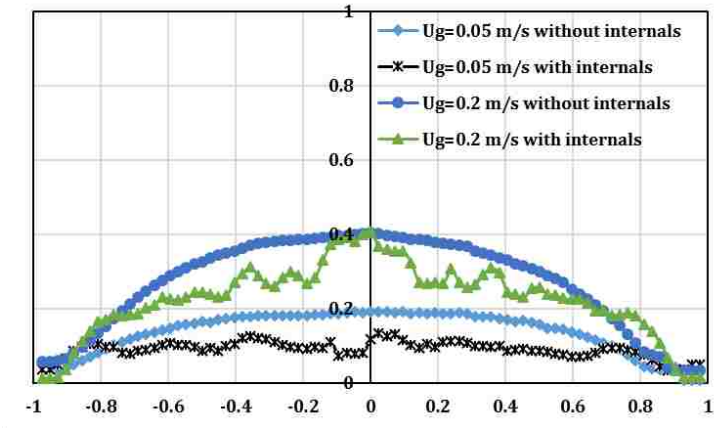

Figure 18. The effect of the presence of internals on the time-averaged gas holdup distribution in Ug=0.05 m/s and Ug=0.2 m/s

4.7. THE EFFECT OF THE INTERNALS CONFIGURATION AND THE INTERNALS SIZE ON TIME-AVERAGED GAS HOLDUP DISTRIBUTION

The effect of the internals configuration on the time-averaged gas holdup profiles has been conducted numerically under operation condition of superficial gas velocity U_g= 0.2 m/s, therefor, two arrangements of hexagonal and circular for this purpose were used,

which are occupying the same cross-section area (CSA) of column and the same internals tube size 0.5-inch. The simulation results of the bubble column equipped with circular configuration validated with the experiment results are illustrated in Figure 20. Data obtained show that the simulation results exhibit a good agreement with the experimental data with a percentage of averaged absolute relative difference about (AARD = 20.4%).

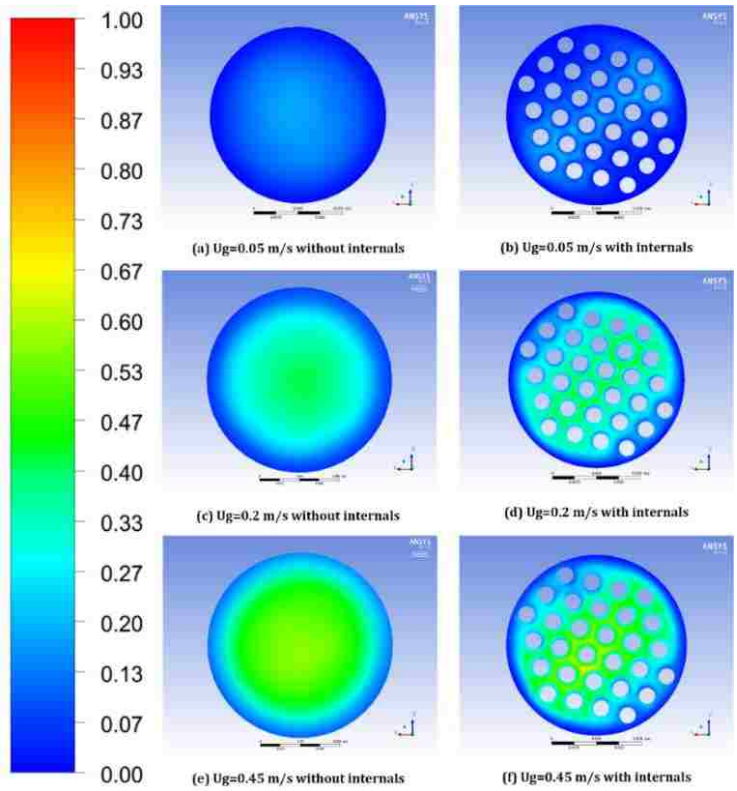

Figure 19. CFD scan images of time-averaged cross-section gas holdup distributions at different gas velocities based on the free (CSA) of bubble column with and without internals

Figure 21 illustrates the effect of different configurations (i.e., hexagonal and circular) on the time-averaged gas holdup distributions. As shown, the bubble column with the hexagonal and circular configurations of tubes exhibit a uniform gas holdup profile

with a remarkable increase in the magnitude value of the gas holdup, close to the wall region (dimensionless radius, r/R=0.8), an about 57% and 63% at employed the hexagonal and circular configurations, respectively. Figure 21 further reveals that using internals with hexagonal configuration shows a higher magnitude value of gas holdup comparing with the circular configuration in the central region of bubble column (i.e., dimensionless radius, r/R = 0.2 to r/R = -0.2), while, less gas holdup in the wall region comparing to the circular configuration. According to that, internals of circular arrangement exhibits a semi-flat gas holdup profile, while, the hexagonal arrangement provides high gas holdup. This findings are agree with results were reported by Sultan et al. [4]. However, the changing in the configuration of internals would significantly impacts on the gas holdup profiles.

The effect of the variation in the internals tube size on the time-averaged gas holdup distributions has been conducted numerically under operation condition of superficial gas velocity U_g= 0.2 m/s, therefore, for this purpose using two bubble columns have been equipped with internals of circular configuration 0.5-inch and circular configuration 1-inch. The simulation results was validated with experimental results that reported by Sultan et al. [3] as illustrated in Figure 22. The results of validation exhibit a good agreement with the experimental data with a percentage of averaged absolute relative difference about (AARD = 18.4%). However, Figure 23 illustrates the effect of the internals tube size on the time-averaged gas holdup at operation condition of superficial gas velocity U_g= 0.2 m/s. As shown in Figure 23, the bubble column with 1-inch internals provides a higher gas holdup than the bubble column with 0.5-inch internals at region between r/R = 0.15-0.4 and the region between r/R = 0.6-0.8.

In addition, the bubble column without vertical internal tubes exhibited a gas holdup profile for all studied superficial gas velocities shaped as a smooth parabola. The parabolic gas holdup profile of the bubble column without vertical internals, which was obtained in the current study and reported in the literature Rados et al. [88], Shaikh and Al-Dahhan [89] under the churn turbulent flow regime also followed a similar profile (i.e., parabolic shape), which is typical of coarse gas distributor (i.e., holes diameter greater than 1 mm) [90]. However, the bubble columns equipped with dense vertical internal tubes displayed wavy-shaped profiles along with a parabolic trend for all investigated configurations with vertical internals. These wavy profiles for the bubble columns with vertical internal tubes varied according to the configurations of the vertical internals in the bubble column. This variation in the gas holdup profiles among the bubble columns with vertical internals was due to the different arrangements of tubes over the CSA of the column, the shape of the pitch for each configuration, and the space (clearance) between the bundle of vertical internals and the column wall. Each concave area of these profiles represents the azimuthal average of the values of the gas holdup in the spaces among the vertical internal tubes. These kinds of wavy gas holdup profiles have not been reported in the literature for a bubble column with dense vertical internals when measured by optical probes. In the literature, parabolic profiles were only obtained in the columns with vertical internals, which were similar to those achieved in the bubble column without vertical internal tubes. However, wavy profiles were reported by [1] when they measured the gas holdup in the bubble column with dense vertical internals using the CT technique.

Figure 24 (a-d) illustrate the 2D images of the CFD scan for the time-averaged cross-section gas holdup in bubble column without internals and in bubble column

equipped with a different configuration of internals (hexagonal and circular) and different internals tubes diameters (0.5-inch and 1-inch). As can be seen, that in the bubble column without internals the higher magnitude value of gas holdup is in the core of the bubble column, while, the lower gas holdup is in the wall region of the column. This phenomenon still obtains in the presence of internals in different configurations and in different internals tubes diameters as shown in Figure 24(b, c, and d). Further, a similar observation was indicated in Figure 19 in terms various superficial gas velocities, where the magnitude of the gas holdup increased with increases in the superficial gas velocities in bubble columns with and without internals. However, this phenomenon agrees with the results that have been reported by Sultan et al. [3]. Based on their visualization that explains this phenomenon by that the common core-annulus (ascending of liquid in the center and liquid descending on wall region) liquid circulation very similar to the one obtained in the bubble column without internals.

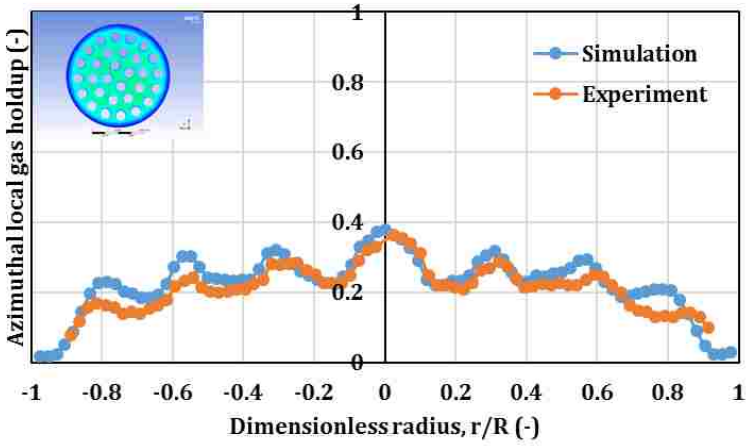

Figure 20. The validation of simulation results of bubble column equipped by internals with circular configuration of 0.5-inch tube size

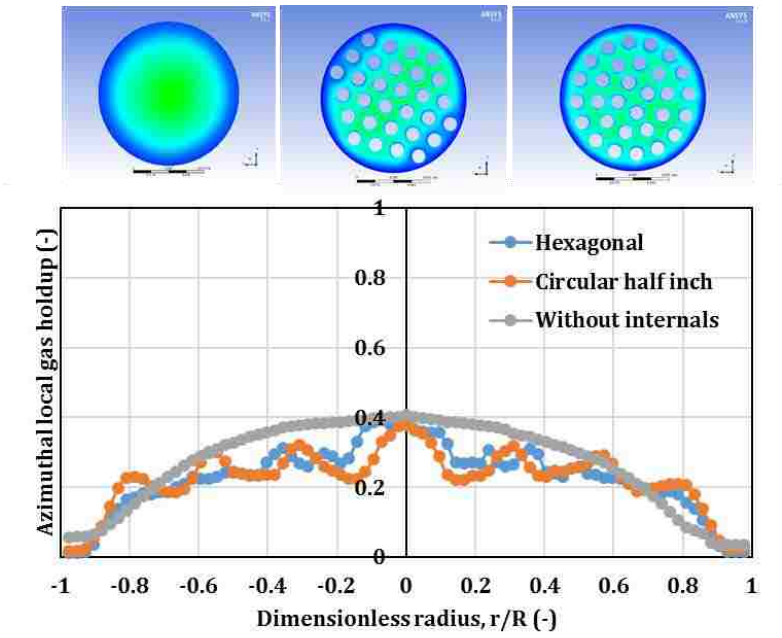

Figure 21. The effect of the internals configuration on the time-averaged gas holdup distribution, U_g=0.2 m/s

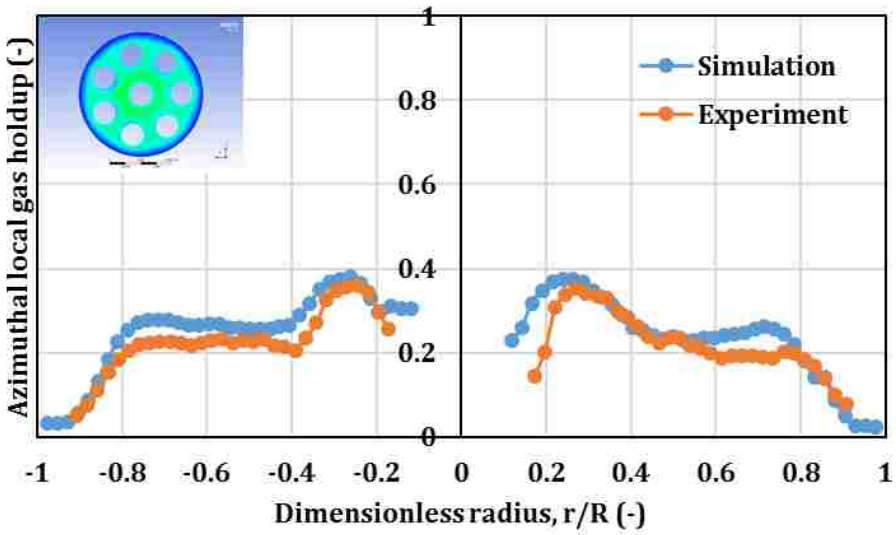

Figure 22. The validation of simulation results of bubble column equipped by internals with circular configuration of 1-inch tube size

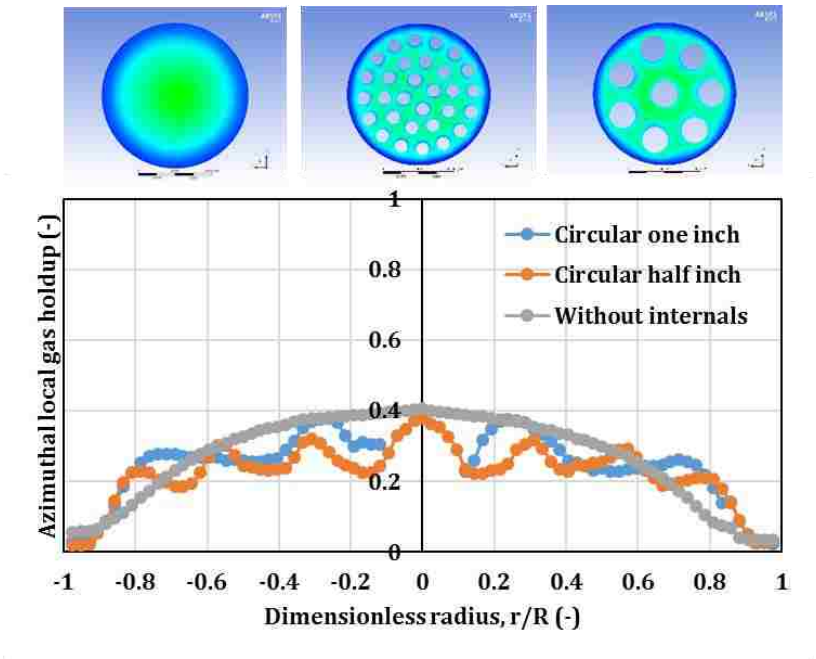

Figure 23. The effect of the internals tube size on the time-averaged gas holdup distribution, U_g=0.2 m/s

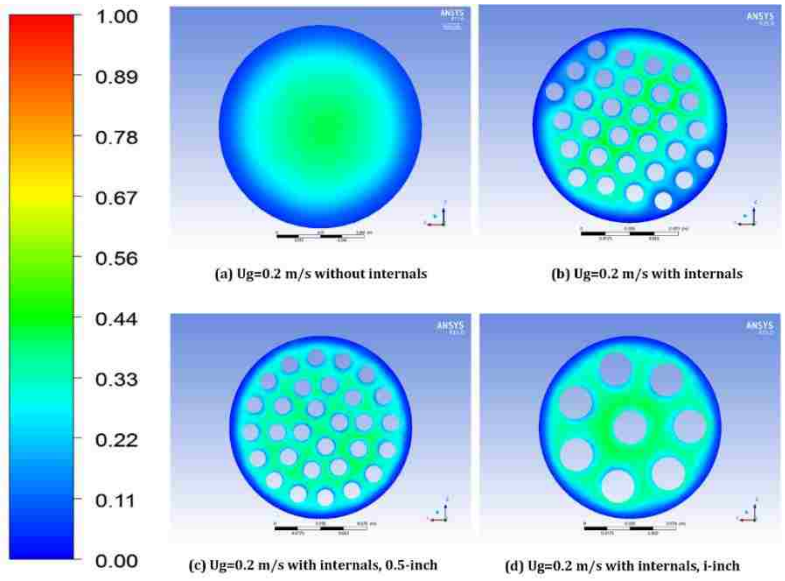

Figure 24. The CFD scan images of the effect of internals configurations and internals tube diameter on the gas holdup on the time-averaged cross-section gas holdup distributions

5. REMARKS

3D time-dependent simulations of two-phase bubble columns using commercial CFD code have been accomplished to validate the turbulent models, including RNG ($k-\varepsilon$) and stander ($k-\varepsilon$), and the interfacial forces, including drag force, lift force, wall lubrication force, and turbulent dispersion force. Furthermore, addressing the effect of the presence of internals, the configurations of internals (hexagonal and circular arrangements), and the internals tube diameters on the time-averaged gas holdup distributions. Accordingly, the current simulation results reveal the following remarks:

The validation results indicated that inability of using the drag force as a singular interfacial force to predict the hydrodynamics of the bubble column. While, applying the combine of interfacial forces of the drag, lift, wall lubricating, and turbulent dispersion properly would significantly improve the simulation results in terms to the profile and the magnitude value of the gas hold.

Interfacial forces models including the drag force, the wall lubrication force, and the turbulent dispersion force that proposed by Grace et al. [57], Antal et al. [65], and Simonin and Viollet [67], respectively, exhibit better prediction results, in terms of the average absolute relative difference (AARD = 17%), for the time-averaged of the gas holdup distributions. Meanwhile, the prediction of liquid velocity using turbulent model of RNG ($k-\varepsilon$) shows a good agreement with the experimantal results about (AARD = 17.6%), in particular, in the central and the wall regions of the bubble column and the reflecting point that is located at r/R ~0.69, whereas, stander ($k-\varepsilon$) model lost the prediction in these regions.

Incorporation the population balance model PBM, in turn, improves the performance of the numerical solution in wide range of the used superficial gas velocity (the bubbly flow and the churn turbulent flow regimes). However, the simulation results of the time-averaged of the gas holdup distributions, operated at turbulent flow regime U_g= 0.2 m/s, illustrate high sensitivity toward the variation in the numbers of bubble groups, further reveal, that the used classes of bubbles with twenty groups illustrate a good agreement for the simulation results with the experimental results about (AARD=16.8%).

Validated CFD closures (i.e., interfacial forces and the turbulent model) exhibit the capability to predict the hydrodynamics of the bubble column that estimated based on comparison with the experimental results by the average absolute relative difference (AARD). In case of the bubble column without internals the average absolute relative difference are AARD= 14.6%, 16.8%, and 16.2% for gas velocities U_g= 0.05, 0.2 and 0.45 m/s, respectively. While, in the case of bubble column with internals the average absolute relative difference are AARD = 29.5%, 24.8% and 15.9% for gas velocities U_g= 0.05, 0.2 and 0.45 m/s, respectively. Furthermore, the numerical solution appears the capability to capture the effect of the variation in the internals design that including different configurations and different internals tubes diameters on the gas holdup profiles. Hence, expecting that the numerical solution will provide the opportunity to understanding the transport phenomena in bubble column that operated in severe operating conditions (high temperature and pressure), in terms to the low cost of experiment and the flexibility in designing.

In the bubble column with and without internals, the magnitude value of the time-averaged gas holdup was increased significantly with increase the superficial gas velocity,

particularly, in the central region of the column. Furthermore, the simulation results, obtained in low superficial gas velocity U_g= 0.05 m/s, appear that the gas holdup profiles over the cross-section of the bubble column with and without internals have semi-flat shape. As the superficial gas velocity increases, the gas holdup profiles being steeper (i.e., increase the difference in magnitude value of the gas holdup between the central region and the wall region). This phenomenon leads to fact that the increase in the superficial gas velocity will promote the liquid circulation in the bubble column.

The 2D images of the CFD scan for the time-averaged cross-section gas holdup in the bubble column without internals and bubble column equipped with the all used designed internals reveal that the core-annular liquid circulation pattern, which commonly prevalent in the bubble column without internals still exist in bubble column internals.

The simulation results exhibit no significant effect for the presence of internals (the all used designed internals) on the time-averaged gas holdup distributions in the central region of the bubble column, whereas, the presence of internals significantly increases the gas holdup closed to the wall region of the bubble column.

At a high superficial gas velocity, the time-averaged gas holdup distributions over the cross-section of the bubble column without internals appears in smooth-line parabolic. Whereas, in the present of internals (at the all used designed internals) the gas holdup distributions exhibit in wavy line uniform profiles. Therefore, the different curvatures in the gas holdup profiles have been related to the numbers of internals tubes, the gaps between the tubes, and the size of the internals tubes

The results of the effect of internals diameter exhibit that the gas holdup was remarkably increased in the center and the wall regions of the bubble column equipped by

internals of 1-inch diameter more than the other used designed internals. Meanwhile, the effect of internals configurations reported that the internals with hexagonal arrangement increases the gas holdup in the center region more than the circular arrangement (of 0.5-inch), and less in the wall region comparing with the circular arrangement. Accordingly, the time-averaged gas holdup distributions exhibit significant altered in terms the profiles and the magnitude towards the variation in the internals configuration and internals tubes diameters.

REFERENCES

[1] M. K. Al Mesfer, A. J. Sultan, and M. H. Al-Dahhan, "Impacts of dense heat exchanging internals on gas holdup cross-sectional distributions and profiles of bubble column using gamma ray Computed Tomography (CT) for FT synthesis," *Chem. Eng. J.*, vol. 300, pp. 317–333, 2016.

[2] M. K. Al Mesfer, A. J. Sultan, and M. H. Al-Dahhan, "Study the Effect of Dense Internals on the Liquid Velocity Field and Turbulent Parameters in Bubble Column for Fischer–Tropsch (FT) Synthesis by Using Radioactive Particle Tracking (RPT) Technique," *Chem. Eng. Sci.*, vol. 161, pp. 228–248, 2017.

[3] A. J. Sultan, L. S. Sabri, and M. H. Al-Dahhan, "Influence of the size of heat exchanging internals on the gas holdup distribution in a bubble column using gamma-ray computed tomography," *Chem. Eng. Sci.*, vol. 186, pp. 1–25, 2018.

[4] A. J. Sultan, L. S. Sabri, and M. H. Al-Dahhan, "Impact of heat-exchanging tube configurations on the gas holdup distribution in bubble columns using gamma-ray computed tomography," *Int. J. Multiph. Flow*, vol. 106, pp. 202–219, 2018.

[5] C. Wu and M. Al-Dahhan, "Heat Transfer Coefficients in Mimicked Fischer-Tropsch Slurry Bubble Columns," *Ind. Eng. Chem. Res.*, vol. 51, no. 4, pp. 1543–1548, 2012.

[6] S. Barghi, A. Prakash, A. Margaritis, and M. A. Bergougnou, "Flow Regime Identification in a Slurry Bubble Column from Gas Holdup and Pressure Fluctuations Analysis," *Can. J. Chem. Eng.*, vol. 82, no. October, pp. 865–870, 2004.

[7] R. Rzehak, M. Krauß, P. Kováts, and K. Zähringer, “Fluid dynamics in a bubble column: New experiments and simulations,” *Int. J. Multiph. Flow*, vol. 89, pp. 299–312, 2017.

[8] S. Rabha, M. Schubert, and U. Hampel, “Intrinsic flow behavior in a slurry bubble column: A study on the effect of particle size,” *Chem. Eng. Sci.*, vol. 93, pp. 401–411, 2013.

[9] S. Sasaki, K. Uchida, K. Hayashi, and A. Tomiyama, “Effects of column diameter and liquid height on gas holdup in air-water bubble columns,” *Exp. Therm. Fluid Sci.*, vol. 72, pp. 67–74, 2017.

[10] H. Al-Naseri, J. P. Schlegel, and M. H. Al-Dahhan, “The Effects of Internals and Low Aspect Ratio on The Flow Development and Bubble Dynamics in Pilot-Plant Bubble Column for Fischer-Tropsch synthesis,” *Exp. Therm. Fluid Sci.*, vol. submitted, 2018.

[11] G. Yang, K. Guo, and T. Wang, “Numerical simulation of the bubble column at elevated pressure with a CFD-PBM coupled model,” *Chem. Eng. Sci.*, vol. 170, pp. 251–262, Oct. 2017.

[12] O. M. Basha, L. Weng, Z. Men, and B. I. Morsi, “CFD Modeling with Experimental Validation of the Internal Hydrodynamics in a Pilot-Scale Slurry Bubble Column Reactor,” *Int. J. Chem. React. Eng.*, vol. 14(2), no. 2, pp. 599–619, 2016.

[13] H. Al-Naseri, J. P. Schlegel, and M. H. Al-Dahhan, “The Impact of Low Aspect Ratio on Flow Regime Transition in Industrial-Sized Pilot Plant Bubble Column Reactor,” *Chem. Eng. J.*, vol. submitted, 2018.

[14] A. H. Syed, M. Boulet, T. Melchiori, and J. M. Lavoie, “CFD simulation of a slurry bubble column: Effect of population balance kernels,” *Comput. Fluids*, vol. 175, pp. 167–179, 2018.

[15] A. A. Youssef, M. E. Hamed, J. T. Grimes, M. H. Al-Dahhan, and M. P. Duduković, “Hydrodynamics of pilot-scale bubble columns: Effect of internals,” *Ind. Eng. Chem. Res.*, vol. 52, no. 1, pp. 43–55, 2013.

[16] A. A. Youssef and M. H. Al-Dahhan, “Impact of internals on the gas holdup and bubble properties of a bubble column,” *Ind. Eng. Chem. Res.*, vol. 48, no. 17, pp. 8007–8013, 2009.

[17] L. Gemello, C. Plais, F. Augier, A. Cloupet, and D. L. Marchisio, “Hydrodynamics and bubble size in bubble columns: Effects of contaminants and spargers,” *Chem. Eng. Sci.*, vol. 184, pp. 93–102, 2018.

[18] B. N. N. Thorat *et al.*, "EFFECT OF SPARGER DESIGN AND HEIGHT TO DIAMETER RATIO ON FRACTIONAL GAS HOLD-UP," *Trans. IChmE*, vol. 76, no. October, pp. 823–834, 1998.

[19] Y. K. Doshi and A. B. Pandit, "Effect of internals and sparger design on mixing behavior in sectionalized bubble column," *Chem. Eng. J.*, vol. 112, no. 1–3, pp. 117–129, 2005.

[20] C. Wu, M. H. Al-Dahhan, and A. Prakash, "Heat transfer coefficients in a high-pressure bubble column," *Chem. Eng. Sci.*, vol. 62, no. 1–2, 2007.

[21] X. Guan, Z. Li, L. Wang, Y. Cheng, and X. Li, "CFD simulation of bubble dynamics in bubble columns with internals," *Ind. Eng. Chem. Res.*, vol. 53, no. 42, pp. 16529–16538, 2014.

[22] A. K. Das, P. K. Das, and J. R. Thome, "Transition of Bubbly Flow in Vertical Tubes: New Criteria Through CFD Simulation," *J. Fluids Eng.*, vol. 131, no. 9, p. 091304, 2009.

[23] J. M. van Baten and R. Krishna, "CFD Simulations of a Bubble Column Operating in the Homogeneous and Heterogeneous Flow Regimes," *Chem. Eng. Technol.*, vol. 25, no. 11, pp. 1081–1086, 2002.

[24] A. A. Troshko and F. Zdravistch, "CFD modeling of slurry bubble column reactors for Fisher-Tropsch synthesis," *Chem. Eng. Sci.*, vol. 64, no. 5, pp. 892–903, 2009.

[25] L. Gemello, V. Cappello, F. Augier, D. Marchisio, and C. Plais, "CFD-based scale-up of hydrodynamics and mixing in bubble columns," *Chem. Eng. Res. Des.*, vol. 136, no. 69, pp. 846–858, 2018.

[26] V. H. Bhusare *et al.*, "CFD simulations of a bubble column with and without internals by using OpenFOAM," *Chem. Eng. J.*, vol. 317, pp. 157–174, 2017.

[27] M. T. Dhotre, K. Ekambara, and J. B. Joshi, "CFD simulation of sparger design and height to diameter ratio on gas hold-up profiles in bubble column reactors," *Exp. Therm. Fluid Sci.*, vol. 28, no. 5, pp. 407–421, 2004.

[28] K. Ekambara, M. T. Dhotre, and J. B. Joshi, "CFD simulations of bubble column reactors : 1D , 2D and 3D approach," *Chem. Eng. Sci.*, vol. 60, no. 23, pp. 6733–6746, 2005.

[29] M. An, X. Guan, N. Yang, Y. Bu, M. Xu, and Z. Men, "Effects of internals on fluid dynamics and reactions in pilot-scale slurry bubble column reactors: A CFD study for Fischer-Tropsch synthesis," *Chem. Eng. Process. - Process Intensif.*, vol. 132, no. August, pp. 194–207, 2018.

[30] M. Kagumba and M. H. Al-Dahhan, “Impact of internals size and configuration on bubble dynamics in bubble columns for alternative clean fuels production,” *Ind. Eng. Chem. Res.*, vol. 54, no. 4, pp. 1359–1372, 2015.

[31] A. A. Jasim, A. J. Sultan, and M. H. Al-Dahhan, “Impact of heat exchanging internals configurations on the gas holdup and bubble properties in a bubble column,” *Int. J. Multiph. flow*, vol. 112, pp. 63–82, 2019.

[32] A. A. Jasim, A. J. Sultan, and M. H. Al-Dahhan, “Influence of heat-exchanging tubes diameter on the gas holdup and bubble dynamics in a bubble column,” *Fuel*, vol. 236, no. March 2018, pp. 1191–1203, 2019.

[33] D. Law, F. Battaglia, and T. Heindel, “Stability issues for gas-liquid flows in bubble columns,” pp. 1–9, 2007.

[34] E. Delnoij, F. A. Lammers, J. A. M. Kuipers, and W. P. M. Van Swaaij, “Dynamic simulation of dispersed gas-liquid two-phase flow using a discrete bubble model,” *Chem. Eng. Sci.*, vol. 52, no. 9, pp. 1429–1458, 1997.

[35] E. Delnoij, J. a. M. A. M. Kuipers, and W. P. M. P. M. van Swaaij, “Dynamic simulation of gas-liquid two-phase flow: effect of column aspect ratio on the flow structure,” *Chem. Eng. Sci.*, vol. 52, no. 21–22, pp. 3759–3772, 1997.

[36] E. Delnoij, J. A. M. Kuipers, and W. P. M. Van Swaaij, “Computational fluid dynamics applied to gas-liquid contactors,” *Chem. Eng. Sci.*, vol. 52, pp. 3623–3623, 1997.

[37] M. R. Rampure, “Modeling of Gas-liquid / Gas-liquid-solid Flows in Bubble Column Reactor : Experiments and CFD Simulations,” *Can. J. Chem. Eng.*, vol. 81, no. August, pp. 692–706, 2003.

[38] J. Sanyal, S. V, S. Roy, and M. P. Dudukovic, “Numerical simulation of gas- liquid dynamics in cylindrical bubble column reactors,” *Chem. Eng. Sci.*, vol. 54, pp. 5071–5083, 1999.

[39] A. Sokolichin and G. Eigenberger, “Gas—liquid flow in bubble columns and loop reactors: Part I. Detailed modelling and numerical simulation,” *Chem. Eng. Sci.*, vol. 49, no. 24, pp. 5735–5746, Dec. 1994.

[40] Y. Pan, M. P. Dudukovic, and M. Chang, “Numerical investigation of gas-driven flow in 2-D bubble columns,” *AIChE J.*, vol. 46, no. 3, pp. 434–449, 2000.

[41] S. M. Monahan, V. S. Vitankar, and R. O. Fox, “CFD predictions for flow-regime transitions in bubble columns,” *AIChE J.*, vol. 51, no. 7, pp. 1897–1923, 2005.

[42] F. Larachi, D. Desvigne, L. Donnat, and D. Schweich, “Simulating the effects of liquid circulation in bubble columns with internals,” *Chem. Eng. Sci.*, vol. 61, no. 13, pp. 4195–4206, 2006.

[43] J. Sanyal, S. Vásquez, S. Roy, and M. P. Dudukovic, “Numerical simulation of gas-liquid dynamics in cylindrical bubble column reactors,” *Chem. Eng. Sci.*, vol. 54, no. 21, pp. 5071–5083, 1999.

[44] X. Guo and C. Chen, “Simulating the impacts of internals on gas–liquid hydrodynamics of bubble column,” *Chem. Eng. Sci.*, vol. 174, pp. 311–325, 2017.

[45] X. Guan and N. Yang, “CFD simulation of pilot-scale bubble columns with internals: Influence of interfacial forces,” *Chem. Eng. Res. Des.*, vol. 126, pp. 109–122, 2017.

[46] Zhang Yu, L. Jia, W. Lijun, and LI Xi, “Studies on hydrodynamics of turbulent slurry bubble column(Ⅲ) Effect of vertical pipe bundles,” *J. Chem. Ind. Eng. Soctial China*, vol. 60, pp. 1135–1140, 2009.

[47] S. Agahzamin and L. Pakzad, “A comprehensive CFD study on the effect of dense vertical internals on the hydrodynamics and population balance model in bubble columns,” *Chem. Eng. Sci.*, vol. 193, pp. 421–435, 2019.

[48] A. Youssef, “Fluid Dynamics and Scale-up of Bubble Columns with Internals,” Washington University in St. Louis, 2010.

[49] R. T. Lahey Jr and Donald A. Drew, “Application of General Constitutive Principles To the Derivation of Multidimensional Two-Phase Flow Equations,” *Int. J. Multiph. Flow*, vol. 5, pp. 243–264, 1979.

[50] Y. Sato, M. sadatomi, and K. Sekoguchi, “Momentum and heat transfer in two-phase bubble flow-I,” *Int. J. Multiph. flow*, vol. 7, pp. 167–177, 1981.

[51] M. Pourtousi, P. Ganesan, and J. N. Sahu, “Effect of bubble diameter size on prediction of flow pattern in Euler-Euler simulation of homogeneous bubble column regime,” *Meas. J. Int. Meas. Confed.*, vol. 76, pp. 255–270, 2015.

[52] M. Pourtousi, J. N. Sahu, P. Ganesan, S. Shamshirband, and G. Redzwan, “A combination of computational fluid dynamics (CFD) and adaptive neuro-fuzzy system (ANFIS) for prediction of the bubble column hydrodynamics,” *Powder Technol.*, vol. 274, pp. 466–481,

[53] A. Behzadi, R. I. Issa, and H. Rusche, “Modelling of dispersed bubble and droplet flow at high phase fractions,” *Chem. Eng. Sci.*, vol. 59, no. 4, pp. 759–770, 2004.

[54] A. Azimi Yancheshme, J. Zarkesh, D. Rashtchian, and A. Anvari, "CFD Simulation of Hydrodynamic of a Bubble Column Reactor Operating in Churn-Turbulent Regime and Effect of Gas Inlet Distribution on System Characteristics," *Int. J. Chem. React. Eng.*, vol. 14, no. 1, pp. 213–224, 2016.

[55] G. H. Yeoh and J. Tu, *Computational techniques for Multi-Phase Flows*, First edit. Elsevier Ltd., 2010.

[56] G. Li, X. Yang, and G. Dai, "CFD simulation of effects of the configuration of gas distributors on gas-liquid flow and mixing in a bubble column," *Chem. Eng. Sci.*, vol. 64, no. 24, pp. 5104–5116, 2009.

[57] J. R. Grace, T. Wairegi, and T. H. Nguyen, "SHAPES AND VELOCITIES OF SINGLE DROPS AND BUBBLES MOVING FREELY THROUGH IMMISCIBLE LIQUIDS.," *Trans Inst Chem Eng*, vol. 54, no. 3, pp. 167–173, 1976.

[58] A. Tomiyama, "Struggle with computational bubble dynamics," *Multiph. Sci. Technol.*, vol. 10, no. 4, pp. 369–405, 1998.

[59] S. A. Morsi and A. J. Alexander, "An investigation of particle trajectories in two-phase flow systems," *J. Fluid Mech.*, vol. 55, no. 2, pp. 193–208, Sep. 1972.

[60] L. Schiller and Z. Naumann, "A Drag Coefficient Correlation," *VDI Zeitung*, vol. 77, pp. 318–320, 1935.

[61] Inc. ANSYS, "ANSYS FLUENT Theory Guide," *ANSYS Fluent Theory Guide*, vol. v. 15, no. November. pp. 510–572, 2015.

[62] D. Bothe, M. Schmidtke, and H. J. Warnecke, "VOF-simulation of the lift force for single bubbles in a simple shear flow," *Chem. Eng. Technol.*, vol. 29, no. 9, pp. 1048–1053, 2006.

[63] D. Lucas, E. Krepper, and H. M. Prasser, "Use of models for lift, wall and turbulent dispersion forces acting on bubbles for poly-disperse flows," *Chem. Eng. Sci.*, vol. 62, no. 15, pp. 4146–4157, 2007.

[64] G. H. Yeoh, C. P. Cheung, and J. Tu, *Multiphase Flow Analysis Using Population Balance Modeling*. Elsevier Ltd., 2014.

[65] S. P. P. Antal, R. T. L. JR, J. E. E. Flaherty, R. T. Lahey Jr., and J. E. E. Flaherty, "Analysis of Phase Distribution in Fully Developed Laminar Bubbly Tow-Phase Flow," *Int. J. Multiph. flow*, vol. 17, no. No.5, pp. 635–652, 1991.

[66] T. Frank, J. M. Shi, and A. D. Burns, "Validation of Eulerian multiphase flow models for nuclear safety application," *3rd Int. Symp. Two-Phase Flow Model. Exp. Pisa, 22-24 Sept. 2004*, no. September, pp. 22–24, 2004.

[67] O. Simonin and P. Viollet, "Modelling of turbulent two-phase jets loaded with discrete particles," *Phenom. Multiph. Flows*, pp. 259–269, 1990.

[68] A. D. Burns, T. Frank, I. Hamill, and J.-M. M. Shi, "The Favre Averaged Drag Model for Turbulent Dispersion in Eulerian Multi-Phase Flows," *Fifth Int. Conf. Multiph. Flow, ICMF-2004*, no. 392, pp. 1–17, 2004.

[69] M. Kagumba, H. Al-Naseri, and M. H. Al-Dahhan, "A new contact time model for the mechanistic assessment of local heat transfer coefficients in bubble column using both the four-optical fiber probe and the fast heat transfer probe-simultaneously," *Chem. Eng. J.*, vol. 361, no. December 2018, pp. 67–79, 2019.

[70] D. Ramkrishna, *Population Balances: Theory ans Applications to Particulate System in Engineering*. Academic Press, 2000.

[71] H. Luo and H. S. F., "Theoretical model for drop and bubble breakp in turbulent dispersions," *AIChE J.*, vol. 42, no. 5, pp. 1225–1233, 1996.

[72] H. Luo, "Coalescence, Breakup and Liquid Circulation in Bubble Column Reactors," the Institute of Norwegian Institute, The University of Trondheim, 1993.

[73] X. Liang, H. Pan, Y. Su, and Z. Luo, "CFD-PBM approach with modified drag model for the gas-liquid flow in a bubble column," *Chem. Eng. Res. Des.*, vol. 112, pp. 88–102, 2016.

[74] A. J. Sultan, L. S. Sabri, and M. H. Al-Dahhan, "Investigating the influence of the configuration of the bundle of heat exchanging tubes and column size on the gas holdup distributions in bubble columns via gamma-ray computed tomography," *Exp. Therm. Fluid Sci.*, vol. 98, no. February, pp. 68–85, 2018.

[75] R. Krishna, J. Ellenberger, D. E. Hennophof, D. E. Hennephof, and D. E. Hennophof, "Analogous description of the hydrodynamics of gas-solid fluidized beds and bubble columns," *Chem. Eng. J.*, vol. 53, no. 1, pp. 89–101, 1993.

[76] J. Ellenberger and R. Krishna, "A unified approach to the scale-up of gas-solid fluidized bed and gas-liquid bubble column reactors," *Chem. Eng. Sci.*, vol. 49, no. 24, pp. 5391–5411, 1994.

[77] Y. Wu and M. H. Al-Dahhan, "Prediction of axial liquid velocity profile in bubble columns," *Chem. Eng. Sci.*, vol. 56, no. 3, pp. 1127–1130, 2001.

[78] L. C. Mutharasu *et al.*, “Experimental study and CFD simulation of the multiphase flow conditions encountered in a Novel Down-flow Bubble Colum,” *Chem. Eng. J.*, vol. 350, no. April, pp. 507–522, 2018.

[79] M. K. Silva, M. A. D'ávila, and M. Mori, “Study of the interfacial forces and turbulence models in a bubble column,” *Comput. Chem. Eng.*, vol. 44, pp. 34–44, 2012.

[80] M. V Tabib, S. A. Roy, and J. B. Joshi, “CFD simulation of bubble column — An analysis of interphase forces and turbulence models,” *Chem. Eng. J.*, vol. 139, pp. 589–614, 2008.

[81] S. Yamoah, R. Martínez-Cuenca, G. Monrós, S. Chiva, and R. Macián-Juan, “Numerical investigation of models for drag, lift, wall lubrication and turbulent dispersion forces for the simulation of gas-liquid two-phase flow,” *Chem. Eng. Res. Des.*, vol. 98, pp. 17–35, Jun. 2015.

[82] P. Chen, J. Sanyal, and M. P. Dudukovic, “CFD modeling of bubble columns flows: Implementation of population balance,” *Chem. Eng. Sci.*, vol. 59, no. 22–23, pp. 5201–5207, 2004.

[83] H. K. Versteeg and M. W, *An Introduction to Computational Fluid Dynamics*. 2007.

[84] S. B. Kumar, “Computed Tomographic Measurements of Void Fraction and Modeling of the Flow in Bubble Coulnms,” Washington Univeristy, St. Louis, MO, 1994.

[85] N. Rados, A. Shaikh, and M. H. Al-Dahhan, “Solids flow mapping in a high pressure slurry bubble column,” *Chem. Eng. Sci.*, vol. 60, no. 22, pp. 6067–6072, 2005.

[86] S. Nedeltchev and A. Shaikh, “A new method for identification of the main transition velocities in multiphase reactors based on information entropy theory,” *Chem. Eng. Sci.*, vol. 100, pp. 2–14, 2013.

[87] J. Chen *et al.*, “Fluid dynamic parameters in bubble columns with internals,” *Chem. Eng. Sci.*, vol. 54, no. 13–14, pp. 2187–2197, 1999.

[88] N. Rados, A. Shaikh, and M. H. Al-Dahhan, “Phase Distribution in a High Pressure Slurry Bubble Column via a Single Source Computed Tomography,” *Can. J. Chem. Eng.*, vol. 83, no. February, 2005.

[89] A. Shaikh and M. Al-Dahhan, “Characterization of the hydrodynamic flow regime in bubble columns via computed tomography,” *Flow Meas. Instrum.*, vol. 16, pp. 91–98, 2005.

[90] G. Besagni and F. Inzoli, “Bubble size distributions and shapes in annular gap bubble column,” *Exp. Therm. Fluid Sci.*, vol. 74, pp. 27–48, Jun. 2016.

SECTION

2. RECOMMENDATIONS

In this study, for the first time, the effect of the presence industrial-scale heat exchanging internals, the solids loading, the variation in the low aspect ratio in industrial-sized pilot plant bubble/slurry bubble column on the bubble dynamics and the flow regime transition have been investigated. However, data obtained exhibit that the studied design parameters have a significant effect on the bubble dynamics and the flow regime transition. Therefore, the new knowledge in this investigation have been revealed in terms the presence of internals, low aspect ratio, and the solids loading the following suggestions that have been made for future work to be performed.

1. Investigate the impact of the presence of heat exchanging internals, the solids loading at low aspect ratio ($H/D \leq 5$) in industrial-sized pilot plant bubble/slurry bubble column on the liquid dynamics, including the liquid velocity, Reynolds stresses, turbulent kinetic energy, and turbulent eddy diffusivities, by using radioactive particle tracking (RPT) technique.
2. Investigate the impacts of the sparger design on the bubble dynamics and liquid dynamics using the advanced four-point optical probe technique and radioactive particle tracking (RPT) technique, respectively, at low aspect ratio in bubble/slurry bubble column with and without internals.
3. Investigate the impact of the presence heat exchanging internals at low aspect ratio ($H/D \leq 5$) in an industrial-sized bubble/slurry bubble column on the heat transfer

coefficient and mass transfer coefficient since the current data obtained exhibit that bubble properties have been impacted by the studied parameters.

4. Investigate the effect of solids loading with different particle sizes diameter on the bubble dynamics, heat transfer, and mass transfer, since some studies have reported increase in heat transfer coefficient while others a decrease and it is thought the different phenomena observed can be attributed to different gas-liquid-solid systems employed.
5. 3D time-depend simulate of the actual conditions in terms industrial-sized for the bubble/slurry bubble column with and without the presence of internals using numerical solution, since the current study provide benchmarking data that can be used to validate the numerical solution to enhance the fundamental understanding of the hydrodynamics of bubble columns with and without internals in industrial scale.
6. Simulate the bubble/slurry bubble column with and without the presence of internals using CFD codes under relevant industrial conditions (i.e., Fischer-Tropsch conditions), using mimicked liquid of similar physical properties, operating under high temperature, pressure, and loading of the fine catalyst.

REFERENCES

[1] L.E. Doman, L.E. Singer, M. Bowman, International Energy Outlook 2016 Liquid fuels, 2016. doi:DOE/EIA-0484(2014).

[2] M. Kagumba, Heat transfer and bubble dynamics in bubble and slurry bubble columns with internals for Fischer-Tropsch synthesis of clean alternative fuels and chemicals, Missouri University of Science and Technology, 2013.

[3] J. Hu, F. Yu, Y. Lu, Application of Fischer–Tropsch Synthesis in Biomass to Liquid Conversion, Catalysts. 2 (2012) 303–326. doi:10.3390/catal2020303.

[4] snehesh shivananda Ali, S. Dasappa, Biomass to liquid transportation fuel via Fischer Tropsch synthesis – Technology review and current scenario, Renew. Sustain. Energy Rev. 58 (2016) 267–286. doi:10.1016/j.rser.2015.12.143.

[5] L.-Q. Wang, Y.-H. Dun, H. Tang, T.-Z. Wang, A biomass gasification system for synthesis gas from the new method, Nat. Sci. 01 (2009) 195–203. doi:10.4236/ns.2009.13026.

[6] A. de Klerk, E. Furimsky, Catalysis in the Refi ning of Fischer-Tropsch Syncrude, Platin. Met. Rev. 55 (2011) 263–267.

[7] R. Krishna, S.T. Sie, Design and scale-up of the Fischer–Tropsch bubble column slurry reactor, Fuel Process. Technol. 64 (2000) 73–105. www.elsevier.comrlocaterfuproc.

[8] S.C. Saxena, Bubble Column Reactors and Fischer-Tropsch Synthesis, Catal. Rev. 37 (1995) 227–309. doi:10.1080/01614949508007096.

[9] R. Krishna, J.W.A. de Swart, J. Ellenberg, G.B. Martina, C. Maretto, Gas holdup in slurry bubble columns: Effect of column diameter and slurry concentrations, A.I.Ch.E. J. 43 (1997) 311.

[10] A. Youssef, Fluid Dynamics and Scale-up of Bubble Columns with Internals, Washington University in St. Louis, 2010. doi:10.1017/CBO9781107415324.004.

[11] M.P. Dudukovic, Opaque Multiphase Reactors: Experimentation, Modeling and Troubleshooting, Oil Gas Sci. Technol. 55 (2000) 135–158. doi:10.2516/ogst:2000008.

[12] B.I. Kamara, J. Coetzee, Overview of high-temperature Fischer-Tropsch gasoline and diesel quality, Energy and Fuels. 23 (2009) 2242–2247. doi:10.1021/ef800924z.

[13] C.N. Setterfield, G.A. Huff, Mass transfer limitations in Fischer-Tropsch slurry reactors, Chem. Eng. Sci. 36 (1981) 791–792. doi:10.1016/0009-2509(81)85102-0.

[14] S. Schlüter, A. Steiff, P.-M. Weinspach, Heat transfer in two- and three-phase bubble column reactors with internals, Chem. Eng. Process. Process Intensif. 34 (1995) 157–172. doi:10.1016/0255-2701(94)04002-8.

[15] M.K. Al Mesfer, A.J. Sultan, M.H. Al-Dahhan, Study the Effect of Dense Internals on the Liquid Velocity Field and Turbulent Parameters in Bubble Column for Fischer–Tropsch (FT) Synthesis by Using Radioactive Particle Tracking (RPT) Technique, Chem. Eng. Sci. 161 (2017) 228–248. doi:10.1016/j.ces.2016.12.001.

[16] M.K. Al Mesfer, A.J. Sultan, M.H. Al-Dahhan, Impacts of dense heat exchanging internals on gas holdup cross-sectional distributions and profiles of bubble column using gamma ray Computed Tomography (CT) for FT synthesis, Chem. Eng. J. 300 (2016) 317–333. doi:10.1016/j.cej.2016.04.075.

[17] A.J. Sultan, L.S. Sabri, M.H. Al-Dahhan, Investigating the influence of the configuration of the bundle of heat exchanging tubes and column size on the gas holdup distributions in bubble columns via gamma-ray computed tomography, Exp. Therm. Fluid Sci. 98 (2018) 68–85. doi:10.1016/j.expthermflusci.2018.05.005.

[18] B.C. Ong, P. Gupta, A. Youssef, M. Al-Dahhan, M.P. Duduković, Computed Tomographic Investigation of the Influence of Gas Sparger Design on Gas Holdup Distribution in a Bubble Column, Ind. Eng. Chem. Res. 48 (2009) 58–68. doi:10.1021/ie800516s.

[19] J. Xue, Bubble Velocity, Size and Interfacial Area Measurements in Bubble columns, Washington Univeristy, Saint Louis, 2004. doi:10.1002/aic.

[20] J. Xue, M. Al-Dahhan, M.P. Dudukovic, Bubble Velocity, Size, and Interfacial Area Measurements in a Bubble Column by Four-Point Optical Probe, AIChE J. 54 (2008) 350–363. doi:10.1002/aic.

[21] C. Wu, K. Suddard, M.H. Al-Dahhan, Bubble Dynamics Investigation in a Slurry Bubble Column, AIChE J. 54 (2008) 1203–1212. doi:10.1002/aic.

[22] A.A. Youssef, M.E. Hamed, J.T. Grimes, M.H. Al-Dahhan, M.P. Duduković, Hydrodynamics of pilot-scale bubble columns: Effect of internals, Ind. Eng. Chem. Res. 52 (2013) 43–55. doi:10.1021/ie300465t.

[23] A.A. Youssef, M.H. Al-Dahhan, Impact of internals on the gas holdup and bubble properties of a bubble column, Ind. Eng. Chem. Res. 48 (2009) 8007–8013. doi:10.1021/ie900266q.

[24] M. Kagumba, M.H. Al-Dahhan, Impact of internals size and configuration on bubble dynamics in bubble columns for alternative clean fuels production, Ind. Eng. Chem. Res. 54 (2015) 1359–1372. doi:10.1021/ie503490h.

[25] A. Shaikh, M. Al-Dahhan, Characterization of the hydrodynamic flow regime in bubble columns via computed tomography, Flow Meas. Instrum. 16 (2005) 91–98. doi:10.1016/j.flowmeasinst.2005.02.004.

[26] A. Forret, J.M. Schweitzer, T. Gauthier, R. Krishna, D. Schweich, Influence of scale on the hydrodynamics of bubble column reactors: An experimental study in columns of 0.1, 0.4 and 1 m diameters, Chem. Eng. Sci. 58 (2003) 719–724. doi:10.1016/S0009-2509(02)00600-0.

[27] G. Hebrard, D. Bastoul, M. Roustan, Influence of the gas sparger on the hydrodynamic behavior of bubble columns, Chem. Eng. Res. Des. 74 (1996) 406–414.

[28] S.B. Kumar, Computed Tomographic Measurements of Void Fraction and Modeling of the Flow in Bubble Coulnms, Washington Univeristy, St. Louis, MO, 1994.

[29] P. Rollbusch, M. Becker, M. Ludwig, A. Bieberle, M. Grünewald, U. Hampel, R. Franke, Experimental investigation of the influence of column scale, gas density and liquid properties on gas holdup in bubble columns, Int. J. Multiph. Flow. 75 (2015) 88–106. doi:10.1016/j.ijmultiphaseflow.2015.05.009.

[30] S. Sasaki, K. Uchida, K. Hayashi, A. Tomiyama, Effects of column diameter and liquid height on gas holdup in air-water bubble columns, Exp. Therm. Fluid Sci. 72 (2017) 67–74. doi:10.1016/j.expthermflusci.2015.10.027.

[31] M.W. Haque, K.D.P. Nigam, J.B. Joshi, Optimum gas sparger design for bubble columns with a low height-to-diameter ratio, Chem. Eng. J. 33 (1986) 63–69. doi:10.1016/0300-9467(86)80035-1.

[32] O.M. Basha, B.I. Morsi, Effects of Sparger and Internals Designs on the Local Hydrodynamics in Slurry Bubble Column Reactors Operating under Typical Fischer-Tropsch Process Conditions - I, Int. J. Chem. React. Eng. 0 (2017) 1–19. doi:10.1515/ijcre-2017-0058.

[33] B.N. Thorat, J.B. Joshi, Regime transition in bubble columns: Experimental and predictions, Exp. Therm. Fluid Sci. 28 (2004) 423–430. doi:10.1016/j.expthermflusci.2003.06.002.

[34] G. Besagni, L. Gallazzini, F. Inzoli, Effect of gas sparger design on bubble column hydrodynamics using pure and binary liquid phases, Chem. Eng. Sci. 176 (2018) 116–126. doi:10.1016/j.ces.2017.10.036.

[35] J. Chen, P. Gupta, S. Degaleesan, M.H. Al-Dahhan, M.P. Duduković, B.A. Toseland, Gas holdup distributions in large-diameter bubble columns measured by computed tomography, Flow Meas. Instrum. 9 (1998) 91–101. doi:10.1016/S0955-5986(98)00010-7.

[36] G. Besagni, F. Inzoli, G. De Guido, L.A. Pellegrini, The dual effect of viscosity on bubble column hydrodynamics, Chem. Eng. Sci. 158 (2017) 509–538. doi:10.1016/j.ces.2016.11.003.

[37] S. Nedeltchev, A. Shaikh, M. Al-Dahhan, Flow regime identification in a bubble column based on both statistical and chaotic parameters applied to computed tomography data, Chem. Eng. Technol. 29 (2006) 1054–1060. doi:10.1002/ceat.200600162.

[38] W.T. Medjiade, A.R. Alvaro, A. Schumpe, Flow regime transitions in a bubble column, Chem. Eng. Sci. 170 (2017) 263–269. doi:10.1016/j.ces.2017.04.010.

[39] X. Shen, T. Hibiki, H. Nakamura, Developing structure of two-phase flow in a large diameter pipe at low liquid flow rate, Int. J. Heat Fluid Flow. 34 (2012) 70–84. doi:10.1016/j.ijheatfluidflow.2012.02.004.

[40] S. Nedeltchev, S. Aradhya, F. Zaid, M. Al-Dahhan, Flow Regime Identification in Three Multiphase Reactors Based on Kolmogorov Entropies Devived from gauge Pressure Fluctuations, J. Chem. Eng. Japan. 45 (2012) 757–764.

[41] S. Barghi, A. Prakash, A. Margaritis, M.A. Bergougnou, Flow Regime Identification in a Slurry Bubble Column from Gas Holdup and Pressure Fluctuations Analysis, Can. J. Chem. Eng. 82 (2004) 865–870.

[42] J.J. Wu, D. Wang, L. hua Li, J.T. Zhou, Characterization of Flow Regimes in Bubble Columns through CCF Analysis of Pressure Fluctuations, Chem. Eng. Technol. 28 (2005) 1109–1113. doi:10.1002/ceat.200500155.

[43] B. Gourich, C. Vial, A.H. Essadki, F. Allam, M.B. Soulami, M. Ziyad, Identification of flow regimes and transition points in a bubble column through analysis of differential pressure signal - Influence of the coalescence behavior of the liquid phase, Chem. Eng. Process. Process Intensif. 45 (2006) 214–223. doi:10.1016/j.cep.2005.09.002.

[44] W. Li, W. Zhong, B. Jin, Y. Lu, T. He, Flow patterns and transitions in a rectangular three-phase bubble column, Powder Technol. 260 (2014) 27–35. doi:10.1016/j.powtec.2014.04.002.

[45] H. Al-Naseri, J.P. Schlegel, M.H. Al-Dahhan, The Impact of Low Aspect Ratio on Flow Regime Transition in Industrial-Sized Pilot Plant Bubble Column Reactor, Chem. Eng. J. submitted (2018).

[46] J.P. Zhang, J.R. Grace, N. Epstein, K.S. Lim, Flow regime identification in gas-liquid flow and three-phase fluidized beds, Chem. Eng. Sci. 52 (1997) 3979–3992.

[47] M. Shiea, N. Mostoufi, R. Sotudeh-Gharebagh, Comprehensive study of regime transitions throughout a bubble column using resistivity probe, Chem. Eng. Sci. 100 (2013) 15–22. doi:10.1016/j.ces.2013.01.047.

[48] G. Besagni, F. Inzoli, Influence of internals on counter-current bubble column hydrodynamics: Holdup, flow regime transition and local flow properties, Chem. Eng. Sci. 145 (2016) 162–180. doi:10.1016/j.ces.2016.02.019.

[49] M.C. Ruzicka, J. Drahos, M. Fialova, N.H. Thomasb, Effect of bubble column dimensions on flow regime transition, Chem. Eng. Sci. 56 (2001) 6117–6124.

[50] S. Orvalho, M. Hashida, M. Zednikova, P. Stanovsky, M.C. Ruzicka, S. Sasaki, A. Tomiyama, Flow regimes in slurry bubble column: Effect of column height and particle concentration, Chem. Eng. J. 351 (2018) 799–815. doi:10.1016/j.cej.2018.06.115.

[51] G. Besagni, F. Inzoli, The effect of liquid phase properties on bubble column fluid dynamics: Gas holdup, flow regime transition, bubble size distributions and shapes, interfacial areas and foaming phenomena, Chem. Eng. Sci. 170 (2016) 270–296. doi:10.1016/j.ces.2017.03.043.

[52] S. Nedeltchev, U. Jordan, O. Lorenz, A. Schumpe, Identification of various transition velocities in a bubble column based on Kolmogorov entropy, Chem. Eng. Technol. 30 (2007) 534–539. doi:10.1002/ceat.200600344.

[53] J. Chen, F. Li, S. Degaleesan, P. Gupta, M.H. Al-Dahhan, M.P. Duduković, B.A. Toseland, M.P. Dudukovic, B.A. Toseland, Fluid dynamic parameters in bubble columns with internals, Chem. Eng. Sci. 54 (1999) 2187–2197. doi:10.1016/S0009-2509(99)00003-2.

[54] A.J. Sultan, L.S. Sabri, M.H. Al-Dahhan, Impact of heat-exchanging tube configurations on the gas holdup distribution in bubble columns using gamma-ray computed tomography, Int. J. Multiph. Flow. 106 (2018) 202–219. doi:10.1016/j.expthermflusci.2018.05.005.

[55] A.J. Sultan, L.S. Sabri, M.H. Al-Dahhan, Influence of the size of heat exchanging internals on the gas holdup distribution in a bubble column using gamma-ray computed tomography, Chem. Eng. Sci. 186 (2018) 1–25. doi:10.1016/j.ces.2018.04.021.

[56] F. Larachi, D. Desvigne, L. Donnat, D. Schweich, Simulating the effects of liquid circulation in bubble columns with internals, Chem. Eng. Sci. 61 (2006) 4195–4206. doi:10.1016/j.ces.2006.01.053.

[57] G. Li, X. Yang, G. Dai, CFD simulation of effects of the configuration of gas distributors on gas-liquid flow and mixing in a bubble column, Chem. Eng. Sci. 64 (2009) 5104–5116. doi:10.1016/j.ces.2009.08.016.

[58] X. Guo, C. Chen, Simulating the impacts of internals on gas–liquid hydrodynamics of bubble column, Chem. Eng. Sci. 174 (2017) 311–325. doi:10.1016/j.ces.2017.09.004.

VITA

Hayder Akram Arif Al-Naseri born in Basrah, Iraq. He received his Bachelors of Engineering (B.E.) in Chemical Engineering and the first Master Science (M.Sc.) in Chemical Engineering from Tikrit University, Iraq in 1999 and 2002, respectively. In 2003, he was employed as a process engineer, for five years, in the petrochemical industry in Arabic Company for Chemicals Detergent (ARADET), Iraq. Then in 2006, he was employed as an instructor in the Chemical Engineering Department at Tikrit University in which he earned his bachelor's and master's degree in 2006. In 2012, he was awarded a scholarship by the Iraqi government that represented by the Higher Committee for Education Development (HCED) in Iraq to earn his Doctor of Philosophy degree (Ph.D.) in Chemical Engineering at Missouri University of Science and Technology in the United States. He started at Missouri S&T during the fall semester of 2014 to work under the supervision of Dr. Muthanna Al-Dahhan. He obtained his second M.S. in Chemical Engineering from Missouri S&T in May 2016. Hayder is a member of Iraqi Engineers Union (IEU) since 1999, and a member of American Institute of Chemical Engineer (AIChE) since 2016. Additionally, he published two journal papers in Chemical Engineering Journals (CEJ) and Experimental Thermal Science Fluid (ETSF). Further, he submitted four journal papers, which are under review. In May 2019, he received his Ph.D. in Chemical Engineering from Missouri University of Science and Technology.